Structure and function of the social brain in primates

Léa ROUMAZEILLES

New College

University of Oxford

A Thesis submitted for the degree of Doctor of Philosophy

Michaelmas term 2021

Declaration

This thesis has only been submitted to the University of Oxford for the degree of Doctor of Philosophy and no part has been accepted or is currently being submitted for any degree, diploma or certificate or other qualification in this University or elsewhere. All data, interpretations and materials presented in this thesis are my own work with contributions from my two supervisors Profs Jerome Sallet and Rogier Mars and from others as outlined below.

Funding for this project was provided by a fees-only BBSRC Studentship and a 1379 Society Old Members Scholarship from New College (University of Oxford) as well as an in-vivo skills award from the BBSRC for chapter 2 data acquisition. The functional magnetic resonance imaging study (chapter 2) was performed at the Biomedical Science Services (University of Oxford) and facilitated by their technicians. *Post mortem* samples for chapters 3, 4 and 5 were acquired through the Zoological Society of London (gorilla, chimpanzee, squirrel monkey), the Copenhagen Zoo (lemurs, squirrel monkeys), the Caribbean Primate Research Center (free-ranging macaques) and the University of Oxford Biomedical Science Services (laboratory macaques). Scanning of these *post mortem* samples for the chapters 3, 4 and 5 was facilitated by Alexander Khrapitchev at the University of Oxford. *In vivo* chimpanzee data (chapter 3) was obtained from the National Chimpanzee Brain Resource collected at the Yerkes National Primate Research Centre. Human data were obtained from the Human Connectome Project (HCP). Data for chapter 2, 3 and 4 are available online (details in the associated publications).

Approximate word count: 55,800 words.

Acknowledgments

This thesis would not have been possible without the support of several people.

I would like to thank my two supervisors, Jérôme Sallet and Rogier Mars for their guidance and support throughout the thesis. They provided me with a great environment to do a PhD, always enthusiastically encouraging my work, sharing great advice and able to help me rebound in tough times.

From my master thesis, I would like to thank Sébastien Bouret who have raised my interest and knowledge in comparative neuroscience and Caroline Jahn who has helped me so much in applying for a PhD.

The Neuroecology lab has given me an inspiring environment with diverse people, always available. Particularly, Nicole Eichert's great skills, that she was always willing to share, Katherine Bryant's wide knowledge of primate brains and anthropology and Matthias Schurz's insights in functional MRI analysis and theory of mind have helped me a lot throughout the PhD.

I would also like to thank Matthew Rushworth and his whole lab, who welcomed me as their own and have provided so much help and everyday motivation. Particularly, Davide Folloni who showed me the ropes of monkey fMRI research and Kevin Marche, my control room buddy, a great listening ear and full of (bad) jokes! Nadescha Trudel who has provided much fun and support throughout my PhD as well as sharing great scientific input together with Marco Wittman. Alizée Lopez, from Paris to Oxford to Paris again, it's always so enlightening to talk to you about anything.

Thanks to the DTC for offering lots of opportunities during the PhD and a great cohort. So much thanks go to my housemates Sofía and Anna for providing the best home environment where we were always able to rant as much as we needed. Thanks to Signe, Vero, and Daria for their supporting friendships throughout the PhD.

I also need to thank all the monkeys who have participated in my thesis and particularly my own three: Vass, Voodvood and Warw, as well as the whole BSB team who are taking great care of them.

Thanks to Lola, Hind and Pénélope, in 10 years of friendship you never gave up wanting to visit the different countries I was living in! It was so great to reset with you in Corsica every summer.

Thanks to my family, although they do not really understand what I do, they have always been supporting me and my choices.

Last but not least, thanks to Axel, always present, in the best and the worst part of the PhD, tirelessly helping me go through every hurdle and pushing me to reveal my best at all times. You have had such a big impact on this thesis and my overall personal growth over the years.

Thank you all. Merci à tous.

Table of Contents

Abstract

Social abilities differ between primate species, with some thought to be specifically human, such as theory of mind (TOM). It has been argued that brain expansion and reorganisation throughout the primate evolutionary history has accompanied these differences (reviewed in **chapter 1**). In this thesis, we aimed to characterise how the primate social brain function and anatomy have evolved to shed light onto the evolutionary roots of the human social brain. We tackled this goal with a comparative approach and using magnetic resonance imaging (MRI). First, we designed a novel functional MRI experiment testing for the computational properties underlying TOM in the macaque brain in **chapter 2**. Our results showed that, as the temporo-parietal junction (TPJ) in humans, a middle superior temporal sulcus (midSTS) area in macaques can support TOM computations. We suggest that the macaque midSTS could have undergone reorganisation and specialisation as a precursor for the human TPJ. Then, in **chapter 3**, we investigated the architecture of the white matter temporal lobe underlying its cortical expansion and reorganisation from macaques to humans. By integrating several great ape species, we were able to suggest a stepwise evolutionary trajectory for the connectivity of the temporal lobe. We further characterised the evolution of primate brain organisation in **chapter 4**, by establishing a common methodology to study lemurs, squirrel monkeys and macaques. We identified a simian fronto-parietal and temporo-parietal elaboration in terms of cortical and connectivity expansion. In **chapter 5**, we set out to expand our understanding of the ontogeny of the macaque brain organisation by exploring the changes observed throughout their lifespan. We pinpointed a period in their early life where most of the changes occurs and revealed connectivity refinement throughout their life. Overall, this thesis suggests an evolutionary trajectory for the primate social brain (**chapter 6**) and paves the way for further investigation.

Abbreviations

ACC	Anterior Cingulate Cortex
ACPC	Anterior Commissure-Posterior Commissure
AF	Arcuate Fascicle (tract)/Anterior Fundus (face patch)
AFI	Actual Flip-angle Imaging
AL	Anterior Lateral
AM	Anterior Medial
ANTs	Advanced Normalization Tools
AR	Acoustic Radiation
AS	Arcuate Sulcus
ATC	Anterior Temporal Cortex
ATR	Anterior Thalamic Radiation
BOLD	Blood-Oxygen-Level Dependent
CalS	Calcarine Sulcus
CB	Cingulum Bundle
CeS	Central Sulcus
Cing	Cingulate sulcus
CPRC	Caribbean Primate Research Centre
CST	Cortico-Spinal Tract
DMN	Default Mode Network
DW	Diffusion-Weighted
EPI	Echo Planar Imaging
EV	Explanatory Variable
FA	Fractional Anisotropy
FDR	False Discovery Rate
FEF	Frontal Eye Field
FFA	Fusiform Face Area
FG	Fusiform Gyrus
FrA	Frontal Aslant
FSL	FMRIB Software Library
FST	Fundus of Superior Temporal area
FWE	Family-Wise Error
FWHM	Full Width at Half Minimum
FX	Fornix
GLM	Generalized Linear Model
GM	Grey Matter
GRE	Gradient-Refocused Echo
HCP	Human Connectome Project
IFOF	Inferior Fronto-Occipital Fascicle
ILF	Inferior Longitudinal Fascicle
IOS	Inferior Occipital Sulcus
IPL	Inferior Parietal Lobule
IPS	Intra-Parietal Sulcus
ITG	Inferior Temporal Gyrus
KL	Kullback-Leibler
LaS	Lateral Fissure
LuS	Lunate Sulcus

MD	Mean Diffusivity
MdLF	Middle Longitudinal Fascicle
MF	Middle Fundus
midSTS	Middle Superior Temporal Sulcus
ML	Middle Lateral
MMORF	MultiMOdal Registration Framework
MNI	Montreal Neurological Institute
MPD	Mean Positional Distance
MPFC	Medial Pre-Frontal Cortex
MRI	Magnetic Resonance Imaging
MST	Medial Superior Temporal area
MT	Middle Temporal
MTG	Middle Temporal Gyrus
NIH	National Institutes of Health
OFA	Occipital Face Area
OFC	Orbito-Frontal Cortex
OR	Optic Radiation
PBS	Phosphate-Buffered Saline
PCC	Posterior Cingulate Cortex
PDF	Probability Density Function
PF	PreFrontal
PFC	PreFrontal Cortex
PL	Posterior Lateral
PS	Principal Sulcus
ROI	Region Of Interest
SD	Standard Deviation
SLF	Superior Longitudinal Fascicle
SNR	Signal to Noise Ratio
SPA	Social Prediction Area
SSFP	Steady-State Free Precession
STG	Superior Temporal Gyrus
STR	Superior Thalamic Radiation
STS	Superior Temporal Sulcus
TE	Echo Time
TFCE	Threshold-Free Cluster Enhancement
TIR	Turbo-Inversion Recovery
TOM	Theory of Mind
TPJ	Temporo-Parietal Junction
TPO	Temporo-Parietal-Occipital association area
TR	Repetition Time
TSE	Turbo Spin-Echo
TUS	Transcranial Ultrasound Stimulation
UAR	Understanding Animal Research
UNC	Uncinate Fascicle
VOF	Vertical Occipital Fascicle
WM	White Matter
YNPRC	Yerkes National Primate Research Center

List of Figures

List of Tables

Chapter 1 - Introduction

1.1. Premises of the thesis: brain evolution and function

Humans are widespread all over the surface of the earth, but humankind represents only a small part of the evolutionary history. If the earth was 24 hours old, humans would have existed for just a bit more than a minute, while life on earth originated 20 hours ago. Indeed, life on earth emerged around 3.8 billion years ago. Since then, life forms have diversified through the power of evolution, shaping the traits of different species to adapt to the changing environment. The Darwin-Wallace theory of evolution posits that natural selection will favour progenies of parents with characteristics that have allowed them to survive and reproduce in their environment (Darwin, 1859). From this evolutionary process, primates including humans, have inherited, among other things, a particularly large brain and complex social abilities. How and why evolution have favoured these traits in primate and human evolution is a particularly thrilling question.

The search to understand the brain has received many interests since the antiquity. From being thought as a blood cooling organ to a host of the soul, its functions and links to behaviour are not fully understood even today. Phrenology associating bumps on the skull to mental trait and ability, dominated at the beginning of the 19th century (usually associated with Franz Joseph Gall). It was followed by localizationism, influenced by Paul Pierre Broca, which associated brain functions to physical brain regions relying on lesion studies from head injuries. Lesion studies also led to the emergence of connectivism in the second half of the 19th century (with for instance Karl Friedrich Burdach, Johann Christian Reil and Carl Wernicke), arguing that complex brain functions are the result of interactions between connected brain areas while more basic functions could be limited to particular areas (Duffau, 2018). Therefore, connectivism emphasized the importance of interaction between brain areas

and accompanied the emergence of the term ‘neuron’ from Santiago Ramón de Cajal’s work (López-Muñoz et al., 2006). Methods have been developed and refined constantly in the 20th and 21st century to make possible the study of the brain at many different levels. From molecular to connectome study, investigating genetic, function and anatomy and how they relate to behaviour, the field of neuroscience is now encompassing many different disciplines.

Comparative neuroscience which studies the nervous system of different species has been emerging as a tool to better understand the human brain and its evolutionary origins. Indeed, to study human brain evolution per se, one would have to focus on their closest ancestors which are mostly extinct and as the brain does not fossilize, common methods cannot be used. Instead, paleo-neurologists study endocranial casts, the casts of the cranial cavity representing the approximate brain size and structure. Although endocasts have allowed for the identification of gross morphological changes in human brain evolution, they are limited in the level of details they can provide and how they can relate to the species ecology and behaviour. Comparative neuroscience has been focusing on species still present on earth such as our closest relatives, the chimpanzees, with whom we share a common ancestor around 6 million years ago, but for ethical and practical reasons, some research cannot be conducted with chimpanzees. Preferably, investigating the whole primate order allows to combine diverse methods and, when interpreted in an evolutionary framework, these comparative studies allow to apprehend the extent of evolutionary processes leading to modern human brain and social behaviour (see overview of primate evolution in Figure 1.1).

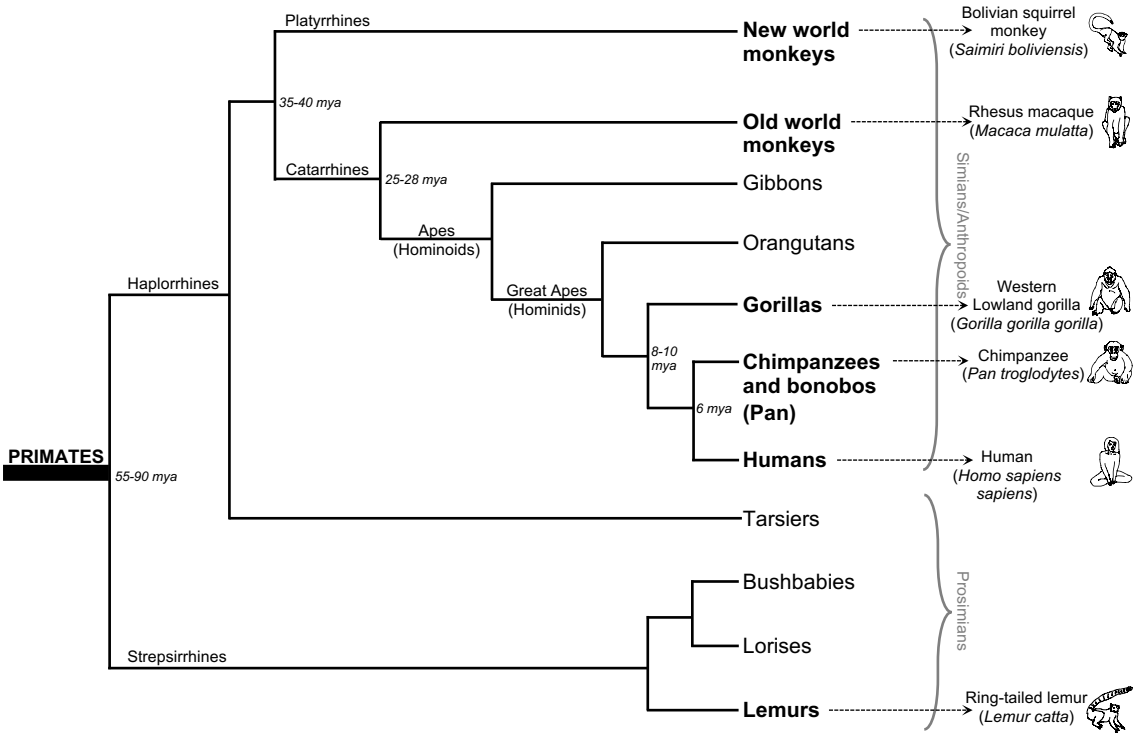

Figure 1.1 Primates phylogenetic tree

Overview of the primate evolution, highlighting the suborders, infraorders, parvorders, superfamilies and families relevant for this thesis with the exact species represented on the right-hand side. Mya: million years ago.

In this introduction, we will lay the ground knowledge that have inspired this thesis. We start by discussing the similarities and differences in primate social abilities and behaviours with a particular focus on theory of mind. Then, we detail the current knowledge about the human social brain in terms of its anatomy, function, and underlying computation. We follow by introducing evolutionary concepts and comparative methods that have led to the current knowledge of the social brain in non-human primates. Next, we bring in neuro-developmental insights to discuss the link between evolution and development. Finally, we summarize the methodological issues encountered in the field that we aim to tackle with this thesis.

In this thesis, we benefit from the study of several primate species and the emergence of new methods to develop a comparative approach to study primate brain

evolution in the context of social abilities complexification. We combine functional and anatomical study with an emphasis on connectivity to investigate brain evolutionary trajectories that could explain differences observed in social behaviour across primates.

1.2. Social abilities in primates

Primates are usually described as very social species, with social interactions occupying a large portion of their time. We will highlight here some of the impressive primate social skills and how they differ across species, before discussing more precisely the theory of mind abilities.

1.2.1. A common ground of social skills

Identity-matching

Complex social behaviours between individuals rely on the ability to recognise each other and identify unique individuals. Different sensory cues might be used to perform identity matching. The most prominent among primates are the visual cues, such as faces (Perrodin et al., 2015). Most primates are innately drawn to faces and their first order configuration is described as sharing the same basic features and general organisation enabling to discriminate between face and non-face objects (Parr, 2011). Second order configuration is needed to establish the unique identity of a face, it is described as the relative spatial position of features and their surface-based characteristics (colour, shading…). The face inversion effect has been widely used to test for face identity matching across primate's species. It relies on the fact that identifying faces upside down is more difficult than for other non-face objects. This effect has been observed in humans and chimpanzees so far, but the results are less clear for monkeys. It is actually thought that monkeys might be less sensitive to second order configuration than chimpanzees or humans (Parr, 2011). Ethological considerations

regarding the social organisation of different species might be able to explain these differences.

Faces are not the only visual stimuli used by primates to recognize individuals, body gestures are also used in humans (O'Toole et al., 2011), while in chimpanzees behinds have been shown to be processed similarly to faces, at least at the behavioural level (Kret and Tomonaga, 2016). Olfactory cues have gathered less attention in primates, but ring-tailed lemurs have been shown to match olfactory and auditory signatures of the same individuals (Kulahci et al., 2014), therefore displaying a multi-sensory representation. Multisensory representations have also been shown in different primates concerning visual and auditory cues such as speech or calls (Sliwa et al., 2011; Habbershon et al., 2013; Maciej et al., 2013).

Communication/language

To function in social groups, primates are also able to communicate. As with the previous description of identity matching, they rely on several sensory cues that can also be used in combination. To be defined as supporting communication, these cues must be perceived by others, interpreted, and eventually answered. In the visual domain, primates share basic repertoire of facial display which may have evolved from non-communicative gesture associated with arousal or defensive behaviours (Andrew, 1963). Tactile communications have also been noticed to signal dominance or affinity (Peters and Ploog, 1973).

In the auditory domain, non-vocal signals are produced by specific movement of hands, feet, lips, and tongue (Peters and Ploog, 1973). Combination of visual and auditory cues in communication has been observed in macaques, cebus, chimpanzees and humans (Ghazanfar, 2013). The size of the social group in anthropoid primates has

actually been associated with the extent of the facial (Dobson, 2009) and vocal (McComb and Semple, 2005) expression repertoire. Vocal signals are described as calls in non-human species and as speech in humans. Human speech, when defined in its narrow sense, has been associated with the recursion and combinatorial pattern of vocal communication found uniquely in humans (Hauser, 2002). But more recent work has also described the vocal abilities as a continuum where humans are the most advanced (Jarvis, 2019). However, further debate around the evolution of human speech is not in the scope of this thesis.

Gaze following

A particular communication skill has attracted attention as being a key developmental building block in social interaction. The emergence of a gaze control system in primates is thought to have participated to their refined foraging abilities, as they were now able to locate food without having to move much (Cisek, 2019). This system has then been associated with attention and social function. Social gaze allows individual to share their focus of attention and hidden intentions. It not only comprises following the eyes but also the head and body orientation. Most taxa of primates are at least responsive to others' gaze (Rosati and Hare, 2009) and respond to coarse metrics of visual orientation. Most haplorrhines studied (apes and several species of monkeys) have been shown to be able to follow gaze of their conspecifics in a reflexive and voluntary way. This allows them to represent space outside of their own visual field (Shepherd, 2010; Meunier, 2017; Isoda et al., 2018; Spadacenta et al., 2019) and exploit several sensory information to integrate understanding of others' perspective which strepsirrhines are not able to perform (Krupenye, 2021).

It is also thought that gaze following capacity allows observational learning in most primates (Emery, 2000), as an individual must direct its attention to where another is looking in order to learn from them. Gaze following is therefore usually associated with joint attention. Joint attention describes the behaviour of two individuals attending the same object because one used the attentional cue from the other. Previous studies have shown the importance of joint attention in humans compared to apes and monkeys (Emery, 2000; Shepherd, 2010). These findings have contributed to the suggestion of the cooperative eye hypothesis, which posits that humans have unusually visible eyes (due to the white sclera) because the eye has evolved to support their cooperative social interaction through gaze following and joint attention (Tomasello et al., 2007). Furthermore, gaze following and joint attention are thought to be building blocks for theory of mind (discussed in section 1.2.2).

Structured social network

Primates are commonly described as living in elaborated and relatively stable social groups. Although, several characteristics can differ between primate species (e.g., group size, hierarchy status…), their social network is structured. Different measures to characterise these social networks have been suggested to describe them in their complexity rather than attributing a single term such as 'egalitarian' or 'hierarchical' (Kasper and Voelkl, 2009). Indeed, stemming from graph theory, network analysis is combining the multitude of affiliative and aggressive behaviours displayed between individuals of the same group to understand the fitness implications of group life (Sueur et al., 2011). Among these implications, it has been noted that increased social complexity could lead to better chance of survival (Silk, 2003; Brent et al., 2017),

decreased predation risk and increased foraging efficiency (Sueur et al., 2011; Chang et al., 2013a).

Competition/Cooperation

The advantages of living in large groups stand on cooperative and affiliative behaviours which benefit the social group cohesion and the access to resources (Sussman et al., 2005). Cooperative behaviours have been associated with pro-sociality, and it has been argued that humans and non-human primates display prosocial behaviour even when there is no obvious benefit for them (de Waal et al., 2008; de Waal and Suchak, 2010). This kind of prosocial behaviours have been linked with the ability to feel empathy for others (Lockwood et al., 2016). However, primates are also famous for their highly competitive interactions with their conspecifics because the resources are usually present in a finite amount. This complex balance between competition and cooperation has been associated with human intelligence evolution through the Machiavellian intelligence hypothesis (Byrne, 1996). It argued that the capacity to out-compete others with very sophisticated cognitive abilities have been selected throughout primate evolution. The importance of competition in the primate social life has implications for the design of relevant social tasks (Hare, 2001; Schmelz and Call, 2016). However, it should also be noted that competition behaviours differ between species, even when phylogenetically close such as chimpanzees and bonobos for instance. With an environment in which food resources are more available, the bonobos have developed a less aggressive social system (Gruber and Clay, 2016).

We have highlighted here different primate social abilities allowing for the complexity of their social life and how primates share common characteristics. We will

now touch upon the more elaborated social skills observed mainly in humans and referred to as 'theory of mind'.

1.2.2. The hot debate: Theory of mind

Definition, theories, levels

Theory of mind (TOM), also called mentalizing, refers to the ability to infer someone else thoughts and beliefs, in other words their mental states. It has been originally proposed by Premack and Woodruff in 1978. In this seminal paper, they insist on the term 'theory' as the mental states are not directly observable and because this system can be used to make predictions about others behaviour (Premack and Woodruff, 1978). While this original study focused on evidence of theory of mind in chimpanzees, the term has been later on adopted by developmental psychologists to describe the ontogeny of mental representation in infants and children (Leslie, 1987).

Different views of mentalizing are classically opposed. The nativist view posits that mentalizing is an evolved mechanism innately present in humans, while the constructivist view emphasizes the importance of the individual environment in the development of mentalizing abilities (Heyes, 2014). These two views can be reconciled if one considers that mentalizing can be a dual-process with implicit and explicit forms (Apperly and Butterfill, 2009). This distinction has been suggested by several authors to explain the discrepancy observed during theory of mind tasks in infants (Low and Perner, 2012; Butterfill and Apperly, 2013; Heyes, 2014). Indeed, it was previously thought that theory of mind developed at around the age of 4 years old in humans. However, non-verbal tasks have identified this ability as early as 2 years old. Therefore, implicit mentalizing, a fast and automatic uncontrolled behaviour, could be the system present at young age. Explicit mentalizing would appear at a later developmental stage

and is described as a slow and controlled system involving language to deliberate about mental states (Heyes, 2014). It has been further argued that explicit mind reading could be culturally inherited and passed on *via* verbal instructions (Heyes and Frith, 2014). The term submentalizing has also been proposed to refer to behaviours that resemble implicit mentalizing but without involving thinking about mental states at all and driven by domain general cognitive mechanisms (such as attentional reorientation and spatial coding) (Heyes, 2014).

The theoretical framework around theory of mind has also been divided between the *theory theory* and the *simulation theory*. The former proposing that mental states are interpreted based on past experiences observed from others while the latter proposes an impersonation phenomenon, putting ourselves in the same situation as others to interpret their mental states (Alcalá-López et al., 2018). Because the simulation theory cannot account for all the mentalizing abilities, it has been suggested that a hybrid theory, combining both processes suggested by the two theories, would better explain the extent of theory of mind abilities (Mitchell, 2005; Saxe, 2005). It is clear from this description that theoretical and philosophical questions remain in the definition of theory of mind (Kulke et al., 2019).

Uniquely human?

The question of the human uniqueness of theory of mind has also been intensely debated. It is now agreed that other primates can demonstrate some forms of theory of mind but the extent to which they resemble the human theory of mind (also referred to as full-blown mind-reading) is still unclear. From the previously mentioned gaze following, joint attention studies and others, it has been long though that macaques are able to track others' perspectives but not others' beliefs (Marticorena et al., 2014;

Drayton and Santos, 2016) while apes were able to represent beliefs but only if they did not differ from their own (Call and Tomasello, 2008; Martin and Santos, 2016).

This brings us to an important aspect of the theory of mind field which concerns false beliefs, defined as the ability to infer someone else's belief even if known to be false or different from our own. Therefore, it implies to understand that others' beliefs are based on their own knowledge, a difficult mental process that was thought to be a hallmark of human theory of mind (Meunier, 2017). However, results from recent studies suggest that apes and Japanese macaques are able to track simple false beliefs (Krupenye et al., 2016; Kano et al., 2019; Hayashi et al., 2020). Although, one must be cautious in interpreting these results as they use an anticipatory looking paradigm which are prone to replicability limitations (Horschler et al., 2020).

It is also complicated to affirm the existence of one form of theory of mind or another in non-human primates because of the incomplete data spanning a very limited range of species. But considering the current state of the research, there are some mentalizing processes that are thought to be uniquely humans (Krupenye, 2021). First, there is the ability to perform level 2 perspective taking, which allows us to understand how a given object is perceived by others and not only its presence or absence from the other's field of view (Meunier, 2017). Second, the ability to perform recursive or embedded levels of theory of mind has not been observed yet in other species (Devaine et al., 2014, 2017). Finally, it is also thought that the shared intentionality demonstrated by humans in cooperative activity makes a crucial difference between humans and non-human primates (Tomasello et al., 2005).

Usual tests and their caveats

To fully understand current knowledge about theory of mind and its evolutionary origins, it appears necessary to discuss some of the main methods used in this research field. Importantly, methodological issues arise in this field because, as per the parsimony principle, some results could actually be explained by simple cognitive low-level abilities rather than proper theory of mind skills (Povinelli and Vonk, 2012; Heyes, 2015). Classical original tests for theory of mind abilities in humans include false belief stories as the famous 'Sally and Anne' (Wimmer and Perner, 1983), and other trait judgement and social strategic games, which all require some kind of language and reading skills, to deal with pictures, texts or videos stimuli. These tests, although implementing adequate controls, have been criticized because they are mainly based on observation, they relate to third person perspective.

A 'goggles experiment' has been suggested to overcome this issue, because in this test participants need to use their own experience to infer what others see (Heyes, 1998). However, in order to overcome most of the current critics, ecologically valid and second person perspective tests where participant directly engage with theory of mind as well as more culturally diverse research, are needed (Byom and Mutlu, 2013; Quesque and Rossetti, 2020).

Because most of human theory of mind research depends on language and reading, adapting the protocols to infant and non-human primate protocols has proven very difficult. To replace language-based, competitive, and interactive helping tasks as well as looking time studies and anticipatory looking methods have been developed (Ong et al., 2020; Arre and Santos, 2021). The usual concerns with non-human primate tests of theory of mind usually refer to the small sample size and the low reproducibility rate as well as the difficulty of interpretation (Kulke et al., 2019). It is interesting to note

that from early experiments trying to prove the existence of false belief ability in apes, such as the seminal work by Premack and Woodruff, the bar has now been dramatically lowered in terms of research goals to ask if non-human primates possess any of the low-level abilities (Heyes, 2015).

Overall, the field of theory of mind is still a debated area where further progress in theoretical definitions, evolutionary research and methodological considerations is needed to better understand this complex and invaluable social skill. This will be further explored in chapter 2.

1.3. Anatomy and function of the social brain

What has been dubbed the social brain comprises a network of grey matter areas associated with social functions and white matter fibres connecting them. As social cognition involves high level processes, it is important to introduce here a distinction between types of brain areas. Two main types are of interest for further anatomical discussion in this thesis, the primary areas, and the multimodal association areas. Primary areas, which can be either sensory or motor, are concerned with unimodal sensation or motor action. Multimodal association areas are able of combining several stimuli and are thought to be responsible for high level cognitive processes such as language or mentalizing. They are principally located in the prefrontal, posterior parietal, and lateral temporal cortices.

1.3.1. The human social brain

Brain areas involved in social tasks

Grey matter brain areas of the human social brain have been previously identified, mainly using Magnetic Resonance Imaging (MRI) to identify their

coactivation with social task parameters. They have been summarized as comprising the following areas (see summary in Figure 1.2A): the medial Prefrontal Cortex (PFC) including the Anterior Cingulate Cortex (ACC), the Superior Temporal Sulcus (STS), the Anterior Temporal Cortex (ATC), the Temporo-Parietal Junction (TPJ), the amygdala and the striatum (Rushworth et al., 2013; Tremblay et al., 2017; Wittmann et al., 2018). They have been associated with different social functions and interestingly the size of some of them has been shown to have a positive correlation with the social network size of a given individual (ventro-medial PFC, ATC, TPJ, ACC) (Bickart et al., 2011; Kanai et al., 2012; Noonan et al., 2018).

Concerning life in complex social environment, the ATC has been shown to be critical for representing and retrieving social knowledge (Olson et al., 2013), the pSTS has been associated with altruistic behaviour (Morishima et al., 2012) and processing social interactions (Masson and Isik, 2021) and the ventro-medial PFC and striatum are involved in the social valuation system, as well as the Orbito-Frontal Cortex (OFC) (Ruff and Fehr, 2014).

Theory of mind abilities have been associated mainly with the TPJ, particularly its posterior part (Mars et al., 2012b), and medial PFC in humans, but some of the tasks also involve the precuneus, the ATC and the STS (Schurz et al., 2014). Some regions associated with the human social brain are actually involved in more general processes which can in turn be generalized to social processes (Wittmann et al., 2018; Lockwood et al., 2020). Recent works have tried to suggest a theoretical framework to disentangle the socially specific neural processes and the ones shared with other non-social abilities (Lockwood et al., 2020). Other networks and their neuronal computation can also inform the underlying computation of the social brain.

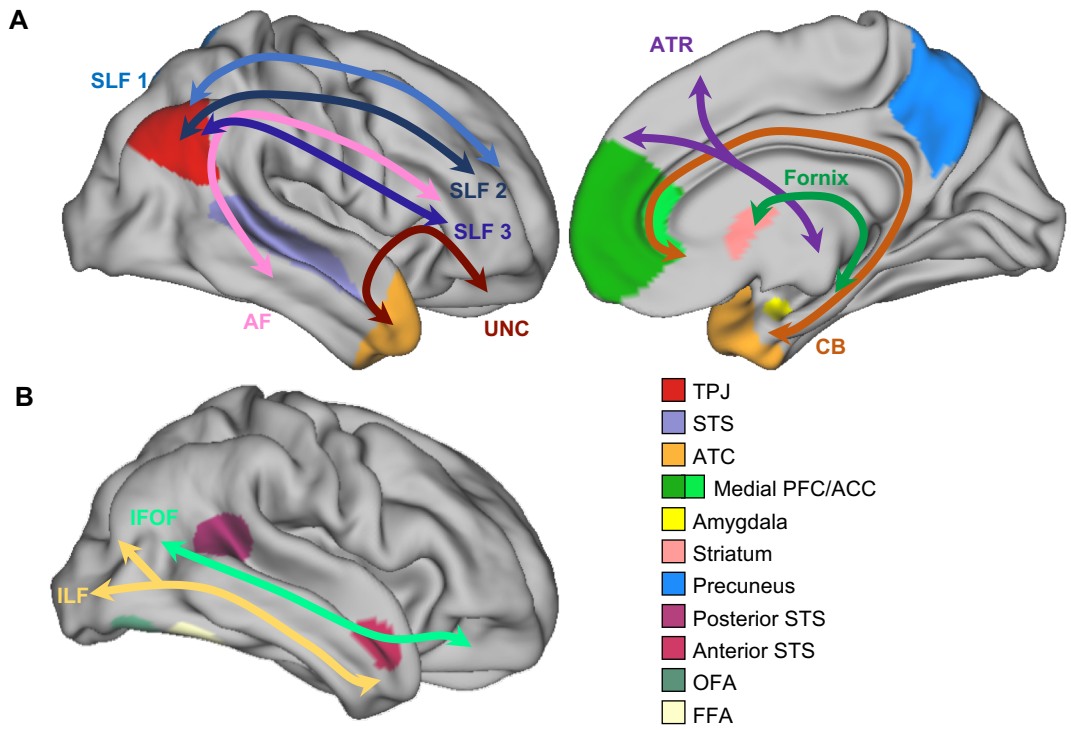

Figure 1.2 The anatomy of the human social brain

A. Approximate location of the brain regions and white matter tracts involved in social cognition, represented on mid-thickness lateral (left) and medial (right) surface representations. **B.** Approximate location of face responsive areas and associated white matter tracts. ACC: Anterior Cingulate Cortex; AF: Arcuate Fascicle; ATC: Anterior Temporal Cortex; ATR: Anterior Thalamic Radiation; CB: Cingulum Bundle; FFA: Fusiform Face Area; IFOF: Inferior Fronto-Occipital Fascicle; ILF: Inferior Longitudinal Fascicle; OFA: Occipital Face Area; PFC: PreFrontal Cortex; SLF: Superior Longitudinal Fascicle; STS: Superior Temporal Sulcus; TPJ: Temporo-Parietal-Junction; UNC: Uncinate Fascicle.

The case of the Temporo-Parietal Junction

The TPJ deserves specifically more focus in the scope of this thesis as it will be discussed further in the following chapter (chapter 2) and is generally approximately defined. Indeed, the TPJ is a region mostly defined by its function related to attention and social cognition (Patel et al., 2019). Anatomically, it has been defined as the cortical area at the junction of the posterior end of the superior temporal sulcus (STS), the inferior parietal lobule (IPL), and the lateral occipital cortex, spanning the angular and supramarginal gyri (Mars et al., 2012b; Patel et al., 2019). Based on connectivity-

based parcellations it has been identified as consisting of distinct anatomical areas (Mars et al., 2012b; Igelström et al., 2015), of which specific part seemed essential for theory of mind processing (Schurz et al., 2017) and others for attentional processing (Patel et al., 2019).

Underlying computation

From the description of the anatomical network, we can notice some overlaps in terms of brain regions involved between the social valuation system and the value-based reward system (ventro-medial PFC, striatum, and OFC). These similarities extend to the computation underlying these processes as well. Indeed, the reward system uses reinforcement learning to learn about reward related information while social learning relies on information from or about others. In reinforcement learning, an agent will learn the outcomes associated with a certain action to eventually be able to predict them (Sutton and Barto, 1998). A prediction error occurs when a certain action does not lead to the expected outcomes anymore. From low-level social processes such as face detection or gaze-following to higher levels such as theory of mind, studies have identified expectation forming processes in social contexts similar to reward contexts (de Bruin and Michael, 2021). They rely on the predictive coding framework in which an unexpected outcome would trigger more activity in a given brain region because the difference between the predicted and observed stimuli is higher, in other words the prediction error is more important. Brain areas such as the striatum and the ACC encode others and reward related information similarly, possibly in slightly different subregions (Chang et al., 2013b) and this information can be further combined in the PFC (Behrens et al., 2008). It appears that self-learning and learning about others share biological characteristics (Joiner et al., 2017).

In the context of theory of mind, the predictive coding framework is thought to allow for inferences about others' goals, thoughts, and personality (Koster-Hale and Saxe, 2013), with prediction error activity identified in the TPJ and the temporal cortex as well (Behrens et al., 2008). Since its conceptualization, the simplification of social cognition processes into predictive coding framework has received attention as a potential solution for the design of experimental tasks in natural settings (which will be further explored in chapter 2).

Face responsive system

The face responsive areas are thought to be part of the social brain, but this system involves slightly different regions (see summary in Figure 1.2B). The most common regions associated with face response in the human brain are located in the inferior part of the brain and named Fusiform Face Area (FFA) and Occipital Face Area (OFA) (Tsao et al., 2008). Other extended networks have been shown to also be involved with face-related activity, such as areas in the posterior and anterior STS and the amygdala (Haxby et al., 2000). Altogether these face areas are able to perceive facial features, eye gaze and expression, identify individual identity and link these to other emotional, attentional or biographical information.

This dispersed set of brain regions involved in social functions rely on white matter connectivity for communication in the network and the study of connectivity is therefore fundamental to fully understand the function of a brain region.

White matter tracts

Associating anatomical entity with function is much less straightforward when talking about white matter bundles compared to grey matter areas, but connectivity between brain areas ensured by white matter is also crucial for the correct functioning of complex social processes (Wang and Olson, 2018; Thiebaut de Schotten et al., 2020; Filley, 2021). The investigation of white matter involvement in social processes has mainly focused on correlating structural characteristics with social parameters and causal studies from patients with white matter impairments. As for the grey matter in this system, the size of the social network correlates with white matter in the fronto-temporal system (Hampton et al., 2016; Noonan et al., 2018). Two white matter pathways have been repeatedly associated with social processes, the Inferior Longitudinal Fascicle (ILF) and the Inferior Fronto-Occipital Fascicle (IFOF) (Wu et al., 2016; Herbet et al., 2018). They are thought to be the main ones associated with face perception as they are connecting occipital and temporal regions and occipital and frontal regions respectively (Figure 1.2B) (Pyles et al., 2013). Associated with social cognition processes such as empathy and emotion regulation are the Superior Longitudinal Fascicle (SLF) connecting frontal and parietal areas, the Uncinate Fascicle (UNC) connecting anterior temporal and frontal areas, the Anterior Thalamic Radiation (ATR) connecting subcortical and prefrontal areas and the fornix, the main subcortical limbic tract (Figure 1.2A) (Wang et al., 2018). Mentalizing abilities have been associated with the cingulum bundle, running along the cingulate gyrus it connects its anterior and posterior parts as well the medial temporal cortex (Herbet et al., 2014). The role of the Arcuate Fascicle (AF) in mentalizing has also been suggested, although it is more commonly associated with language abilities due to its connectivity to the major language areas. Previously disregarded, white matter connectivity is gaining more

attention recently and as the methods improve, our understanding of its involvement in social processes will progress as well.

1.3.2. Association with other systems

To better comprehend the social brain, we need to also describe other brain systems sharing anatomical or functional aspects.

Mirror system

The mirror neuron system, linked with the social brain, has received attention due its importance for understanding others action. Specific types of visuomotor neurons have first been identified in macaques premotor and intraparietal cortex, that respond when the individual would perform an action but also when they would watch the same action performed by another (Rizzolatti et al., 1996; Fogassi et al., 2005). Since then, a mirror system has also been identified in humans in similar areas of the brain (Rizzolatti and Craighero, 2004) and effort has been put in understanding its link with the mentalizing system. Indeed, while they both encode information about others, the mirror system is mainly concerned with action and biological motion while the mentalizing system comes into play when the information becomes more abstract (Van Overwalle and Baetens, 2009). It had been suggested that by understanding intention underlying others' motor act, the mirror system could support the simulation theory in the mentalizing domain, as this description fits with the impersonation aspect of the theory. However, the computation behind the mirror system does not seem high level enough to explain the complex processes of mentalizing (Rizzolatti and Fogassi, 2014; Alcalá-López et al., 2018). The mirror and mentalizing systems have recently been shown to be distinct in that, with everything else matched, the first one processes action while the second one is concerned with moods (Geiger et al., 2019). Evidence is arguing

for a complementary relationship between the mirror and mentalizing systems, although possible evolutionary links with language functions and emotion perceptions are still under scrutiny (Rizzolatti, 2005; Keysers and Fadiga, 2008).

Default mode network

A very large network of the brain has also received attention recently and its overlap with the social brain is quite striking. It had first been identified as a network of brain regions that were more active during the passive control of a task or at rest than during the goal-directed task itself and therefore it had been named the Default Mode Network (DMN) (Raichle et al., 2001). Because of this original definition, it has been thought that this network was mainly concerned with passive processes, however it is now commonly associated with mind-wandering and self-generated thought and interaction with executive control systems (Andrews-Hanna, 2012; Schurz et al., 2020; Yeshurun et al., 2021). It has further been defined by resting-state connectivity study identifying its main regions as the medial PFC, the Posterior Cingulate Cortex (PCC), the medial temporal lobe, the angular gyrus, the TPJ and the lateral temporal cortex along the STS (Yeo et al., 2011). Subcortically, the basal forebrain and anterior and mediodorsal thalamic nuclei have been associated with the DMN (Alves et al., 2019). Large scale connectivity mapping of the brain has also proposed the DMN as the higher functional level (where primary sensory areas are the lowest) because of its capacity to combine transmodal information not related to immediate sensory input (Margulies et al., 2016). As with any large system, it has also been divided into smaller parts with a core made of the PCC, angular gyrus and medial PFC representing personally relevant information. The medial temporal sub-system would be in charge of combining associative information to construct a coherent scene and finally the dorso-medial and

TPJ sub-system would serve to reflect upon information related to self (Andrews-Hanna et al., 2014). This last sub-system has evident overlap with the mentalizing network and is thought to be related to introspection about mental states of others as well. Further links of the DMN with the social brain can also be noted as its coupling with the ACC and dorso-lateral PFC increases with the size of the social network (Noonan et al., 2018). The DMN has been identified in several species, although different data (resting-state, tract tracing…) and analysis methods (independent component, seed-based, gradient…) have yields slightly different anatomical boundaries, the overlap between the DMN and the social brain has also been observed in non-human primates (Mars et al., 2012a; Schwiedrzik et al., 2015; Buckner and Margulies, 2019; Liu et al., 2019). It appears clear that social cognition relies at least in part on the DMN which opens possibilities for the study of social cognition and its evolutionary roots.

1.3.3. Associated disorders

As social cognition makes up a large part of human life, a range of social cognition disorders have been identified (Kennedy and Adolphs, 2012). A lot of them have been related to theory of mind impairment which can account for some of the social behavioural deficits in children and adults, with the most studied two examples: Autism Spectrum Disorder and Schizophrenia (Brüne and Brüne-Cohrs, 2006).

Autism Spectrum Disorder and Schizophrenia

Autism is a developmental condition diagnosed in early childhood (appearing around the age of 3 years old). It is usually associated with the avoidance of social contact, with the failure to establish relationship and engagement in stereotypical behaviour. Theory of mind seems to be specifically impaired in autism leading to

difficulties in appreciating mental states of others, while autistic individuals can perform social cognitive tasks independent of theory of mind (Baron-Cohen, 1991).

Schizophrenia is usually described as a disorder distorting the perception of self and others, of emotions and behaviours, leading to hallucination, delusion, and difficulties to communicate. It has been associated with theory of mind deficits in relating one's own intention to executive behaviour and monitoring of others' intentions which could also in turn impair the language (Brune, 2005).

In line with their association to theory of mind, both autism and schizophrenia have been associated with dysfunction in the temporo-frontal cortex, the limbic system, and the cerebellum (Brambilla, 2003; Karlsgodt et al., 2010; Sugranyes et al., 2011; Ecker, 2012). Schizophrenia has particularly been described as a disconnection syndrome, affecting connectivity between specific brain regions through white matter alteration in the SLF, CB, UNC and ILF for instance (Kyriakopoulos et al., 2008).

Personality disorders

Further personality disorders have been investigated in relation to social cognition and theory of mind, but it is not always straightforward to understand the processes at play. For instance, psychopathy, which is characterized by anti-social disorders seems to not particularly impact theory of mind abilities per se but mostly the empathic side of it. Therefore, psychopath could understand others but in instrumental terms, devoid of empathic feeling (Blair et al., 1996). Personality pathologies have been thought to be related to an impaired theory of mind because of early-life experiences which did not allow a proper development of mentalizing skills and instead favourited the inhibition of these skills as a defence mechanism (Fonagy et al., 2018). Antisocial personality behaviour and psychopathy have been mainly associated with an alteration

of prefrontal and limbic circuits particularly when processing emotional stimuli (McCloskey et al., 2005).

Social anxiety

Finally, social anxiety, the persistent and excessive fear of social situation, has also been associated with theory of mind. Interestingly, inversely from autistic people, persons suffering from social anxiety will attribute more intense emotions and greater meaning to others' mental states compared to control participants (Hezel and McNally, 2014). Social anxiety has been associated with dysfunction in the brain functional connectivity, involving several networks such as the DMN and affective network (ACC, amygdala, temporal pole, and insula) but also some lower-level cognitive network such as the visual network and the sensory-motor network (Liu et al., 2015b).

This overview of disorders associated with social cognition is by no means complete but provide an overview of the possible applications of theory of mind research and demonstrate the need for a better understanding of cognitive and neural processes behind such disorders.

1.4. Evolutionary perspectives on the social brain

Evolutionary processes have shaped the evolution of the brain to select traits that would confer higher fitness results. Uncovering which fitness problematic these traits are solving will lead to a better understanding of how modern human brains work. For the scope of this thesis, we will focus mainly here on primate evolution, but evolutionary principles could sometimes be discussed in a wider range of species. In the

course of the next pages, it might be useful to refer to Figure 1.1 representing primate evolutionary tree.

1.4.1. Brain evolution theories

Primate brain evolution is characterized by unusually large brain, but as this comes as a cost in terms of energetic and physiological demands, they must have been selected for providing a certain advantage. Evolutionary theorists have tried to uncover what could support this trend toward large brains mainly by looking at correlation with other factors. We describe here some of the most influential theories.

Ecological intelligence hypothesis

The important impact of foraging abilities on fitness and the frugivorous diet of primates have led to the formulation of the ecological intelligence hypothesis (Milton, 1988). It argued that frugivory, being more demanding on cognitive capacities, as it requires an extensive mental mapping and multi-information tracking, would lead primates to evolve larger brains (DeCasien et al., 2017). Others have reformulated this hypothesis in terms of the innovation rate, which more generally relies on the ability to learn and adapt to cope with the environment and is correlated with the size of the brain in a large range of species and not only primates (Lefebvre et al., 2004). Field studies have allowed us to comprehend better the various advanced cognitive skills required for successful foraging, such as using fruiting synchronicity or memories of already visited trees (Zuberbühler and Janmaat, 2010; Janmaat et al., 2012, 2013). This ecological intelligence hypothesis is particularly attractive because it provides a somewhat direct link between the energy expenditure coming with the enlargement of the brain. Indeed, because fruits constitute a high-quality food it is thought that therefore primates could actually afford a more energetically expansive brain. The evolution of complex foraging

abilities associated with larger brains may have in turn allowed primates to develop complex social skills (Zuberbühler and Janmaat, 2010). But critics of this foraging hypothesis have argued the opposite: that large brains have evolved for other reasons, and it is to cope with the demand in energy that in turn foraging skills have developed. The ecological hypothesis has also been criticised in terms of its reduced explanatory capacity because while primate brain sizes differ massively between species, the foraging strategies do not differ as much (Dunbar and Shultz, 2017).

Social brain hypothesis

Usually seen as an opponent to the ecological intelligence hypothesis, another very influential theory is the social brain hypothesis. It was first formulated as a quantitative relationship between group size and brain size in mammals but specifically in primates, such that the information processing capacity required in large primate social group would explain their large brain (Dunbar, 1998). It has been later refined on several points. First, regarding the brain measure, it has been suggested that a more accurate measurement would be to consider the size of the neocortex in relation to body size or whole brain size (Dunbar and Shultz, 2007a, 2007b), as it is the part of the brain that has mostly expanded in primates. Second, in terms of the social parameter studied, it has been argued that considering group size as a proxy for social complexity was an important shortcut. Instead, the quality of primate social relationship has been put forward as a critical parameter, specifically in the case of Anthropoid primates. Their ability to apply pair-bonding relationships as observed in other taxa to non-reproductive relationships has been put forward as a better explanation of increased cognitive pressures which would have led to larger brains (Dunbar, 2009). Critics against the social brain hypothesis have arisen (de Ruiter et al., 2011; Acedo-Carmona and Gomila,

2016). They are mainly pointing out the shortcomings of focusing on one linear relationship which cannot capture the complexity of brain and behaviour evolution. But this theory is still prominent in the field and some studies have in the contrary reassessed the robustness of the link between brain size and social complexity (Sandel et al., 2016).

Ecological and social hypotheses overlaps

Going further into the interpretation of the social brain hypothesis, it has been suggested that large groups with complex social interactions could be a benefit in terms of predation and food-finding. Predation has also been suggested as an important factor that could have been at the origin of the evolution of large brains and complex sociality (van der Bijl and Kolm, 2016). Regarding food-finding it has also been suggested that increase sociality could be linked with the ability to learn from others and apply the learned skills to deal with ecological pressure such as finding food (Reader and Laland, 2002).

These interpretations suggest that both the ecological and the social brain hypothesis should be considered when investigating primate brain evolution and there exist obvious links between them (Dunbar and Shultz, 2017). In terms of neuroanatomy, we have seen that the social and reward processing system partially overlap in terms of brain areas and computations involved (see 3.1 and 3.2). Some skills such as language are thought to have evolved thanks to both the enlargement of group size but also to the navigational system stemming from foraging abilities, combining the two hypotheses (Ferretti, 2016). Interactions between ecological and social hypotheses are not so surprising, as specific foraging challenges would emerge from large social groups but in turn foraging innovation could impact upon the social group. It has also been argued

that it could be the increase in development duration in primates that permitted large sized brains, in turn allowing to adapt in complex social and ecological environment (Charvet and Finlay, 2012). However, it seems that it is the functional constraints that by favouring specific brain systems led to more complex developmental mechanisms (Montgomery et al., 2016). Overall, the two hypotheses -ecological and social- could be reconciled by arguing that both have explanatory power regarding the size of the primate brain but in different specific domains of cognition (Rosati, 2017).

Cultural intelligence

To further complete the social brain hypothesis, a cultural intelligence hypothesis has been suggested (Carpenter and Tomasello, 1995; Whiten and van Schaik, 2007; Whiten and van de Waal, 2017). It associates social learning abilities and social complexity from the social brain hypothesis to culture. Culture here is defined on a spectrum from simple social learning exploiting information to complex tradition arising from elaboration on earlier ones. Social abilities influence culture which in turn influences social abilities producing a spiralling effect (Whiten and van Schaik, 2007). This hypothesis has been used to explain the differences between human cognition and brain size with that of other species, as the more elaborated level of culture has so far mostly been observed in humans (Tomasello et al., 1993, 2005). On this account, cultural learning has further been associated with human abilities for theory of mind and language (Heyes and Frith, 2014; Lameira, 2017). However, the cultural intelligence hypothesis has been criticised because of the difficulties to apply it to other species than primates (Dunbar and Shultz, 2017).

The three aforementioned hypotheses are useful in that they try to formulate a common overarching principle of brain evolution, but we need to be careful in interpreting them, as they could seem oversimplified to interpret the complete complexity of the brain. It appears that more investigation is needed, refining the methods and enlarging the sample size, to design a coherent model of brain enlargement in primates.

1.4.2. A neuro-comparative framework to investigate brain evolution

We will now discuss the principles and methods behind the investigation of brain evolution. They rely on comparative studies as extinct species cannot be investigated.

Main principles

From the previous discussion of brain evolution theories, it appears clearly that the size is an important measure of evolutionary pressure. Allometric principles have been used widely in the study of evolution. Allometry refers to the principle that a certain biological characteristic change with the size of the organism or parts of it. It appears evident that the size of surrounding elements would cause an increase in the size of the encased one, such as in the case of body and brain sizes. Therefore, it has been argued that allometry relations can be used to distinguish a change of proportion due to size dependent issue, from adaptation for another reason, giving clues about the evolutionary pressure at play (Gould, 1966).

However, critics for the consideration of brain size only have emerged. It has been argued that while brain size increases, there must be some reorganisation episodes of specific systems happening. This more modular view of brain evolution has further been formulated as the *mosaic evolution* of the brain, postulating that size changes

selectively in functionally distinct systems (Barton and Harvey, 2000). A striking evidence has been put forward with the study of the neocortex size that has a five folds difference between primates and insectivores compared to the rest of brain. But it is also interesting to note that there is a correlation in size changes between regions anatomically or functionally connected such as the olfactory bulb and olfactory cortex (Barton and Harvey, 2000). Further studies have focused specifically on anthropoid primates to show that specific regions are consistently enlarged, such as the prefrontal and motor control areas and cortico-cerebellar system (Smaers and Soligo, 2013; Smaers and Vanier, 2019). Therefore, although size will be limited by the energetic factor, it must not be considered as the only factor; specific cognitive demand will also play a role as demonstrated by localized increases in brain areas relative to the whole brain.

The study of overall brain size, still considered as an interesting measure, need to be completed by the understanding of the systems that contribute to it, such as microscopic features (axon diameter, neuronal density, white matter enlargement…) (Barton, 2006). With the increase of brain size or specific components comes the question of the brain shape changes to accommodate the changes in size. However, a study focusing on primate brains has shown that allometric effect on brain shape were only present in catarrhine primates, possibly associated with more complex behaviours (Sansalone et al., 2020). The complexity of the brain and its evolution is calling for more complex comparative measures which are currently emerging.

Comparative measures and their caveats

To move further than the consideration of brain size, researchers have focused on the size of specific brain regions as described earlier but also on several other

innovative measures that we are going to describe briefly here. Brain organisation can be studied in terms of its gyral and sulcal patterns which interestingly have been shown to be associated with brain functions as well (Bodin et al., 2018; Lopez-Persem et al., 2019). Few studies have investigated the sulcal morphology in different species showing that they could provide insights into the evolution of frontal cortex organisation and superior temporal sulcus function (Leroy et al., 2015; Amiez et al., 2019).

Content of myelin has also been used as a comparative measure. It is thought that when brain size enlarged, the areas that used to be connected will be located further apart and to conserve the efficacy of information transport along the axons, they are insulated by a higher myelin content. This causes white matter to increase disproportionately with brain size (Barton, 2006; Herculano-Houzel et al., 2010). Myelin maps have been useful to compare brain anatomy between species because myelin amount is inversely correlated with intracortical circuits complexity (Glasser et al., 2014); therefore, brain regions can be mapped between species in terms of their processes (low myelin content would correspond to associative areas while high content would correspond to sensory areas) (Bryant et al., 2019; Eichert et al., 2020).

Concerning the comparison of connectivity, further measures can be used between species such as the structural connectivity through the study of major white matter tracts anatomy (Rilling et al., 2008; Thiebaut de Schotten et al., 2011a; Eichert et al., 2018; Barrett et al., 2020; Warrington et al., 2020) or the functional connectivity through the study of the resting-state activity patterns (Mars et al., 2013; Sallet et al., 2013; Vijayakumar et al., 2019). These methods can lead to the establishment of connectivity fingerprint which can be compared between species (Mars et al., 2018b). While they allow for the investigation of a large number of species, albeit using

sometime slightly modified version of the methods, these two connectivity measures still need to rely on some existing knowledge and are usually focused on specific areas of the brain. Their generalization into the investigation of the whole brain organisation is possible through connectome studies, mapping comprehensively the neural connection of a given brain. They can highlight differences in brain network architecture to infer evolutionary trajectory in terms of both brain regions organisation and white matter structures (Van Essen et al., 2013; Ardesch et al., 2019). The combination of different measures throughout the brain is important to fully understand connectivity changes since they could be due to a set of different causes from reorganisation of connection quantitatively and qualitatively to reorganisation of brain areas (Mars et al., 2018a, 2021). The investigation of whole brain network has led to studies looking at brain connectivity gradient throughout the brain from macroscopic to microscopic scale (Margulies et al., 2016; Paquola et al., 2019). These gradients constitute yet another measure comparable between species and can be related to functional relevance and microstructural characteristics (Margulies et al., 2016; Goulas et al., 2018; Blazquez Freches et al., 2020; Xu et al., 2020; Vos de Wael et al., 2021).

Interindividual variability

While all the previously mentioned principles and measures usually focus on comparing averaged values across a group of individuals belonging to one species, it is also important to consider the interindividual variability observed in the brain. Variability between individuals has been observed structurally, in the connectivity anatomy and in the sulcal morphology of the brain (Ochiai et al., 2004; Thiebaut de Schotten et al., 2011b; Amiez et al., 2019, 2021). Differences in sulcal morphology have been shown to have an influence on the functional organisation of the brain

(Amiez et al., 2013; Lopez-Persem et al., 2019). Variability also represents a driving force of evolution, as it allows new traits to emerge which can be selected by natural selection. This variability can be genetically mediated or a phenotypic adaptation to a particular environment (Krubitzer and Kaas, 2005). A relationship between variability and evolution has been previously reported, showing that areas that have more greatly expanded from the macaque brain to the human brain show greater variability; inversely areas that have evolved less recently would be more stable with less interindividual variability (Croxson et al., 2018). It is interesting to note that these recently evolved areas showing great variability correspond broadly to multimodal areas in both humans and macaques. However, one main difference in structural variability was observed between the two species and concerned the amount of hemispheric asymmetry in variability which was left-lateralized in humans (Croxson et al., 2018). Variability between individuals is therefore an important evolutionary driver that should be taken into account in comparative studies.

Overall, as new methods emerge to study brain evolution, they need to be generalized to more species and larger sample to build a more complete picture. While we have here detailed the measures that species can be compared on, it is important to consider the comparison methods as well, which we will detail later (see 6.2).

1.4.3. Primate brain evolution

Shared aspects of brain organisation

Comparative measures described previously assumes a certain degree of similarity in principles of brain organisation in order to compare them between species. All mammals present a layered neocortex and a common plan of cortical organisation

(Krubitzer and Kaas, 2005). This is particularly true for primates as we will try to highlight now. A first striking element concerns the relatively conserved shape of the brain across primate species with the particular emergence of the temporal lobe, considered different from other mammals' lateral expansion (Bryant and Preuss, 2018). Primates are overall characterised as having large brains but also a complex and elaborated visual system. Folding patterns have been related to white matter expansion as the number of axons increases the tension in the white matter which in turn causes cortical folding (Herculano-Houzel et al., 2010). This relation is thought to be conserved across primates but different from other mammals such as rodents (Ventura-Antunes et al., 2013).

Concerning cortical regions, it is suggested that the addition of new cortical association fields from eutherian mammals to primates constitute a hallmark of their difference and lead to an increase in connectivity (Krubitzer, 2009). General important principles of connectivity are also observable, not only across primates but across mammals in general. Two regions will be more likely to be connected if they are adjacent, they have a similar microstructural composition and they connect to similar other regions (Ercsey-Ravasz et al., 2013; Barbas, 2015; Horvát et al., 2016). The efficiency of communication between regions has been shown to be conserved across a large range of mammals, as possessing fewer interhemispheric connection is associated with better intra-hemispheric connectivity (Assaf et al., 2020). Further characterisations of brain connectivity have led to the idea that to minimize the cost associated with wiring the brain, networks are organised in rich-club. Rich club are communities of topologically close brain regions that serve specialized function and communicate highly through short range connections, while communication between rich club is

assured by a limited number of long-range connections (Bullmore and Sporns, 2012; van den Heuvel et al., 2016).

Primates, as being closely phylogenetically related, share common principles of brain organisation but they also demonstrate some differences that make each species different.

Elaborations down the primate evolutionary tree

Some elaborations have occurred during primate evolution, we will briefly describe here the most influential ones and we purposely leave out some considerations of the primate social brain evolution that will be tackled separately later (see 1.4.4). Although this is driven by the availability of the data, main differences in brain organisation between primates have been observed at particular points in the primate phylogenetic classification: at the separation between prosimians and simians, then at the emergence of the great apes and finally the emergence of the human genus. Prosimians and simians have diverged around 40 million years ago and one important brain difference between the two infraorders is thought to concern the further addition of association areas and their associated connectivity (Krubitzer, 2009). Particularly the parieto-frontal system has been suggested to be reinforced in simian primates, associated with complexification of their lifestyles and environment (Genovesio et al., 2014). Frontal areas of the brain have received further attention in terms of granular areas present. Granular areas are characterized by their enrichment in granular cells and while some of them are already present in prosimian primates as a primate specialization, further granular areas appeared in simians and are thought to allow them

to make better foraging choices in a more complex ecological and social environment (Passingham and Wise, 2012).

Studies on the prefrontal cortex, region usually associated with high-level cognitive processes, have also suggested that there was an enlargement of this part of the brain in great apes specifically (Semendeferi et al., 2002; Smaers et al., 2017). Another enlargement is visible in the great ape's temporal lobe with the emergence of additional gyri, the middle temporal gyrus and the fusiform gyrus (Bryant and Preuss, 2018). This localized expansion is thought to cause reorganisation of the area. For instance, the MT/V5 region, easily identifiable with its high myelin content, appears to relocate more ventrally in humans specifically, suggesting a further temporal expansion in humans compared to other apes (Glasser and Van Essen, 2011; Large et al., 2016; Bryant et al., 2019).

A lot of research has been dedicated to look for human specific characteristic of brain organisation, we will briefly summarize some of the accounts from this field. Further reinforcement of the connectivity between frontal and parietal regions has been observed in human brains compared to chimpanzee brains (Ardesch et al., 2019). Regarding brain properties, increased plasticity and asymmetry have been specifically associated with the human brain. Plasticity, describing the ability of the brain to be remodelled according to changes in the cognitive demands, is thought to have had an impact in shaping specific human behaviours for adaptation to the environment (Gómez-Robles and Sherwood, 2016). Asymmetry between the two hemispheres has now been observed in non-human primates as well but not as pronounced as humans indicating differential brain organisation that is thought to have participated to the emergence of human behaviour such as language (Gómez-Robles et al., 2013; Leroy et al., 2015; Hou et al., 2019).

This summary, by no means complete, is already suggesting recurrent patterns in the evolution of the primate brain and we will now enrich it with particular considerations of the social brain evolution.

1.4.4. The social brain in non-human primates

Homologies and observed differences

From the previous description of the anatomy of the human social brain (see 1.3.1-1.3.2), the areas implicated can be divided into three different anatomical categories: the frontal regions, the parietal regions, these two comprising regions on both lateral and medial part of the brain and finally the temporal regions. Homologs, in terms of connectivity, architectonic and overall organisation, of the human frontal brain areas, have been identified in the macaque brain (Mackey and Petrides, 2010; Sallet et al., 2013; Neubert et al., 2014, 2015). They are associated with similar functions (Wittmann et al., 2018). For instance, the macaque medial PFC is also associated with false-belief (Hayashi et al., 2020). Moreover, overall pattern of frontal connectivity to the rest of the brain seems to have been conserved from macaques to humans (e.g., the SLF, UNC and ATR) (Thiebaut De Schotten et al., 2012; Wilson et al., 2015; Folloni et al., 2019a; Rocchi et al., 2021). The nature of social interactions also seems to drive the connectivity between the frontal and temporal lobes in macaques (Sallet et al., 2011; Ainsworth et al., 2021). Still, slight differences were observed between humans' and macaques' frontal cortex. Human brains dedicate a greater proportion of white matter to frontal lobe connections with a particular increase between frontal regions and posterior auditory areas, compared to macaques, potentially pertaining to the human language ability (Kelly et al., 2010; Neubert et al., 2014; Barrett et al., 2020).

Similar observations have been made concerning the parietal cortex. Fundamental similarities have been observed in the parietal areas function, organisation and connectivity between humans and macaques (Margulies et al., 2009; Caspers et al., 2011; Mars et al., 2011; Caminiti et al., 2015; Borra and Luppino, 2017; Catani et al., 2017). The main difference pointed out concerns the connectivity of the central inferior parietal lobule (IPL) with the anterior PFC, which is more pronounced in humans possibly supporting some language and decision strategy computations (Caspers et al., 2011; Mars et al., 2011).

Due to morphological differences of the temporal lobe emerging in great apes, as mentioned previously (see 1.4.3), the comparison of temporal lobe organisation between humans and macaques has proven more difficult. Recent studies have compared chimpanzee and human temporal lobe revealing very similar white and grey matter networks (Mars et al., 2019) but also differences in terms of the connectivity to auditory core. The connectivity of the anterior temporal lobe to auditory regions appears to be a specific human characteristic while the general temporal connectivity to auditory core is more pronounced in chimpanzees and humans compared to the macaque (Bryant et al., 2019). These findings are in line with the connectivity differences observed from frontal and parietal cortices as well and could reflect the acquisition of more complex vocal communication in chimpanzees compared to macaques and the further complexity of human speech (Lameira, 2017).

Although the precise influence of the change in gyral anatomy has not been precisely studied, the temporal white matter system is assumed to be similar between macaques, chimpanzees, and humans, such as the anatomy of the ILF and UNC is generally considered conserved (Bryant and Preuss, 2018; Barrett et al., 2020; Bryant et al., 2020) but this will be further explored in chapter 3. More recently the IFOF, initially

thought to link frontal to occipital regions through the temporal lobe only in humans, has been recognised as having similar anatomy between a range of primate species (Mars et al., 2016a; Schaeffer et al., 2017; Decramer et al., 2018; Barrett et al., 2020; Bryant et al., 2020). However, one major tract, the AF, has been repeatedly shown to be different between humans and the other primate species. Its more pronounced invasion of the temporal lobe in humans and leftward asymmetry has put this tract forward as supporting some uniquely human language abilities (Rilling et al., 2008; Eichert et al., 2018, 2020).

We can note from this brief overview that a strong foundation for the human social brain is already present in macaques. Connectivity differences have been observed mainly regarding language related areas in humans. As the comparative anatomy of the temporal lobe appears more difficult and supporting larger differences, we will detail further the current state of the literature in this field.

Expansion and reorganisation: the case of the temporal lobe

We have already mentioned the case of the ventral relocation of area MT/V5 in humans compared to macaques (Glasser and Van Essen, 2011; Large et al., 2016; Bryant et al., 2019). Another well-documented reorganisation emerging in the temporal lobe concerns the face processing system (see Figure 1.3). The human face system is associated with several regions in the fusiform gyrus and with the posterior and anterior STS (see 1.3.1 and Figure 1.2), and a similar network has been observed in chimpanzees as well (Parr et al., 2009). However, the apparent lack of fusiform gyrus is macaques prevent straightforward homologies to be found (Bryant and Preuss, 2018). Instead, the main face processing areas in macaques are distributed along the STS (Tsao et al., 2003, 2008; Schwiedrzik et al., 2015; Bell et al., 2016; Liu et al., 2016). The face

network in the two species present some homologies in terms of overall spatial arrangement and selectivity to form parallel and hierarchical systems (Pinsk et al., 2009; Yovel and Freiwald, 2013; Pitcher and Ungerleider, 2021). In this framework, macaque face patches located in the dorsal bank and fundus of the STS could correspond to the human lateral face processing regions such as the posterior and anterior STS, while the macaque ventral bank face patches could correspond to the human ventral regions such as OFA and FFA (see Figure 1.3).

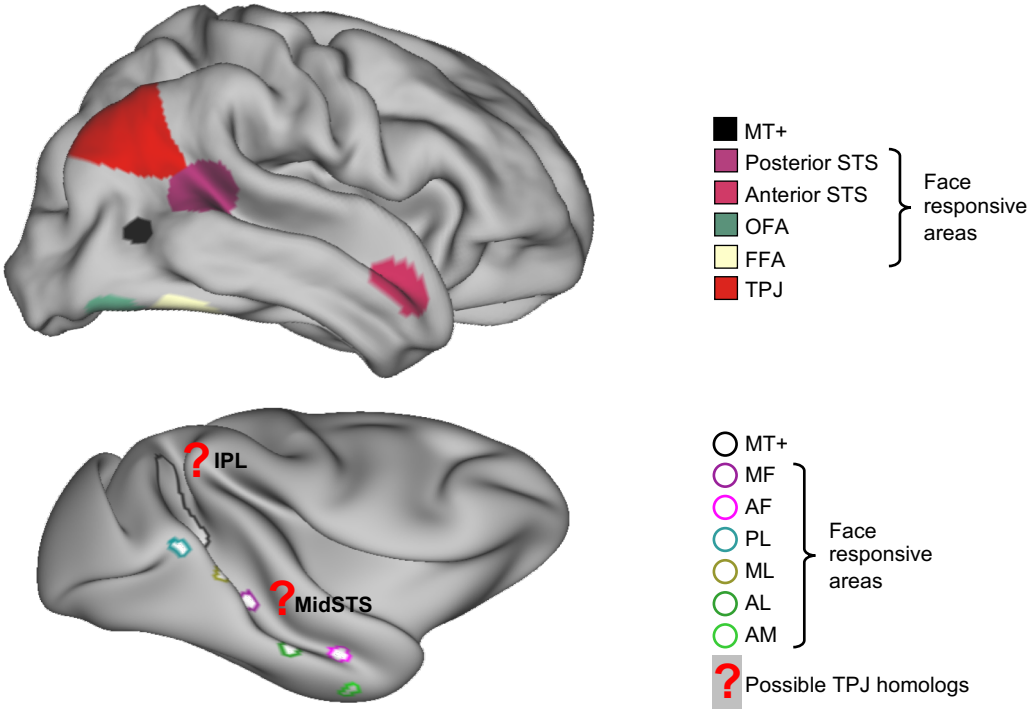

Figure 1.3 Evolutionary reorganisation of the temporal lobe

Temporal lobe areas in humans (top) and macaques (bottom) represented on their mid-thickness surface. MT+ is represented as a homologous area in both species and face responsive areas are represented in both species. TPJ is represented in humans and its suggested macaque homologs are represented in red question marks (IPL and midSTS). AF: Anterior Fundus; AL: Anterior Lateral; AM: Anterior Medial; FFA: Fusiform Face Area; IPL: Inferior Parietal Lobule; MF: Middle Fundus; midSTS: middle STS; ML: Middle Lateral; OFA: Occipital Face Area; PL: Posterior Lateral; STS: Superior Temporal Sulcus; TPJ: Temporo-Parietal-Junction.

A major issue in the research for homologies between macaques' and humans' temporal cortex comes from the case of the TPJ. Indeed, emerging from a high expansion area, the extent of this junction appears much broader in humans than in macaques, making a straightforward correspondence difficult (Hill et al., 2010; Patel et al., 2019; Vos de Wael et al., 2021). Combined with its implication in theory of mind abilities, it has been put forward as a likely candidate for a social region specific to humans. The IPL has been proposed as a possible TPJ equivalent in the macaque brain for several reasons (see Figure 1.3). It seems located in a similar location of the brain and is also included in the macaque default mode network (Vincent et al., 2007; Mantini et al., 2011). Functionally, it has been shown to be implicated in the processing of social interaction (Sliwa and Freiwald, 2017). The further expansion of TPJ and posterior STS in humans is thought to support a role as social cognitive processes hub for more complex social behaviours (Patel et al., 2019). However, the macaque IPL differs from the human TPJ in terms on connectivity to the rest of the brain. Instead, an area located in the macaque middle STS (midSTS, see Figure 1.3) shares strong similarities in terms of connectivity patterns with the human TPJ (Mars et al., 2013). This area has been associated in macaques with social hierarchy, network size and social strategy (Sallet et al., 2011; Noonan et al., 2014; Ong et al., 2020) and is thought to be part of a visual pathway specialized for social perception (Pitcher and Ungerleider, 2021). The evolutionary precursor of the human TPJ is therefore still debated and will be further investigated in chapter 2.

This account of the evolutionary trajectory of the social brain in primates is however quite incomplete. Indeed, most studies focus on comparing macaques and humans while they have separated from a common ancestor around 25 million years

ago. Furthermore, macaques, as anthropoids, are known to share extensive neuroanatomical similarities with humans while other primate species in different lineages are still understudied.

1.5. The developmental perspective

The observation of comparatively large brains in primate species brings developmental considerations to this research field. We will give a brief account of ontogeny in primates, starting with biological development, then psychological development, to finish by describing the relationship between development and evolution.

1.5.1. Principles of brain development

Early brain development

Very briefly, we want to introduce the basic principles and events behind brain development in humans, more details can be found in reviews on the topic (Stiles and Jernigan, 2010; Budday et al., 2015). Brain development is a long process, from embryonic stage to late adolescence and possibly throughout the lifespan of an individual. It depends on a variety of factors from molecular events such as gene expression to environmental input. It starts at the third gestational week with the differentiation of neural progenitor cells and their proliferation and migration to form the basic compartments of the nervous system by the end of the embryonic period (gestational week 8). These compartments correspond to what will later be referred to as the forebrain, the midbrain, the hindbrain, and the spinal cord. The further foetal development sees a dramatic growth of the nervous system and the formation of cortical and subcortical structures as well as the major white matter tracts when neurons began to make connections with each other.

The human brain continues to increase in size postnatally reaching 90% of adult age volume around the age of 6 and stabilizes at the end of adolescence (Courchesne et al., 2000). As the infant brain is not a down-scaled version of the adult brain, structural and functional changes in grey and white matter accompany the brain growth and are associated with changes in behaviour. The development is rapid during childhood, slower during adolescence and a plateau or reversal of developmental processes is observed during adulthood. An important principle for the scope of this thesis concerns the order of neurogenesis of brain region (Finlay and Darlington, 1995; Finlay et al., 2001). Indeed, as the later developing brain regions appear to become the most enlarged regions, the study of development and factors influencing it could greatly inform the reasons behind neuroanatomical features of different brains. Even more so because these late developing and enlarged regions encompass most of the association cortex in charge of the most complex social behaviour. By developing later, they are also more prone to endure impacts from the individual experience onto their developmental trajectory.

White matter developmental characteristics

Another major principle during brain development concerns the connectivity of the brain. It has been observed that the connectivity of the early post-natal brain is much more important than in adults. During the early development, a process called pruning is responsible for the selective loss of some projections throughout the brain in order to design a precise pattern of connectivity as seen in the adult brain (O'Leary, 1992; Innocenti and Price, 2005). This process is thought to confer flexibility and robustness to neuronal connections. It is accompanied by the process of myelination, which is the acquisition of myelin sheath around the axons acting as an electrically insulating layer.

White matter and grey matter volumes appear to be inversely correlated throughout development. While white matter volume steeply increases in the first part of life up to around 40 years old, it then decreases with age. Grey matter volume instead first decreases with age to stabilize after 40 years old (Bendlin et al., 2010; Lebel et al., 2012). White matter microstructural changes have also been observed throughout human brain development with different timelines associated with different white matter tracts (Lebel et al., 2012; Slater et al., 2019).

Comparison of developmental patterns in primates

Very few studies have so far compared developmental processes between different primate species. An inherent limitation being to establish corresponding developmental stages between species. Study of the macaque development is also complicated because the monkey brain matures quickly, and major developmental and myelination processes have already happened at birth. However, the trajectories of macaque brain development, including the relative volumetric growth and the white matter microstructure have been shown to follow a similar pattern than in human development with a fast developing pace in early development which slows down around adolescence and finally stabilize in adult (Knickmeyer et al., 2010; Shi et al., 2013; Kim et al., 2020).

The frontal cortex circuit maturation seems to share conserved features across humans and Old World primates, in terms of connectomic and transcriptomic data. The expansion of cortico-cortical pathways in this area is more important in primates than rodents (Charvet et al., 2021). However, differences have been observed in the timing of prefrontal connectivity maturation, while monkeys seem to demonstrate matured connectivity early on, chimpanzees and humans prefrontal connectivity maturation is

delayed but more rapid for humans than chimpanzees (Sakai et al., 2011). Recently, the engineering of *in vitro* cellular models called organoids has allowed us to investigate neuro-developmental processes in fine detail. For instance, brain expansion in humans seems to depend on the duration of a developmental transitional state controlled by a transcription factor which could explain differences in brain expansion with other great apes (Benito-Kwiecinski et al., 2021).

1.5.2. Development and ageing of social cognition

Social skills development

From infant mimicking facial expression (Meltzoff and Moore, 1983) to the adult theory of mind, the development of human social skills has attracted a lot of attention and debates over the years. It is not in the scope of this thesis to dwell into the complex field of developmental psychology, but we will try to provide here a brief account from chosen sources to demonstrate how the study of development can inform the study of social behaviour.

Developmental psychology always refers to two very influential theorists: Jean Piaget (1896-1980) and Lev Vygotsky (1896-1934). They mainly differ in the progressive construction of knowledge which is a more solitary and individual process for Piaget while Vygotsky argues that it is mainly driven by social interaction (Lourenço, 2012). This more social view has been used by others to justify some uniquely human social behaviour (as summarized in a recent book (Tomasello, 2019)). It is important to bear in mind that the development of social skills happens in parallel and in close interaction with the development of other executive functions and the development of language ability. It has been proposed that from a young age human infants develop a shared intentionality through joint attention, gaze following and

pointing behaviour. Around 3 to 4 years old, their communication skills improve, they are capable of collaboration and active social learning, they understand others perspective and therefore possess at least some theory of mind abilities. These abilities further develop so that around 6-7 years old, they acquire the ability of second order false belief and are able to coordinate multiple perspectives. Increased executive function and social complexity during adolescence has also put this period forward as very sensitive in the socio-cultural development of individuals (Blakemore and Mills, 2014).

Given this process of postnatal development, personal experience in the social domain will shape our social abilities and therefore our brain particularly at an early age (Atzil et al., 2018) and reorganisation of the social brain will continue in adolescence (Blakemore, 2010). Early infancy is a critical time for the wiring of the social brain as the quality of social interaction in infancy has been shown to predict later social abilities in life in humans as well as in non-human primates (Carpendale and Lewis, 2004; Stevens et al., 2009; Nelson and Guyer, 2011; Kaburu et al., 2016; Howell et al., 2019).

Ageing effect

On the other end of the developmental process lies ageing effects. Brain ageing has been associated with some macroscopic, microscopic, and molecular changes such as a decrease in brain volume and in number and size of neurons (Esiri, 2007; Chen et al., 2013). It is therefore expected that ageing would have an impact on the functioning of the brain. Concerning social skills, the impact of age has received mixed evidence. It is thought that there is a decline in social cognition with normal ageing, but it is not clear how much it depends on the general decline of cognitive and executive functions (Kemp et al., 2012; Rakoczy et al., 2012; Moran, 2013). As for developmental

processes, environmental factors such as social interactions are thought to influence this decline (Pearlman-Avnion et al., 2018). Regarding neurogenerative disorders associated with old age, Alzheimer's and Parkinson's diseases are associated with a general impairment of executive functions but not specifically social cognition (Brüne and Brüne-Cohrs, 2006; Kemp et al., 2012). Frontotemporal dementia has been associated with changes in executive functions, personality, and social behaviour with individuals particularly impaired in theory of mind tasks (Gregory et al., 2002; Neary et al., 2005). This observation is not so surprising considering the anatomical location of this disorder contingent with the social brain.

Overall, as they begin to associate the emergence of social skills and their associated brain structure, developmental studies can shed light on the ontogeny of the social brain.

1.5.3. Evo-Devo: how the study of development and evolution inform each other

Comparative developmental psychology

Any phenotypic traits, such as the ones described for social cognition, are products of development and evolution, and these two processes inform each other (Montgomery et al., 2016). Therefore, they are both useful in trying to understand the roots of human social cognition and the combination of developmental and comparative studies has been argued to be necessary to reach this goal (Maestripieri and Roney, 2006; Rosati et al., 2014; Nielsen and Haun, 2016). Few studies have compared developmental processes between different primate species.

Differences in development between species can be due to different mechanisms: a difference in the pace of cognitive development or a difference in the pattern (how the acquisition of certain traits can influence the acquisition of others) (Rosati et al., 2014). The social development of primates seems, at first sight, comparable, in terms of their social dependence at young age for instance. Most primates rely on close relatives early on for feeding, grooming and protection, relatives remain a secure source later on when they start exploring further (Stevens et al., 2009). However, differences in brain ontogeny between species have been suggested to account for the differences observed in social cognition between humans and other primates (Hare, 2011). One hypothesis concerns the length of the juvenile period which is longer in primates in general but even more so in humans and has been put forward as a possible mean for the acquisition of more complex skills (Kaplan et al., 2000). Although, in early infancy humans and chimpanzees seem to share a similar development, the pace accelerates in terms of social cognition in humans from around 1 year old, particularly in the acquisition of joint attention and goal understanding (Wobber et al., 2014). This difference in developmental pace is thought to be crucial for the acquisition of further competence and not only social ones. The evo-devo (evolutionary-development) field is therefore growing and receiving more interest as parallels between developmental and evolutionary processes are made (Raff, 2000). We should still remain careful to not overinterpret this theory, as development should not be considered are a short summary of evolution.

Example similarities between development and evolution processes

We provide a few examples of striking similarities between developmental and evolutionary processes that have influenced this thesis. First, concerning the expansion of the brain (Hill et al., 2010), the developmental pattern in humans suggest a

nonuniform expansion after birth which leads to greater expansion of frontal, parietal and lateral temporal cortices compared to the rest of the brain. In agreement with the previously mentioned order of neurogenesis, the expansion of these regions is associated with a late and slow maturation compared to the others. The evolutionary pattern of expansion observed from a macaque to a human brain is remarkably similar to this developmental pattern, so that regions that have expanded more recently in terms of evolutionary time seems to mature later in humans. It is interesting to note here that the regions at stake -frontal, parietal, lateral temporal- are high order association areas, also involved in social cognition (Rilling, 2006). Second, concerning the development of the white matter supporting human language function, it has been suggested that the AF, and particularly its temporal segment, is not mature at birth and its slow maturation during childhood coincides with the acquisition of better and more complex language abilities (Friederici, 2012). The study of the evolution of the AF have shown that its temporal segment, although present in human adult is very reduced in chimpanzees and not present at all in macaques (Rilling et al., 2008), as discussed in chapter 3 as well. This AF segment has therefore been suggested as a necessary component to the unique human language ability (Catani and Bambini, 2014).

Developmental and evolutionary processes together can provide a new framework to understand the differences in social cognitive abilities observed among primate's species.

1.6. The need for better methodological considerations

This introduction so far has already pointed out some of the main issues in comparative neuroscience that will be summarized here.

1.6.1. Investigating non-human primates

As animal research is constantly under scrutiny, we will highlight here some of its benefits and caveats as well as possible improvements.

Benefits

Animal research has always made up an important part of neuroscience research. Its propensity to perform experiments where the environment and life history of the individuals can be precisely controlled and where the same protocol is completely reproducible, has made it an important tool for behavioural study. Similarly, the possibility of using more invasive method or a combination of methods not necessarily available in humans, makes it an invaluable tool to study brain mechanisms. Although primate studies constitute a small part of all animal research (0.16% in Great Britain in 2019, source: UAR), their similarity to humans make them essential for neuroscience research. By being close phylogenetically to humans, they also share major biological and behavioural responses, which makes them prone to be good models for genetic, physiopathology, social behaviour, complex cognition, development, and ageing (Phillips et al., 2014). Because of these similarities, non-human primate research is more translational, advances made in understanding the normal and pathological function of the primate brain have led to the development of therapeutics for humans (Perretta, 2009; Friedman et al., 2017). Their use in neuroscience and social neuroscience more precisely has been supported by several researchers over the years (Isoda et al., 2018; Mitchell et al., 2018).

However, this similarity with humans also implies the need for important ethical considerations, which are consistently refined to take into account the welfare of the primates. Animal research has also been seen as a way to preserve endangered species from extinction. Indeed, from developing cure to animal diseases to helping in their

reproduction, animal research program can play a part in understanding better these endangered species, increase the awareness and participate in their conservation (Shaw et al., 2021).

Need for more species

It appeared clearly throughout the course of this introduction that only a few primate species are actually studied. This sparsity of the data means that there are important gaps in the primate evolutionary tree of studied species which lead to gaps in our understanding of primate evolution. The focus on macaque and human studies have implied that there is a single massive change between the two species without considering the possible steps that have led to these changes. As macaques and humans are old world monkeys, the restriction to these two species also lead to a lack of knowledge for other primates. Although studies on new world monkeys such as marmosets and squirrel monkeys are gaining interests (Royo et al., 2021), studies on prosimians are still very rare. These discrepancies in the species studied arise from ethical considerations (regulation on the use of great apes in research for instance) and practical considerations (some species cannot be kept in laboratories without major impairment to their welfare). New initiatives, such as the Primate Brain Bank (non-profit initiative at the Netherlands Institute for Neuroscience), are trying to cope with this knowledge gaps by collecting samples from deceased primates in zoos (Kaas and van Eden, 2011).

While we have highlighted the importance of the research models, it is also necessary to define a proper framework for the acquisition and analysis of comparative data.

1.6.2. The search for a unified approach

As discussed earlier (see 1.2.2), behavioural tests across species are tremendously hard to design and interpret but new protocols are emerging to test similar cognitive function in primates. We will discuss here methodological consideration regarding the study of the brain in different primate species.

MRI: promising methods for similar data acquisition

Magnetic Resonance Imaging (MRI) methods have been put forward as able to cope with both the need to investigate more species and to have similar methods across species for better comparison. Using the same method in a wide range of species allows to bridge the gap between microscopic methods mostly used in non-human animals and macroscopic methods mostly used in humans (Barron et al., 2021). MRI data can be used to study multiple aspects of the brain, from its structural aspect to functional responses and white matter organisation that can in turn be related to behaviour. Although neuro-imaging methods have a relatively poor spatial resolution compared to other methods, it allows for more species to be studied in a fast, repeatable, and multi-modal fashion (Friedrich et al., 2021). Recent advances in terms of data acquisition, elaboration of new analysis methods and collaborative effort (Milham et al., 2018), have also enabled better comparison between species (Mars et al., 2014).

We will now focus on one of these innovative analysis frameworks specifically useful for comparative neuroscience.

Defining a common space

Another methodological issue that has emerged throughout this introduction concerned the difficulty of comparing different brains (see 4.2). While brain expansion

is one element of difference between brains, expansion leads to reorganisation at multiple levels which can in turn suggest different hypotheses for the differences observed between two brains. It could suggest a regional expansion of an existing area, a differentiation or separation of a given area or a change in connectivity by creating or changing the existing connection (Mars et al., 2018a). Therefore, to understand what is really a unique feature of a given brain, it has been suggested to look for common organisation principle. This common space approach has been further characterised recently as a framework to compare brains meaningfully between species (Mars et al., 2021). Making use of large and multimodal data now available, it suggests that describing brains in terms of their shared features would allow one to investigate their organisational differences. Shared features allow to build abstract spaces that are reliably comparable across species because taking out dimensions for which the mapping between species is uncertain. Brain connectivity has been used previously to define a common space between different species. It is assumed that brain regions with similar function would retain similar connectivity across species, even if some reorganisation has occurred (Mars et al., 2016b, 2018b). Functional connectivity at rest can be used to establish fingerprints of connection between brain areas that can then be compared across species but only if prior knowledge of homology is already existing (Neubert et al., 2014, 2015; Balsters et al., 2020). White matter tracts can be used to represent the whole brain connectivity in terms of a common tracts space, called a blueprint, which can then be used to compare brain connectivity between species (Mars et al., 2018c). In this framework, several features can be combined to elaborate a coherent hypothesis of brain evolution in specific brain areas (Eichert et al., 2020).

Methods used throughout this thesis try to combine the previous observations: considering a wider range of species, using appropriate behavioural test and similar MRI data acquisition to make use of the common space approach.

1.7. Aims and methods of the thesis

The overarching goal of this thesis is to study the social brain organisation, function, and connectivity in different primate species to shed light onto the evolutionary roots of the human social brain. We first addressed the debated topic of theory of mind neural precursors in non-human primates. We designed a non-linguistic fMRI task for macaques based on the social prediction framework. Combined with other classical social tasks and a resting-state connectivity analysis, we pointed out similarities and differences between human and macaque social brain, in terms of computation and relation between different social processes.

The temporal lobe being the host of social function and a primate specialisation, we then focused more precisely on its connectivity and organisation across several primate species. Using unified tractography protocols, we established tract anatomy in the temporal lobe of macaques, gorillas, chimpanzees, and humans. We also built a common space to study cortical connectivity. By including great ape species, this study allowed us to capture the nature and order of changes in the temporal lobe white matter anatomy between macaques and humans.

We then extended the study of connectivity to other primate species to investigate organisational changes from early primates to macaques. Using recently developed methods for template and cortical surface elaboration, we were able to investigate the cortical anatomy and conduct tractography to establish white matter organisation in the ring-tailed lemur, squirrel monkey and rhesus macaque. This study

allowed us to characterise further temporal lobe connectivity modifications during primate evolution as well as posterior parietal and prefrontal elaboration.

Finally, we applied the same methods in a developmental framework, establishing age-related connectivity principles in the macaque brain. This study, one of the first investigating extensively both developmental and ageing effect on the macaque brain connectivity, provides foundations for further brain developmental studies linked with social parameters and genetics.

Chapter 2 - Identification of a precursor for Theory of Mind ability

Roumazeilles L, Schurz M, Lojkiewiez M, Verhagen L, Schüffelgen U, Marche K, Mahmoodi A, Emberton A, Simpson K, Joly O, Khamassi M, Rushworth MFS, Mars RB, Sallet J (2021) Social prediction modulates activity of macaque superior temporal cortex. *Sci. Adv* 7. DOI: 10.1126/sciadv.abh2392

2.1 Abstract

The ability to attribute thoughts to others, also called theory of mind (TOM), has been extensively studied in humans, however, its evolutionary origins have been challenged. Computationally, the basis of TOM has been interpreted within the predictive coding framework and associated with activity in the temporo-parietal junction (TPJ). Here, we revealed, using a non-linguistic task and functional magnetic resonance imaging, that activity in a region of the macaque middle superior temporal cortex was specifically modulated by the predictability of social situations. As in human TPJ, this region could be distinguished from other temporal regions involved in face processing. Our result suggests the existence of a precursor for the TOM ability in the last common ancestor of human and Old World monkeys.

2.2 Introduction

The ability to attribute mental representations to others, called Theory of Mind (TOM (Premack and Woodruff, 1978)) is key to complex human social interactions (Koster-Hale and Saxe, 2013; Heyes and Frith, 2014). While TOM's neural bases have been extensively studied in humans, the question of its evolutionary origins has been disputed since the concept was first introduced (Premack and Woodruff, 1978; Call and Tomasello, 2008; Heyes and Frith, 2014; Meunier, 2017).

Behavioural paradigms have been developed to specifically address the question of TOM ability in animals (Hare et al., 2000), but despite ingenious designs, the interpretation of performances on TOM-like tasks across primate species has been debated (Heyes and Frith, 2014; Drayton and Santos, 2016; Krupenye et al., 2016; Meunier, 2017). Difficulties in addressing the question of TOM in animal models are

partly due to the reliance of human TOM studies on linguistic stimuli (Schurz et al., 2014). Two recent studies have nevertheless attempted to solve this problem, by designing innovative nonverbal false-belief task, a canonical test in the study of TOM (Báez-Mendoza and Williams, 2020). They showed that great apes and even Japanese macaques were able to anticipate other agents' behaviours driven by false belief (Kano et al., 2019; Hayashi et al., 2020), suggesting the emergence of TOM abilities as ancient as the common ancestor of humans and Old World monkeys. Some authors, however, warn that such results should be considered cautiously (Horschler et al., 2020).

Brain networks supporting TOM abilities in humans have been most notably identified as the medial prefrontal cortex (MPFC) and the temporo-parietal junction (TPJ) (Behrens et al., 2009; Schurz et al., 2014). Both areas have been shown to undergo great expansion between the macaque and human brains (Hill et al., 2010), and the ensuing reorganization of the TPJ and posterior superior temporal sulcus (STS) between species is still unclear (Patel et al., 2019). However, MPFC has been shown to maintain a broadly similar anatomical organization in macaques and humans (Sallet et al., 2013). Furthermore, using functional connectivity, a middle STS (midSTS) area was shown to share similar connectivity patterns with the human TPJ (Mars et al., 2013). Evidence of shared neuroanatomical properties suggests that the macaque MPFC and midSTS could share similar functions with the human MPFC and TPJ (Passingham et al., 2002). In support of this hypothesis, both the MPFC and the midSTS have been associated with processing social information (Tsao et al., 2008; Ku et al., 2011; Sallet et al., 2011; Yoshida et al., 2012; Chang et al., 2013b; Marciniak et al., 2014; Popivanov et al., 2014; Sliwa and Freiwald, 2017; Ong et al., 2020) and complex social interactions (Yoshida et al., 2012; Haroush and Williams, 2015; Ong et al., 2020), although the question of TOM was not directly tested in these studies.

Theoretical developments in computational neuroscience propose an alternative method to compare human and animal social abilities. Rather than looking for TOM itself in other species, it may be profitable to seek evidence of more basic computational processes linked to TOM (Butterfill and Apperly, 2013; Schurz and Perner, 2015; Wittmann et al., 2018; Lockwood et al., 2020). Computational models describe human TPJ and MPFC activation during social tasks within a predictive coding framework (Behrens et al., 2008; Koster-Hale and Saxe, 2013). This framework predicts that deviations from expected social behaviours should lead to change of activity in these areas. It allowed us to design a non-linguistic task for functional magnetic resonance imaging (fMRI), to investigate the existence of neural architecture supporting the computation of TOM in macaques and its relationship to other social circuits.

2.3 Materials and methods

2.3.1. Data Acquisition

Animals

14 healthy rhesus macaque monkeys (*Macaca mulatta*, 13 males and 1 female) performed a set of free-watching tasks over a period of six months. All procedures were conducted under licenses from the United Kingdom (UK) Home Office in accordance with the UK Animals (Scientific Procedures) Act 1986. See Table 2.1 for a detailed account of the number of runs per condition and per monkey.

Monkey ID	Age (years)	Weight (kg)	Social prediction	Object prediction	Social animation	Faces	*Repli-cation* Social prediction	*Repli-cation* Object prediction
O1	13	12	10	-	11	13	-	-
O2	13	12	4	-	7	9	-	-
O3	13	12	9	-	6	13	-	-
P1	12	11	11	-	11	12	-	-
P2	12	11.5	8	-	9	9	-	-
P3	12	11.5	10	-	10	9	-	-
P4	12	11.5	10	-	13	11	-	-
S1*	9	7.5	8	8	11	10	-	-
T1	8	11.5	5	10	7	10	-	-
T2	8	14	10	10	11	9	6	6
T3	8	12	10	9	11	9	6	6
T4	8	13	8	11	9	10	6	6
U1	7	13	11	10	9	10	-	-
U2	7	11	10	8	12	11	-	-
V1	-	-	-	-	-	-	6	6
Total			124 (n=14)	66 (n=7)	137 (n=14)	145 (n=14)	24 (n =4)	24 (n=4)

*Female

Table 2.1 Detail of the monkeys and number of runs per subjects and per conditions selected for analysis.

Stimuli

Pictures and videos recorded at the breeding centre and at the Oxford research colony were the basis of the video clips used in four experimental conditions (https://git.fmrib.ox.ac.uk/rlea/macaque_social_prediction/tree/master/Stimuli). In addition, two other experimental conditions based on non-social stimuli were also used. Together, these six conditions and an awake resting-state acquisition (not included in this study) were presented in pseudo-randomized order. Four conditions described below have been used for the purpose of the current study (Figure 2.1). No more than three repetitions of a given condition were presented per day, the same condition was never repeated consecutively, and two different orders of presentation of the videos/pictures for a given condition were used to further limit habituation. For all conditions, the animals were not asked to fixate their gaze to conserve the most natural behaviour. No reward delivery occurred during the presentation of stimuli. Reward was instead delivered in between two runs to maintain animal attention to the stimuli. The videos were selected to represent real-life events of the monkeys' daily life. This means that the videos were not controlled for matching on some specific parameters (e.g., different types of social interaction). By introducing variety across videos for every single condition, we also reinforce the salience for the common attribute that defines each condition (e.g., the predictability of the social scenes).

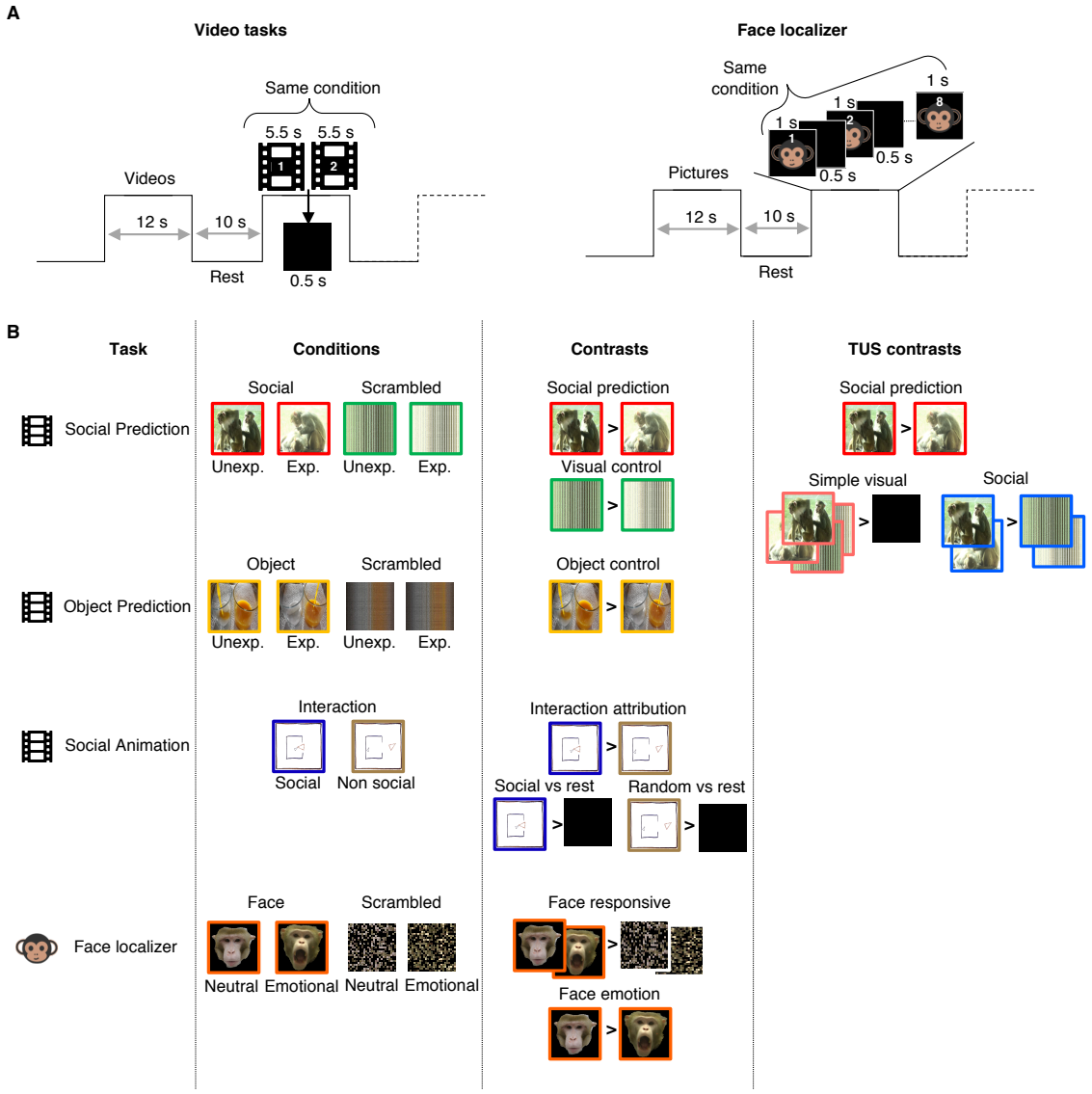

Figure 2.1 Summary of tasks used.

A. Schematic representing the timings for video-based tasks and the face localizer. Three blocks of each task are represented here. **B.** Details of the conditions and contrasts: an example frame for each condition is represented and they illustrate contrasts of interest for the study, as well as the control contrasts used after perturbation by Transcranial Ultrasound Stimulation (TUS). Unexp. stands for unexpected and Exp. for expected.

First, we selected videos containing expected (e.g., grooming or playing) and unexpected (e.g., unexpected deviation from grooming or playing) social behaviours that were highly ecologically valid for the monkeys. The videos were presented for 5.5 s each and were combined in a 12 s block with 0.5 s of black screen before each video.

Each block was followed by 10 s of rest (black screen). We presented three blocks of social unpredicted, three blocks of social predicted and three blocks for each of their scrambled versions respectively, in random order.

On the basis of a similar principle (deviation from expected situation), we created videos showing expected and unexpected object situation based on simple physical regularity. In keeping with the social videos, object scenes showed events that could be unpredicted based on either location (object appearing at an unexpected location), identity (a new object appears), or movement (sudden change in movement patterns shown up to now). For instance, a video in which objects are falling at constant rate is considered predictable, while an unpredictable scenario would see this rate suddenly changed without an obvious cause. The timings for these conditions were the same than for the social prediction. We presented three blocks of object unpredicted situations, three blocks of object predicted situations and three blocks for each of their scrambled version, respectively. This task was only done on 7 of the 14 monkeys.

For the social animation, we used stimuli from a previous study (Castelli et al., 2013) showing abstract geometric shape behaving either socially or randomly. The timings for the social animation task are the same as that for the social prediction. There were 6 blocks of social interaction and 6 blocks of non-social interaction, with each block followed by 10 s of rest (black screen).

For the face localizer, the task followed a block design with each block of 12 s consisting of the presentation of eight images for 1 s each followed by 500 ms of black screen. A resting period of 10 s (black screen) was inserted between the face blocks. Each run was composed of three blocks of neutral faces, three blocks of emotional faces (aggressive or lip-smacking) and six blocks of scrambled faces. This type of face localizer is known to capture face-responsive areas (Hadj-Bouziane et al., 2008).

Awake fMRI

The fMRI data were acquired in a horizontal 3 Tesla MRI scanner with a full-size bore using a four-channel, phased-array, receive-only radio-frequency coil in conjunction with a local transmission coil (Windmiller Kolster Inc, Fresno, USA). The animals were head-fixed in a sphinx position in an MRI-compatible chair (Rogue Research, CA). fMRI data were acquired using a gradient-echo T2* echo planar imaging (EPI) sequence with the following parameters: 1.5 × 1.5 × 1.5 mm resolution, 36 axial interleaved slices with no gap, TR of 2280 ms, TE of 30 ms and 130 volumes per run. Proton density weighted images using a gradient-refocused echo (GRE) sequence (TR = 10 ms, TE = 2.52 ms) were acquired as reference for offline image reconstruction.

Anaesthetized fMRI

Resting-state fMRI data and anatomical scans were collected under anaesthesia for the same animals according to a previously used protocol (Sallet et al., 2013). fMRI resting-state connectivity patterns are well conserved under anaesthesia (Vincent et al., 2007) and have been used for conducting human-macaque comparisons (Vincent et al., 2007; Mars et al., 2013; Sallet et al., 2013). Anaesthesia was induced using intramuscular injection of ketamine (10 mg/kg) combined with either xylazine (0.125 to 0.25 mg/kg) or midazolam (0.1 mg/kg) and buprenorphine (0.01 mg/kg). Macaques also received injections of atropine (0.05 mg/kg), meloxicam (0.2 mg/kg), and ranitidine (0.05 mg/kg). Anaesthesia was maintained with isoflurane. Isoflurane was selected because it has been demonstrated that resting-state networks are still present using this agent for anaesthesia (Vincent et al., 2007). The anesthetized animals were placed in an MRI-compatible stereotactic frame (Crist Instrument) in a sphinx position within a

horizontal 3 T MRI scanner with a full-size bore. The same coils as for awake scans were used for data acquisition. Whole-brain blood-oxygen-level dependent (BOLD) fMRI data were collected using the following parameters: 1.5 × 1.5 × 1.5 mm resolution, TR of 2280 ms, TE of 30 ms, 36 axial interleaved slices with no gap and 1600 volumes. Structural scans were acquired in the same session using a T1-weighted MP-rage sequence (no slice gap, 0.5 × 0.5 × 0.5 mm resolution, TR of 2500 ms, TE of 4.01 ms and 128 slices).

2.3.2. Preprocessing

All data were preprocessed and analysed using tools from the FMRIB Software Library (FSL, version 5.0.10) (Jenkinson et al., 2012), the Advanced Normalization Tools (ANTs, version 2.1.0) and the Connectome workbench software (www.humanconnectome.org). We also used Matlab (version R2016a, The MathWorks, Inc., Natick, Massachusetts, United States) and bash codes from the Magnetic Resonance Comparative Anatomy toolbox (MrCat, www.neuroecologylab.org) and custom-made codes.

Task-fMRI preprocessing

Task-fMRI data were preprocessed following a dedicated nonhuman primate fMRI processing pipeline as part of the MrCat toolbox. In short, after offline SENSE reconstruction of the EPI image (Windmiller Kolster Scientific, USA), motion-induced time-varying slice distortions were corrected using restricted nonlinear registration, first to a run-specific high-fidelity EPI, then to each animal's T1w structural image, and finally to group-specific template in CARET macaque F99 space (Van Essen and Dierker, 2007). Brain extraction, bias correction, and template registration of the T1-

weighted structural image were achieved in an interdependent iterative approach. The resultant high-fidelity removal of nonbrain tissue could be back-projected to the EPI following nonlinear registration. A nuisance regressor design matrix was created to account for volumes with excessive movement, signal variability associated with motion-induced distortion artifacts and nonbrain noise components. For the video tasks, we did not use the regressors for the nonbrain component, as they were correlated with the timing of the task. Further steps were implemented using the FEAT toolbox. We performed spatial smoothing using a Gaussian of 3 mm FWHM (full width at half minimum) kernel, grand mean intensity normalization and high-pass temporal filtering (Gaussian-weighted least-squares straight-line fitting, with sigma = 100 s).

To assess for a proper coverage of the brain by the coils, we calculated the temporal signal to noise ratio (tSNR) associated with our data. For each session of the social prediction study, we obtained the mean intensity of the preprocessed time series, divided by the standard deviation of the intensities at each voxel, and averaged these images across sessions (Figure 2.2). The result demonstrated a good coverage of the brain and particularly the frontal cortex, which is usually known for its poor tSNR.

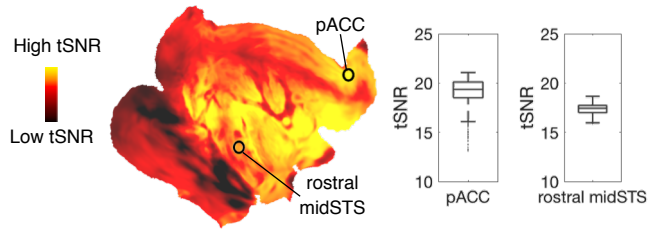

Figure 2.2 Temporal signal to noise ratio.

Flat map representing the right hemisphere tSNR calculated across all sessions of the social prediction task and box plot of tSNR in two regions of interest: the pACC and the rostral midSTS. On each box, the central mark indicates the median, and the bottom and top edges of the box indicate the 25th and 75th percentiles, respectively. The whiskers extend to the most extreme data points not considered outliers. Outliers are represented with dots. midSTS: middle superior temporal sulcus; pACC: perigenual anterior cingulate cortex; tSNR: temporal signal to noise ratio.

Resting-state fMRI preprocessing

The detailed preprocessing pipeline for the resting-state fMRI has been described elsewhere (Folloni et al., 2019b; Verhagen et al., 2019). Briefly, after reorientation to the same convention for all functional EPI datasets, the first volumes were discarded to ensure a steady radio frequency excitation state. EPI timeseries were motion-corrected using *MCFLIRT* (Jenkinson et al., 2002). Brain extraction, bias correction, and registration were achieved for the functional EPI datasets in an interdependent iterative manner. The mean of each functional dataset was registered to its corresponding T1w image using rigid-body boundary-based registration (*FLIRT* (Jenkinson and Smith, 2001; Jenkinson et al., 2002)). EPI signal noise was reduced in both the frequency and temporal domain. The functional timeseries were high-pass filtered with a frequency cut-off at 2000 s. Temporally cyclical noise, for example, originating from the respiration apparatus, was removed using band-stop filters set dynamically to noise peaks in the frequency domain of the first three principal components of the timeseries. To account for remaining global signal confounds, we considered the signal timeseries in white matter and meningeal compartments, and their confound parameters were regressed out of the BOLD signal for each voxel. Following this confound cleaning step, the timeseries were low-pass filtered with a cutoff at 10 s. The data were transformed to the surface space using the F99 template and spatially smoothed using a 2.8 mm FWHM gaussian kernel, while considering the folding of the cortex. Last, the data timeseries were demeaned to prepare for functional connectivity analyses.

2.3.3. Analysis

Contrasts

For the awake fMRI, the first-level analysis was carried out using FEAT for each run (Woolrich et al., 2001, 2004). Simple generalized linear model (GLM) designs were defined. For the social prediction task, we used four explanatory variables (EVs), accounting for the social expected scene, social unexpected scene, and one for each of their scrambled versions. The main contrast of interest was between social unpredicted versus social predicted. We defined one more contrast as the scrambled unpredicted versus scrambled predicted to control for activity related to visual features (e.g., motion and luminance). We used a similar approach for the object prediction. For the social animation task, we used two EVs representing the social and random conditions. The main contrast was defined as social versus random. We also defined two more contrasts as social animation versus rest and random animation versus rest to further investigate both conditions. For the face task, four EVs were used to account respectively for the neutral face blocks, the emotional face blocks, the neutral scrambled blocks, and the emotional scrambled blocks. The main contrasts were defined as face images versus scrambled images and emotional faces versus neutral faces.

In each task, on top of the main contrasts, we defined a control contrast to detect neural activation when an image or video was present on the screen compared to rest period to confirm whether the monkeys were engaged during the task. Indeed, as the task did not provide reward to the animals, they could disengage and fall asleep. We therefore excluded runs in which this control contrast elicited no or limited activation in the visual cortex. This method excluded 5 runs for the social prediction task and 3 runs for the object prediction task.

We applied a gamma hemodynamic response function convolution with a phase of 0 s, a standard deviation of 1.5 s and a delay of 3 s and the same temporal filtering as for the data. The movement regressors previously described were also used as additional confounds.

In the second-level analysis, after registration to standard space, we pooled together runs from the same monkeys. A fixed-effect analysis was performed at the subject level. Finally, a third-level analysis was carried out to obtain the results at the group level using FLAME 1 as mixed-effects analysis with a cluster-forming z-threshold of 3.1 and corrected for family-wise error (FWE) at $p<0.05$. The z-thresholds were chosen according to previous literature (Eklund et al., 2016), which advises using the threshold of 3.1 with Flame 1 mixed-effect to avoid false positives. To test for a potential overlap of object prediction with social prediction, we used a more liberal threshold at $z=2.3$. In fact, when no complete overlap is expected, as here, this approach increases the sensitivity of the test, allowing more stringent inferences.

Conjunction

We verified the specificity of the modulation by the social prediction videos by performing a series of conjunction analysis at the group level. All conjunctions are performed according to previous literature (Nichols et al., 2005). We defined an STS mask comprising the grey matter of the STS excluding the very posterior parietal portion to restrict the conjunction and set the cluster-forming threshold at $z=3.1$ and $p<0.05$. For the conjunction between object prediction and social prediction we used only the same seven animals available in both datasets. Because no significant conjunction was found between the object and social prediction at the $z>3.1$ threshold,

we lowered the threshold to 2.3, as above, to increase the sensitivity and account for the smaller number of animals in this condition.

Comparison of mean uncorrected z-statistic

To further confirm that this result was not due to a thresholding effect, we conducted additional analyses. We defined a region of interest (ROI) around the coordinates found in an anterior study (Mars et al., 2013) (most similar connectivity profile to human TPJ) with a 5-voxel radius. First, we computed the mean uncorrected z-statistic across voxels in this ROI for our three conditions (social prediction, visual control, and object control). The standard deviation is defined as the square root of the variance of the z-statistic. We performed a Wilcoxon signed-rank test between conditions and corrected for multiple comparison using the Bonferroni method. Second, we performed the same third-level contrasts as before but restricting the statistics to the rostral midSTS ROI as defined before. Because the extent of this ROI is quite small, we performed both cluster- and voxel-thresholding corrections.

Hemispheric and regional specificity

We also investigated the hemispheric specificity of the social prediction modulation by analysing the same contrast with an ROI either on the left or on the right hemisphere as performed in the literature (Chau et al., 2015). The ROI was defined as a coronal mask (5 slices) encompassing the whole STS at the level of the small ROI mentioned earlier, around the coordinates found in the anterior study (Mars et al., 2013). This ROI was defined to overcome the issue of thresholding by reducing the number of voxels and to enlarge the search area so that we could capture clusters even if they were overlapping the borders of the small ROI (accounting for interindividual differences).

The MPFC has also been identified as part of the social brain in macaques (Sallet et al., 2011). Therefore, we conducted another ROI analysis targeting the Anterior Cingulate Cortex (ACC) to restrict the statistics to this previously identified region (Sallet et al., 2011). No activity modulation of the ACC by the social prediction was revealed with this analysis.

Resting-data fMRI analysis

For the anaesthetized resting-data fMRI, in each monkey individually, we identified bilateral face patches from peak activation at the second-level analysis and based on the definitions of a previous study (Tsao et al., 2008). We obtained the middle fundus (MF) and middle lateral (ML) in all monkeys, the anterior lateral (AL), the anterior fundus (AF) and the anterior medial (AM) in 13 monkeys and the posterior lateral (PL) in 12 monkeys. When the face patch was present on only one hemisphere, we defined the opposite hemisphere face patch as its symmetric voxels. We carried on the analysis on the 12 monkeys where we could find all the face patches in at least one hemisphere. Each face patch location was mapped to surface space and an ROI was made of a circle of 2 mm geodesic distance, giving all ROIs the same size. We followed the same procedure for the social prediction area (SPA) and defined an anterior SPA ROI that was part of the same cluster but could be found in all monkeys, ensuring that we cover the entirety of the modulation location. We extracted the time series of each of these ROIs (six for face patches and two for social prediction) and computed their correlation with timeseries of the whole brain. We also performed a partial correlation where we regressed out the mean time series of all face patches from the SPA and the time series of the SPA from the face patches to obtain their specific connectivity. We then computed the correlation of these more specific time series to the whole brain. We

therefore obtained two maps describing how each ROI connects to the rest of the brain for each monkey using both full correlation and partial correlation. We merged all monkeys for each seed and performed a nonparametric permutation inference using PALM (Winkler et al., 2014) and performing the maximum number of permutations (in this case, sign flipping for a one-sample t test). Clusters were defined with the threshold-free cluster enhancement (TFCE) method, which enhances the cluster-like structures but keeps the voxel dimension of the data and were corrected for multiple comparison using the FWE method.

For visualization, some of the results were projected onto the F99 surface using tools from the HCP workbench and the inflated surfaces from a published study (Van Essen et al., 2017).

2.3.4. Human data

For the face task, we used the Neurosynth platform (Created and maintained by Tal Yarkoni, supported by NIH award R01MH096906) for automated meta-analysis that we probed with the word ‘faces’. The resulting meta-analysis map from 864 studies was then z-stats thresholded at 2.3 and projected onto a standard MNI surface. The map is corrected using a false discovery rate (FDR) approach, with an expected FDR of 0.01.

For the resting-state human study, data were provided by the Human Connectome Project, WU-Minn Consortium (Principal Investigators: David Van Essen and Kamil Ugurbil; 1U54MH091657) funded by the 16 NIH Institutes and Centers that support the NIH Blueprint for Neuroscience Research; and by the McDonnell Center for Systems Neuroscience at Washington University. We specifically used the group-average structural and functional MRI data from the HCP S1200 data release (March

2017). This dataset, available on-line at www.humanconnectome.org, allowed us to access task-related data but also resting-state connectivity network and atlases. The connectivity of TPJ was obtained from an ROI of 2 mm geodesic distance around the TPJ coordinates defined as in a previous study (Mars et al., 2012b).

2.3.5. Replication and transcranial ultrasound stimulation

One year after the first acquisition batch, we were able to acquire additional data for four animals (T2, T3, T4 and an additional monkey V1). Therefore, we conducted a replication study using 6 sessions for each of the conditions per animal (social prediction: 24 sessions, visual control: 24 sessions and object control: 24 sessions). An additional animal was excluded because of the high level of head movement. We followed the exact same procedure, except for some technical acquisition and analysis details that we describe here. Data were collected with a 3 T MRI scanner with a full size bore, and we used the four-channel, phased-array, receive-only radio-frequency coil in conjunction with a local transmission coil (Windmiller Kolster Inc, Fresno, USA). We used the exact same acquisition protocol. Concerning the analysis, we restrained our analysis to two levels because of the limited amount of data and because this is the most commonly used approach when having the same number of sessions for each animal. At threshold level 3.1, we did not obtain any significant result, but this was expected considering the lower amount of data. Therefore, we lowered the threshold to 2.3 and performed the same conjunction analysis and calculated the mean uncorrected z-statistic across voxels in this ROI as in the initial study.

We performed Transcranial Ultrasound Stimulation (TUS) on the same macaques used for the replication just before the fMRI free-viewing task, to assess whether the Frontal Eye Field (FEF), through its attentional or oculomotor activity,

could explain the modulation by social prediction in the SPA. Indeed, the FEF is involved in attention and oculomotor movement such as saccades (Deffieux et al., 2013; Pouget et al., 2020), its activity at rest is correlated with STS activity (Hutchison et al., 2012; Sallet et al., 2013), and was also revealed in our social prediction analysis. As a control region, we stimulated the ACC, which is involved in the extended social brain. The impact of TUS on FEF and ACC and their consequence on behaviour have already been demonstrated (Deffieux et al., 2013; Folloni et al., 2019b; Fouragnan et al., 2019; Pouget et al., 2020). We also collected control data for which no stimulation was performed (note that these are the data used in the replication). For these three stimulation conditions, we acquired 6 runs per monkey per condition (social prediction, visual control, and object control). Control days were interleaved with TUS sonication days. TUS was performed using the same protocol as previously published (Fouragnan et al., 2019; Khalighinejad et al., 2020), adapting the focal depth of the transducer to the desired coordinates. A sequential stimulation was performed to target the left and right FEF (Khalighinejad et al., 2020). A unique stimulation was performed on the midline for achieving a bilateral ACC stimulation (Fouragnan et al., 2019).

Briefly, a single-element ultrasound transducer was used for 40s. It was positioned with the help of the Brainsight neuronavigation system (Rogue Research) so that the focal spot was centred on the targeted brain region, namely the FEF on the anterior bank of the arcuate sulcus (left FEF MNI coordinates +/-Standard Deviation (SD): x = -14.4+/-0.9, y = 4.9+/-2.5, z = 13.3+/-1.4; right FEF: x = 15+/-1.2, y = 4.2+/-1.6, z = 11.8+/-1.5) and the controlled region: the ACC rostral to the genu of the corpus callosum (MNI coordinates +/-SD : x = 0 +/- 0.9, y = 15.5 +/- 1.5, z = 6.5 +/- 1.0). The ultrasound wave frequency was set to the 250 kHz resonance frequency and 30 ms bursts of ultrasound were generated every 100 ms (duty cycle 30%) with a digital

function generator (Handyscope HS5, TiePie engineering, Sneek, the Netherlands). Overall, the stimulation lasted for 40 s. A 75 W amplifier (75A250A, Amplifier Research, Souderton, PA) was used to deliver the required power to the transducer. A TiePie probe (Handyscope HS5, TiePie engineering, Sneek, The Netherlands) connected to an oscilloscope was used to monitor the voltage delivered. Note that one FEF session for one animal was conducted with a higher intensity and longer duration (60% duty cycle instead of 30% for 60s instead of 40s) which resulted in a localized skin trauma. The recorded peak-to-peak voltage was constant throughout the stimulation session. Voltage values per session ranged from 128 to 136 V and corresponded to a peak negative pressure ranging from 1.15 to 1.29 MPa, respectively, as measured in water with an in-house heterodyne interferometer (Constans et al., 2017). On the basis of a mean 66% transmission through the skull (Wattiez et al., 2017), the estimated peak negative pressures applied were between 0.75 and 0.85 MPa at the target in the brain.

fMRI data acquisition, preprocessing and analysis were performed as described for the replication. To compare control condition contrasts with stimulation condition contrasts, we performed a two-sample paired t test, regressing out the mean of each subject so that it would not interfere with the estimation of the difference between stimulation conditions. To assess that the stimulations had any effect, we compared a simple visual contrast (videos versus black screen) and a social contrast (social videos versus scrambled). Having established that stimulations did change some of the brain task-related modulation, we compared the contrast of interest: the social prediction. We used a whole brain analysis and an ROI analysis. This ROI combined the left and right ROI defined for the hemispheric analysis, resulting in a coronal mask encompassing the whole STS bilaterally at the level of the small ROI mentioned earlier. This ROI was defined to overcome the issue of thresholding and inter-individual difference.

2.4 Results

2.4.1. Macaques' midSTS is modulated by social expectation

To investigate whether macaque brain areas signal deviation from social expectation, we presented 14 rhesus macaques with a free-viewing fMRI paradigm consisting of videoclips of macaques interacting socially. This approach has been successfully used to identify brain networks supporting social cognition in macaques (Sliwa and Freiwald, 2017) but has not yet been used to identify computations supported in those circuits. In our videos, social situations either followed an expected scenario (e.g., continuous grooming or playing) or were interrupted by an unexpected event (e.g., grooming or playing interrupted by a fight). Several brain areas showed higher activation for the unexpected than expected social events, including regions belonging to the visual cortex and oculomotor-related regions (Figure 2.3A, Table 2.2). Two clusters in the midSTS were also identified, which we will refer to as caudal midSTS and rostral midSTS (Figure 2.3B, Table 2.2). The rostral midSTS has often been associated with the macaque social brain (Sallet et al., 2011; Mars et al., 2013; Kilintari et al., 2014).

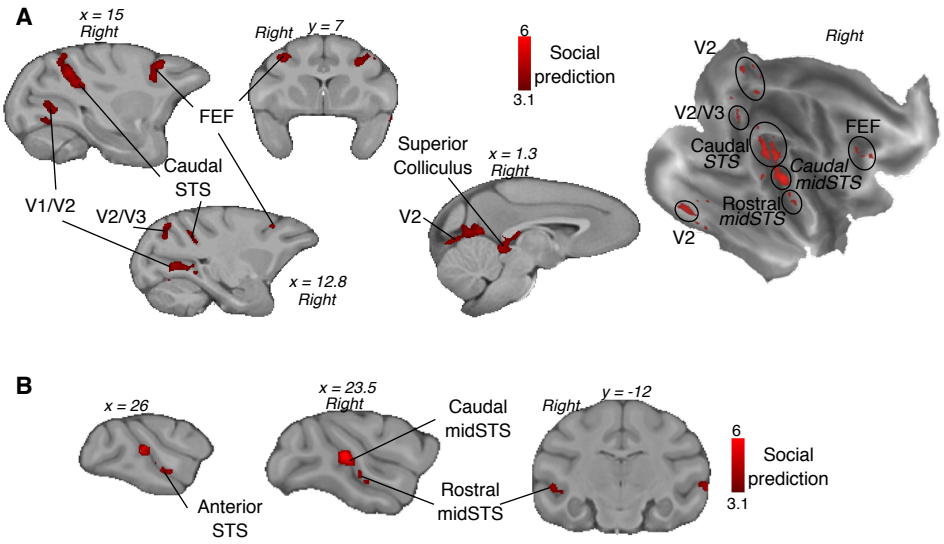

Figure 2.3 Social prediction contrast.

A. Group contrast of unexpected versus expected social situation revealed activity in FEF, Superior Colliculus, Visual area V1/V2 and Visual area V2/V3 (extending into V4) as seen on F99 slices (left) and flat map (right) (n=14, cluster-corrected at $z>3.1$, $p<0.05$ FWE corrected). **B.** Group contrast of unexpected versus expected social situation also revealed activity in rostral and caudal midSTS (n=14, cluster-corrected at $z>3.1$, $p<0.05$ FWE corrected). FEF: frontal eye field; FWE: family-wise error; STS: superior temporal cortex.

To rule out explanations in terms of basic visual features, we first contrasted the neural response to scrambled videos of unexpected versus expected social situations, which were matched in terms of luminosity and movement to the original videos (visual control). The visual control contrast elicited higher activation in the caudal midSTS but not in the more rostral part of the midSTS (Figure 2.4AC, Table 2.2). Unexpected social situation videos contain, by definition, more unexpected movement and therefore, it is expected that this visual control would recruit regions in caudal midSTS that include the motion-sensitive areas: middle temporal (MT), fundus of the superior temporal visual area (FST) and medial superior temporal area (MST) (Nelissen et al., 2006; Kilintari et al., 2014).

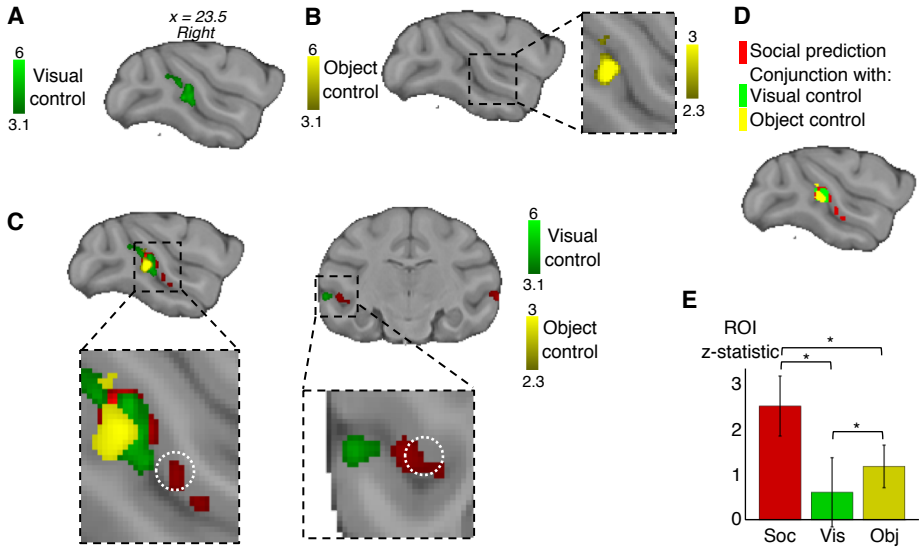

Figure 2.4 Control conditions.

A. Visual control: group contrast of unexpected versus expected scrambled social scenes revealed activity in caudal midSTS only (n=14, cluster-corrected at z>3.1, p<0.05 FWE corrected). **B.** Non-social prediction (object) control: group contrast of unexpected versus expected object scenes revealed no activity (n=7, cluster-corrected at z>3.1 and p<0.05 FWE corrected). At lower threshold (insert), the contrast revealed activity in caudal midSTS only (cluster-corrected at z>2.3, p<0.05 FWE corrected). **C.** Overlap between responses to social prediction and control conditions (visual control: n=14, cluster-corrected at z>3.1; object control: n=7, cluster-corrected at z>2.3 and both p<0.05 FWE corrected). The white dotted circle represents a macaque TPJ-like region identified previously (Mars et al., 2013). **D.** Conjunction results between the social prediction contrast and the control contrasts (cluster-corrected at z>3.1 for visual feature control and at z>2.3 for object control, p<0.05 FWE corrected). **E.** Mean Z-statistic obtained in the ROI (white circle in C) for social prediction (soc), visual control (vis), and object control (obj). Error bars represent standard deviation (Wilcoxon signed-rank test, Bonferroni corrected for multiple comparison p<0.05, social × visual: p=6.10-43, social × object: p=3.10-43, object × visual: p<1.10-21). FWE: family-wise error; ROI: region of interest.

We then tested the social specificity of the modulation of activity observed for social prediction in a subset of subjects (n=7/14, object control) using non-social scenes containing inanimate objects. To match closely with the social situation videos, these videos were designed to represent situations with or without a departure from an expected and established physical regularity, such as the location, identity, or movement. Regardless of whether we examined activity at the original threshold (z>3.1) or at a more liberal threshold (z>2.3) to account for the smaller number of

animals, there was no evidence for activity in rostral midSTS but only in caudal midSTS for this object control (Figure 2.4BC, Table 2.2). A conjunction analysis between the social prediction contrast and each of our two control conditions (Figure 2.4D) confirmed the specificity of the modulation of activity by social predictability in rostral midSTS cluster.

	Social prediction			**Visual control**			**Object control**		
	x	**y**	**z**	**x**	**y**	**z**	**x**	**y**	**z**
midSTS rostral	24.6	-11.6	-2.5						
midSTS caudal	22.6	-16.6	3.02	22.1	-17.1	1.51	23.1	-17.1	1.01
FEF	15.1	7.04	16.6						
V2/V3	8.05	-37.2	18.1						
V1 lateral	13.6	-33.2	1.01						
V2 medial	1.51	-31.2	6.54						
Superior colliculus	2.52	-20.1	1.51						

Table 2.2 Peak activation coordinates of social prediction and controls at the group level.

Coordinates given for the right hemisphere in mm in F99 standard space (Social prediction and visual control: n=14, cluster-corrected at $z>3.1$ and $p<0.05$ FWE corrected, object control: n=7, cluster-corrected at $z>2.3$ and $p<0.05$ FWE corrected). FEF: frontal-eye field; FWE: family-wise error; midSTS: middle superior temporal sulcus.

From here on, we will refer to this specific rostral midSTS region as 'social prediction area' (SPA). It overlaps with cytoarchitectonically defined temporo-parieto-occipital association area (TPO), and PG associated area of STS (PGa) (Reveley et al.,

2017). From this location, we can also rule out an overlap with body-responsive areas that have been identified either posteriorly or ventrally to the SPA (Popivanov et al., 2014; Sliwa and Freiwald, 2017). It has also recently been shown that strategic social signalling in the rostral midSTS involves a different set of neurons than the ones responding to faces and bodies (Ong et al., 2020). Importantly, the rostral midSTS that we identified corresponds to a midSTS region previously identified for its connectivity pattern most resembling that of human TPJ (Mars et al., 2013). In this independently defined region of interest (ROI), we observed that social prediction induced significantly higher activation than control conditions (Figure 2.4E).

To confirm that the social prediction modulation in the SPA was not due to a thresholding effect and illustrate the specificity of its activity, we performed the three contrasts (social prediction, visual control, and object control) using the same independent ROI identified previously (Mars et al., 2013) to restrict the statistics. We observed a significant activation in the ROI only in the social prediction contrast and not the two others with a cluster correction (Figure 2.5, top). Because the extent of this ROI is quite small, we also performed voxel correction which showed again the specificity of activation in this region for the social prediction contrast (181 voxels significant out of the 257 voxels of the ROI) and only a few voxels for the other two on the posterior edge of the ROI (12 for the visual control and 3 for the object control, Figure 2.5, bottom).

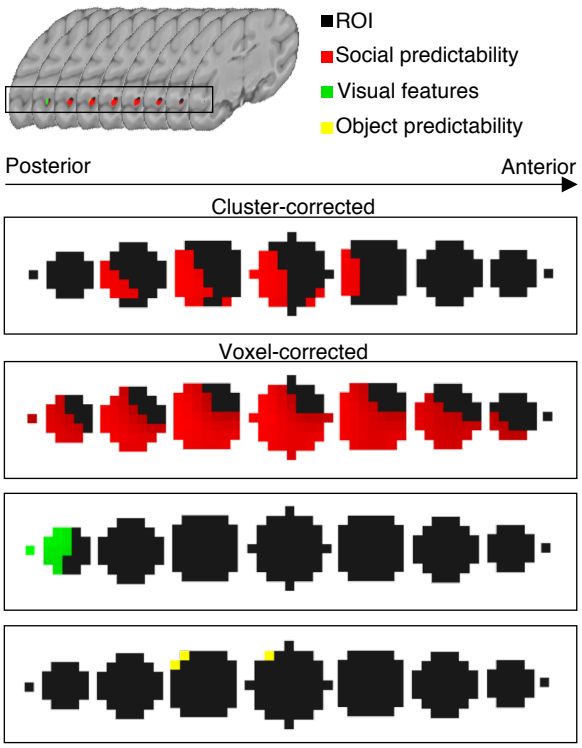

Figure 2.5 ROI analysis cluster and voxel corrected.

Representation of the midSTS ROI from previous study (Mars et al., 2013), from posterior to anterior coronal slices. When cluster-corrected ($z>3.1$) only the social prediction contrast was significant. When voxel-corrected ($p<0.05$), a few voxels in the two other controls were significant. ROI: region of interest.

While we observed midSTS clusters bilaterally, some hemispheric differences were noticeable. The right caudal midSTS cluster, unlike the left caudal midSTS, extended toward the end of the STS, including V4t on its ventral bank (Reveley et al., 2017). On the left hemisphere, the rostral midSTS cluster was located in a different area than the right SPA and had a more lateral position, extending from the dorsal bank of the STS to area TE on the lateral surface. To investigate whether the lack of social prediction modulation in the left SPA was indicative of a thresholding issue or a lateralized function, we defined a large ROI encompassing the whole STS around the coordinates of the previously mentioned midSTS region sharing neuroanatomical similarities with the human TPJ (Mars et al., 2013). With the same social prediction contrast but restricted on either the left or right hemisphere of this enlarged ROI, we

found that a cluster survives the statistical correction in both hemispheres. Rather than a purely lateralized function, these results show that the modulation by social prediction in the SPA was bilateral but less robust in the left hemisphere (Figure 2.6).

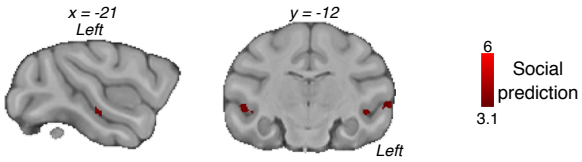

Figure 2.6 Hemispheric analysis.

Group contrast of unexpected versus expected social situation restricted on a rostral midSTS ROI revealed activity in the rostral midSTS on the left hemisphere (n=14, cluster-corrected at $z>3.1$, $p<0.05$ FWE corrected). FWE: family-wise error; midSTS: middle superior temporal sulcus.

2.4.2. MidSTS modulation is robust to replication and disruption of oculomotor/attentional system

Finally, we conducted a separate free-viewing experiment with a different set of four monkeys. Our first goal was to test for the robustness of the social prediction modulation in SPA in a replication study. Our second goal was to determine the impact of a disruption of the frontal eye field (FEF) on the computation performed by SPA. The FEF is usually associated with the attentional system and connectivity at rest between the FEF and the STS has been reported (Hutchison et al., 2012; Sallet et al., 2013). Because of the activity observed in the FEF in our social prediction contrast, we were concerned that a top-down attentional signal could mediate the modulation of activity observed in the SPA. Due to the passive nature of the task, it was not possible to causally and directly address the role of the midSTS. Instead, we used repetitive transcranial ultrasound stimulation (TUS) protocol to disturb brain activity over key

regions of interests, for at least two hours after stimulation (Verhagen et al., 2019), to check for potential confounding effects.

We used the sessions without previous stimulation as a replication of the social prediction study, revealing the same rostral midSTS region as specifically modulated by social prediction (Figure 2.7A, Table 2.3). In the replication, the visual and object control contrasts did not yield any significant results in rostral midSTS and there was no conjunction with the social prediction contrast (Figure 2.7BCD).

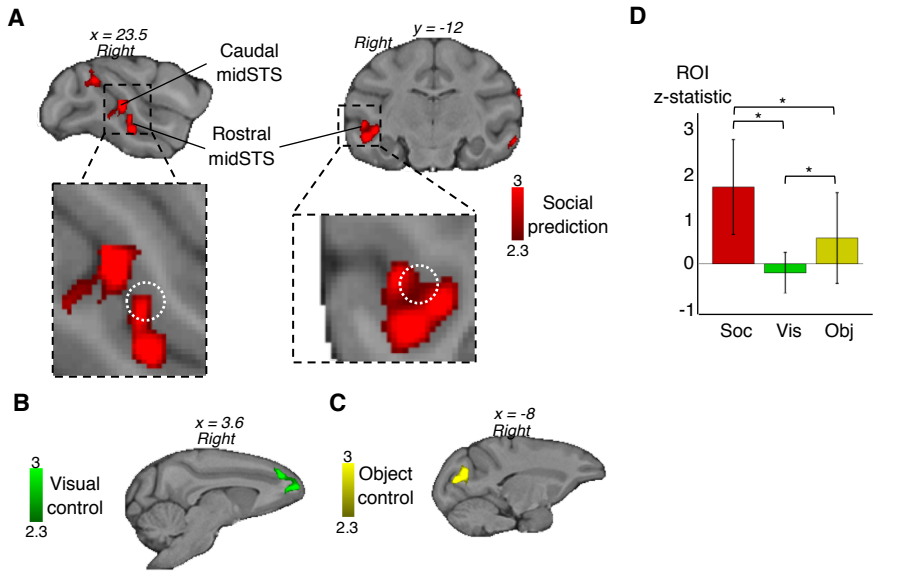

Figure 2.7 Replication of the modulation of macaque STS activity.

A. Social prediction: group contrast of unexpected versus expected social situation revealed activity in rostral and caudal midSTS (n=4, cluster-corrected at $z>2.3$, $p<0.05$ FWE corrected). Inserts show the white dotted circle representing a macaque TPJ-like region identified previously (Mars et al., 2013). **B.** Visual control: group contrast of unexpected versus expected scrambled social (n=4, cluster-corrected at $z>2.3$, $p<0.05$ FWE corrected). **C.** Non-social prediction (object) control: group contrast of unexpected versus expected object scenes (n=4, cluster-corrected at $z>2.3$ and $p<0.05$ FWE corrected). **D.** Mean Z-statistic obtained in the ROI (white circle) for social prediction (soc), visual control (vis), object control (obj). Error bars represent standard deviation (Wilcoxon signed-rank test, Bonferroni corrected for multiple comparison $p<0.05$). FWE: family-wise error; midSTS: middle superior temporal sulcus; ROI: region of interest.

	Social prediction		
	x	y	z
midSTS rostral	21	-12.6	-4.9
midSTS caudal	20.1	-20.6	4.02
FEF	-18.1	7.04	20.1
Parietal area PG	10.6	-37.2	19..6
aSTS	-28.2	-10.1	-8.05

Table 2.3 Peak activation coordinates of social prediction at the group level for the replication study.

Coordinates given in mm in F99 standard space (n=4, cluster-corrected at z>2.3 and p<0.05 FWE corrected). FEF: frontal-eye field; FWE: family-wise error; a/midSTS: anterior/middle superior temporal sulcus.

In both the original and replicated studies, we observed a cluster just anterior to the genu of the arcuate sulcus, an oculomotor region often referred to as the FEF. To rule out a putative attentional or oculomotor confound with the social prediction modulation, we used, before the awake fMRI data acquisition, a repetitive TUS of the FEF. In separate sessions the anterior cingulate cortex (ACC), a region known for its role in social cognition (Sallet et al., 2011; Chang et al., 2013b; Sliwa and Freiwald, 2017), was targeted as an active control region. The efficacy of the stimulations was revealed by causal perturbation of activity in distant brain regions observed in two relevant contrasts: a simple visual contrast (videos versus black screen) and a social contrast (social videos versus scrambled) (Figure 2.8ABC). However, in our contrast of interest - the social prediction - no difference between stimulation and non-stimulation sessions could be observed (Figure 2.8D). These results show that SPA was modulated by the predictability of social situation, independently of attentional or oculomotor

effect led by the FEF. They confirmed the social specificity of the activity modulation in the SPA.

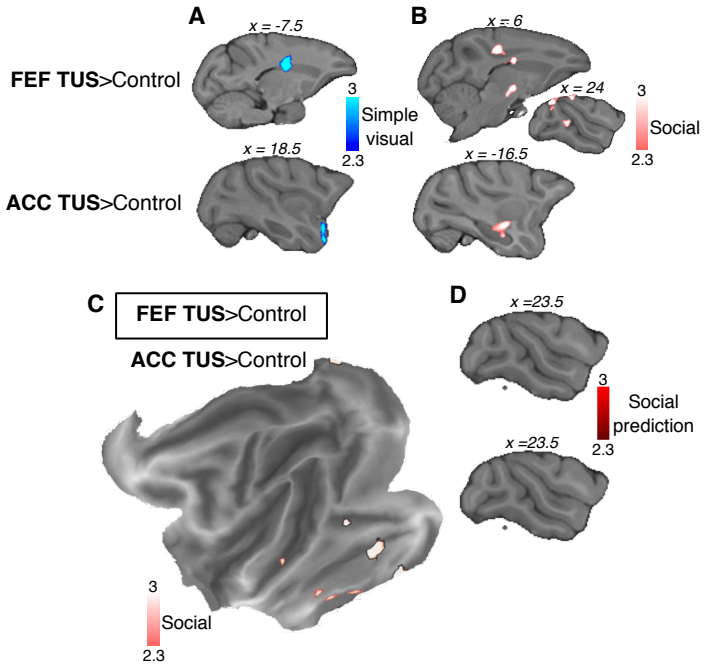

Figure 2.8 Effect of ultrasound stimulation.

A. Simple visual: two-sample paired t-test for higher activation in FEF stimulation condition (top) or ACC (bottom) compared to control for the group contrast of videos versus black screen (n=4, cluster-corrected at $z>2.3$, $p<0.05$ FWE corrected). **B.** Social: two-sample paired t-test for higher activation in FEF stimulation condition (top) or ACC (bottom) compared to control for the group contrast of social videos versus scrambled videos (n=4, cluster-corrected at $z>2.3$, $p<0.05$ FWE corrected). **C.** Two-sample paired t-test for higher activation in FEF stimulation condition (black-outline) or ACC (no outline) compared to control for the group contrast of social videos versus scrambled videos represented on a flat map (n=4, cluster-corrected at $z>2.3$, $p<0.05$ FWE corrected). **D.** Social prediction contrast: two-sample paired t-test for higher activation in FEF stimulation condition or ACC compared to control for the group contrast of unexpected versus expected social situation (n=4, cluster-corrected at $z>2.3$, $p<0.05$ FWE corrected, nothing significant). ACC: anterior cingulate cortex; FEF: frontal eye field; FWE: family-wise error.

2.4.3. Attribution of mental states to geometric shapes

We also presented animals with a non-linguistic task used to study TOM in humans that is relying on animation of geometric shape acting either socially or

randomly (Castelli et al., 2013). Although this task has been criticized as not being a proper TOM task (Schurz et al., 2020), discriminating between social and random interactions of the abstract shapes has been associated with modulation of activity in the vicinity of the TPJ and posterior STS in humans (Castelli et al., 2013). In macaques, contrasting activity between the two types of videos did not reveal different brain activity in SPA. Contrasting each video type with rest blocks revealed that modulations of activity for both social and random interactions were located in visual areas, confirming that macaques were looking at the videos but did so similarly for both (Figure 2.9).

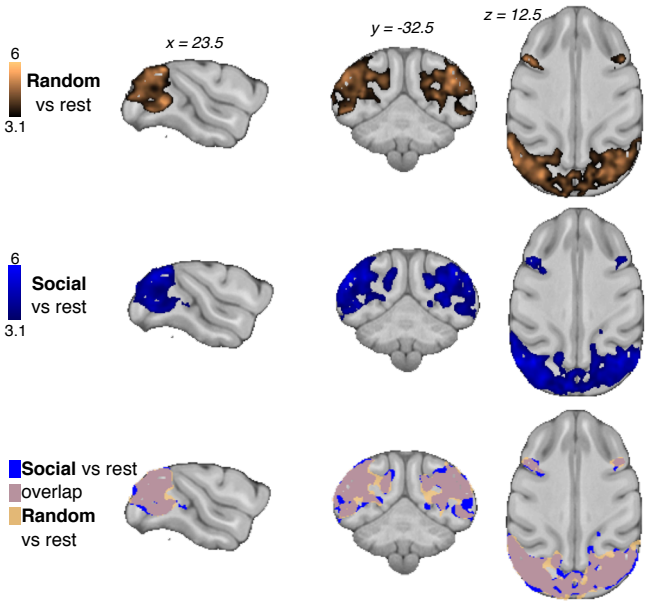

Figure 2.9 Social animation.

Group contrast of abstract shape videos versus rest blocks when acting either randomly (copper) or socially (blue) and their overlap (n=14, cluster-corrected at z>3.1, p<0.05 FWE corrected). FWE: family-wise error.

2.4.4. Relationship of SPA with the face-responsive brain network

To further test the specificity of SPA responses and their relationship with known STS functions, we investigated how SPA is related to face patches, a set of face-

responsive areas located in STS and inferotemporal cortex (Tsao et al., 2008). We analysed awake fMRI data from a face localizer collected in our initial group of 14 rhesus macaques. Our localizer consisted of pictures of neutral and emotional (e.g., lip-smacking, open mouth…) macaque faces and their scrambled equivalent during fMRI. This method has been shown to identify the face-responsive brain regions as opposed to the face-selective brain regions by using a localizer combining face, body, and object pictures (Hadj-Bouziane et al., 2008). In 12 of 14 animals, we were able to identify all six face patches previously reported (Tsao et al., 2008; Arcaro et al., 2020): posterior lateral (PL), middle lateral (ML), middle fundus (MF), anterior lateral (AL), anterior fundus (AF) and anterior medial (AM) (Figure 2.10A, Table 2.4).

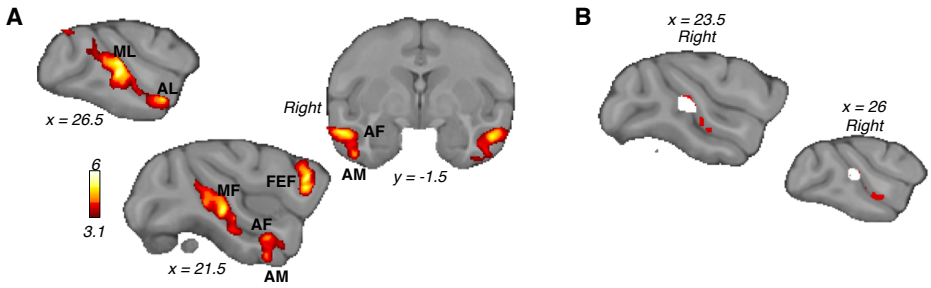

Figure 2.10 Face-responsive areas in macaques.

A. Macaque group contrast of face versus scrambled pictures (n=14, cluster-corrected at $z>3.1$, $p<0.05$ FWE corrected). **B.** Conjunction analysis (white) of social prediction contrast activation (red) and face patches (cluster-corrected at $z>3.1$, $p<0.05$ FWE corrected). AF: anterior fundus; AL: anterior lateral; AM: anterior medial; FEF: frontal eye field; FWE: family-wise error; MF: middle lateral; MF: middle fundus.

	Right			Left		
	x	**y**	**z**	**x**	**y**	**z**
AM	22.1	-1.5	-16.3	-20.5	-0.7	-14.7
AF	22.6	-2	-10.1	-20.5	-5.2	-9.8
AL	24.6	-0.9	-9.5	-22.5	-1.17	-10.8
MF	25.2	-15.6	-0.5	-22.0	-14.6	-4.6
ML	30.7	-16.1	4.5	-27.6	-17.2	2.5
FEF	21.1	10.6	8.6	-21.1	10.6	6.54

Table 2.4 Peak activation coordinates of the face localizer at the group level.

Coordinates given for the right and left hemisphere in mm in F99 standard space (n=14, cluster-corrected at $z>3.1$ and $p<0.05$ FWE corrected). AF: anterior fundus; AL: anterior lateral; AM: anterior medial; FEF: frontal eye field; FWE: family-wise error; MF: middle lateral; MF: middle fundus.

A conjunction analysis revealed no significant overlap between face patches and SPA (Figure 2.10B). At the single-subject level, we noticed that SPA peaks tended to be located in a more dorsal/fundus section of midSTS, and therefore, in a distinct cytoarchitectonic area compared to face patches (Figure 2.11). Our results are supported by recent findings showing that neurons in the ventral bank of the midSTS signal selectively cooperative social behaviour, independently of visual sensitivity to faces and bodies (Ong et al., 2020).

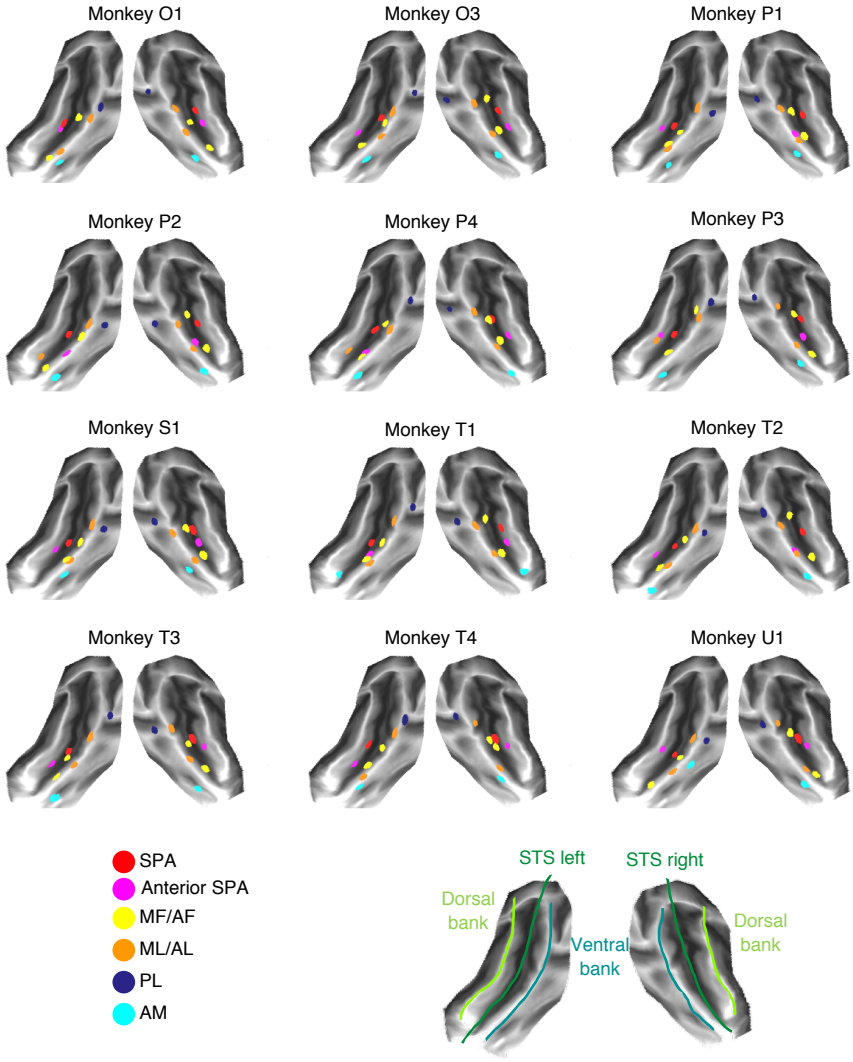

Figure 2.11 Peak activities for individual macaques.

Peak activity for the SPA and for the face patches represented on a flat F99 surface showing the STS with its dorsal and ventral bank. AF: anterior fundus; AL: anterior lateral; AM: anterior medial; FEF: frontal eye field; MF: middle lateral; MF: middle fundus; PL: posterior lateral; SPA: social prediction area; STS: superior temporal sulcus.

We then conducted a resting-state fMRI analysis to determine the relationship between the SPA and the face patches. We computed the functional connectivity profiles of macaques' SPA with both full correlation as available in humans and a more specific partial correlation. The full correlation revealed that macaques' SPA connectivity profile comprised face responsive regions and other visual areas (Figure

2.12A) but these were absent for human TPJ connectivity profile (coordinates from (Mars et al., 2013), HCP resting-state data (Van Essen et al., 2013), Figure 2.12B). However, computing the partial connectivity, by regressing out the time series of all face patches, reveals that SPA is specifically coupled with dorsal STS, posterior cingulate and prefrontal cortex, resembling the human TPJ connectivity profile (Figure 2.12C). Similarly, computing the partial connectivity of the face patches, by regressing out the time series of the SPA (and its anterior section) revealed a network involving mostly STS and the visual cortex (Figure 2.12C). In summary, connectivity results not only provide further evidence for the distinction of face patch and SPA systems but also reveal stronger interactions between the two systems in macaques than in humans.

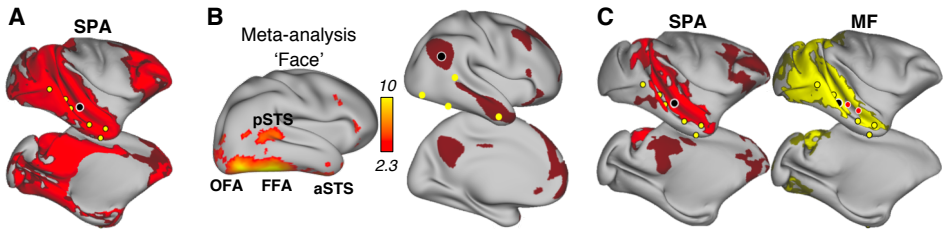

Figure 2.12 Face-patch system and resting-state functional connectivity in macaques and humans.

A. Resting-state connectivity associated with SPA (black circle) from a full correlation to the whole brain (face patches are yellow circles). **B.** Human comparison. Left: meta-analysis results (Neurosynth) for 'face', displayed on right hemisphere. Right: resting-state connectivity of TPJ (Cohen's d effect size thresholded at 0.6). **C.** Resting-state connectivity associated with SPA (black circle) from a partial correlation to the whole brain while accounting for face patches connectivity (left, red). Resting-state connectivity associated with MF (black circle) from a partial correlation to the whole brain while accounting for SPA connectivity (right, yellow, SPA and its anterior section are red circles). For all macaque resting state: n=12, TFCE corrected, FWE corrected at $p<0.01$ in bright colour and $0.01<p<0.05$ in dark colour. FFA: fusiform face area; FWE: family-wise error; MF: middle fundus; OFA: occipital face area; a/pSTS: anterior/posterior superior temporal sulcus; SPA: social prediction area; TFCE: threshold-free cluster enhancement; TPJ: temporo-parietal junction.

2.5 Discussion

Overall, our results revealed a brain region in macaques' rostral midSTS that is specifically sensitive to expectation violation during free viewing of social scenes. Its location on the dorsal bank/fundus of the STS is compatible with a functional module identified as being responsive to natural social scenes (Fisher and Freiwald, 2015) and strategic cooperation (Ong et al., 2020) but is distinct from previously identified modules associated with face patches, gaze following, or body patches (Tsao et al., 2008; Marciniak et al., 2014; Popivanov et al., 2014; Arcaro et al., 2020). Here, we were able to characterize a computational property associated with this region. We interpret this response in a predictive coding framework providing the signature of the neurocomputational mechanism supporting mentalizing abilities in humans (Koster-Hale and Saxe, 2013). Evidence for this type of coding has been uncovered in adjacent regions of the temporal cortex for processing non-social information in macaques (Bell et al., 2016). Furthermore, the midSTS region sensitive to prediction in the social domain corresponds to the region that was previously shown to share similar connectivity profiles with the human TPJ (Mars et al., 2013). Unlike in human studies (Behrens et al., 2009; Schurz et al., 2014), our social prediction analysis did not reveal any change of activity in macaque MPFC. This may reflect the nature of the passive free-viewing tasks compared to the active decision-making tasks used in humans (Behrens et al., 2008; Wittmann et al., 2016).

Our results suggest an evolutionary trajectory in brain organization that in humans has resulted in area TPJ. The connectivity of face-responsive areas and the SPA differs in both humans and rhesus macaques, but the two circuits are more integrated in macaques; macaque SPA retains connectivity to face patches, while human TPJ shares little connectivity with the face-responsive system. On one hand, the stronger

independence between TPJ and the visual system in humans might enable TOM computations to be applied to abstract information. On the other hand, midSTS interactions with the visual system in macaques might reflect stronger dependencies of TOM-related computations on visuo-social information. This constraint might explain why macaques did not distinguish between socially and randomly interacting abstract shape as previously observed (Schafroth et al., 2021) despite their abilities for face pareidolia (Taubert et al., 2017). These between-species differences might reflect greater specialization of TPJ in humans that may have occurred in association with the expansion and reorganization (Patel et al., 2019) of the temporal cortex in the hominid evolution.

Limitations and future studies

The debate around TOM and its evolutionary origins is a delicate one to tackle because of many hurdles faced in the design of tests and their interpretations. Our study, using a free-viewing paradigm, was designed in the computational framework of predictive coding rather than in the classical false-belief framework. Both approaches have been shown to recruit the mentalizing system in humans (Schurz et al., 2020). As only one female was used here, future studies should seek to balance the ratio of male and female subjects. Although the same social prediction modulation in SPA was observed in males and in this female subject, possible sex differences cannot be ruled out. The videos for the free-viewing paradigm, were selected to represent natural life events and therefore contain inherent variability in the context around the condition tested, such as the number of monkeys involved or the type of behaviour. Nevertheless, this variability allows us to associate the modulation of activity in the SPA with the computation of social prediction in any social situation and rule out the possibility that

it is specific to a type of behaviour. Future studies could build on our approach by distinguishing the predictability of social agents interacting with other social agents or with non-social items.

Conclusion

Altogether our approach, built on theoretical debates about cross-species differences in TOM (Butterfill and Apperly, 2013; Heyes and Frith, 2014; Meunier, 2017), provides new evidence for the existence in the last common ancestor to humans and macaques of a precursor neural architecture supporting computations associated with TOM in human TPJ (Figure 2.13) (Butterfill and Apperly, 2013).

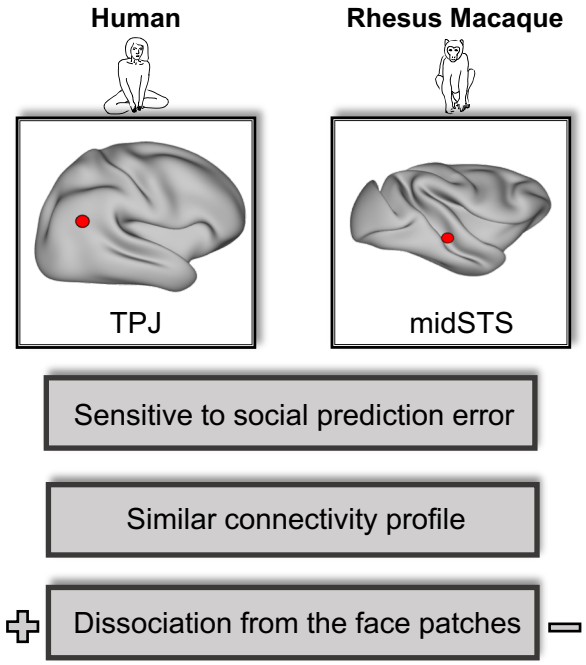

Figure 2.13 Summary figure.

MidSTS: middle superior temporal sulcus; TPJ: temporo-parietal junction.

Chapter 3 - White matter architecture and the organisation of the temporal cortex in primates

Parts of this chapter were published in the following manuscript.

Roumazeilles L, Eichert N, Bryant KL, Folloni D, Sallet J, Vijayakumar S, Foxley S, Tendler BC, Jbabdi S, Reveley C, Verhagen L, Dershowitz LB, Guthrie M, Flach E, Miller KL, Mars RB (2020) Longitudinal connections and the organization of the temporal cortex in macaques, great apes, and humans. *PLOS Biol* 18:e3000810. DOI: 10.1371/journal.pbio.3000810

3.1. Abstract

The temporal association cortex is considered a primate specialization and is involved in complex behaviours, with some, such as language, particularly characteristic of humans. The emergence of these behaviours has been linked to major differences in temporal lobe white matter in humans compared with monkeys. It is unknown, however, how the organization of the temporal lobe differs across several anthropoid primates. Therefore, we systematically compared the organization of the major temporal lobe white matter tracts in the human, gorilla, and chimpanzee great apes and in the macaque monkey. We show that humans and great apes, in particular the chimpanzee, exhibit an expanded and more complex occipital–temporal white matter system; additionally, in humans, the invasion of dorsal tracts into the temporal lobe provides a further specialization. We demonstrate the reorganization of different tracts along the primate evolutionary tree, including distinctive connectivity of human temporal grey matter.

3.2. Introduction

Understanding the organization and function of the brain requires an appreciation of its phylogenetic context. In the study of primate brain evolution, the temporal lobe is of particular interest. Indeed, the temporal cortex as found in Primates is thought to be unique to this order and distinct from expansions of the lateral brain surface seen in Proboscidea, Cetacea, and Carnivora (Bryant and Preuss, 2018). Within the Primate order, the external morphology of the temporal lobe differs substantially, ranging from nearly lissencephalic, possessing only the Sylvian fissure, to highly gyrified with multiple longitudinal sulci in great apes (Bryant and Preuss, 2018). Functionally, the temporal association cortex is involved in some of the most high-level behaviours of primates, including categorization and conceptual

processing (Miller et al., 2003; Lambon Ralph et al., 2010), social cognition (Sallet et al., 2011; Schurz et al., 2014), and in the human semantic processing for language (Price, 2000). However, how the internal organization of the temporal lobe differs across species and how this relates to their different behavioural repertoires remains unknown.

To reliably investigate the organization of the temporal cortex in different species, one must first be able to identify precisely how one brain relates to the other. Most comparative studies used to focus only on generic measures, such as whole brain size, but brains can differ in many aspects of their organization (Mars et al., 2018a; Smaers and Vanier, 2019; Eichert et al., 2020). Ideally, one would create maps of brain organization of a large range of species that can be formally compared with one another (Striedter et al., 2014). However, such maps are laborious to create and difficult to compare using traditional anatomical techniques. More recently, advances in neuroimaging techniques allow the investigation of grey matter organization and connectivity. Such data can be obtained in a reliable fashion and in a relatively short time (Mars et al., 2014; Lerch et al., 2017). Although neuroimaging does not always have the resolution of the gold-standard techniques, it does have the potential to allow direct comparison of brain organization across species on a macroscopic scale.

One way to compare temporal lobe architecture between species is by comparing the longitudinal white matter connections that can be reliably detected using neuroimaging, both *in vivo* and *ex vivo* (Mars et al., 2016a). Earlier work has identified a major difference between humans and other primates in the extension of the arcuate fascicle (AF), a major longitudinal tract running mostly dorsally to the Sylvian fissure between the frontal and posterior temporal cortex (Rilling et al., 2008; Eichert et al., 2018). However, it has been suggested that other aspects of temporal cortex also differ across primates. One example concerns the relocation of areas due to differential cortical expansion between macaques and

humans (Orban et al., 2004; Mars et al., 2013). More recently, it has also been suggested that connectivity of temporal association cortex from tracts originating from primary visual and auditory cortices increased in humans and chimpanzees compared with macaques (Bryant et al., 2019). Recent data from both Klingler dissections and tractography indicate that the inferior longitudinal fascicle (ILF), which connects inferior temporal cortex with occipital regions, is composed of multiple subcomponents in humans (Latini et al., 2017). This could suggest that this fibre system has undergone further specialization in humans in comparison with macaques, in which only one component has been described. Therefore, to understand temporal lobe organization, it is necessary to systematically compare the architecture of temporal tracts across a range of primate species. Besides the ILF, we also included two other longitudinal tracts running through the primate temporal lobe: the middle longitudinal fascicule (MdLF) and the inferior fronto-occipital fascicule (IFOF). The MdLF, was previously only recognised in macaques but its existence is now established in humans as well (Makris et al., 2009). Its anatomy has been described as running through the superior temporal gyrus to the inferior parietal lobule and occipital lobe (Makris et al., 2013) and it is thought to be involved in functions related to attention, visual-processing and language (Menjot De Champfleur et al., 2013; Bryant and Preuss, 2018). The IFOF anatomy has been described as linking frontal to occipital regions through the temporal lobe. It was previously thought to be present in this form only in humans, while the macaque equivalent would not reach the occipital regions, however it has now been has been recognised as having a similar anatomy -reaching occipital areas- in a range of primate species including macaques (Mars et al., 2016a; Schaeffer et al., 2017; Decramer et al., 2018; Barrett et al., 2020; Bryant et al., 2020).

To understand how the expansion of the temporal cortex in the ape and human lineages is reflected in changes in its macroscale connectivity, we here compared the

longitudinal white matter tracts running along the temporal lobe and the dorsal AF between the human, chimpanzee and gorilla great apes, and macaque monkey brains using diffusion-weighted magnetic resonance imaging (MRI). We start by demonstrating that diffusion MRI tractography in macaques is able to reconstruct white matter tracts close to their definition by other methods such as tracers and dissection. Then, we use the same procedure to reconstruct the same tracts in the other species so that we can reliably compare their organization.

Importantly, any differences in the longitudinal tracts between species are likely to result in differences in the connectivity profile of parts of the temporal cortex grey matter. It has been suggested that each cortical area has a unique set of connections with the rest of the brain, the so-called connectivity fingerprint, and that this fingerprint is a crucial determinant of an area's function (Passingham et al., 2002; Mars et al., 2018c). Therefore, we also use the reconstructed white matter tracts to undertake a systematic comparison of the temporal lobe grey matter between the macaque and the human, with the aim to investigate how observed white matter differences between species affect their connectivity fingerprints.

3.3. Material and methods

3.3.1. Ethics Statement

All *in vivo* data (human and chimpanzee) are from publicly available databases. The human data were obtained from the Human Connectome Project (HCP), and the approved consent procedure is fully described in the core HCP literature referenced here (www.humanconnectome.org). The chimpanzee data were obtained from chimpanzeebrain.org and collected at the Yerkes Primate Center under procedures that were carried out in accordance with protocols approved by YNPRC and the Emory University Institutional Animal Care and Use Committee (approval no. YER-2001206). All *in vivo* chimpanzee scans were done prior to 2012 and thus prior to the 2015 implementation of

United States Fish and Wildlife Service and National Institutes of Health regulations governing research with chimpanzees. The *ex vivo* data were acquired from deceased animals that died of causes unrelated to this research project. As such, the research did not require a Home Office License as defined by the Animals (Scientific Procedures) Act 1986 of the United Kingdom.

3.3.2. Data acquisition and preprocessing

Diffusion MRI data

Four rhesus macaque brains (*Macaca mulatta*, one female, between four and 14 years old at the time of death) were obtained *post mortem*. The brains were stored in formalin, rehydrated in a phosphate-buffered saline solution one week prior to scanning and placed in fomblin for the scanning procedure. *Ex vivo* diffusion-weighted MRI data were acquired from the whole brain using a 7T preclinical MRI scanner. We used a 2D diffusion-weighted spin echo multi slice protocol with single line readout (DW-SEMS; TR = 10000 ms; TE = 25 ms resolution: 0.6 x 0.6 x 0.6 mm^3, number of slices: 128). Nine non-diffusion-weighted (b = 0 s/mm^2) and 131 diffusion-weighted (b = 4000 s/mm^2) volumes were acquired with diffusion encoding directions evenly distributed over the whole sphere (single shell protocol). These data have been used in previous reports (Eichert et al., 2018, 2020; Mars et al., 2018c; Folloni et al., 2019a).

Human *in vivo* data were provided by the Human Connectome Project (HCP), WU-Minn Consortium (Principal Investigators: David Van Essen and Kamil Ugurbil; 1U54MH091657) funded by the 16 NIH Institutes and Centers that support the NIH Blueprint for Neuroscience Research; and by the McDonnell Center for Systems Neuroscience at Washington University. We used the datasets of ten subjects from the Q2 release. Data acquisition and preprocessing methods are described in detail elsewhere

(Glasser et al., 2013; Sotiropoulos et al., 2013; Ugurbil et al., 2013). In brief, diffusion-weighted MRI data were acquired from the whole brain using a customized 3T Siemens Skyra scanner. A slice-accelerated gradient echo EPI readout was used with a resolution of 1.25 x 1.25 x 1.25 mm^3. Sampling in q-space included 3 shells at b= 1000, 2000, and 3000 s/mm^2. For each shell, 90 diffusion encoding gradient directions and six non-diffusion-weighted (b = 0 s/mm^2) were obtained twice, with the phase encoding direction reversed to enable susceptibility-related distortion correction.

In vivo data from three chimpanzees (*Pan troglodytes*, three females, between 13 and 36 years old) were obtained from the National Chimpanzee Brain Resource (www.chimpanzeebrain.org) supported by the NIH National Institute of Neurological Disorders and Stroke (grant no. R24NS092988). Data were obtained from a data archive of scans obtained prior to the 2015 implementation of U.S. Fish and Wildlife Service and National Institutes of Health regulations governing research with chimpanzees. All the scans reported in this publication were completed by the end of 2012. Diffusion-weighted MRI data were acquired at the Yerkes National Primate Research Center (YNPRC) on a 3T MRI scanner under propofol anaesthesia (10 mg/kg/h), using previously described procedures (Chen et al., 2013). All procedures were carried out in accordance with protocols approved by YNPRC and the Emory University Institutional Animal Care and Use Committee (approval no. YER-2001206). A single-shot spin-echo echo planar sequence (TR = 5900 ms; TE = 86 ms; resolution: 1.8 x 1.8 x 1.8 mm^3, number of slices: 41) was used to acquire two diffusion-weighted images for each of 60 diffusion directions (b = 1000 s/mm^2). Each with one of the possible left–right phase-encoding directions and four repeats, to enable susceptibility-related distortion correction. Eight averages of diffusion weighted MRI were collected and in total, 40 volumes (5 per averages) without diffusion weighting (b = 0 s/mm^2)

were also acquired with matching imaging parameters. These data were used in previous reports (Chen et al., 2013; Mars et al., 2019).

The data processing for the EPI-based protocols (*in vivo* chimpanzees and humans) consisted of correcting for susceptibility-related distortions using FSL's *TOPUP* (Andersson et al., 2003) and correcting for eddy-current using FSL's *eddy* tool (Andersson and Sotiropoulos, 2016). For all macaque, human and in-vivo chimpanzee data, fitting of a diffusion tensor model was done using FSL's *dtifit*. Following preprocessing, *bedpostX* was used to fit a crossing fibre-model to the data, allowing for three fibre orientation (Behrens et al., 2007). They were also registered to their specific standard space, F99 for macaques, MNI152 for humans and Yerkes129 for chimpanzees.

Post mortem brains from one Western Lowland gorilla (*Gorilla gorilla gorilla*, male, 12 years old at time of death) and one chimpanzee (*Pan troglodytes*, female, 28 years old at time of death) were obtained from the London Zoological Society and the Primate Brain Bank, respectively. Both samples were stored in formalin, rehydrated using a phosphate-buffered saline solution one week prior to scanning and placed in fluorinert for the scanning procedure. As the left frontal lobe of the gorilla brain was damaged during extraction, we have only used the diffusion MRI data from the right hemisphere. The left hemisphere in the chimpanzee sample was slightly flattened in the extraction protocols, making it hard to interpret any results on this hemisphere, so we will also focus on the right hemisphere. Both samples were imaged using a 7T whole body scanner with a 28-channel knee coil (QED). Diffusion MRI data were acquired using a 3D diffusion weighted steady state free precession (DW-SSFP) pulse sequence (Miller et al., 2012; Foxley et al., 2014). DW-SSFP data comprising of 240 diffusion-weighted ($q = 300$ cm^{-1}, flip angle = 39°, TR = 28 ms, TE =21 ms, resolution = 0.6 x 0.6 x 0.6 mm^3) and six non-diffusion weighted ($q = 20$ cm^{-1}) imaging

volumes were acquired over the whole *post mortem* brains. Two repeats of this protocol were performed for the gorilla, with a single repeat for the chimpanzee. To account for the T1, T2 and flip-angle dependencies of the DW-SSFP signal (Buxton, 1993; McNab and Miller, 2010), T1, T2 and B1 datasets were acquired via a turbo inversion-recovery (TIR) (TIs = 30, 60, 120, 240, 480 and 939 ms, TR = 1000 ms, TE = 13 ms, resolution = 0.4 x 0.4 x 1.0 mm^3), turbo spin-echo (TSE) (TEs = 12, 25, 37, 49, 61 and 74 ms, TR = 1000 ms, resolution = 0.4 x 0.4 x 1.0 mm^3) and actual flip-angle imaging (AFI) acquisition (flip angle = 80°, TR1 = 7 ms, TR2 = 21 ms, resolution = 1.5 x 1.5 x 1.5 mm^3 for the gorilla, flip angle = 60°, TR1 = 17 ms, TR2 = 11 ms, TE = 1.5 ms, resolution = 2.8 x 2.8 x 3.0 mm^3 for the chimpanzee) (Yarnykh, 2007).

Prior to processing, a Gibbs ringing correction (Kellner et al., 2016) was applied to the DW-SSFP, TIR and TSE datasets. Quantitative T1 and T2 maps were generated from the TIR and TSE datasets assuming mono-exponential signal evolution. A B1 map was generated from the AFI data following the methodology described elsewhere (Yarnykh, 2007). All coregistrations within and between imaging modalities were performed with *FLIRT* (Jenkinson and Smith, 2001; Jenkinson et al., 2002) via a six degrees of freedom (translation and rotation) transformation. The DW-SSFP data, along with the T1, T2 and B1 maps were fitted with the full DW-SSFP signal equation (Buxton, 1993) to both a diffusion tensor model and a ball and two stick model using cuDIMOT (Hernandez-Fernandez et al., 2019).

Key parameters and information on the diffusion data are summarized in Table 3.1.

	Number of samples	Type of sample	Protocol of acquisition	Resolution (mm^3)	b-values (s/mm^2) or q-values (cm^{-1})
Macaque	4	*Post mortem*	2D diffusion-weighted spin-echo multislice (single shell)	0.6 × 0.6 × 0.6	b = 4,000
Gorilla	1	*Post mortem*	3D DW-SSFP	0.6 × 0.6 × 0.6	q = 300
Chimpanzee *post mortem*	1	*Post mortem*	3D DW-SSFP	0.6 × 0.6 × 0.6	q = 300
Chimpanzee *in vivo*	3	*In vivo*	Single-shot spin-echo echo planar (single shell)	1.8 × 1.8 × 1.8	b = 1,000
Human	10	*In vivo*	Slice-accelerated gradient echo EPI (multishell)	1.25 × 1.25 × 1.25	b = 1,000, 2,000, 3,000

Table 3.1 Overview of diffusion data.

Structural and surface data

For macaques, we used a model of the cortical surface in the standard space F99. Human T1- and T2-weighted images were acquired using an MPRAGE sequence at 0.7 x 0.7 x 0.7 mm^3 resolution and aligned to the diffusion space as part of the HCP's minimum preprocessing pipeline (Glasser et al., 2013). The HCP pipeline reconstructs the pial and white/grey matter interface surface by combining T1- and T2-weighted scans. The surfaces were modelled for each individual as provided through the HCP pipeline (Glasser et al., 2013), and an HCP average surface was used to display the results. Similarly, for the chimpanzee *in vivo* data, T1- and T2-weighted images were processed using a modified version of the HCP pipeline (Glasser et al., 2013; Donahue et al., 2016). The surfaces were modelled for each individual and an average surface was used to display the results (Yerkes129).

Cortical surfaces for the *ex vivo* gorilla and chimpanzee specimens were generated using CARET version 5.65 (Van Essen et al., 2001). For the chimpanzee, a structural scan was generated using a true fast imaging with steady free precession (TRUFI) sequence (Miller et al., 2012). Four high resolution *ex vivo* TRUFI datasets were acquired over the entire *post mortem* brain, where each dataset was obtained with a different phase increment per TR (resolution = 0.21 x 0.21 x 0.19 mm^3, flip angle = 30°, TE = 6.78 ms, TR = 13.56 ms, phase increments = 0°, 90°, 180° and 270°). The four TRUFI datasets were averaged via root sum of squares to form a structural scan that is uncorrupted by the banding artefacts found in individual images (Bangerter et al., 2004). For the gorilla, we formed a structural scan from the mean diffusion attenuation map (diffusion weighted / non-diffusion weighted) over all directions from the acquired DW-SSFP data (See 3.3.2. Data acquisition and preprocessing: *Diffusion MRI data* for details of this acquisition). We did not use the conventional T1-weigthed images for these *post mortem* samples because they do not have a good contrast in fixed brains due to the T1 values of grey and white matter converging. TRUFI (chimpanzee) and diffusion attenuation (gorilla) images have a good contrast but opposite to conventional T1-weighted. Therefore, we needed to include further pre-processing to approximate the T1-weighted *in vivo* intensity profile required for surface reconstruction by CARET. This intensity correction was done as follows after bias correcting these structural scans using FSL's *FAST* (Zhang et al., 2001). Using the Mango MRI editing software (Lancaster et al., 2011) a region of interest (ROI) was carefully constructed semi-manually so that it only contained white and grey matter brain voxels. The range of voxel values within the ROI was normalized to the interval 0 to 1 and then subtracted from 1 to invert the intensities. All voxels outside the ROI were set to 0. These pre-processed data were imported into CARET 5.65 and reoriented to be approximately parallel to the anterior commissure–posterior commissure (ACPC) line. Accurate surfaces were obtained semi-automatically by iteratively

generating and adjusting “Surefit” segmentations within CARET. The resulting surfaces were smoothed in the medial wall and lesioned areas. We applied smoothing in the medial wall because this non-cortical area would not be defined otherwise on the cortical surface. The lesioned areas needed to be smoothed to recover the true anatomy of these areas otherwise misunderstood by the algorithm.

3.3.3. Reconstruction of ILF, MdLF and IFOF

Our first aim was to reconstruct the three major longitudinal tracts running through the temporal cortex in all four species: the ILF, MdLF, and IFOF (sometimes referred to as extreme capsule fibre complex (Mars et al., 2016a)). Given that these tracts have not been previously described in chimpanzee and gorilla, we developed an unbiased connectivity-based clustering approach to define tractography seed and waypoint masks in the temporal lobe white matter of all species. We established and validated the approach using human and macaque data because the tracts have been previously identified in these two species (Schmahmann et al., 2007; Makris et al., 2009; Latini et al., 2017). Briefly, our approach was divided into two steps. We first used a connectivity-based parcellation of three coronal ROIs in the temporal lobe white matter of each individual to identify the bodies of each of the longitudinal tracts based on their connectivity profile to the rest of the brain (Figure 3.1A). The clusters obtained, belonging to our tracts of interests, were subsequently used in the second step of tract reconstruction as seed and waypoint masks (Figure 3.1B).

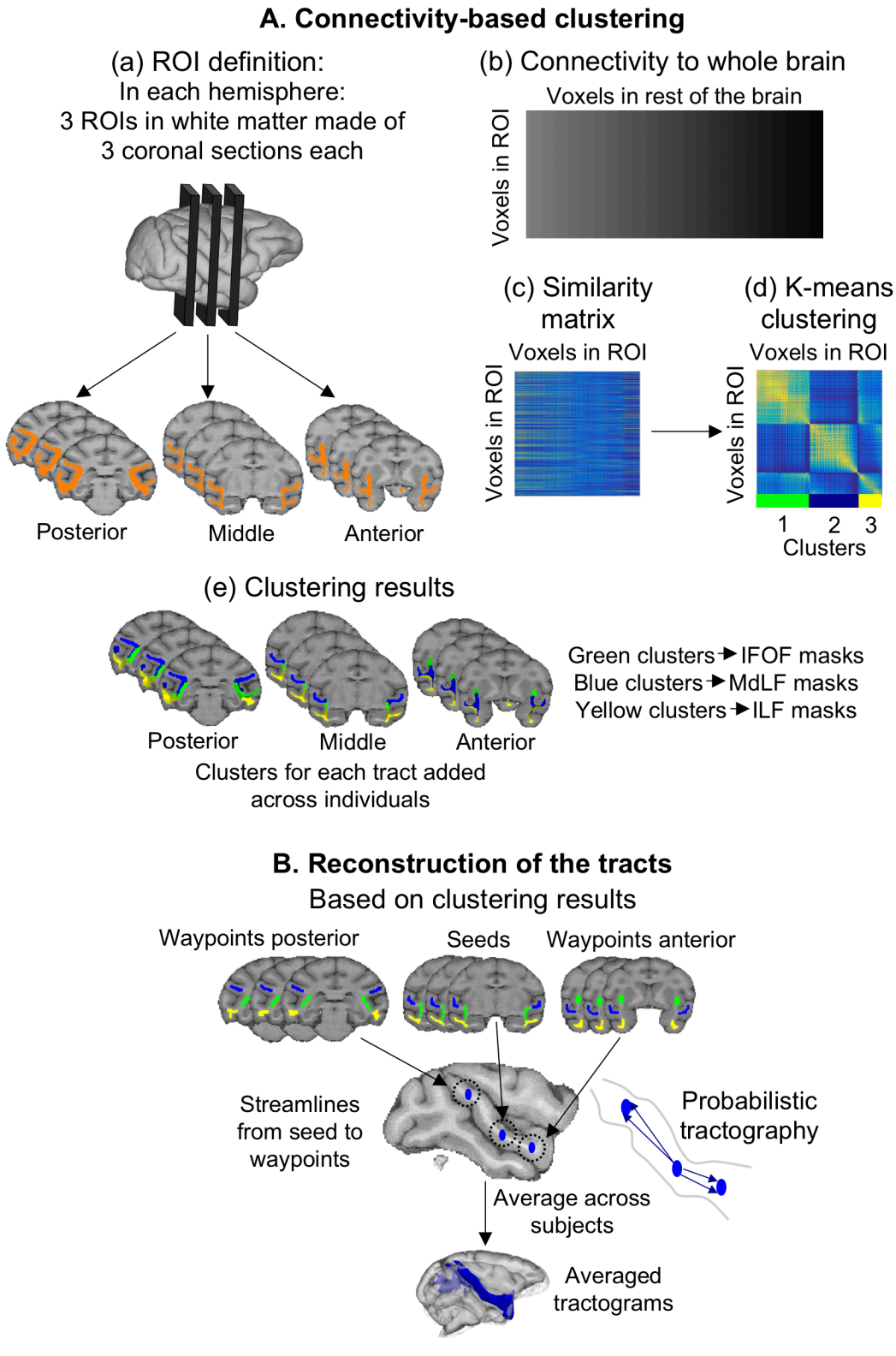

Figure 3.1 Methods overview

(figure legend continues on the following page)

The macaque is shown as the example; the same methods were used for the other species, except that *post mortem* analyses were fully performed in subject space. **A.** Connectivity-based clustering: (a) In each hemisphere, we defined three coronal ROIs in the white matter of the temporal lobe (excluding the area of the cingulum bundle). We transformed these ROIs to the diffusion space of each individual. (b) We then performed tractography from all the voxels in the ROI to the rest of the voxels in the whole brain. (c) We then computed the similarity matrix, representing the similarity in whole-brain connectivity of all voxels in each ROI. (d) We clustered the similarity matrix using the k-means algorithm, which resulted in clusters in the white matter ROI showing which voxels have similar connectivity to the rest of the brain. (e) These clusters were back projected onto each individual brain and transformed to standard space to give what we refer to as the "clustering results" (detailed in Figure 3.2 and Figure 3.3). **B.** Probabilistic tractography: from the clusters obtained at the clustering step, we established the masks for the tract reconstruction (detailed in Figure 3.2 and Figure 3.3). Probabilistic tractography was performed as follows: streamlines were sent from the seed and were kept only if they went through one of the waypoints. The resulting tractograms were averaged across individuals. IFOF: inferior fronto-occipital fascicle; ILF: inferior longitudinal fascicle; MdLF: middle longitudinal fascicle; ROI: region of interest.

Connectivity-based parcellation

The clustering step was first applied in the macaque and human to validate the approach and was performed as follows. For both species, we defined three ROI masks (anterior, middle, and posterior) in standard space (MNI152 1 mm for humans and F99 0.5 mm for macaques), each composed of three consecutive coronal sections and containing only the temporal lobe white matter (Figure 3.1Aa). The area corresponding to the body of the cingulum bundle was excluded. These ROI masks were transformed to each subject's diffusion space prior to performing probabilistic tractography using FSL's *probtrackx* from all the voxels in the ROI to all the voxels in the brain. This completely unconstrained tractography is part of the clustering step and is not intended as a method to define the whole tracts but to set up constraints for the actual tractography performed in the later tract reconstruction step. We thus obtained for each ROI a matrix of dimensions "number of voxels in ROI" × "number of voxels in the brain," representing the connectivity of each voxel in the white matter ROI to the rest of the brain and transformed it back to standard space (Figure 3.1Ab). From this matrix, we derived a similarity matrix of dimensions "number of voxels in ROI" × "number of voxels in ROI", representing the similarity between each white

matter ROI voxels regarding their connectivity to the rest of the brain (Figure 3.1Ac). The three similarity matrices (one for each ROI: anterior, middle, and posterior) were each submitted to k-means clustering to group together those voxels that have a similar profile of connections to the rest of the brain (Figure 3.1Ad) (Mars et al., 2011; Eickhoff et al., 2015). The logic of this approach is that all voxels belonging to the same fibre tract will show a similar connectivity profile, which enables us to infer each tract's most likely location in the temporal white matter ROIs.

From the current knowledge of tract anatomy in the temporal lobe (Schmahmann et al., 2007; Catani and Thiebaut De Schotten, 2008; Latini et al., 2017), we could then determine which cluster belonged to each tract for each subject. In macaques, we set three clusters in the middle and posterior ROI, which was presumed to reconstruct MdLF, ILF, and IFOF, except for the most anterior slice, in which we set it to four clusters to account for the presence of the uncinate fascicle. These assumptions are based on previous tract tracing literature (Schmahmann and Pandya, 2006a). In humans, we set one more cluster in each ROI because it has been shown that the ILF could be subdivided (Latini et al., 2017; Panesar et al., 2018). We justify a lower number of clusters in macaques by hypothesizing a more complex organization of temporal lobe white matter in humans than in macaque. This hypothesis has been verified by various measures that we detail in Appendix 1.

After identifying which cluster belonged to each tract for all individuals in one species, we then added the clusters belonging to the same tract in each coronal ROI to obtain a probability map of cluster position for each tract and ROI. Thus, we obtained probability maps for anterior, middle, and posterior positions of each tract. We refer to these probability maps as "clustering results" (Figure 3.1e and Figure 3.2, top row). Based on these maps, we defined the seed (from middle position) and waypoint masks (from anterior and posterior positions) for the subsequent tract reconstruction (Figure 3.2, bottom row). All the masks for

a given species were made of the same number of voxels across tracts, and masks from different tracts did not overlap.

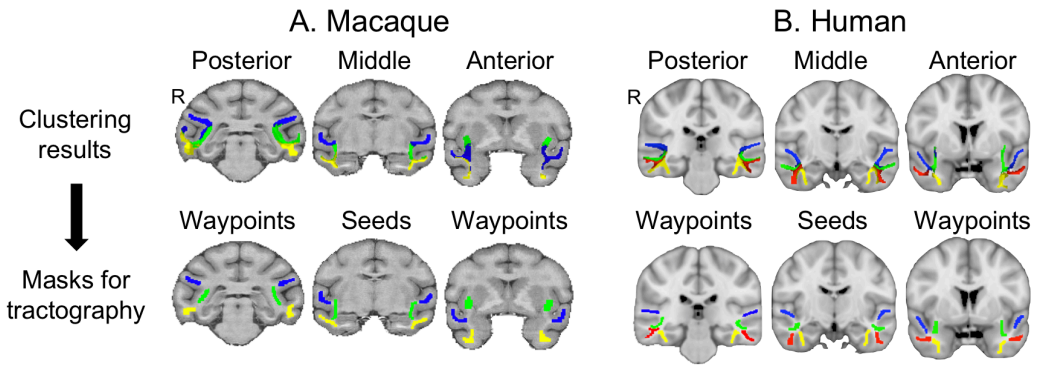

Figure 3.2 Tractography masks (bottom row) derived from clustering results (top row) in macaques and humans.

A. In macaques, the clustering results are thresholded to show the overlap between at least two subjects out of four. **B.** In humans, the clustering results are thresholded to show the overlap between at least four subjects out of 10. Blue, MdLF; green, IFOF; yellow, ILF (macaque) or ILFmed (humans); red, ILFlat. R denotes right hemisphere. IFOF: inferior fronto-occipital fascicle; ILF: inferior longitudinal fascicle; ILFlat: inferior longitudinal fascicle lateral; ILFmed: inferior longitudinal fascicle medial; MdLF: middle longitudinal fascicle.

Tract reconstruction

Following the clustering step to identify the bodies of all tracts in three different positions along the anteroposterior axis, we reconstructed, in a second step, each tract by performing probabilistic tractography informed by the clustering step. For each tract, the tractography started from the middle seed mask defined in the previous step and was constrained by two waypoints that were anterior and posterior to the seed and also defined in the clustering step. Probabilistic tractography, as implemented in FSL's *probtrackx* algorithm, started streamlines in the seed, and each streamline then followed local orientations sampled from the posterior distribution given by *bedpostX* (Behrens et al., 2007); only streamlines that passed through one or the other waypoint were retained. To further constrain the tractography, we also defined exclusion masks based on the anatomical

description of the tracts in previous literature (Schmahmann and Pandya, 2006; Catani and Thiebaut De Schotten, 2008; Makris et al., 2009; Mars et al., 2016a; Latini et al., 2017; Eichert et al., 2018). Streamlines hitting these exclusion masks were deleted (Figure 3.1B). The exclusion masks were drawn as follows: for all tracts, we used sagittal midline sections to avoid tract crossing to the other hemisphere; a dorsal exclusion mask to avoid self–back projection from the longitudinal tracts; and exclusion masks for the fornix, cingulum bundle, and AF seed (defined as described below), as well as the medial section of the optic radiation and the temporal section of the uncinate fascicle. For each tract, waypoints and seeds of the other tracts were also used as exclusion masks. Subcomponents of ILF, however, were not used as exclusion masks for each other. To avoid tracts erroneously crossing grey matter, we also used a termination mask consisting of the entire grey matter defined in subject space (using *FAST* from FSL (Zhang et al., 2001) for macaques and using the individual surface for humans). When reaching these termination masks, the streamlines were terminated but not deleted. Because the macaques' grey matter masks were less precise, we added an exclusion mask in insular cortex and putamen. The resulting tractogram was normalized for each subject by dividing its path distribution by the total number of generated streamlines not rejected by waypoint or exclusion mask criteria. We then averaged the tract distribution over all subjects and down-sampled the average tractogram to 1-mm resolution (isotropic voxels) in F99 space for macaques and 2 mm in MNI152 space for humans. For visualization, 3D renderings of the log-transformed and thresholded average tractograms were generated using in-house Matlab code.

Parcellation and tract reconstruction in chimpanzees and gorillas

Having performed these analyses for the human and the macaque, we then applied the same procedure to the chimpanzee and gorilla data. The *in vivo* chimpanzee data were treated

exactly as the human and macaque data. We performed a clustering procedure by setting the number of clusters to four because of the similar anatomy of the temporal lobe gyri and sulci between humans, gorillas, and chimpanzees. Indeed, although previous studies have shown differences in the gyral pattern between hemisphere, including notably an asymmetry of the Sylvian fissure and occipital bending between chimpanzees and humans (Hou et al., 2019), their overall sulci pattern remains more similar than compared with the macaque, which lacks defined middle temporal and fusiform gyri (Bryant and Preuss, 2018). We performed a similar analysis as in humans and macaques to confirm that this was an optimal number of clusters (Appendix 1). For the chimpanzees, the measures used pointed toward the solution using a high number of clusters. However, for the gorilla, the different measures do not uniformly point toward solutions using a high or low number of clusters, and having only one hemisphere available for this species, we cannot strongly conclude on this issue (Appendix 1).

In this manner, we were able to define four tracts in the temporal lobe: the IFOF, MdLF, ILF lateral (ILFlat), and ILF medial (ILFmed). From the clustering results (Figure 3.3, top rows), we defined the masks used in the tract reconstruction (Figure 3.3, bottom rows). The probabilistic tractography algorithm used the same exclusion masks as described for the macaques as well as the grey matter termination masks. The tract distributions obtained were averaged over three subjects and down-sampled to 1-mm resolution in Yerkes29 space. For the two *post mortem* ape samples (gorilla and chimpanzee), we used the same procedure as described above, except that all the analyses were only performed in the diffusion space of each subject and not transformed to a standard space because only one sample per species was available. Again, for visualization, 3D renderings of the log-transformed and thresholded average tractograms were generated using Matlab code made in-house. We also generated a surface representation of the tracts in great apes using tools from

Connectome Workbench (Marcus et al., 2011). For the *in vivo* chimpanzees, we projected the averaged tracts to the Yerkes29 template (previously created from 29 chimpanzee scans) and we used the respective individual surfaces in T1 space for the *post mortem* gorilla and chimpanzee.

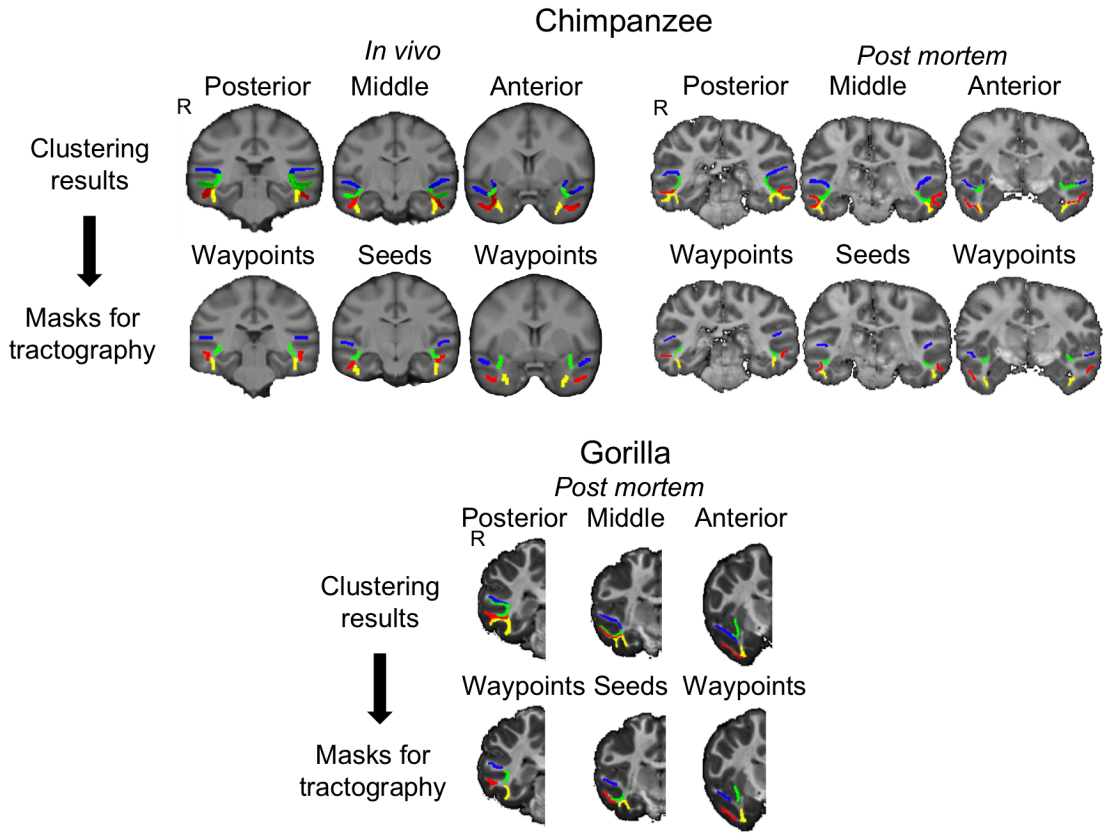

Figure 3.3 Tractography masks (bottom row) derived from clustering results (top row) in great apes.

In chimpanzee *in vivo*, the clustering results show the three subjects overlapped (no thresholding is applied). One subject was available for each of the chimpanzee and gorilla *post mortem* samples. Blue, MdLF; green, IFOF; yellow, ILFmed; red, ILFlat. R denotes right hemisphere. IFOF: inferior fronto-occipital fascicle; ILF: inferior longitudinal fascicle; ILFlat: inferior longitudinal fascicle lateral; ILFmed: inferior longitudinal fascicle medial; MdLF: middle longitudinal fascicle.

For the tract reconstruction, we used the same tractography settings in all species (10,000 samples, 2,000 steps, curvature threshold 0.2), except for the step length to account

for differences in brain size and relative resolution (0.5 mm in humans and chimpanzees *in vivo*, 0.3 in gorilla and chimpanzee *post mortem*, and 0.25 in macaque *post mortem*).

3.3.4. Reconstruction of AF

The AF is a dorsal longitudinal tract that runs from the inferior frontal cortex in a posterior direction and, in the human brain, curves ventrally to terminate in the temporal cortex. Because of its variability between species (Rilling et al., 2008), we could not use the temporal cortex coronal ROI sections to identify it in all species with the clustering approach outlined above. We therefore adapted the method used previously by Eichert and colleagues (Eichert et al., 2018) to reconstruct the tract from a manually defined seed outside the temporal cortex, just posterior to the level of the central sulcus (illustrated in the results section). We also placed an axial mask as a posterior waypoint in the parietal–temporal white matter, posterior to the caudal end of the Sylvian fissure. The mask was placed in a comparable location in all species to not bias the tract's posterior course (illustrated in the results section). To make the tractography comparable to that of the other longitudinal tracts outlined above, we added an anterior waypoint to the protocol of Eichert and colleagues (Eichert et al., 2018), allowing us to track from a middle seed to anterior and posterior waypoints as well. We used the same exclusion masks for all species as in Eichert and colleagues (Eichert et al., 2018): a midline mask, two subcortical white matter and extreme/external capsule masks, and one mask through the superior parietal cortex.

The clustering and all tract reconstruction steps have also been performed with alternative tractography techniques to validate our approach (Appendix 2).

Great apes surface representation

In the great apes, we examined where the tractogram approached the grey/white matter border to represent their tractograms on the cortical surface. We normalized, log transformed, smoothed with a kernel of 2 mm full-width half maximum (FWHM), and thresholded these surface tractograms.

3.3.5. Comparison of macaque and human temporal lobe connectivity blueprints

To establish the effects of any differences in the longitudinal temporal tracts across species on the connectivity profiles of temporal cortex grey matter, we established the white matter connectivity of each part of the temporal cortex grey matter, the so-called "connectivity blueprint," using the method established by Mars and colleagues (Mars et al., 2018c). The connectivity blueprint is in effect a matrix that describes how well each vertex of the temporal lobe grey/white matter border, as defined in the surface, is reached by each of the white matter tracts of the temporal lobe. Each row of this matrix describes the "connectivity fingerprint" of each vertex of the temporal lobe with each white matter tract (Figure 3.4A). Therefore, the connectivity fingerprint is a subset of the connectivity blueprint focusing on a particular vertex instead of the whole brain. Each column of the blueprint matrix corresponds to one tract. Because the tracts are defined in a similar way in the different species, they present a common space that allows us to compare connectivity fingerprints across the two brains, testing whether there are unique connectivity fingerprints in one brain compared with the other.

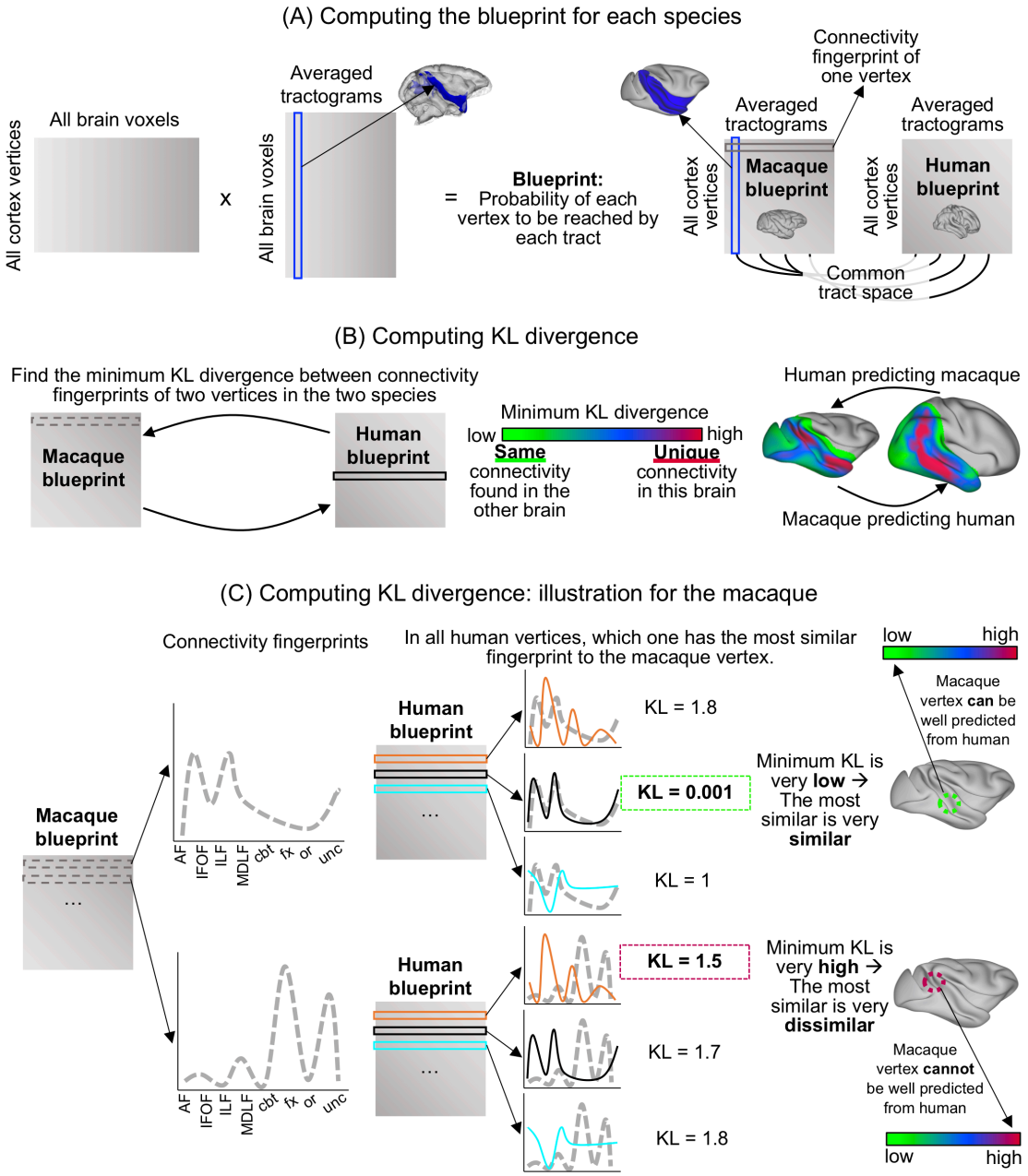

Figure 3.4 Blueprint method to assess connectivity divergence between macaque and human temporal cortex.

A. To compute the blueprint, we multiplied a matrix representing the connectivity of each cortical vertex (surface space) to each brain voxel (volume space) with a matrix representing how each brain voxel (volume space) is reached by each tract. Because we reconstructed the same tracts in both macaques and humans, the columns of the blueprint define a common space to compare the connectivity of the temporal cortex. The rows of the blueprint correspond to the connectivity fingerprint of each voxel. The columns of the matrix correspond to the surface tractograms. **B.** Using the KL divergence measure to compare every vertex in one brain to every vertex in the other brain, we can identify vertices in the two brains in which the smallest divergence is found. If this smallest divergence is very low (green on the scale), it means that the same connectivity profile can be found at these vertices for both brains. *(figure legend continues on the following page)*

If the smallest divergence is very high (pink on the scale), it means that the connectivity profile at this vertex is very different to any connectivity profile of the other brain vertices. **C.** Illustration of the KL divergence computation for two macaque vertices. For each of the vertices, a connectivity fingerprint representing how the vertex is connected to each tract was computed. Using a KL divergence measure, this connectivity fingerprint was compared with connectivity fingerprints of all human vertices. The vertex with the connectivity fingerprint most similar to the macaque one, therefore with the smallest KL divergence, is picked, and this KL divergence value is assigned to the monkey vertex. AF: arcuate fascicle; cbt: temporal part of the cingulum bundle; fx: fornix; IFOF: inferior fronto-occipital fascicle; ILF: inferior longitudinal fascicle; KL: Kullback–Leibler; MdLF: middle longitudinal fascicle; or: optic radiation; unc: uncinate fascicle.

We directly compared these blueprints between the macaque and the human brain (Figure 3.4). We focused on these two species because they are the most studied species among the ones presented in the current study. Furthermore, the course and connectivity of other nonlongitudinal tracts reaching the temporal lobe, such as the uncinate fascicle (UNC), the cingulum bundle (CB), the optic radiation (OR) and the fornix (FX), have been well established in these species (Schmahmann et al., 2007; Mars et al., 2018c).

We established the connectivity blueprint using the tractograms of ILF, MdLF, IFOF, and AF as established above and supplemented them with tractograms of the other major white matter tracts in the temporal lobe—namely, the temporal part of the CB (CBt), the FX, the OR, and UNC—using established tractography protocols (Mars et al., 2018c). A tractogram can be represented as a column vector describing how well each voxel is reached by the tract (Figure 3.4A). By concatenating the vectors corresponding to each tract, we obtained a matrix representing how each voxel (row) is reached by each tract (column). Second, we also calculated whole-hemisphere vertex wise connectivity matrices obtained by tracking from all vertices in the grey/white matter border of the surface file to all voxels in the brain in volumetric space (Figure 3.4A). These matrices were computed for both hemispheres and for each subject individually before creating an average for each hemisphere and species. Then, we multiplied the tractogram's matrix with this averaged matrix in both species, obtaining the blueprint matrix (Figure 3.4A). We also individually extracted each

column of this matrix to obtain a surface representation of the different tracts, which we will refer to as "surface projections."

The connectivity blueprints of different species can be compared by calculating the Kullback–Leibler (KL) divergence between the connectivity profiles of each vertex in one brain with that of each vertex in the other brain (Figure 3.4B). The KL divergence measures how the probability distribution of likelihoods of one vertex to be reached by each of the temporal lobe tracts is different in one brain from the probability distribution of each vertex in the other brain. For each vertex in one brain, we could then determine another vertex in the other brain that had the minimum KL divergence —in other words, the most similar connectivity profile. If a vertex in one species has a very similar connectivity profile to that of a vertex in the other brain, meaning that they are reached by a similar combination of tracts, the minimum KL divergence will be low. If, on the other hand, a vertex's fingerprint connectivity profile is unique in one brain, its minimum KL divergence will be high (Figure 3.4C).

We first defined the blueprints based on the well-established tracts: the CBt, the FX, the OR, and the UNC. Because we did not expect these tracts to be massively different between the two species, we expected the KL to be very low and, therefore, this comparison to serve as a reference point for the following blueprint comparisons. Then, we added the tracts of interest: MdLF, ILF, IFOF, and AF. To assess the reorganization of the human ILF subcomponents, we generated blueprints with both ILF subcomponents combined or either one or the other while keeping the macaque ILF constant. This manipulation enabled us to compare the ILF subcomponents' distinct prediction of the macaque brain organization. We compared these maps visually by subtracting the KL divergence scores spatial map established with human ILFmed from the one established with human ILFlat. Furthermore, we masked the blueprint to only focus on the temporal, occipital, and inferior parietal lobes.

To assess the divergence between species more quantitatively, we obtained the distribution of the minimum KL divergence scores obtained with each blueprint: with nonlongitudinal tracts; adding MdLF, ILF, and IFOF; adding the AF; with the human ILFlat; and finally, with the human ILFmed. We included only nonzero values, which are the vertices with differences in their connectivity fingerprints. Each distribution of minimum KL divergence scores indicates how similar the connectivity fingerprints of this brain are with that of another brain. All distributions were then compared using the two-sample Kolmogorov–Smirnov test (with $p < 0.01$).

For illustration, but not for establishing the blueprint, we smoothed the surface tracts with a kernel of 2 mm FWHM for macaques and 4 mm for humans. We then log transformed and normalized the surface tract distributions to facilitate the threshold determination.

3.4. Results

3.4.1. Longitudinal tracts in macaque and human

We used connectivity-based parcellations of coronal regions of interest (ROIs) through the temporal white matter to identify the bodies of the main longitudinal tracts of the temporal lobe, which subsequently informed the position of the masks used to perform probabilistic tractography in order to reconstruct the course of the tracts.

In macaques, we were able to reconstruct tracts similar to earlier studies (Schmahmann et al., 2007; Mars et al., 2016a, 2018c) (Figure 3.5A). The superior temporal gyrus contained a single cluster, from which we reconstructed a tract that can be identified as the middle longitudinal fascicle (MdLF) because of its course through the superior temporal gyrus and termination points mainly in the inferior parietal lobe but also branching toward occipital regions. The inferior temporal gyrus contained a single cluster, from which we

reconstructed a tract similar to the ILF, terminating in inferior occipital and inferior parietal regions. Medial to these tracts, we identified a tract that is reminiscent of the inferior fronto-occipital fascicle (IFOF), running from the occipital cortex medially through the temporal cortex at the level of the inferior temporal gyrus. Among the tracts we identified, it was the only one to have very clear projections to the frontal lobe. The IFOF as identified here is likely to be a multisynaptic pathway because we are using the method of tractography and not tract tracing. Indeed, tract tracing identifies a monosynaptic section of the IFOF termed the extreme capsule (Schmahmann et al., 2007). Importantly, a recent dissection study identified an IFOF in the macaque similar to our tractography results, demonstrating a biological basis of our finding (Decramer et al., 2018). We provide a more in-depth comparison of these tracts as obtained using different methodologies in the Appendix 3.

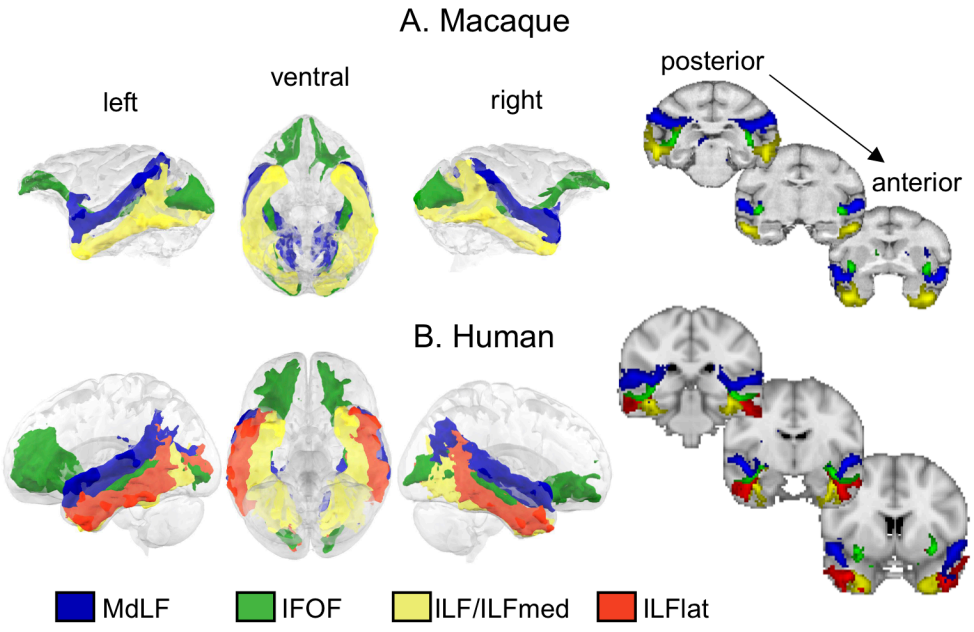

Figure 3.5 Representation in 3D and coronal sections of longitudinal temporal tracts in macaques (A) and humans (B).

Tractograms were log transformed and normalized for display. The coronal sections from left to right are taken from posterior to anterior. Blue, MdLF; green, IFOF; yellow, ILF (macaque) or ILFmed (human); red, ILFlat. Thresholds for the tracts are as follows: 0.7 for MDLF; 0.75 for IFOF; and 0.7 for ILF, ILFmed, and ILFlat. IFOF: inferior fronto-occipital fascicle; ILF: inferior longitudinal fascicle; ILFlat: inferior longitudinal fascicle lateral; ILFmed: inferior longitudinal fascicle medial; MdLF: middle longitudinal fascicle.

The same procedure in humans identified a tract through the superior temporal gyrus similar to the MdLF (Figure 3.5B). In the inferior temporal gyrus, the clustering could reliably identify two clusters with differential connectivity to the rest of the brain where we would expect the territory of the ILF to be (Figure 3.5B). We suggest that the higher number of clusters found in humans reflects a higher complexity in the temporal lobe white matter organization of this species. We interpret this in the light of previous studies supporting a subdivision of the ILF into two subcomponents (Latini et al., 2017; Panesar et al., 2018). Accordingly, the tractography identified different tractograms for the two subcomponents. One of them runs more laterally in the inferior temporal gyrus and slightly invades the middle temporal gyrus, whereas the other runs more medially and ventrally, mainly in the fusiform gyrus, and reaches more inferior occipital regions. We refer to these tracts as the ILF lateral (ILFlat) and ILF medial (ILFmed) subcomponents of the ILF. We identified a tract very similar to the IFOF that runs predominantly through the middle temporal gyrus, although it is located more medially than the other two tracts. Indeed, from the surface projections (Figure 3.6AB, Appendix 4), it can be seen that the middle temporal gyrus in humans is mainly reached by the ILFlat and the IFOF.

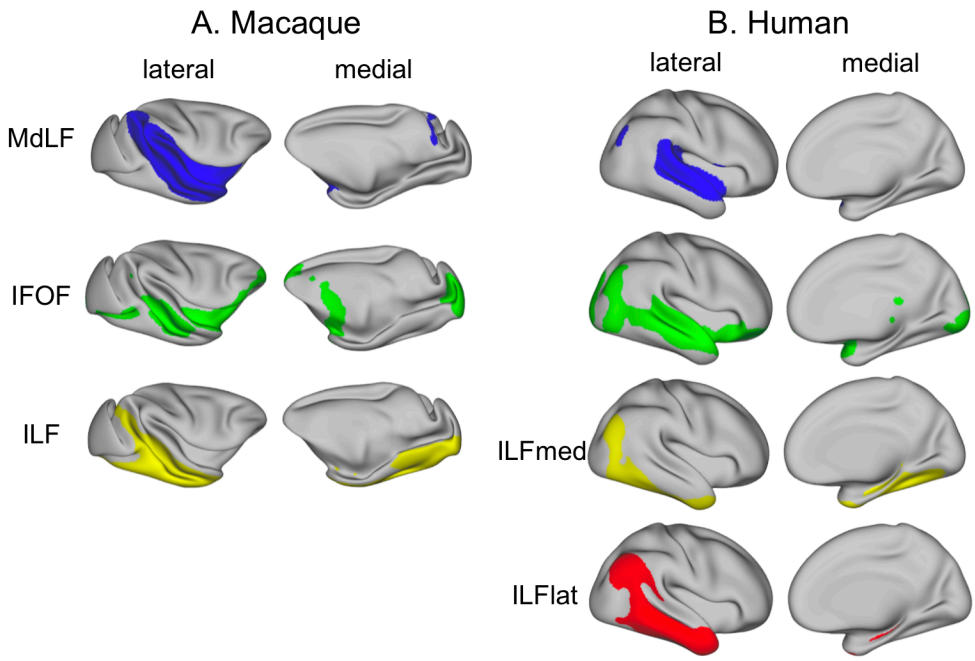

Figure 3.6 Surface projection of longitudinal temporal tracts in macaques (A) and humans (B).

Shown are the group averages of the normalized, log-transformed, and thresholded tracts in the right hemisphere only (left hemisphere results can be found in Appendix 4). Blue, MdLF; green, IFOF; yellow, ILF (macaque) or ILFmed (humans); red, ILFlat. Thresholds for the tracts are as follows: 0.7 for MDLF; 0.75 for IFOF; and 0.7 for ILF, ILFmed, and ILFlat. IFOF: inferior fronto-occipital fascicle; ILF: inferior longitudinal fascicle; ILFlat: inferior longitudinal fascicle lateral; ILFmed: inferior longitudinal fascicle medial; MdLF: middle longitudinal fascicle.

In summary, compared with the macaque, the human IFOF is located more lateral and runs predominantly along the middle temporal gyrus (which is not present in the macaque). Also, unlike macaques, human ILF can be subdivided into two subcomponents. The MdLF has a similar path in both species, which indicates that its main connectivity pattern across species should not be fundamentally different.

3.4.2. Longitudinal tracts in great apes

Using the same procedure of connectivity-based clustering followed by tractography as for humans and macaques, we identified longitudinal temporal tracts in the chimpanzee

and gorilla. We used both *in vivo* and *ex vivo* data in the chimpanzee and obtained comparable results (Figure 3.7AB), indicating that our results generalize across the different imaging protocols. However, because the left hemisphere in the *post mortem* sample was slightly flattened in the extraction protocols, it is hard to interpret the results obtained in that hemisphere.

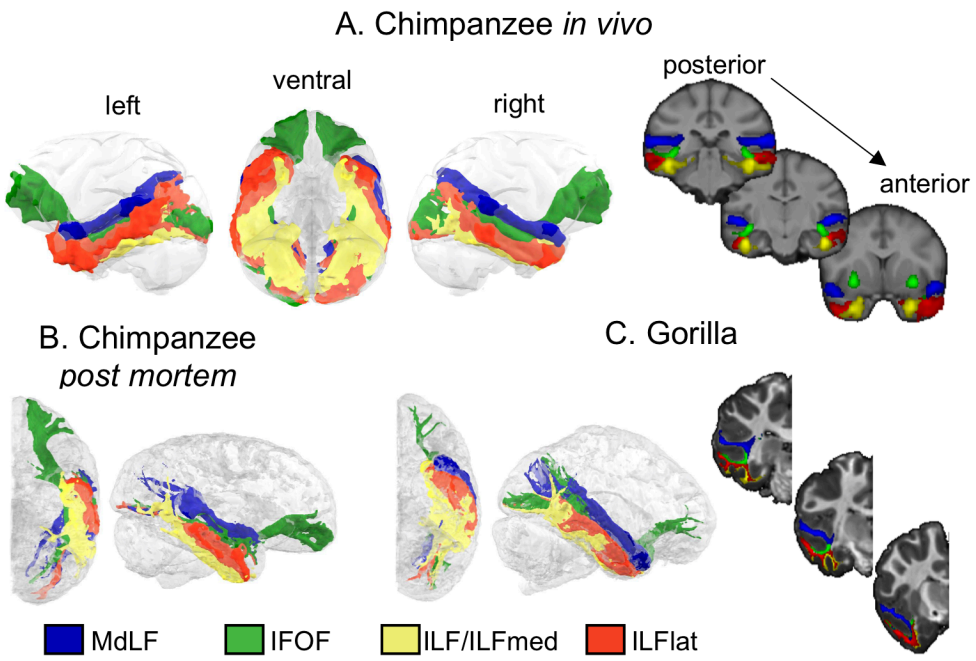

Figure 3.7 Representation in 3D and coronal sections of longitudinal temporal tracts in chimpanzees *in vivo* (A) *post mortem* (B) and gorilla (C).

Tractograms were log transformed and normalized for display. The coronal sections from left to right are taken from posterior to anterior. Blue, MdLF; green, IFOF; yellow, ILFmed; red, ILFlat. Thresholds for the tracts are as follows: 0.7 for MDLF; 0.75 for IFOF; and 0.7 for ILFmed and ILFlat. IFOF: inferior fronto-occipital fascicle; ILF: inferior longitudinal fascicle; ILFlat: inferior longitudinal fascicle lateral; ILFmed: inferior longitudinal fascicle medial; MdLF: middle longitudinal fascicle.

We identified the MdLF running through the superior temporal lobe following a similar course as human and macaque MdLF, reinforcing the argument for a conserved tract across all studied anthropoid primates (Figure 3.7ABC). In the inferior temporal lobe, the territory occupied by the ILF was similar to that in humans and could similarly be divided

into two subcomponents. We therefore will refer to them as ILFlat and ILFmed as well. Although the differentiation is strong in the chimpanzee, specifically in the right hemisphere, the separation of the ILF into two subcomponents in gorilla, although present, is less pronounced. Different methods to assess the number of clusters in the temporal white matter did not reach a consistent conclusion in the gorilla (Appendix 1), suggesting that the gorilla temporal lobe white matter might not be as complex as in chimpanzees and humans. We suggest that this is related to the anatomy of its temporal lobe, with a less prominent fusiform gyrus and a less distinct difference between the inferior and middle temporal gyrus in the gorilla, which is associated with a shallower inferior temporal gyrus, compared with the chimpanzee. The IFOF was also present in great apes, and its course was similar to the human IFOF, running more medially than other tracts as well as in the middle temporal gyrus. In chimpanzee *in vivo*, it seems that the IFOF does not reach as lateral as in the other great ape data. In gorilla, it can be observed that the IFOF is most prominent in its posterior section, whereas it is quite limited in its frontal projections. However, having only one sample for the gorilla because of the presence of a frontal lesion on the left hemisphere, we cannot draw too-strong conclusions from this observation.

To further illustrate these tracts in great apes, we represented their tractograms on the cortical surface (Figure 3.8, Appendix 4). In other words, we examined where the tractogram approached the grey/white matter border. Although one should be cautious in interpreting such results because of the presence of superficial white matter systems (Reveley et al., 2015) and possible gyral bias of tractography toward the surface, it provides an illustration of these fibre tracts in the great ape, in which they are currently underexplored. It allows one to represent not only the differences in tract organization with other species but also the sulcal and gyral patterns of these brains, which are not well known. This showed that for both species, the MdLF reaches mostly superior temporal gyrus areas as it does in the macaque

and human. The ILF subcomponents are similar to those in the human, with the majority of the lateral part of the inferior temporal cortex reached predominantly by the ILFlat and the medial part reached predominantly by the ILFmed. The IFOF is the only one of these tracts that has projections to the frontal cortex.

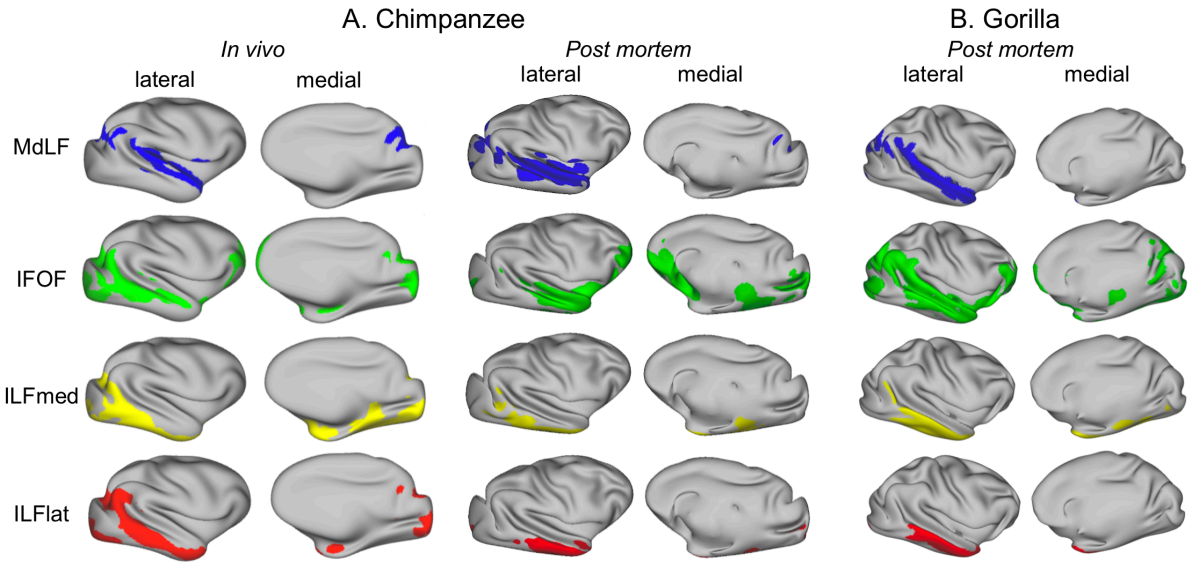

Figure 3.8 Surface representation of longitudinal temporal tracts in chimpanzees (A) and gorilla (B).

Shown are the group average (chimpanzee *in vivo*) or individual results (chimpanzee *post mortem* and gorilla) of the normalized, log-transformed, smoothed, and thresholded right tracts (left hemisphere results can be found in Appendix 4 for chimpanzee *in vivo*). Blue, MdLF; green, IFOF; yellow, ILFmed; red, ILFlat. Thresholds for the tracts are as follows: 0.7 for MDLF; 0.75 for IFOF; and 0.7 for ILFmed and ILFlat. IFOF: inferior fronto-occipital fascicle; ILFlat: inferior longitudinal fascicle lateral; ILFmed: inferior longitudinal fascicle medial; MdLF: middle longitudinal fascicle.

Thus, great apes (including humans) seem to display a similar organization regarding the subcomponents of the ILF running in inferior and fusiform gyri, respectively. The ILFmed reaches an area reminiscent of the fusiform gyrus in all species, which is absent in the macaque, in which we did not detect the subdivision of the ILF. In line with this argument, we notice that these ILF subcomponents are less evident in the gorilla, in which the fusiform gyrus is less prominent than in chimpanzees and humans.

3.4.3. Dorsal longitudinal tract

We have concentrated thus far on the major ventral longitudinal tracts along the temporal cortex. However, a major dorsal longitudinal tract, the AF, runs between the frontal and temporal cortex. Previous studies have developed tractography protocols for this tract in the human, chimpanzee, and macaque, although the details differ between studies and groups (Catani and Thiebaut De Schotten, 2008; Rilling et al., 2008). Here, we used a consistent protocol to track the AF in all four species, creating a comparable result for the three species in which the AF has previously been defined and in the gorilla (Figure 3.9, Appendix 4).

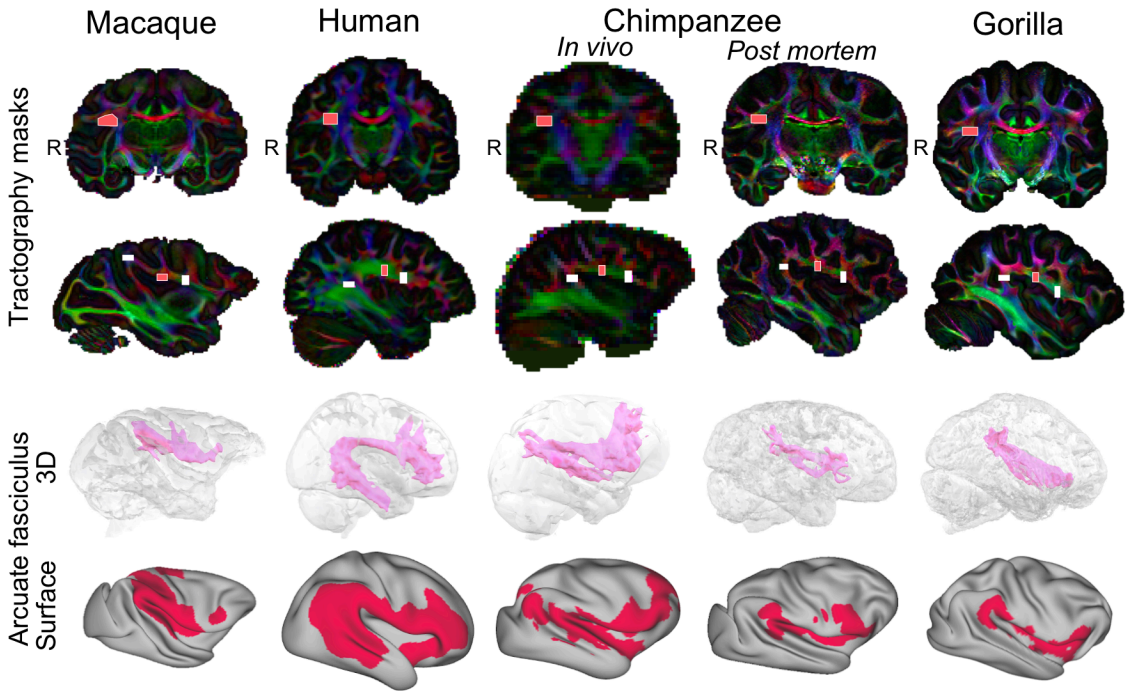

Figure 3.9 AF tractography protocols and results.

Top panel: AF tractography masks example for one individual macaque, human, chimpanzee (*in vivo* and *post mortem*), and gorilla, represented on the principal eigenvector (V1) map weighted by the fractional anisotropy map. The light-pink mask represents the seed, and the white masks represent the anterior and posterior waypoints. Bottom panel: 3D and surface representation of the right tractogram obtained for AF. (Left hemisphere results can be found in Appendix 4) Threshold of 0.75. R denotes right hemisphere. AF: arcuate fascicle.

In macaques, the AF consisted of only a dorsal component, whereas in humans, its course exhibited a sharp curve to end up in the temporal lobe running mainly in the middle temporal gyrus, although quite medially. In chimpanzees, we observed a small curve as well, with AF reaching the superior temporal gyrus but not the middle temporal gyrus, as in humans. An arcuate path similar to that of the chimpanzee could be observed in gorilla. Thus, the AF expansion to the temporal lobe seems to be unique to humans and not present in other great apes studied here.

3.4.4. Divergence in macaque and human temporal cortex connectivity profiles driven by longitudinal tracts

The goal of the present work is to establish similarities and differences between the long-range connections of the temporal lobe across primate species, with the macaque and the human as the two most studied samples. If differences in these long-range connections exist, they should result in different connectivity profiles of temporal cortex grey matter between the two species. To establish whether this is the case, we compared the connectivity profiles of each grey matter vertex of the temporal lobe—in other words, the temporal lobe connectivity blueprint—across species. The logic of the approach is that for each vertex in each species, we quantify how well its connectivity fingerprint with the temporal cortex white matter tracts resembles that of any vertex in the other species. Thus, vertices with a low divergence score have a connectivity fingerprint also present in the other species, whereas vertices with a high divergence score are more likely to have a connectivity that is unique to that species. The connectivity fingerprint profile of a given vertex in this analysis is represented by the probability that the vertex is reached by each tract.

We first restricted the blueprint to four temporal tracts that have been well established in both humans and macaques—namely, the temporal part of the cingulum bundle (CBt), the

fornix (FX), the optic radiation (OR), and the uncinate fascicle (UNC) (Catani et al., 2003; Schmahmann and Pandya, 2006b; Catani and Thiebaut De Schotten, 2008; Folloni et al., 2019a). These tracts are known to be conserved across species, and hence we expect all vertices to have low divergence scores. Indeed, in this blueprint, we can observe that both human and macaque brain organization are predictable from one another (Figure 3.10A, Appendix 4). With those same tracts, but also adding the MdLF, the combined ILF, and the IFOF in the blueprint, we notice a small increase of the divergence score in some areas of the temporal lobe in both species (Figure 3.10B, Appendix 4). The example connectivity fingerprints in Figure 3.10 A and B illustrate how the increase in divergence scores (computed as Kullback–Leibler (KL) divergence) is due to differences in the connections of these parts of the cortical surface with the underlying white matter. When only using the nonlongitudinal tracts (Figure 3.10A), all vertices have a low value because the pattern of connections of any part of the surface can be found in the other species. When adding the ventral longitudinal fibres, some differences are noticeable, and indeed a vertex with a high divergence score has a connectivity profile that differs even from its best matches in the other species (Figure 3.10B). Finally, when adding the AF, the profiles of connections of parts of the cortex are very different even from their best matches in the other species, indicating that this tract contributes most to the distinctive organization of the human temporal lobe (Figure 3.10C, Appendix 4).

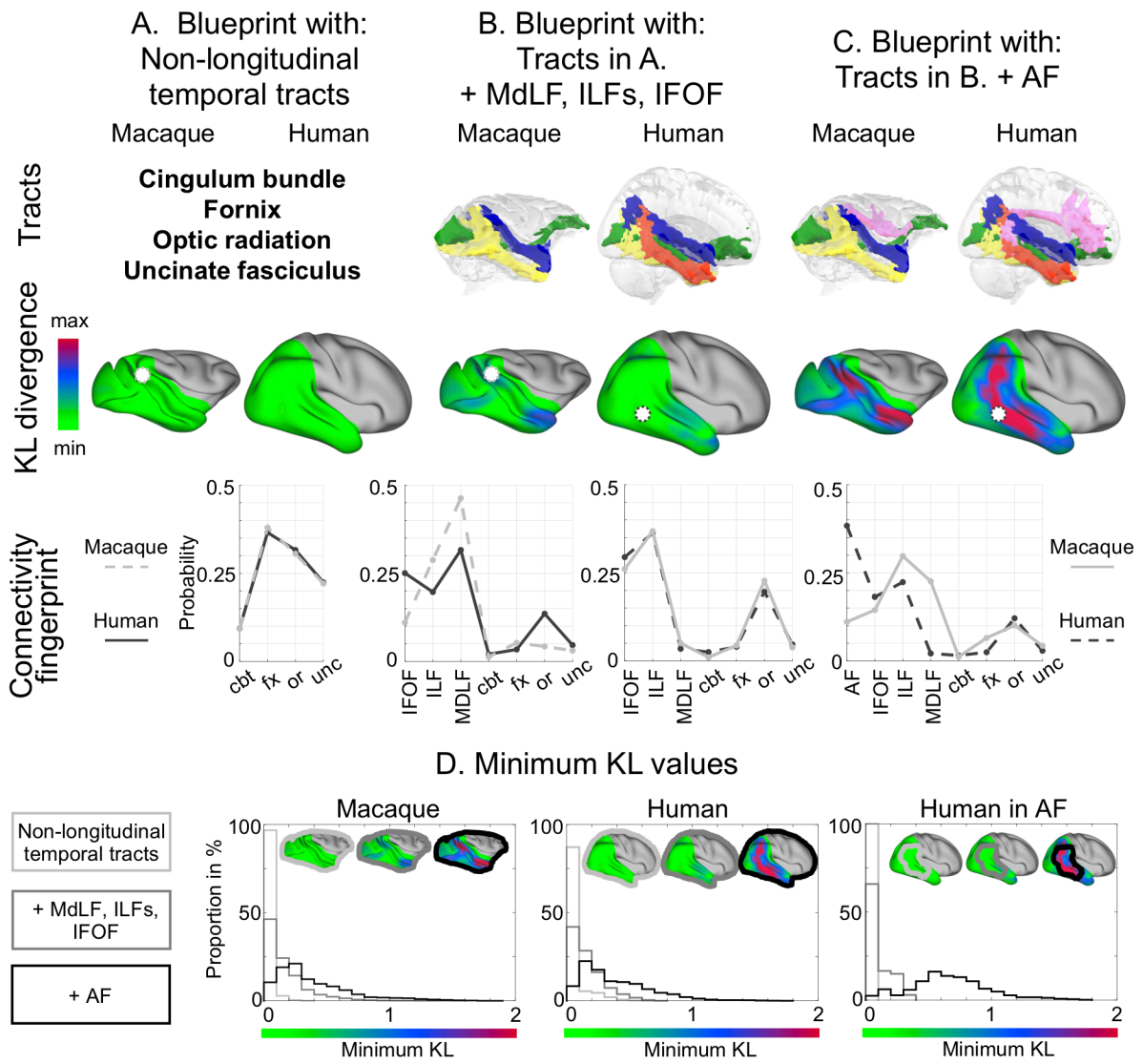

Figure 3.10 Results of the blueprint analysis.

The figure reports results on the right hemisphere (left hemisphere results can be found in Appendix 4) and shows the tracts used (top row), the resulting KL divergence (middle row) for human predicting macaque (left) and macaque predicting human (right), and the connectivity fingerprints (bottom row). The greener the vertices of the KL divergence map in one brain, the more their connectivity profile is similar to that of vertices in the other brain. The connectivity fingerprints show how likely it is for the vertex, highlighted by a white sphere in the brain above, to be reached by each tract (dotted line). The solid line represents how likely each tract is to reach the average of the 10 best-matching vertices in the other species. **A.** Blueprints established using the cbt, the fx, the or, and the unc. **B.** Blueprints established with the tracts in (A) and adding the MdLF, ILF (both subcomponents combined in humans), and IFOF. **C.** Blueprints established with the tracts in (B) and adding the AF. Blue, MdLF; green, IFOF; yellow, ILF (macaque) or ILFmed (human); red, ILFlat; pink, AF. **D.** Distribution of minimum KL values obtained for each blueprint. From left to right for the macaque, the human, and masked with the human AF. Light grey, nonlongitudinal tracts; grey, adding MdLF, ILFs, and IFOF; black, adding AF. AF: arcuate fascicle; cbt: temporal part of the cingulum bundle; fx: fornix; IFOF: inferior fronto-occipital fascicle; ILF: inferior longitudinal fascicle;

(figure legend continues on the following page)

ILFlat: inferior longitudinal fascicle lateral; ILFmed: inferior longitudinal fascicle medial; KL: Kullback–Leibler; MdLF: middle longitudinal fascicle; or: optic radiation; unc: uncinate fascicle.

These results are confirmed by the distribution of the divergence scores obtained with each blueprint (Figure 3.10D, Appendix 4). We can observe a shift toward higher minimum divergence scores in the distributions when adding the AF, which is confirmed by the distributions being statistically different (as assessed by the two-sample Kolmogorov–Smirnov test with $p < 0.01$). This shift is even more dramatic when focusing the human blueprint on the AF territory, confirming its influence on the increase of KL divergence.

One difference we found between the macaques and all the great apes was the dissociability of the two components of the ILF. Using the blueprint method, we next investigated the different impact of the two subcomponents of the ILF on similarity of macaque and human temporal lobe organization. When we ran the same analysis comparing macaque temporal lobe with a human temporal lobe in which the ILF either consists solely of the ILFlat or consists solely of the ILFmed, we observed that macaque temporal lobe contains substantially more vertices with a high KL divergence in the territory of the ILF when we use ILFlat. In other words, macaque and human temporal lobes are more similar if we assume equivalence of macaque ILF and human ILFmed than if we assume equivalence of macaque ILF and human ILFlat (Figure 3.11AB, Appendix 4). Computing the difference between the two divergence maps analysed with the two different subcomponents thus allows one to investigate the putative homology (Figure 3.11C, Appendix 4). On this difference map, we can also notice that when using the ILFmed, the human brain better predicts the areas where the macaque ILF runs, but the macaque brain does not predict the part where the ILFlat runs anymore. When using the ILFlat in humans, it better predicts an area situated more in the domain of the IFOF in macaques. The distribution of the divergence scores in the territory of the macaque ILF, obtained when using one or the other human ILF, also shows a shift toward

higher value when using the human ILFlat compared with the human ILFmed (Figure 3.11D, Appendix 4). The two distributions are statistically different (as assessed by the two-sample Kolmogorov–Smirnov test with $p < 0.01$).

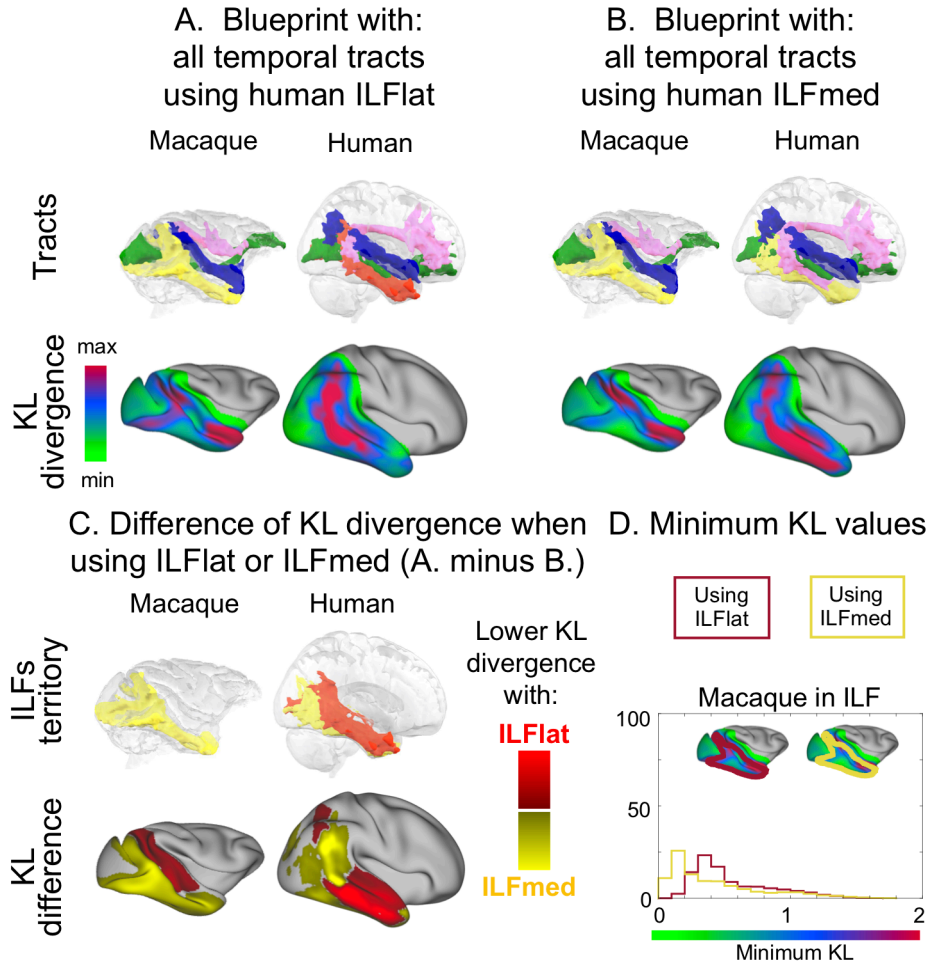

Figure 3.11 Blueprint method to determine differences between the human ILFs.

A. Blueprint established as in Figure 3.10C but with the ILFlat for humans (no ILFmed). **B.** Blueprint established as in (A) but with the ILFmed for humans (no ILFlat). **C.** The different ILF tractograms are represented on the top row. On the bottom row is shown the KL difference between the two maps established in (A) and (B). More yellow vertices means that using ILFmed in humans as macaques' ILF homologous results in lower KL divergence between the two species at these vertices, whereas more red applies to ILFlat. Blue, MdLF; green, IFOF; yellow, ILF (macaque) or ILFmed (human); red, ILFlat; pink, AF. **D.** Distribution of minimum KL values in the macaque's ILF territory obtained for the blueprints with the different human ILF subcomponents. Red, with human ILFlat; yellow, with human ILFmed. IFOF: inferior fronto-occipital fascicle; ILF: inferior longitudinal fascicle; ILFlat: inferior longitudinal fascicle lateral; ILFmed: inferior longitudinal fascicle medial; KL: Kullback–Leibler; MdLF: middle longitudinal fascicle.

3.5. Discussion

Association cortex volume scales differently in monkeys and apes (Glasser et al., 2014; Passingham and Smaers, 2014; Smaers et al., 2017), which can be taken to indicate a grade change with respect to this aspect of brain organization because a grade designates a group of species based on similar morphological traits. Here, we investigate how these differences in volume are accompanied by differences in long-range connectivity. We show that the main longitudinal tracts connecting the temporal lobe are present in the most often studied monkey "model" (the macaque), in two separate great ape species (chimpanzee and gorilla), and in the human brain. Importantly, we identify modifications of these bundles across the different lineages (Figure 3.12). First, the ILF in chimpanzees and humans is reliably separated into subcomponents that were not observed in the macaque. This result is less strong in the gorilla. Second, the middle temporal gyrus, which is present in all species except the macaque, seems to be most heavily connected by the IFOF, which is located more laterally than in the macaque. Finally, the AF's extension into the temporal cortex seems to be a uniquely human specialization, with the lack of expansion previously identified in the chimpanzee replicated here in the gorilla. Although consistent with previous reports of differences in the organization of macaque and human temporal cortex (Rilling et al., 2008; Preuss, 2011; Mars et al., 2018c), our report crucially demonstrates that differences between the two species are not due to a single change at a single moment in time but rather to a series of changes in white matter architecture.

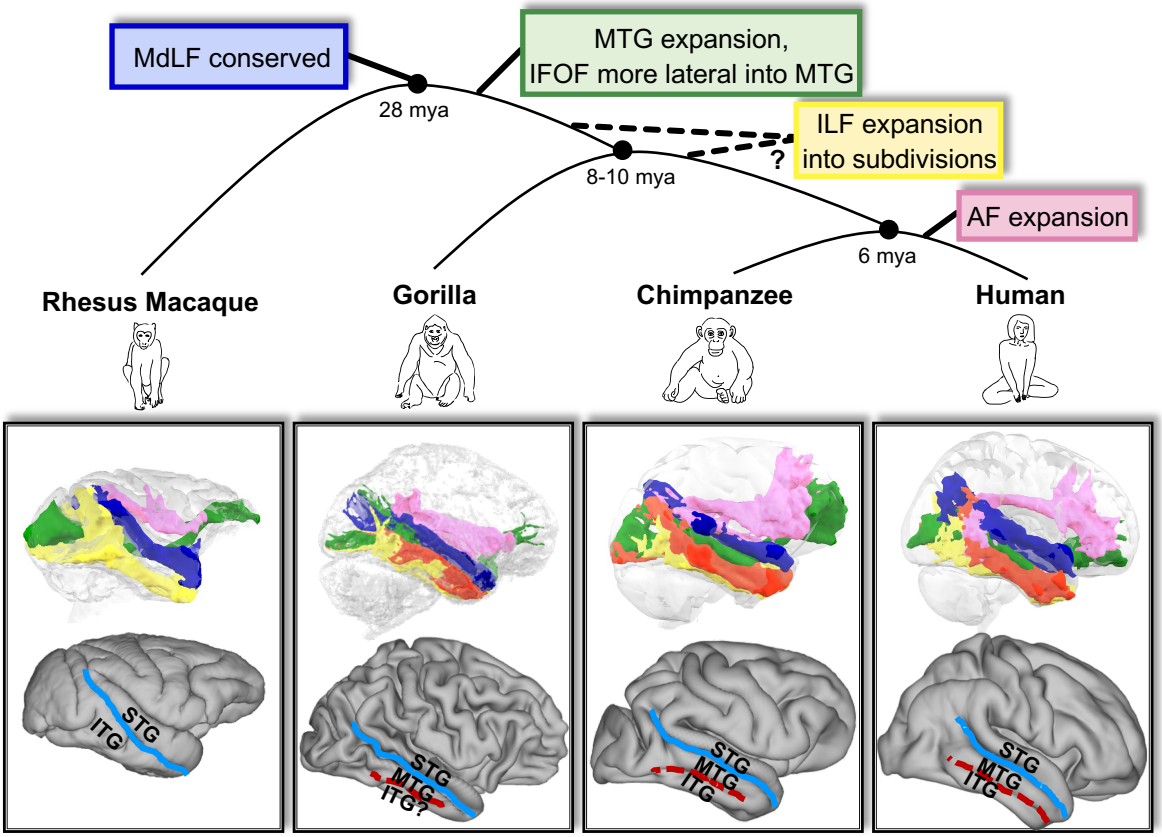

Figure 3.12 Suggested evolutionary trajectory for the longitudinal temporal lobe tracts.

We summarized our findings in the phylogenetic tree represented at the top of the figure. In the bottom part of the panels are represented the major temporal anatomical landmarks in the rhesus macaque, human, chimpanzee, and gorilla (brains not to scale). In top part of the panels, we represented the temporal tracts obtained in the different species. Blue, MdLF; green, IFOF; yellow, ILF (macaque) or ILFmed (human); red, ILFlat; pink, AF. AF: arcuate fascicle; FG: fusiform gyrus; IFOF: inferior fronto-occipital fascicle; ILF: inferior longitudinal fascicle; ILFlat: inferior longitudinal fascicle lateral; ILFmed: inferior longitudinal fascicle medial; ITG: inferior temporal gyrus; MdLF: middle longitudinal fascicle; MTG: middle temporal gyrus; mya: million years ago; STG: superior temporal gyrus.

We studied examples of two nonhuman great apes, the gorilla and the chimpanzee. Although their temporal lobe organization seems generally similar, some differences were apparent. Because it seems that the sulcal anatomy of the gorilla and chimpanzee differs in how clearly defined their fusiform gyrus is, we could expect differences in their long-range connectivity as well, but because of the scarcity of the gorilla's data consisting of one hemisphere, we should be careful in interpreting them. One observation concerns the gorilla's

ILF, which seems less clearly subdivided than in the chimpanzee. We can also notice that the IFOF reaches the frontal lobe to a lesser extent and is more biased toward the posterior projections, as well as not invading the lateral middle temporal gyrus as much, as seen in chimpanzee. Finally, we can also raise the point that the AF shows even less invasion of the temporal lobe than in chimpanzee, looking more similar to that of the macaque. Overall, this study would suggest that the limited expansion of the temporal lobe in the gorilla leads to a less complex pattern of white matter organization than that observed in the chimpanzee.

The IFOF carries fibres from occipital cortex through the length of the temporal cortex into the frontal cortex. This tract is frequently discussed in the human literature, but its existence in the macaque monkey has been controversial (Forkel et al., 2014). It should be noted, however, that most macaque studies are based on tracer injections, which identified monosynaptic pathway, whereas the human results are based on tractography, which identified multisynaptic pathway and therefore usually results in larger white matter bundle. Recent studies using tractography for both species suggested the presence of an IFOF-like bundle extending all the way posteriorly to occipital cortex in both species (Mars et al., 2016a), but it has been argued that this reflects an artifact of the tractography method (Takemura et al., 2017). This issue now seems resolved by recent Klingler dissections in the macaque monkey that provide evidence for a posterior extension of IFOF even in the macaque (Decramer et al., 2018) and by similar reports in another Old World monkey species (Sarubbo et al., 2019).

However, differences in IFOF across species are notable, with human IFOF showing more extended prefrontal projection than macaque IFOF. We also noticed some differences between the two species regarding which frontal areas are mostly reached by the IFOF. The macaques' IFOF projects more to medial frontal regions than the human IFOF, which reaches mainly lateral ones. Concerning the path taken by the IFOF in the temporal lobe, a recent

exploratory study provided evidence of IFOF in the chimpanzee and suggested that most connections seeded from the middle temporal gyrus reach this fibre bundle (Mars et al., 2019). The present results confirm this finding, showing that in all species that have a middle temporal gyrus, the IFOF is the main longitudinal tract reaching it and that it is placed more laterally than in the macaque. This is interesting, given that IFOF has been suggested to carry information between language-related areas in the human brain (Makris and Pandya, 2009), especially those involved in semantic processing (Almairac et al., 2015). A previous study subdividing the human IFOF has also shown that it was the more lateral component of the IFOF that was actually connected to language-related areas as opposed to its medial components, which seem to carry more visual information (Panesar et al., 2017). The present results, showing similarity between human and great ape in possessing a lateral IFOF, suggest that an anatomical substrate enabling cognitive functions related to language existed in the common ancestor of humans and great apes but not in macaques. This demonstrates that cortical features supporting behaviour commonly associated only or especially with humans cannot be assumed to be unique to the human brain.

Evolution of linguistic abilities has often been associated with another longitudinal tract, the AF. Our results confirmed previous studies that have shown differences between primates' species (Rilling et al., 2008; Eichert et al., 2018). In humans, chimpanzees, and gorilla, we observed that the arcuate is innervating the temporal gyrus, whereas it targets only dorsal regions in macaques. Nevertheless, the extent of fibres reaching the middle temporal gyrus is substantially more elaborate in humans than in any other primate species studied to date, accounting for most of the distinctive organization of the human temporal lobe. However, because we are focusing only on the right hemisphere for the gorilla, we should be careful in generalizing this result, particularly because of the left asymmetry of the arcuate observed in humans (Eichert et al., 2018).

We have reported that the great ape ILF can be subdivided into two subcomponents, the medial and the lateral. The medial ILF of humans seems to be most similar to the macaque ILF as classically defined in tracer data (Schmahmann and Pandya, 2006b). We can try to interpret the relevance of these subcomponents for brain function, although of course, we do not claim to ascribe a function to any white matter bundle as one can for a grey matter area. A recent review of neuropsychological studies (Herbet et al., 2018) sheds light on some possible contribution of the ILF to functional networks, with one of the best described being face recognition. Damage to the ILF has indeed been associated with impairment in face tasks in humans (Wang and Olson, 2018). Although face-responsive areas have been identified in both humans and macaques (Tsao et al., 2008), their locations in the temporal lobe differ between the two species (also discussed in chapter 2). In humans, the most often described face area is the fusiform face area (FFA) (Kanwisher et al., 1997). This is located in the fusiform gyrus—a gyrus that monkeys do not possess but which is reached by the ILFmed in the present study. The main face areas in monkeys are scattered throughout the middle superior temporal sulcus and more ventral areas such as temporal area TE (Ku et al., 2011). Therefore, the finding of ILFmed being the most similar to the macaque ILF is consistent with the observation that ILFmed reaches the fusiform gyrus as macaque ILF reaches homologs of the FFA (Schmahmann and Pandya, 2006b; Ku et al., 2011). This argument is also in line with the knowledge of the chimpanzee face-processing system. Indeed, it is located in a similar location to that in humans (in the fusiform gyrus) (Parr et al., 2009), and the current study shows that the chimpanzee ILF could also be subdivided with the ILFmed reaching the fusiform gyrus.

Neuropsychological work also associates the medial part of ILF to other networks, such as the visual memory, scene perception, and the emotion recognition and valuation networks (Herbet et al., 2018), whereas lateral parts of ILF seem to be more associated with

reading, object recognition, and semantic networks. Although we need to be careful with interpreting these linkages, we can observe that the reading and semantic networks, which are more associated with uniquely human cognition, are associated to the ILFlat; the one that we showed here was the most dissimilar to the macaques' ILF.

We have used diffusion MRI data in combination with probabilistic tractography to reconstruct white matter tracts. It should be noted that there have been critiques on certain aspects of the tractography method in recent years. Mostly, these critiques pointed out that tractography can lead to the identification of false positives and that tracking toward the cortical surface is difficult because of the presence of superficial white matter systems near the grey/white matter border (Reveley et al., 2015; Maier-Hein et al., 2017). It is important to point out that the manner with which the tractography was applied here mitigates these concerns. Rather than tracking from a point on the cortical surface to another point at the cortical surface, which indeed can be problematic for tractography (Donahue et al., 2016), we focus here predominantly on the body of the tracts, which we define in a data-driven manner using anatomical priors. Reconstructing the bodies of cortical fibre bundles is generally quite reliable (Catani and Thiebaut De Schotten, 2008). Furthermore, in the one analysis in which we rely on the tracts' connections to the grey matter—namely, the diversion score analyses at the end of the results section—we do not track toward the surface but use a procedure that combines tracking from the body of the tract and tracking from all of the grey matter toward the white matter, which is less susceptible to the problems outlined above (Mars et al., 2018c).

In this study, we have used a greater range of species than is common in comparative diffusion MRI studies (Rilling et al., 2012; Hecht et al., 2013; Mars et al., 2016a; Takemura et al., 2017), which allowed us to build confidence in our conclusions. However, we acknowledge that studies using a wider range of species are still needed. We have studied two

nonhuman great ape species, the chimpanzee and gorilla, but our study neglected the Asian great apes and lesser apes, as well as taking the macaque monkey as the sole representative of the Old World monkeys. The scarcity of data in this field means that other apes and especially other Old World monkeys as well as other primate species remain to be studied, but the accelerating pace of comparative neuroimaging, of which this study is an example, means that these studies can now be considered imminent. Studies on grey matter architecture in a large number of primate species present promising examples (Heuer et al., 2019).

This study does not address the evolutionary pressures that gave rise to the cortical specializations described here. It has been suggested that cortical specializations in the prefrontal cortex along the anthropoid lineage arose from increasingly complex foraging challenges that came with new ecological niches (Passingham et al., 2017). In this framework, humans have further reduced foraging errors by relying more than other surviving great apes on mental trial and error based on mental time travel. A similar argument for temporal cortex is advanced in another monograph (Murray et al., 2016), which suggests temporal lobe modifications might have occurred in great apes and humans when they adapted to their environment by changing their social behaviour. Although it is quite difficult to relate these findings to our study, we are nevertheless able to illustrate here that any structural specialization is derived from a modification of existing machinery present in the ancestral state. Hence, to understand any one brain, understanding the organization of closely related species provides essential information. We must be cautious, however, when inferring evolutionary pressure from brains that come from distant species because they have all continued to evolve since their common ancestor.

When observing differences in white matter anatomy across species, such as those reported here, it is important to ask whether these are differences related to more general changes in brain structure, such as increased cortical folding due to a larger brain size, or

whether they represent specific adaptations to a particular niche. These different types of changes are often difficult to disentangle (Krubitzer and Kaas, 2005; Eichert et al., 2020). It is known that expansion of temporoparietal cortex has occurred many times in the primate lineage (Chaplin et al., 2013), and this might underlie some of the so-called uniquely human organization of the temporal cortex, such as the ventral location of the middle temporal area (Large et al., 2016). However, such general mechanisms cannot describe the phenomenon of "mosaic evolution," which demonstrates that expansion can be selective to certain brain structures in certain lineages (Barton and Harvey, 2000). Similarly, these general mechanisms cannot predict the results observed here, i.e., increased complexity of the ILF in great apes and extension of the AF only in humans. Indeed, the AF extension in humans has been generally interpreted as a unique adaptation rather than a result of general mechanisms in the language literature (Friederici, 2012; Catani and Bambini, 2014; Xiang et al., 2015). Of course, this does not mean that the developmental mechanisms that give rise to these adaptations need not be the same generic mechanisms at work in all primates, but it does imply that the specific tracts can be a unique adaptation (Ardesch et al., 2019).

In sum, we show a more elaborate picture of temporal cortex white matter organization across selected species of the order Primates than previously demonstrated. The human expansion of the AF has become one of the most established results of early comparative diffusion MRI studies, but here we show the beginning of a more complete picture, focusing in particular on occipital–temporal systems subserved by the IFOF and ILF. The changes in these tracts result in unique connectivity profiles of the temporal cortex grey matter in humans and other great apes, which has important implications for differences in their behavioural abilities.

Chapter 4 - Cortical morphology and white matter tractography of three phylogenetically distant primates

Roumazeilles L, Lange FJ, Benn RA, Andersson JLR, Bertelsen MF, Manger PR, Flach E, Khrapitchev AA, Bryant KL, Sallet J, Mars RB (2021) Cortical morphology and white matter tractography of three phylogenetically distant primates: Evidence for a simian elaboration. *Cereb Cortex*. DOI: 10.1093/cercor/bhab285

4.1 Abstract

Comparative neuroimaging has been used to identify changes in white matter architecture across primate species phylogenetically close to humans, but few have compared the phylogenetically distant species such as simians and prosimians. Here, we acquired *post mortem* diffusion imaging data from ring-tailed lemurs (*Lemur catta*), black-capped squirrel monkeys (*Saimiri boliviensis*) and rhesus macaques (*Macaca mulatta*). We were able to establish templates and surfaces allowing us to investigate sulcal, cortical and white matter anatomy. The results demonstrate an expansion of the frontal projections of the superior longitudinal fascicle complex in squirrel monkeys and rhesus macaques compared to ring-tailed lemurs, which correlates with sulcal anatomy and the lemur's smaller prefrontal granular cortex. The connectivity of the ventral pathway in the parietal region is also comparatively reduced in ring-tailed lemurs, with the posterior projections of the inferior longitudinal fascicle not extending toward parietal cortical areas as in the other species. In the squirrel monkeys we note a very specific occipito-parietal anatomy that is apparent in their surface anatomy and the expansion of the posterior projections of the optic radiation. Our study supports the hypothesis that the connectivity of the prefrontal-parietal regions became relatively elaborated in the simian lineage after divergence from the prosimian lineage.

4.2 Introduction

Comparative neuroscience is an important approach for understanding general brain anatomy and function. Macaques are one of the most commonly studied nonhuman primate species for both ethical and practical reasons (Manger et al., 2008; Perretta, 2009). Cercopithecids (Old World monkeys), such as macaques, shared a

common ancestor with the Hominoids (the apes including humans) around 25 million years ago (Perelman et al., 2011). With the Platyrrhines (New World monkeys), the Cercopithecids and Hominoids form the infraorder Simiiformes (simian primates), thought to share extensive neuroanatomical similarities. Such similarities are the basis of the translational paradigm in neuroscience, using model species to understand the human brain. However, primates also demonstrate specific mosaic evolution even when correcting for the size of the brain (Smaers and Soligo, 2013). Therefore, it is important to compare brain organization in a range of different species to understand how closely the neuroanatomy of traditional animal models parallels human brain organization, but also to elucidate broader principles of neuroanatomical diversity across primates, and to reveal potential species-specific specializations.

Neuroimaging techniques, such as magnetic resonance imaging (MRI), have recently come of age as a tool for whole-brain comparative anatomy (Mars et al., 2014; Rilling, 2014). Although MRI provides an indirect quantification of anatomy and is of coarser resolution than classical anatomical techniques, it allows fast, whole-brain quantification of potentially multiple modalities from a single brain (Lerch et al., 2017). These data can, in turn, be related to histological results where they are available (Large et al., 2016; Reveley et al., 2017). Several software packages also permit the reconstruction of cortical brain surfaces from MRI data, which allows investigation of cortical morphology. MRI-based investigations of white matter anatomy in species across the primate order is also facilitated by standardized tools, leading to the creation of white matter atlases of the human, chimpanzee, and macaque brain (Bryant et al., 2020; Warrington et al., 2020).

Comparative neuroimaging studies of white matter architecture in primates have revealed evidence for an expansion of the frontal association tracts in humans compared

to other species (Rilling et al., 2008; Barrett et al., 2020; Eichert et al., 2020), as well as more elaborated white matter organization within the great ape ventral visual stream compared to macaques (chapter 3); however, such studies have rarely included Platyrrhines and Strepsirrhines (prosimian primates), focusing instead on the Cercopithecids. This is despite the fact that important brain characteristics emerged in Simiiformes and continued to evolve in this lineage. Such characteristics include additional granular prefrontal cortical areas and more extensive fronto-parietal connectivity (Preuss and Goldman-Rakic, 1991; Krubitzer, 2009). These novel characteristics have been interpreted as adaptations to specific lifestyles and environments (Passingham and Wise, 2012; Genovesio et al., 2014).

Here, we study the neuroanatomy of ring-tailed lemurs *(Lemur catta)*, black-capped squirrel monkeys *(Saimiri boliviensis)*, and rhesus macaques *(Macaca mulatta)*, using high resolution diffusion MRI in *post mortem* samples. All three species are diurnal primates, live in large multi-male/multi-female groups, and are at least partly arboreal. By taking advantage of newly developed tools, we established robust MRI templates and reconstructed the cortical surfaces. Using tractography in conjunction with the templates, we reconstructed white matter tracts for the three species while the surfaces allowed us to examine their cortical, sulcal and white matter organization. This enabled us to investigate how changes in brain organization, previously seen across simians, compare to differences with species belonging to other phylogenetic lineages. Specifically, we hypothesized that long-range association tracts might be less extensive in prosimian primates compared to simians.

4.3 Materials and methods

4.3.1. Data

For this study we used, three *post mortem* brains from each of the following species: ring-tailed lemurs (*L. catta,* between 3 and 11 years, 3 males), black-capped squirrel monkeys (*S. boliviensis,* between 2 and 19 years old, 1 female, 2 males) and rhesus macaques (*M. mulatta,* between 11 and 15 years old, 1 female, 2 males). The samples were obtained from Copenhagen Zoo (lemurs and squirrel monkeys), the Zoological Society of London (squirrel monkey), and the University of Oxford's Biomedical Sciences (macaques). All brains were extracted and fixed within 24 h after the death of the animal. The brains from the Copenhagen Zoo were obtained after the animals had been euthanized with sodium pentobarbital (intravenous) in line with population management decisions, independent of the current study (Bertelsen, 2019). Once euthanized, the carotid arteries were immediately cannulated, and the heads were perfused with an initial rinse of 0.9% saline (1 l/kg) solution at a temperature of 4°C followed by 4% paraformaldehyde in 0.1 M phosphate buffer (PB) (1 l/kg) at 4°C. The brains, which showed no signs of neuropathology, were removed from the skull and post-fixed in 4% paraformaldehyde in 0.1 M PB (24 h at 4°C). The brains were subsequently formalin-fixed in a phosphate-buffered saline (PBS) solution and shipped to Oxford in PBS. The brain from the Zoological Society of London was obtained after the death of the animal from a range of age-related conditions. No evidence of brain pathology was noticed during the necropsy. The brain was fixed in a 10% neutral buffered formalin solution and transported to Oxford in formalin. The brains from the University of Oxford's Biomedical Sciences were obtained after the animals had been euthanized for reasons unrelated to this study. Immediately after death, the brains were

perfusion fixed with formalin and stored in a 10% neutral buffered formalin solution with azide.

4.3.2. Imaging protocol

All brains were rehydrated in a PBS solution 1 week prior to scanning and placed in fomblin or fluorinert for the scanning procedure. The diffusion-weighted MRI data were acquired from the whole brain using a 7T preclinical MRI scanner (Varian, Oxford UK). The scanner bore diameter is 210 mm, the gradient coil references are the following: 205_120_HD (Varian, Oxford UK) with a Gmax of 50 G/cm. The radiofrequency coil was made by Rapid Biomedical GmbH (Rimpar, Germany) and is a birdcage transmit receive coil with 72mm ID. We used a 2D diffusion-weighted spin-echo multi-slice protocol with single line readout (DW-SEMS; TR = 10 s; TE = 26 ms; Matrix size = 128 x 128 with a sufficient number of slices to cover each brain; resolution for lemurs and squirrel monkeys: 0.5 x 0.5 x 0.5 mm^3, and resolution for macaques: 0.6 x 0.6 x 0.6 mm^3). 16 non-diffusion-weighted (b = 0 s/mm^2) and 128 diffusion-weighted (b = 4000 s/mm^2) volumes were acquired with diffusion encoding directions evenly distributed over the whole sphere (single shell protocol). To assess the data quality, we computed the signal to noise ratio (SNR) for each individual scans from the diffusion weighted volumes. The SNR was defined as the ratio between the mean signal in the brain and the mean signal outside the brain. We also computed the mean fractional anisotropy (FA) and mean diffusivity (MD) in the white matter of each individual, as well as in the corpus callosum. Values for these measures are comparable between individuals, species, and brain providers (Figure 4.1).

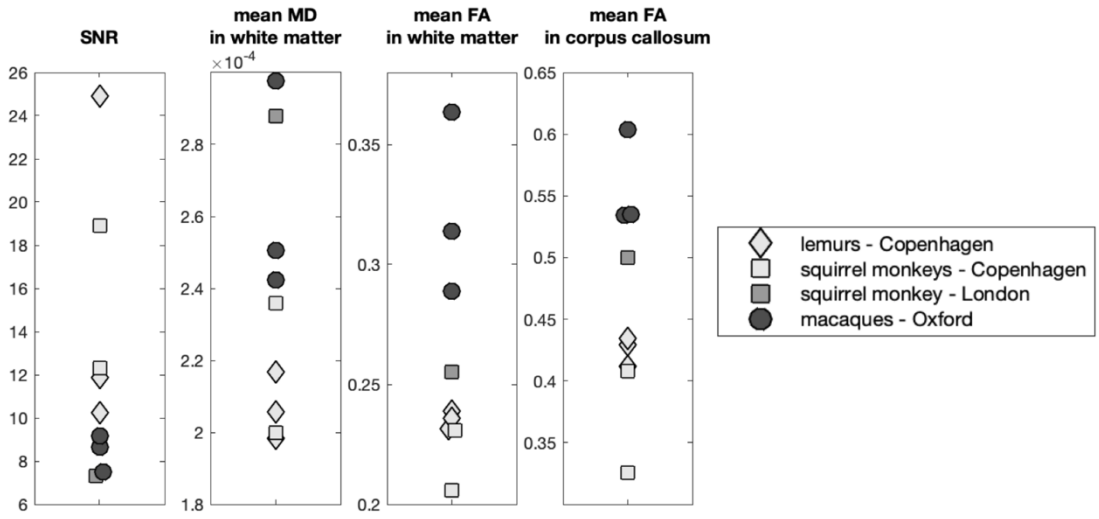

Figure 4.1 Data quality assessment.

For each individual, the values of SNR, mean MD and mean FA in white matter as well as mean FA in the corpus callosum are reported. The marker shape code identifies the different species while the colour code identifies the provenance of the brain as indicated in the legend. FA: fractional anisotropy; MD: mean diffusivity; SNR: signal to noise ratio.

4.3.3. Diffusion MRI data preprocessing

All data were preprocessed using the same protocol implemented in the module *phoenix* of the MR Comparative Anatomy Toolbox (Mr Cat; www.neuroecologylab.org). Briefly, the steps are as follows: We first converted the datasets to NIFTI format, then built an image based on the volumes acquired without a diffusion gradient as well as a binary mask of this image. Using tools from FSL (www.fmrib.ox.ac.uk/fsl), we then fitted a diffusion tensor model using FSL's *dtifit* including saving the tensor image which is used in the subsequent template creation. The principal direction image helped to reorient the data to approximate ACPC (anterior commissure-posterior commissure) conventional orientation which sets the origin at the middle of the anterior commissure, where a small bundle of fibres decussates. Following the preprocessing, *bedpostX* (Behrens et al., 2007) was used to fit a crossing fibre-model to the data, allowing for three fibre orientations.

4.3.4. Template creation

We created templates for each of the species using a method described previously (Lange et al., 2020b). This method employs a registration based, multi-resolution, iterative template creation strategy including spatial unbiasing of both affine and nonlinear shape changes. Registration is performed using the MultiMOdal Registration Framework (MMORF) (Lange et al., 2020a). MMORF is a multimodal registration tool for simultaneous alignment of datasets with both scalar and tensor MRI images. Multimodal registration offers advantages over traditional registration algorithms, as it is able to exploit the fact that different imaging modalities provide distinct types of information (e.g., intensity and orientation) and often contain most information at different locations in the brain. Here, we used the no-diffusion images with T2 contrast (*nodif*) and the tensor images from FSL's *dtifit* (*dti_tensor*). As these images were generated from the same raw diffusion weighted data, they were already co-registered for each individual and have been oriented to approximate the ACPC convention.

Any residual non-brain tissue remaining after dissection was excluded from the images using a manually defined brain mask in order to avoid artefacts in the resulting templates. The scalar images were intensity bias-field corrected using FSL's *FAST* tool (Zhang et al., 2001) and globally intensity normalized. Next, a random individual was chosen as an initial template space and all three individual scalar images were then affine registered to this space using *FLIRT* (Jenkinson and Smith, 2001). The mid-transformation matrix was obtained to unbias the template toward any individual and the scalar images were then resampled to this unbiased reference and voxelwise averaged across subjects. This averaged image required rigid reorientation to match the ACPC orientation. The rigid reorienting matrix was combined with the previous affine

matrix to obtain our final affine transformation matrix. This was then applied to both scalar and tensor images (using FSL's *applywarp* and *vecreg* commands respectively) and the resulting images were averaged across each modality separately, using a log-tensor averaging for the tensor images, creating our initial scalar and tensor templates. Both images from each subject were then smoothed and simultaneously nonlinearly registered to the initial template at a coarse warp resolution (16 mm isotropic). This process was repeated, doubling the warp resolution every other iteration and reducing the amount of smoothing, for a total of 10 iterations (final warp resolution of 0.5 mm isotropic for lemurs and squirrel monkeys and 0.6 mm isotropic for macaques). At each iteration, the warps describing the transformation from the template space to subject space were spatially unbiased and the resampled images obtained with these warps were averaged as before to create the next template iteration. MMORF uses a cubic B-spline elastic transformation with mean squared error as the scalar cost function, mean squared Frobenius norm as the tensor cost function, and regularization based on the singular values of the local Jacobian field to ensure warps remain diffeomorphic. The combination of scalar, tensor and regularization cost functions results in warps which maximize grey and white matter tissue-type overlap, as well as correctly registering location and orientation of white matter bundles, while adhering to biologically plausible set of deformation constraints.

Each individual fractional anisotropy image and mean principal diffusion direction distribution (in vector form, output of *bedpostX*) were transformed to the template space using the *applywarp* and *vecreg* FSL commands respectively. We then averaged these images across individuals of the same species, to obtain mean principal diffusion image and mean fractional anisotropy image in template space.

4.3.5. Surfaces creation and labelling

Surface creation

Surfaces were generated with the preclinical surface pipeline *precon_all (*https://github.com/neurabenn/precon_all). *precon_all* is a minimalist adaptation of Freesurfer's (Fischl, 2012) recon-all pipeline, aiming to provide broad flexibility to reconstruct cortical surface meshes without a known segmentation or parcellation scheme. This allows *precon_all* to generate cortical surface meshes in lesser studied animal models. It consists of a modularly designed pipeline and can run brain extraction, tissue segmentation, white matter filling, and surface generation in a continuous workflow on images with a T1-like contrast. To accommodate this, we converted the T2 contrast of our templates to obtain T1-like contrast images, using FSL tools. We inverted the intensities by multiplying the template image by -1 and adding the maximum intensity of the initial image, making sure the cerebrospinal fluid and ventricle intensities remained at zero.

In all three templates, we ran *precon_all* twice; the first run used the automated segmentation from ANTs Atropos (Avants et al., 2009), and the second used a hand-edited WM mask. The WM segmentation was filled with hand-drawn "subcortical" and "non-cortical" masks. The subcortical mask is an inclusion mask and begins at the superior border of the corpus callosum and fills the subcortex between the outer borders of the left and right lateral ventricles. The non-cortical mask lies directly posterior and inferior to the subcortical mask and includes the cerebellum and brainstem. Both subcortical and non-cortical masks were drawn using ITK-SNAP (www.itksnap.org, (Yushkevich et al., 2006)). The filling process uses these masks to remove the cerebellum and brainstem and fill the subcortex between the lateral ventricles beneath the corpus callosum. This created the prerequisite volumetric image that can be used to

create white, pial, and mid-thickness surfaces. The final surfaces presented here all use a hand-edited WM mask and they were downsampled in connectome workbench to a normal sphere with 10,242 vertices.

Surface labelling

For visual comparison with known anatomical regions, we also labelled sulci and specific areas on the cortical surface. Major sulci were labelled on the cortical surface of the rhesus macaque and squirrel monkey using the terminology used for the macaque by Petrides (2005, 2011). For the ring-tailed lemurs, apparent similarities in sulcal patterns could be observed but only few studies existed on this genus with a lack of consensus on the labelling to be used for some sulci (Mott and Kelley, 1908; Brodmann, 1909; Connolly, 1936; Radinsky, 1975). Therefore, to be consistent with the macaque terminology, we refer to the ambiguous lemur sulci with a ”l” prefix to reflect on their probable homology or at least the shared topography with the macaque sulci.

Cortical labels were drawn from previous illustrations on the surface using Connectome Workbench tools (Marcus et al., 2011). For the lemur, the primary visual (V1) and motor cortex (M1) borders were based on illustrations from histological studies (Mott and Kelley, 1908; Fasemore et al., 2018). For the squirrel monkey these borders were based on the VALiDATe29 atlas, providing surface borders based on histological data (Schilling et al., 2017). For the macaque, V1 and M1 borders were based on several histological atlases that have been adapted to standard macaque surface (von Bonin and Bailey, 1947; Paxinos et al., 2000). For the prefrontal (PF) cortex, we used the definition from Passingham and Wise (2012) which defines PF as all the areas anterior to any of the premotor and supplementary motor areas. For PF and granular areas in the macaque and squirrel monkey, we used illustrations from a

relevant book (Passingham and Wise, 2012), completed by illustrations from another squirrel monkey source (Rosabal, 1967). There exists only a limited amount of studies about the ring-tailed lemur prefrontal cortex, therefore we combined illustrations of another prosimian, the bushbaby (Preuss and Goldman-Rakic, 1991), with the previously mentioned lemurs' illustrations (Mott and Kelley, 1908) to estimate the extent of the lemur PF cortex and its granular areas.

4.3.6. Tractography

The tracts were reconstructed using probabilistic tractography as implemented in the *Xtract* tool (Warrington et al., 2020). We defined tractography seed, target, and exclusion masks in the template space of each species. These were then transformed to the diffusion space of each individual using the warps obtained during the template creation. We defined all masks to be in as similar an anatomical position as possible in all three species, based on anatomical landmarks (see details below). The tractography algorithm starts from the seed, the streamlines follow local orientations sampled from the posterior distribution given by *bedpostX* and only the streamlines that reached or passed through the target and not through the exclusion mask were conserved. All the *Xtract* options were the default, only the step length was adjusted to 0.2 mm to reflect the small voxel and brain size of our data. In each seed voxel 10,000 samples were seeded. The output of the tractography is a tractogram image which represents the fibre probability distribution. For all protocols, a second tractography was run inverting the roles of the seed and target and the resulting tractogram of the two protocols were added and normalized by dividing the path distribution by the total number of generated streamlines not rejected by target or exclusion mask criteria. This normalized tractogram obtained for each subject was transformed back to the template space,

averaged across subjects and log-transformed to obtain a value between zero and one, facilitating the threshold determination. We used a threshold of 0.8 which resulted in selecting the most similar higher densities of streamlines reaching each voxel for all tracts and all species.

We will now detail the tractography recipes used for each tract (Figure 4.2). The recipes are based on the *Xtract* recipes for the macaque and previous literature (Bryant et al., 2020, 2021). As all the tracts reconstructed here are unilateral, all exclusion masks contain a sagittal plane at the midline to avoid streamlines crossing to the other hemisphere.

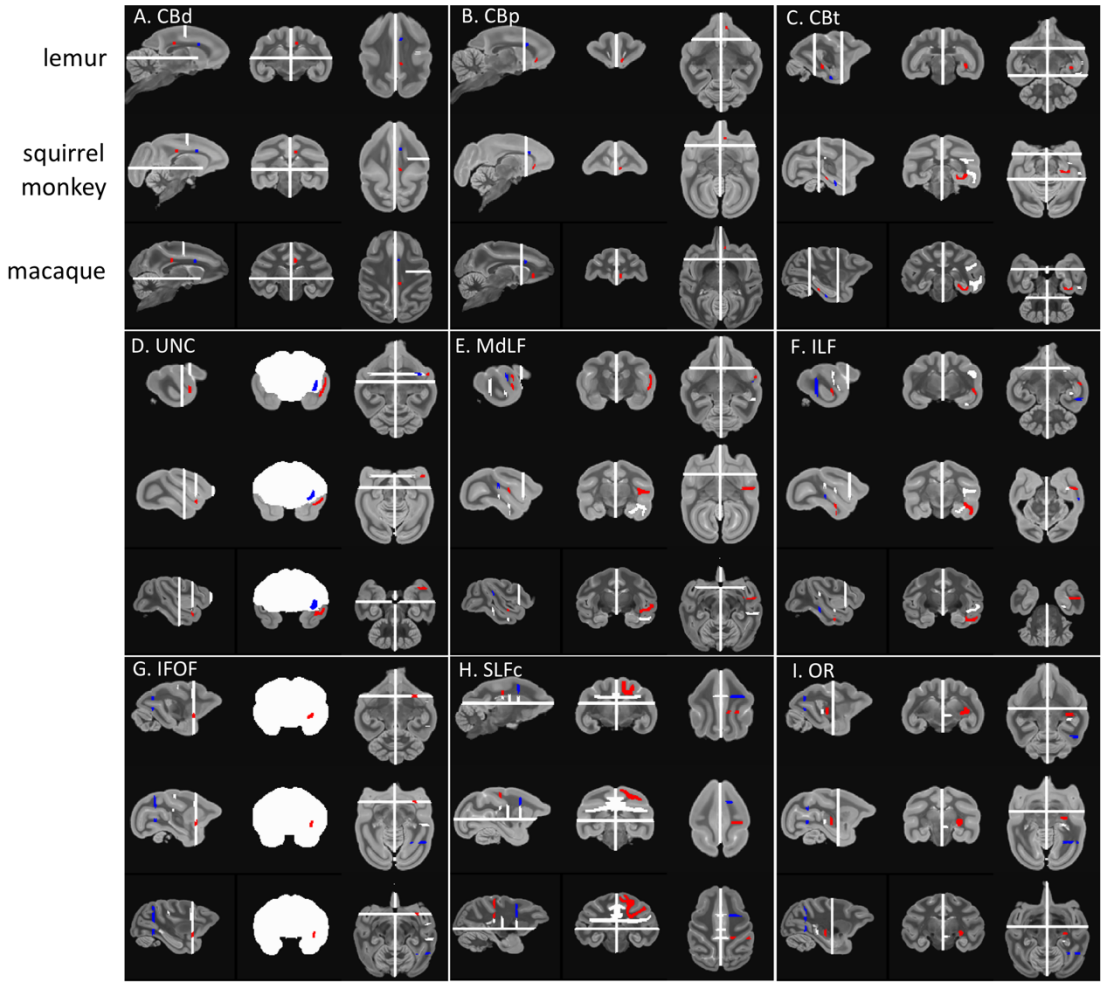

Figure 4.2 Tractography recipes for lemurs, squirrel monkeys and macaques.

The seed mask (red), the target mask (blue) and the exclusion mask (white) are represented for the left hemisphere protocols on the template image for each species in radiological convention. *(figure legend continues on the following page)*

CBd/p/t: dorsal/peri-genual/temporal part of the cingulum bundle; IFOF: inferior fronto-occipital fascicle; ILF: inferior longitudinal fascicle; MdLF: middle longitudinal fascicle; OR: optic radiation; SLFc: superior longitudinal fascicle complex; UNC: uncinate fascicle.

Cingulum bundle (CB)

The CB has previously been segmented based on the presence of fibres connecting specific targets (Heilbronner and Haber, 2014). This segmentation has informed previous tractography protocols reconstructing the CB in primates leading to the adaptation of a three sections protocol to capture the entirety of the CB (Bryant et al., 2020; Warrington et al., 2020). We reconstructed the CB in three different sections: dorsal (CBd), peri-genual (CBp), and temporal (CBt). The seed and target of the CBd were placed in the white matter of the cingulum gyrus. Dividing the corpus callosum in three equal segments, the seed of the CBd was placed at the front of the most posterior segment (Figure 4.2A). Its target was placed at the start of the genu of the corpus callosum. The exclusion mask was made of a coronal mask through the territory of the SLFc at the level of the midpoint of the corpus callosum and an axial mask below the corpus callosum to avoid invading the SLFc territory and the CBt respectively. The seed of the CBp was placed at the ventral terminal point of the genu of the corpus callosum and its target in the dorsal end of the genu (Figure 4.2B). The exclusion mask was made of a coronal plane just anterior to the temporal lobe to restrict the tractography to this specific CB section. The seed and target of the CBt were placed in the white matter just inferior to the parahippocampal gyrus posterior and anterior respectively (Figure 4.2C). The exclusion mask was made of a coronal plane at the level of the midpoint of the extreme/external capsule, a coronal plane posterior to the corpus callosum and the seeds and targets of the MdLF and ILF to avoid invading occipitotemporal or extreme/external capsule fibres.

Uncinate fascicle (UNC)

The UNC was reconstructed by placing a seed in the superior temporal gyrus where the temporal and frontal cortices are first separated and a target in the same coronal section but in the ventral part of the extreme capsule (Figure 4.2D). The exclusion mask was made of a frontal coronal section at the level of the seed and target but excluding the seed and target, a posterior coronal section to avoid invading the temporal tracts and a frontal dorsal coronal section to avoid invading dorsal tracts.

Middle longitudinal fascicle (MdLF)

The MdLF was reconstructed by placing a seed in the superior temporal gyrus on a coronal slice slightly anterior to the central sulcus (Figure 4.2E). Its target was placed posteriorly in the superior temporal gyrus, just anterior to the posterior terminus of the Sylvian fissure. The exclusion mask was made of a frontal coronal mask through the extreme capsule and seeds and targets from the ILF, CBt and IFOF to prevent leakage in these fibres.

Inferior longitudinal fascicle (ILF)

The ILF was reconstructed by placing a seed in the anterior inferior temporal gyrus on a coronal slice slightly anterior to the central sulcus (Figure 4.2F). Its target was placed posteriorly in the inferior temporal gyrus, just anterior to the posterior terminus of the Sylvian fissure. The exclusion mask was made of a frontal coronal mask through the extreme capsule and seeds and targets from the MdLF, CBt and IFOF to prevent invading these fibres.

Inferior fronto-occipital fascicle (IFOF)

We reconstructed the IFOF by placing a seed in the extreme capsule where it connects temporal and frontal cortex and a target as a coronal plane just anterior to the lunate sulcus (Figure 4.2G). The exclusion mask was made of a coronal mask encompassing the whole white matter except the seed at the level of the seed to avoid spurious anterior posterior fibres and the seeds and targets from MdLF, ILF and SLFc to prevent invading these tracts.

Superior longitudinal fascicle complex (SLFc)

We reconstructed the SLFc as a complex of the three SLF branches (Thiebaut de Schotten et al., 2011a). The seed was defined as a large coronal mask in the parietal cortex immediately posterior to the dorsal end of the central sulcus (Figure 4.2H). The target was also a large coronal mask in the territory of the SLFc at the level of the anterior commissure. The exclusion mask was made of an axial exclusion below the corpus callosum to avoid invading temporal tracts, and three coronal masks in the cingulate gyrus, two of them at the same coronal level as the seed and target and one in between, in the region of midpoint of the central sulcus, to avoid invading the cingulum bundle. Three additional coronal exclude masks were placed at the same level in the external and internal capsule to avoid invading these fibres. Finally, the seeds and targets from the MdLF recipe were added to the exclusion to make sure the SLFc did not invade ventral pathways.

Optic radiation (OR)

We reconstructed the OR by placing a seed in the lateral geniculate nucleus and a target as a coronal plane just anterior to the lunate sulcus (Figure 4.2I). The exclusion

consisted of an axial block of the brainstem, a coronal block directly posterior to the lateral geniculate nucleus to select only fibres that curl around dorsally, and a coronal plane just anterior to the seed to prevent invading the longitudinal fibres.

We used a Matlab in-house routine to produce three dimensional visualization of the averaged log-transformed tractograms for each species, to facilitate the study and the representation of the whole tract anatomy (as seen in subpanel A of tract result figure).

Control analyses

We ran two additional control analyses. The first aimed to confirm that the ILF did not reach parietal cortex in the lemur. Our previous protocol reconstructed the tracts based on seeds and targets placed in the core of the tract, letting the extremities to be defined by the tractography algorithm. For this control, we therefore used a modified protocol in which we placed the seed at the posterior extremity in the parietal cortex and the target at the anterior extremity in the temporal pole and assessed the likelihood of reconstructing a white matter bundle with such protocol. We used the MdLF for comparison as it reaches the parietal cortex in all three species and runs parallel to the ILF in the temporal lobe. The modified protocols used the same seed and exclusion for both ILF and MdLF, only the targets changed. In more details, the common large seed was placed in the axial plane encompassing the ventral posterior parietal cortex of the three species (Figure 4.3A). We used the same exclusion masks as previously defined for the main tractography of MdLF and ILF except that we did not include the seeds and targets of these tracts. The ILF target was placed in the anterior inferior temporal gyrus (Figure 4.3B) and the MdLF target in the anterior superior temporal gyrus (Figure

4.3C). These targets contained the same number of voxels for ILF and MdLF in all species. To account for the plausibility of the tracts, we then computed the ratio of streamlines surviving these two tractography protocols. If only a few streamlines survive the target and exclusion criteria, it means that a tractography protocol is unlikely to reconstruct one of the major white matter bundles, such as ILF and MdLF. Therefore, by comparing the number of surviving streamlines with these two similar protocols we can assess how likely the ILF reaches the parietal cortex. If the ratio of streamlines surviving with the MdLF target compared to the ILF is very high, it means that MdLF reaches parietal cortex more than ILF and vice versa.

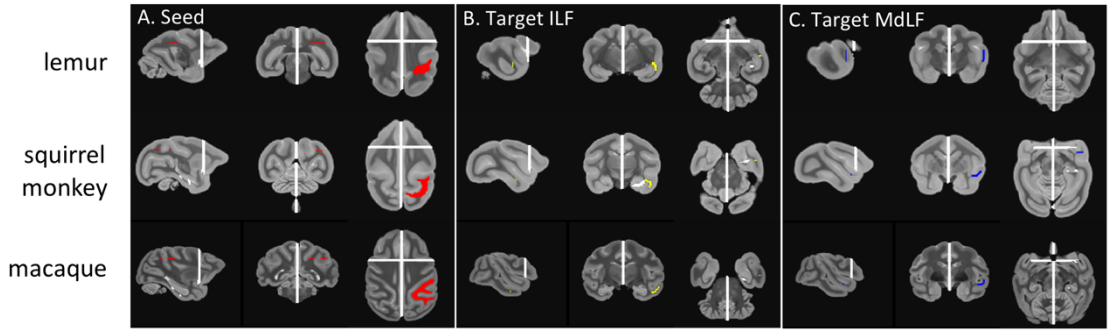

Figure 4.3 Additional tractography recipes.

A. The seed mask (red), **B.** the target mask for ILF (yellow) and **C.** MdLF (blue), and the exclusion mask (white) are represented for the left hemisphere protocols on the template image for each species in radiological convention. ILF: inferior longitudinal fascicle; MdLF: middle longitudinal fascicle.

The second control analysis aimed to confirm the inter-species findings concerning the SLFc and OR. To ensure these effects are not due to changes in overall brain size, we aimed to show that tracts running in similar parts of the brain showed dissociable changes between species. If this proved to be the case, our results cannot simply be ascribed to differences due to overall scaling of the white matter. From the results of the initial tractography, we have noticed that the CB, an evolutionarily

conserved tract (Bubb et al., 2018) follows a similar course across species; its dorsal component runs through the dorsal part of the cortex parallel to the SLFc, while its temporal component runs close to part of OR. Therefore, we calculated the ratio between the number of voxels reached by SLFc and OR and the number of voxels reached by the CB segment running in a similar part of the cortex.

4.3.7. Surface projection maps

Cortical surface representations were obtained for each tract of each species to investigate the cortical territory reached by the tracts. We used a recently developed approach to reduce the issues caused by gyral bias and superficial white matter (Reveley et al., 2015). This approach is to multiply the tractograms obtained with a whole brain connectivity matrix (Mars et al., 2018c). For each species, we obtained an average matrix across subjects representing the connectivity between all the vertices of the cortical surface and all the voxels in the brain volume. We used the brain extracted template image and the template surface generated above for each species. Each of the tracts from the tractography (not log normalized nor thresholded) was multiplied to this average matrix, to obtain a map representing their connectivity with the cortical surface. The result was smoothed using a gaussian surface smoothing kernel of 1 mm using the *cifti-smoothing* command from Connectome Workbench (Marcus et al., 2011) and log transformed and thresholded at 0.8 as per the tractography result.

4.4 Results

In this study, we acquired diffusion MRI data from three primate species representing three distinct lineages: strepsirrhines (ring-tailed lemur), platyrrhines (black-capped squirrel monkey) and cercopithecids (rhesus macaque). The dataset is of

high quality and three individual brains were used for each of the species, allowing us to establish templates using a recently presented multimodal registration method (Lange et al., 2020b), and surfaces using a modified version of previous tools (Benn et al., 2020). In turn, these allowed us to investigate and compare the cortical, sulcal and white matter anatomy of the three species.

4.4.1. Cortical surface

Cortical surface reconstructions reveal that all three species show some degree of cortical folding (Figure 4.4A), but this is most apparent in the macaque, with the squirrel monkey showing the least evidence for deep sulci in the occipital, and to a lesser extent, frontal cortex. Due to the lack of consensus in the literature, we adapted the macaque terminology and added a "l" prefix for the ring-tailed lemur sulci. The squirrel monkey cortical surface shows a very lissencephalic anatomy with only two very pronounced sulci, the lateral sulcus (LaS, also called Sylvian fissure) and the superior temporal sulcus (STS) (Figure 4.4B). We could also observe three other sulci in all three species: the principal sulcus (PS), the central sulcus (CeS), and the intra-parietal sulcus (IPS). However, we are cautious in labelling these sulci in lemurs as previous reports have disagreed in their labelling. It is evident from the surface reconstruction that the PS extends more posteriorly in lemurs than in the other species, even merging with the IPS. This had been previously interpreted as a unique sulcus called the coronal sulcus, similar to what is observed in non-primate mammals (Radinsky, 1975), while others have kept them separated (Mott and Kelley, 1908). Others have argued that the lemur CeS is actually formed by both the CeS (as indicated here) and the posterior portion of the PS (Connolly, 1936). Posteriorly, the IPS is substantially more extensive in lemurs and macaques than in squirrel monkeys. The

border between occipital and parietal cortex (marked with an arrow in Figure 4.4A) suggests that much more of the dorso-caudal surface of the occipital lobe is occupied by visual cortex in squirrel monkeys than in the other species studied.

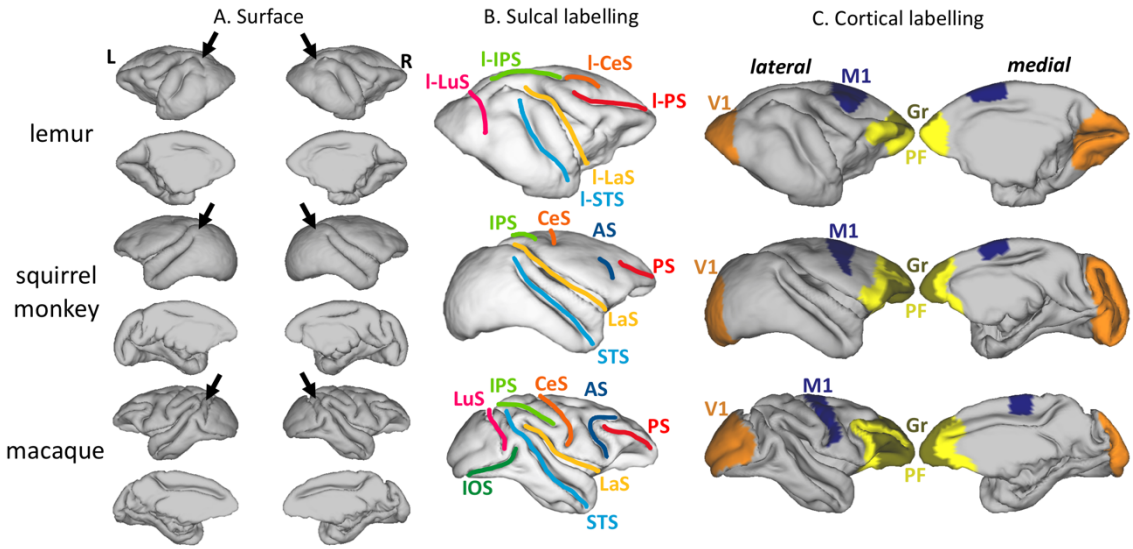

Figure 4.4 Cortical surface labelling.

A. Pial cortical surfaces of ring-tailed lemurs, black-capped squirrel monkeys and rhesus macaques obtained from the template. The arrows indicate the dorsal most location of the occipito-parietal cortex in the three species. L denotes the left hemisphere; R denotes the right hemisphere. **B.** Labelling of the sulci on the lateral mid-thickness surfaces. Note the 'l' prefix for the lemur sulci. **C.** Labelling of the primary visual cortex (V1), primary motor cortex (M1), prefrontal cortex (PF) and its granular areas (Gr) on the right hemisphere mid-thickness cortical surfaces. AS: arcuate sulcus; CeS: central sulcus; IOS: inferior occipital sulcus; IPS: intra-parietal sulcus; LaS: lateral sulcus; LuS: lunate sulcus; PS: principal sulcus; STS: superior temporal sulcus.

To put this cortical labelling in context, it is helpful to compare the sulcal anatomy to known cytoarchitectonic subdivisions in the three species. We labelled primary visual cortex (V1), primary motor cortex (M1), prefrontal cortex (PF) and the granular part of prefrontal cortex (Gr) in the three species (Figure 4.4C) based on existing anatomical atlases (Mott and Kelley, 1908; von Bonin and Bailey, 1947; Paxinos et al., 2000; Schilling et al., 2017), and found that the morphology and cortical territory of V1 differs substantially across species. V1 shows a very different folding

pattern in lemurs compared to the two other species, apparent in the dorsally rotated orientation of the calcarine sulcus. Furthermore, V1 occupies proportionally more cortical surface area in the squirrel monkey (30% of total surface in squirrel monkeys, against 21% and 15% respectively for lemurs and macaques). The absolute size of V1 is also bigger in squirrel monkeys compared to lemurs, which have brains of similar size so we can infer that there is a specific increase in size for V1 in squirrel monkeys compared to lemurs. The expansion of PF in squirrel monkeys and rhesus macaques can be illustrated by comparing on the medial surface the locations and sizes of M1 and PF, which appear further apart, and PF covers more areas in squirrel monkeys and rhesus macaques than in ring-tailed lemurs. The large arcuate sulcus in rhesus macaques also increases the cortical territory of PF on the lateral surface. PF contains more granular territory in squirrel monkeys and rhesus macaques compared to that of ring-tailed lemurs, as is confirmed by the ratios of granular surface to prefrontal surface: 15% in lemurs compared to 30% and 43% respectively in squirrel monkeys and rhesus macaques.

4.4.2. White matter anatomy

We reconstructed several white matter tracts using probabilistic tractography. We employed similar recipes in the three species based on common anatomical features and principal direction images identifying landmarks for white matter tract definition (Figure 4.5). All the tracts are displayed as a 3D reconstruction and as a projection to the cortical surface.

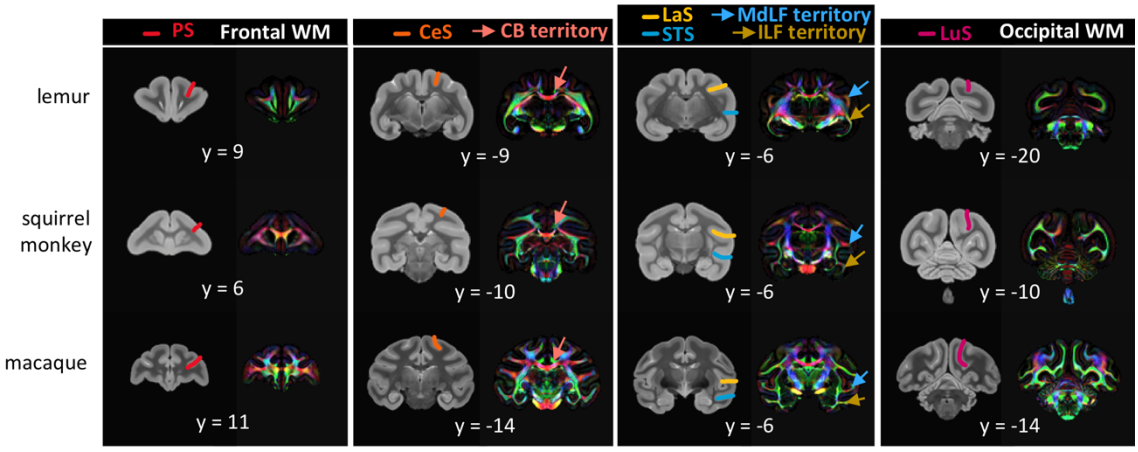

Figure 4.5 Anatomical landmarks for white matter tract definition.

Sulcal landmarks on the template image (left) and the principal diffusion directions modulated by the fractional anisotropy (right) are shown for ring-tailed lemurs, squirrel monkeys, and rhesus macaques in radiological convention. The lemur sulci correspond to the sulci with the "l" prefix as in Figure 4.4. Colours of the principal diffusion images indicate the directions: red left-right, green anterior-posterior and blue dorsal-ventral. CB: cingulum bundle; CeS: central sulcus; ILF: inferior longitudinal fascicle; LaS: lateral sulcus; LuS: lunate sulcus; MdLF: middle longitudinal fascicle; PS: principal sulcus; STS: superior temporal sulcus; WM: white matter.

Cingulum bundle and uncinate fascicle

From the limbic tracts, we reconstructed the cingulum bundle (CB). This is a tract extending from the parahippocampal gyrus, through medial posterior temporal lobe, coursing rostro-caudally superior to the corpus callosum and terminating in medial prefrontal cortex. Because of the sharp curvature of this tract, we reconstructed it in three different sections: peri-genual (CBp), dorsal (CBd), and temporal (CBt). We were able to obtain the whole CB with a very similar anatomy showing prefrontal projections in the three species, while also showing some posterior parietal projections in squirrel monkeys and rhesus macaques (Figure 4.6). It also appears that the posterior end of the dorsal segment is located relatively more rostral in squirrel monkeys compared to rhesus macaques, possibly because of the difference in the anatomy of the visual cortex described above.

The uncinate fascicle (UNC) is a tract that connects the temporal pole to the medial and orbital prefrontal cortex *via* the extreme/external capsule. The UNC is also considered a limbic tract (Alves et al., 2019). The anatomy of the UNC is quite similar in the three species studied. Although it has been shown previously that few fibres reach the frontal pole in macaques as well (Schmahmann et al., 2007), we observe more streamlines reaching the rostral prefrontal cortex in the ring-tailed lemur compared to both the rhesus macaque and squirrel monkey, possibly because of the reduced granular prefrontal cortex in the lemur (Figure 4.6). These observations suggest that similar cortical areas are innervated by this tract. The difference observed highlights the expansion of granular prefrontal cortex in the lineage to which squirrel monkeys and rhesus macaques belong and the relative position of prefrontal cortex areas in the three species (Passingham and Wise, 2012).

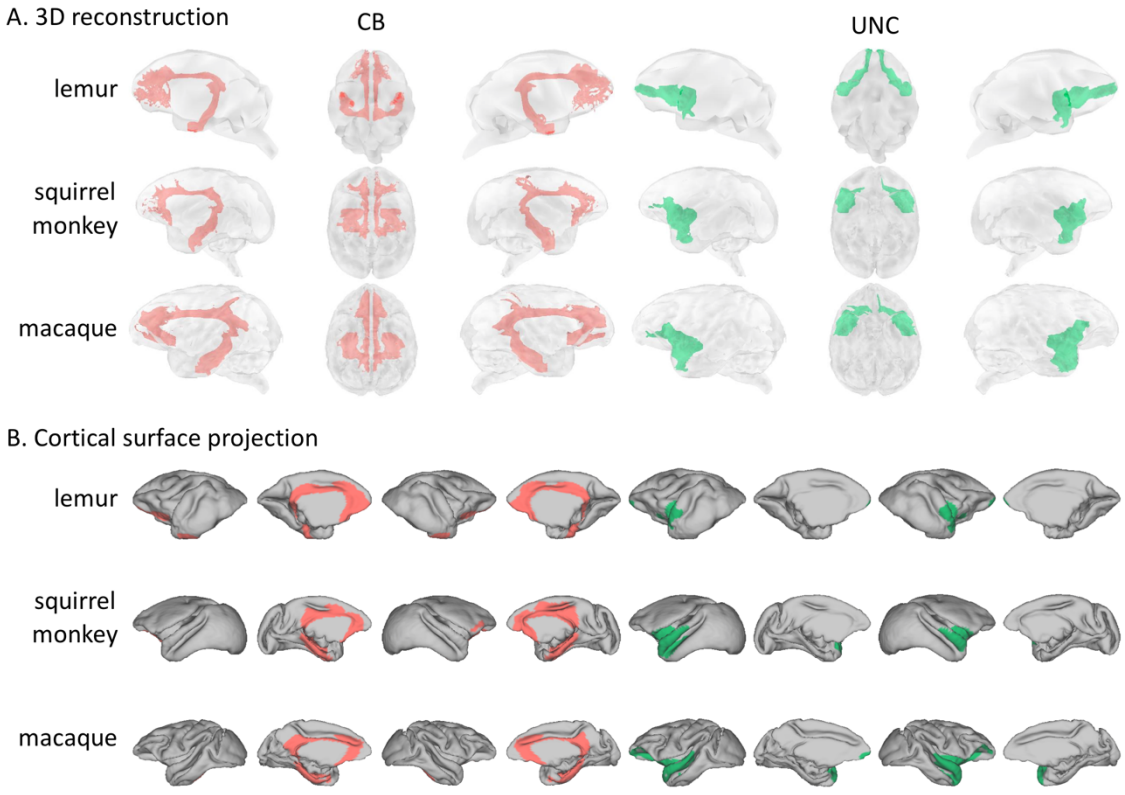

Figure 4.6 Tractography results for the CB and UNC.

(figure legend continues on the following page)

A. We represented the averaged log transformed, thresholded tractogram with a 3D reconstruction showing from left to right: left hemisphere, ventral view, right hemisphere. **B.** The projections to the mid-thickness cortical surface shows left and right hemispheres from both lateral and medial views. CB: cingulum bundle; UNC: uncinate fascicle.

Middle longitudinal fascicle and inferior longitudinal fascicle

The middle longitudinal fascicle (MdLF) is a longitudinal tract spanning the length of the superior temporal gyrus and projecting to the occipital and posterior parietal cortex. It has been shown to exhibit a conserved and similar anatomy in rhesus macaques and great apes such as chimpanzees and humans (Bryant et al., 2020, chapter 3). The anatomy of the MdLF is also very similar in ring-tailed lemurs, squirrel monkeys, and rhesus macaques studied herein, with the only difference occurring in the somewhat broader projections to the occipital cortex in squirrel monkeys compared to the other species (Figure 4.7AB).

The inferior longitudinal fascicle (ILF) is a longitudinal tract running parallel to the MdLF and it has been described in macaques as spanning the length of the inferior temporal gyrus from the temporal pole to occipital and posterior parietal regions (Schmahmann et al., 2007). However, our tractography protocol, although similar in all species, could not identify a parietal projection in ring-tailed lemurs even though it was present in both squirrel monkeys and rhesus macaques (Figure 4.7AB).

To verify this result was not due to issues in the tractography protocols, we performed an additional tractography analysis, using a large seed encompassing the parietal cortex and targets either in the territory of the anterior MdLF or the anterior ILF. We calculated the number of surviving streamlines with these two tractography protocols for each individual and each hemisphere, to investigate the plausibility of a tract running from the parietal cortex to these two anterior temporal locations. We then calculated the ratio between these surviving streamlines for MdLF and ILF protocols.

The results confirmed the observation from the initial tractography. Seeding in ring-tailed lemur parietal cortex showed only minimal fibres reaching the ILF running through the inferior temporal gyrus compared to fibres reaching the MdLF running through the superior temporal gyrus (log ratio around 10) (Figure 4.7C). In contrast, from the parietal cortex of the squirrel monkey, the MdLF was less likely to be reached than the ILF (log ratio close to 0), and the rhesus macaque showed similar connectivity of parietal with MdLF and ILF (log ratio close to 1). This result suggests parietal connectivity of the ILF in squirrel monkeys and rhesus macaques, not present in ring-tailed lemurs.

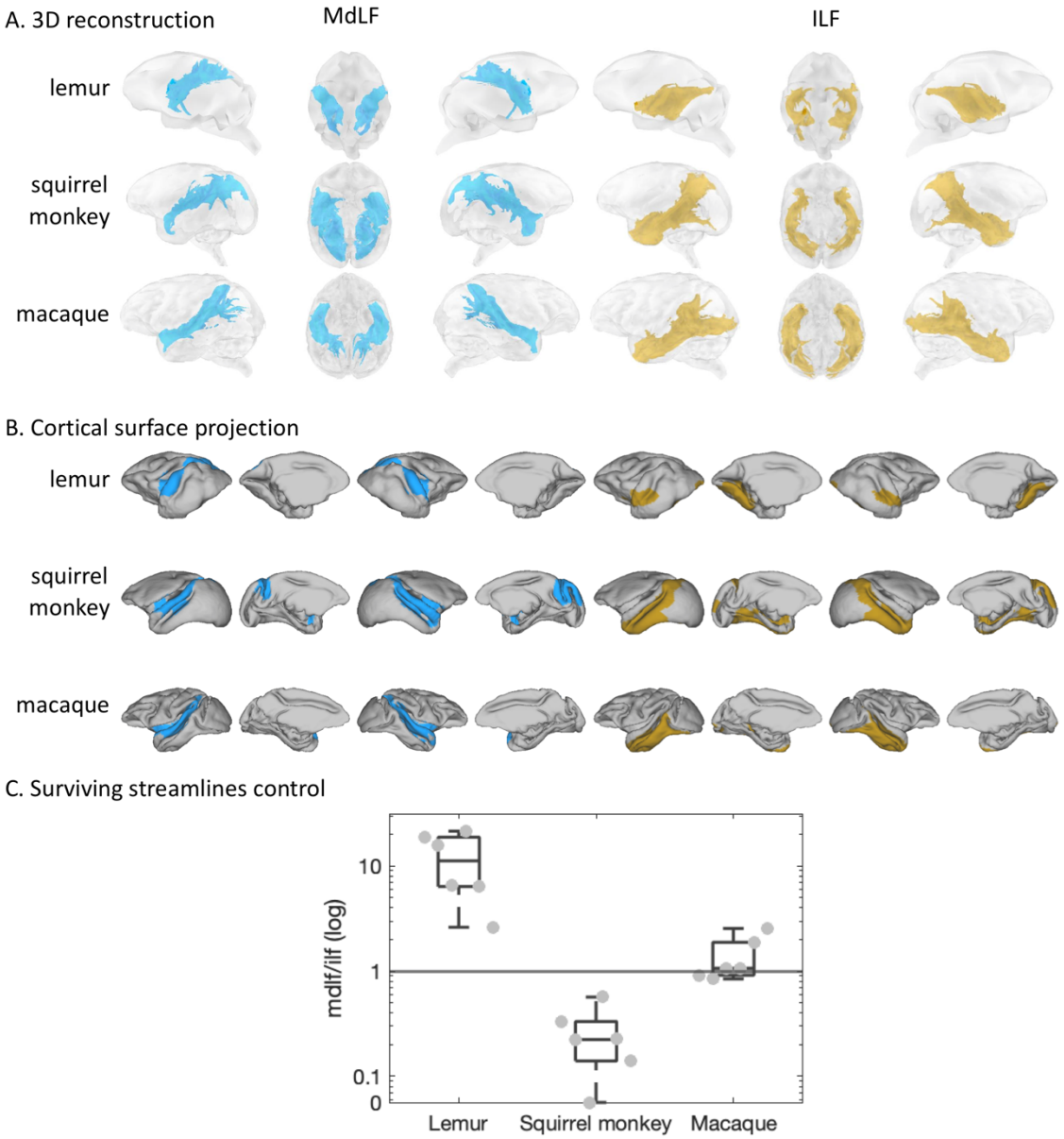

Figure 4.7 Tractography results for the MdLF and ILF.

A. We represented the averaged log transformed, thresholded tractogram with a 3D reconstruction showing from left to right: left hemisphere, ventral view, right hemisphere. **B.** The projections to the mid-thickness cortical surface shows left and right hemispheres from both lateral and medial views. **C.** The boxplot shows the log ratio of surviving streamlines between control protocols using the MdLF or the ILF target. On each box, the central mark indicates the median, and the bottom and top edges of the box indicate the 25th and 75th percentiles, respectively. The whiskers extend to the most extreme data points not considered outliers. Each grey dot represents the ratio for one hemisphere from one individual. ILF: inferior longitudinal fascicle; MdLF: middle longitudinal fascicle.

Inferior fronto-occipital fascicle

The presence of an inferior fronto-occipital fascicle (IFOF), also called the longitudinal fronto-temporal tract or extreme capsule complex, has been established in several species of cercopithecids using both tractography and blunt dissection (Mars et al., 2016a; Schaeffer et al., 2017; Decramer et al., 2018; Barrett et al., 2020; Bryant et al., 2020; Roumazeilles et al., 2020). This multisynaptic tract has been described as connecting the occipital lobe and the frontal lobe *via* the temporal lobe and the extreme/external capsule. Its overall shape appears very similar in all three species studied herein, although its frontal projections appear more robust toward the PF in squirrel monkeys and rhesus macaques than in ring-tailed lemurs, and its occipital projections appear more restricted in squirrel monkeys, particularly compared with the OR projections in that region of the brain (Figure 4.8AB). Sagittal, coronal, and axial brain sections of the three species showing the OR, MdLF and IFOF reinforce the argument that IFOF is a tract that is distinct from other tracts occupying the same region (Figure 4.8C).

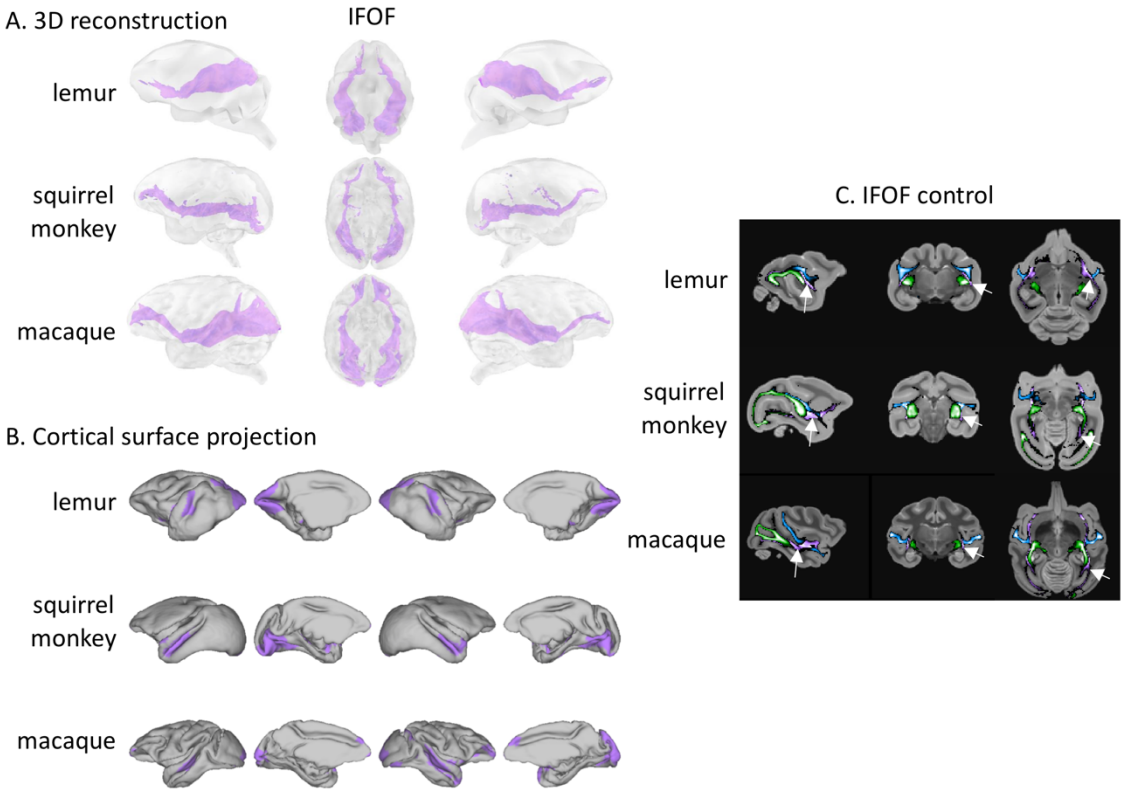

Figure 4.8 Tractography results for the IFOF.

A. We represented the averaged log transformed, thresholded tractogram with a 3D reconstruction showing from left to right: left hemisphere, ventral view, right hemisphere. **B.** The projections to the mid-thickness cortical surface shows left and right hemispheres from both lateral and medial views. **C.** Arrows on the sagittal, coronal, and axial slices point to locations where the IFOF (purple) path is clearly separated from the MdLF (blue) and OR (green). The tracts are shown on the template in radiological convention. IFOF: inferior fronto-occipital fascicle; MdLF: middle longitudinal fascicle; OR: optic radiation.

Superior longitudinal fascicle complex and optic radiation

In the dorsal portion of the telencephalon, we reconstructed a superior longitudinal fascicle complex (SLFc) encompassing the three branches of the SLF usually defined in macaques, as a complex of dorsal longitudinal fibres connecting the frontal lobe with parietal and posterior temporal cortices. We observed that in all three species the SLFc terminates posteriorly in the posterior parietal cortex, but in rhesus macaques and squirrel monkeys the SLFc projects further rostrally than in ring-tailed lemurs (Figure 4.9AB). This can also be seen when comparing the location of the

prefrontal cortex and the SLFc projection on the cortical surface (Figure 4.10). Indeed, it would appear that the SLFc in ring-tailed lemurs shows weaker frontal connectivity, possibly due to the reduced size of their PF.

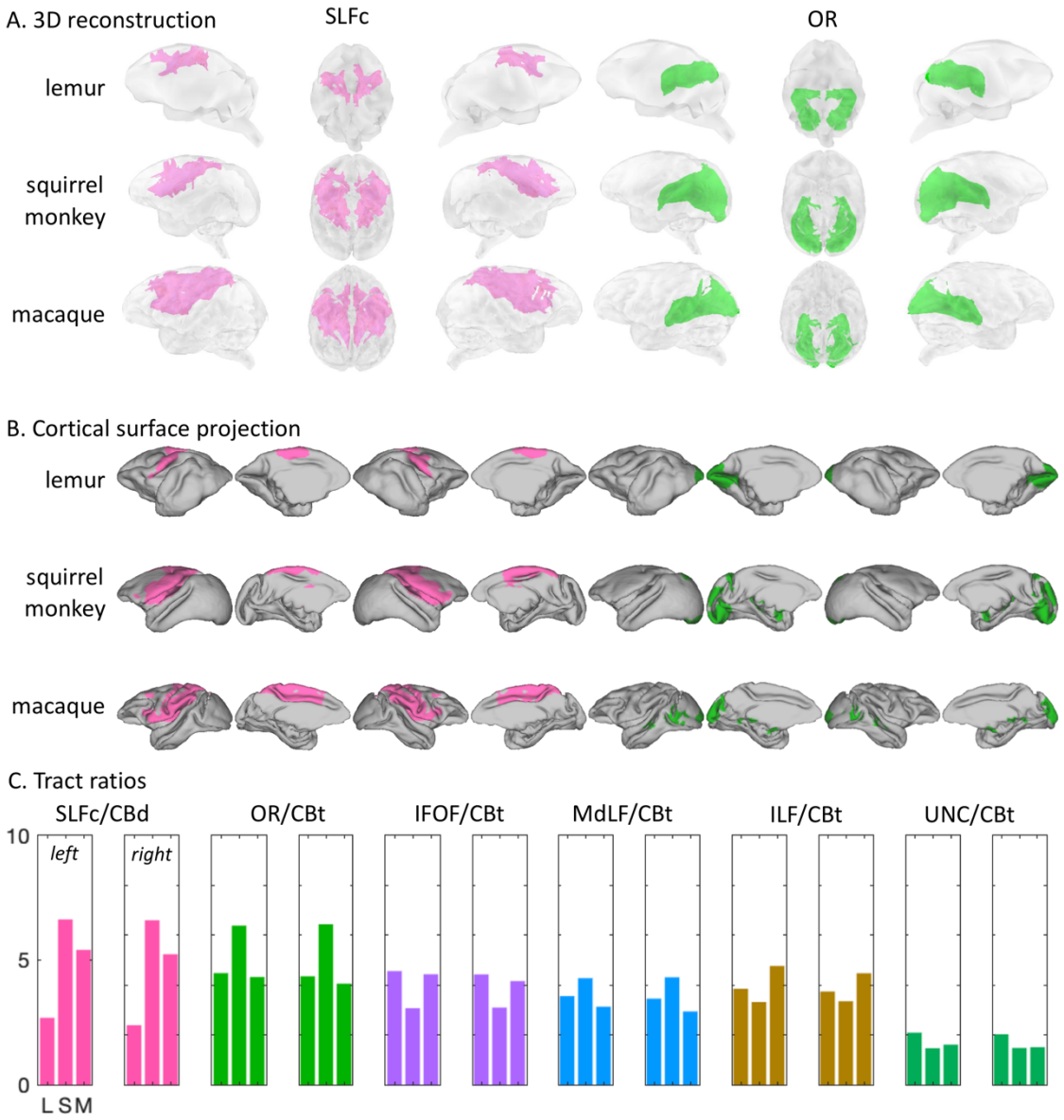

Figure 4.9 Tractography results for the SLFc and OR.

A. We represented the averaged log transformed, thresholded tractogram with a 3D reconstruction showing from left to right: left hemisphere, ventral view, right hemisphere. **B.** The projections to the mid-thickness cortical surface shows left and right hemispheres from both lateral and medial views. **C.** Tract ratios with the CBd and CBt for the tracts of interest: SLFc and OR, as well as the rest of the tracts. Both left and right hemisphere ratios are represented. CBd/t: dorsal/temporal part of the cingulum bundle;

(figure legend continues on the following page)

IFOF: inferior fronto-occipital fascicle; ILF: inferior longitudinal fascicle; L: lemurs; M: macaques; MdLF: middle longitudinal fascicle; OR: optic radiation; S: squirrel monkeys; SLFc: superior longitudinal fascicle complex; UNC: uncinate fascicle.

The optic radiation (OR) was reconstructed as a tract that connects the lateral geniculate nucleus of the thalamus and the primary visual cortex. Its anatomy in the different species confirms the previous observation made on cortical labelling of V1, as this tract's posterior projections highlight the extent of V1. The relative enlargement of V1 in the calcarine fissure in the squirrel monkey is evident also from the OR projections. The lateral position of macaque V1 is also accompanied by weak lateral projections of OR in this species (Figure 4.9AB, Figure 4.10).

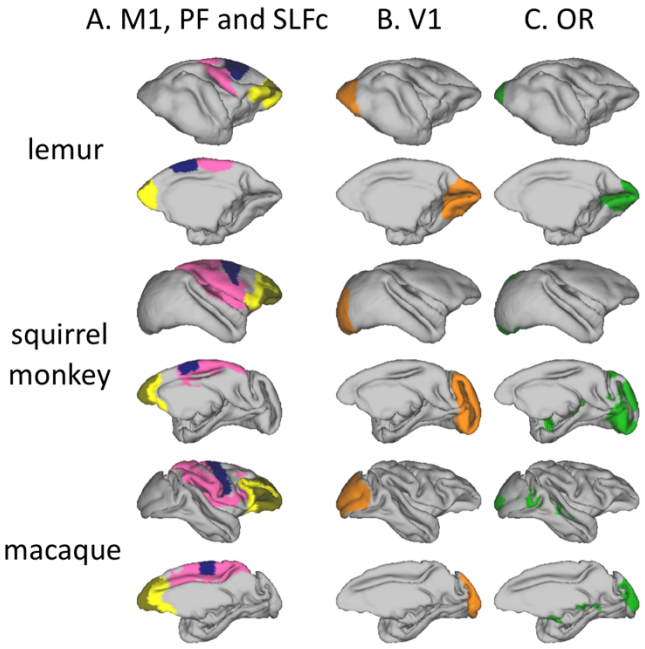

Figure 4.10 Cortical surface labelling and tractography.

A. Right hemisphere mid-thickness cortical surface showing M1 (blue), PF and granular areas (light and dark yellow respectively) and SLFc projections (pink). **B.** Right hemisphere mid-thickness cortical surface showing V1 (orange) and **C.** showing OR projections (green). M1: primary motor cortex; OR: optic radiation; PF: prefrontal cortex; SLFc: superior longitudinal fascicle complex; V1: primary visual area.

To confirm the differences observed in SLFc and OR, namely that SLFc connectivity is reduced in ring-tailed lemurs' frontal cortex, and OR is disproportionately expanded in squirrel monkeys, we performed a ratio analysis with tracts that are similar between the different species and running in similar areas (dorsal and temporo-occipital). The CB runs in both dorsal and temporal areas and is a tract usually considered to be conserved across species (Bubb et al., 2018). Therefore, we performed the ratio of our two tracts of interest with the CB section that runs in a similar territory. These analyses confirmed our observation that the SLFc is proportionately smaller in ring-tailed lemurs, and it also revealed that the macaque SLFc seems proportionately smaller than that of the squirrel monkey SLFc (Figure 4.9C). The OR was demonstrated to be proportionately larger in squirrel monkeys while a very similar ratio with CBt was obtained for ring-tailed lemurs and rhesus macaques.

4.5 Discussion

In the current study, we investigated cortical morphology and white matter architecture in three species of primates, representing three distinct lineages within the order, ring-tailed lemurs (which belong to the suborder Strepsirrhini, family Lemuroidae, also referred to as a prosimian primate), black-capped squirrel monkeys (which belong to the suborder Haplorrhini, parvorder Platyrrhini, family Cebidae, also referred to as New World monkey, simian primate or anthropoid primate), and rhesus macaques (which belong to the suborder Haplorrhini, parvorder Catarrhini, family Cercopithecidae, also referred to as Old World monkey, simian primate or anthropoid primate). To our knowledge, we present the first reconstructions of white matter tracts in the ring-tailed lemur, as well as expanding our knowledge of these tracts in the squirrel monkey. The white matter tracts show a generalized similarity across the

primate species studied here and those studied previously. Our results identified an elaboration of prefrontal and parietal connectivity in squirrel monkeys and rhesus macaques (simians) compared to ring-tailed lemurs (prosimians), among a range of variations that might be considered to represent a simian *versus* prosimian divergence in cortical organization (Figure 4.11). We also observed a very specific occipito-parietal anatomy in the squirrel monkey that distinguishes the squirrel monkey from the other species studied (Figure 4.11).

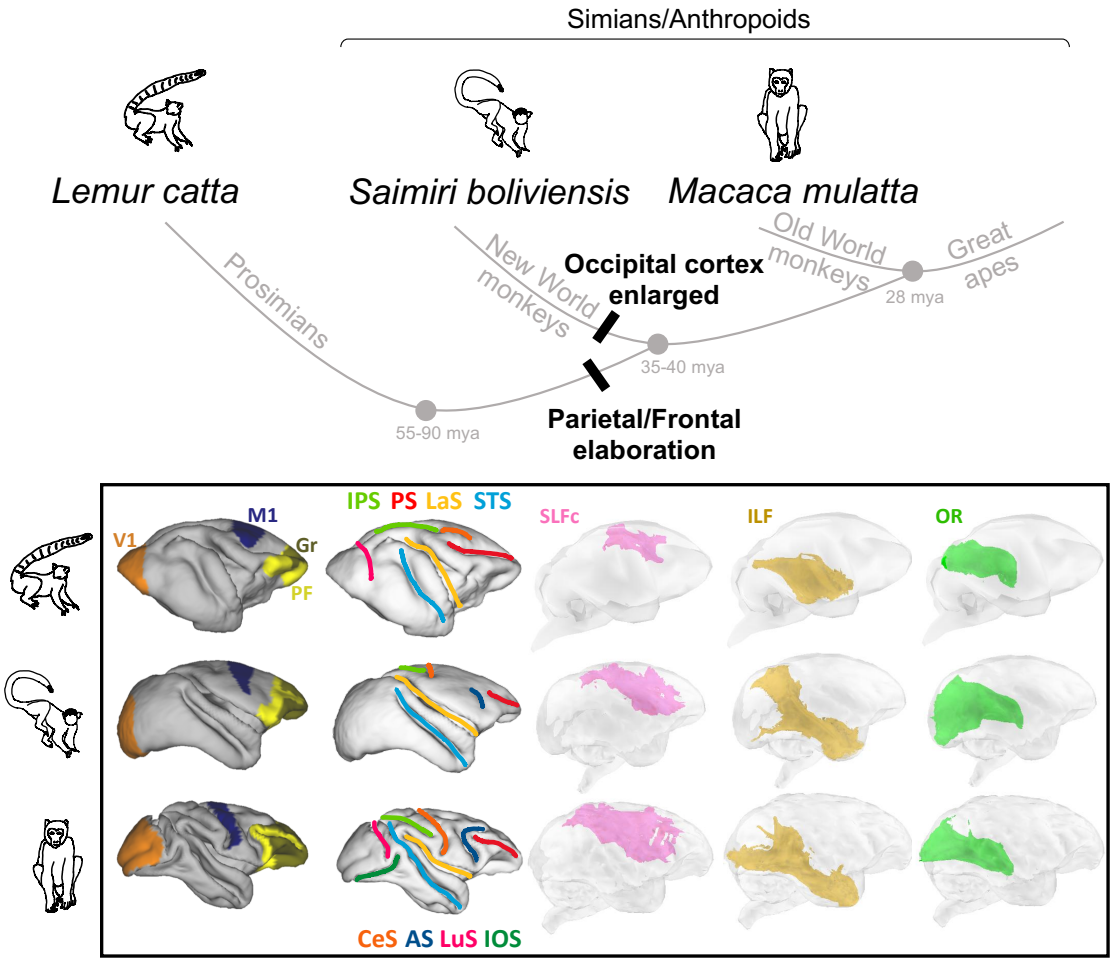

Figure 4.11 Cortical morphology, white matter tractography and suggested evolutionary trajectory for lemurs, squirrel monkeys and macaques.

We summarized our findings in the phylogenetic tree represented at the top of the figure. In the bottom panels, we summarized our cortical and white matter results in the three different species. AS: arcuate sulcus; CeS: central sulcus; Gr: granular areas of the prefrontal cortex; ILF: inferior longitudinal fascicle; IOS: inferior occipital sulcus; IPS: intra-parietal sulcus; LaS: lateral sulcus; *(figure legend continues on the following page)*

LuS: lunate sulcus; M1: primary motor cortex; mya: million years ago; OR: optic radiation; PF: prefrontal cortex; PS: principal sulcus; SLFc: superior longitudinal fascicle complex; STS: superior temporal sulcus; V1: primary visual cortex.

Despite these variations, the white matter tracts show a generalized similarity across the primate species studied here and other primates. Mammals have been shown to share fundamental principles of brain connectivity such as wiring costs and speed of conduction, and more recently, a conserved relationship in which fewer interhemispheric connections are associated with better intrahemispheric connectivity and *vice versa*, maintaining the overall efficiency of communication across a large range of species (Assaf et al., 2020). The addition of new cortical association fields in the different lineages of primates contributes to our knowledge of the evolutionary specializations of this order (Krubitzer, 2009). However, the overall principles of white matter organization appear conserved across the primate order (Rilling et al., 2008; Barrett et al., 2020; Eichert et al., 2020; Roumazeilles et al., 2020) despite differences in brain size and sulcal pattern, representing what might be an order-specific organization of the white matter (Manger, 2005). The seven white matter tracts studied here are consistent with this pattern, showing a conserved organization in terms of topological relationship and connectivity of comparable brain regions, across three primate species that represent three distinct lineages within the order. Despite this overall similarity, interspecific variations were observed, particularly in the connectivity of association areas.

The identified differences between prosimian and simian primates were mainly associated with the frontal and parietal cortical areas. Prefrontal cortex has been previously reported to be proportionately larger in simians than prosimians, with several granular prefrontal cortical areas reported to be present only in simians (Preuss and Goldman-Rakic, 1991). We have illustrated these findings here on the surface brains we

created for the prosimian and the two simians. The comparative neuroimaging analysis undertaken in the current study provided further supportive evidence for these suggestions in terms of white matter organization. Particularly, although we could reconstruct the SLF in all species studied, there were less extensive frontal projections in the prosimian, possibly reflecting a weaker frontal connectivity, which is consistent with the limited size of the prefrontal cortex reported in prosimians. Similarly, the frontal projections of the IFOF appear less robust in the prosimian. In contrast, the UNC, which projects to the granular prefrontal areas that are present in all three species studied, appeared to reach the frontal pole more in the prosimian. This illustrates the reduced size of frontal granular areas observed in prosimians, confined only to the frontal extremity while extending more posteriorly in simians. We also noticed differences in the anatomy of the white matter associated with the parietal cortex when comparing between prosimians and simians. The ILF showed more limited posterior projections in the prosimian as it did not reach the parietal cortex, whereas it did in the two simians studied. In addition, the CB showed projections to the posterior parietal region in the two simians but not in the prosimian. These frontal and parietal variations between prosimians and simians support previous findings showing that the connectivity between frontal, parietal, and temporal areas is more complex in simian primates compared to prosimian primates, giving rise to what has been termed the 'anthropoid elaboration' (Krubitzer, 2009).

The additional granular prefrontal cortical areas in simian primates have been postulated to be associated with certain ecological and social factors and their abilities to forage in a more complex niche than prosimian primates. It has been further argued that these prefrontal networks have increased access to posterior parietal cortex information related to relational metrics, using them for more general decision-making

processes (Genovesio et al., 2014). The findings of the reduced parietal ILF projections in prosimians raise similar questions. Based on tracer work in the macaque monkey, Schmahmann and Pandya identified the ILF as a long association fibre tract of the ventral visual pathway in the occipitotemporal cortices (Schmahmann and Pandya, 2006c). Importantly, they also highlighted its connectivity with parietal cortex, suggesting the importance of integrating the attentional functions of these areas into the visual processing of the ventral stream. Although the current state of knowledge and methods does not allow us to link white matter tracts and functions with certainty, it is interesting to discuss this observation in light of the known functions of areas associated with the ILF. Kaas (2017) highlights an expansion of the ventral visual stream in simians, presumably to enhance the ability to recognize individual faces and objects. The ILF has been specifically associated with providing visual input to this system for facial recognition (Herbet et al., 2018) and it is therefore striking that a species such as the lemur, usually living in smaller groups and relying on audition and olfaction in addition to vision to recognize individuals, would possess a reduced ILF (Kulahci et al., 2014). Furthermore, we have previously showed that the ILF is even more complex in great apes, where it is divisible into two subcomponents, the most ventral of which is homologous to macaque ILF and reaches face responsive areas in all of the anthropoids' species studied as seen in chapter 3 (Roumazeilles et al., 2020).

Our study also highlights specific features of the occipital region for the squirrel monkey. The size of the primary visual cortex, and more generally occipital cortex, is particularly large in the squirrel monkey compared to the two other species studied. This is associated with the posterior projections of the OR projecting more broadly than in the two other species. We also note other subtler differences in tract projections to occipital regions in squirrel monkeys compared to the two other species, including

broader MdLF projections and more restricted IFOF projections. In this context, it is also interesting to note that the ILF appears more dominant in the posterior parietal area in squirrel monkeys than in macaques. These anatomical details in the relative size of different cortical regions and the projections of the associated tracts suggest a potential specialization of the occipital cortex in squirrel monkeys that has not been observed in other primates studied to date. Although all three species examined in this study are diurnal, squirrel monkeys have a lifestyle that is more arboreal-dependent than the two other species. Squirrel monkeys rarely come to the ground, and live and travel through small branches of trees, implying a challenge for neuronal information processing in both visual and locomotor systems. Interestingly, it has been previously noted that arboreal rodents devote more cortical territory to visual processing when compared to their terrestrial counterparts (Campi and Krubitzer, 2010).

Limitations and future studies

It should be noted that changes in proportion of white matter across the brains of different species may be due to allometric scaling (Ventura-Antunes et al., 2013). Inferring departures from allometric scaling rules generally requires analyses that take phylogenetic relationships into account and that include many more species than examined in the present study (Barton and Venditti, 2013). However, the differences reported here are not differences in the relative quantity of cortical white matter, but rather qualitative variances between the cortical territories of a certain white matter tract. We have previously shown that qualitative variations, such as invasion of new cortical territories by a particular white matter tract, can be distinguished from cortical reorganization due solely to the expansion of the brain (Eichert et al., 2018, 2020). Our results are in line with such reorganizations of the intracortical white matter, showing

that there are changes in the relative proportion of tracts in the same cortical areas, such as in the case of the SLFc and the dorsal cingulum, and that these tracts may project to novel parts of the cortex, such as in the case of the parietal connections of ILF in simians.

Tractography is a suitable tool to compare connectivity in different brains, as it allows for standardized protocols that are readily comparable across species; however, tractography is not without its caveats. First, probabilistic tractography applied to diffusion MRI data has been criticized recently for generating false positives and false negatives if not used with proper anatomical constraints (Maier-Hein et al., 2017). Here, we used previously validated protocols in macaques that have been shown to reconstruct tracts accurately (Warrington et al., 2020). Importantly, we were able to use three subjects per species and thus average the individual tractograms and threshold the result, which reduces the probability for false positives and negatives to be conserved in the final tract. Second, finding anatomical landmarks corresponding across species can sometimes be difficult, due to their very different overall anatomy. Taking several points of reference, both cortically and subcortically, which are known to have only limited variance across species, allows for a better approximation of the landmarks. Our tractography results also showed remarkable consistency with inferences made from the size and location of known cytoarchitectonic areas. Such convergence of results across modalities increases our confidence in the validity of our findings (Mars et al., 2021). It is also important to note that some of the tracts we delineated are very similar across species, such as the CB, MdLF and IFOF. These tracts run in similar regions of the white matter to those for which we identified variations across species and were obtained based on similar landmarks. This reinforces confidence in our results. In addition, the reduced SLFc connectivity in lemur prefrontal cortex cannot be explained

by reduced quality in the diffusion data in the frontal part of these brains, since the UNC seems to readily invade this space. It is also interesting to note that similar reduced SLFc connectivity has been observed in another prosimian, the galago (Bryant et al., 2021). Last, we have conducted control analyses when finding differences between species for the ILF, SLFc and OR. Tracking from different areas and investigating appropriate ratios have confirmed our results.

Large-scale comparative neuroscience is often difficult, due to the labour and costs involved. MRI allows one to partially address these issues, but at present high-quality data are only available from a limited number of species. These data are usually acquired *post mortem* which could lead to tissue shrinkage, however this has a limited impact on the final data revealing higher levels of details in *post mortem* compared to *in vivo* imaging (Barrett et al., 2020). Although this study improves on previous methods by studying three individuals for each species, this number is still limited and does not allow for further inter individual and inter sexes investigation, as for instance we could only obtain male ring-tailed lemurs. Fortunately, the situation is rapidly improving facilitated by the increasing collaborative nature of data sharing in nonhuman primate research and the inclusion of more species (Assaf et al., 2020; Milham et al., 2020; Bryant et al., 2021), leading to the requirement for standardized acquisition protocols, templates, and analysis strategies across species. The availability of multiple individuals with high quality data from each species allowed us to create species-specific templates, in effect creating a 'standard space' for each. All tractography protocols were defined in these standard spaces in a manner compatible with the recently released *Xtract* tools. All these resources are made available online to facilitate the easy exchange of information. Combined with other efforts using the same tools, this initiates more formalized phylogenetic comparisons of brain organization across the primate order.

Conclusion

In summary, our study provides evidence in the form of white matter anatomy that supports the concept of the elaboration of prefrontal and posterior parietal systems in simians compared to prosimians. This study provides a baseline from which further studies, using similar standardized methods, can accurately compare brains across different species. This is of interest to allow us to understand the various evolutionary trajectories that influenced the structure of the brain within the different primate lineages and species.

Chapter 5 - Insights of macaque brain development and ageing

This chapter reports unpublished data and results to which the following people contributed during data collection and part of the data analysis:

Roumazeilles L, Lange FJ, Benn RA, Andersson JLR, Roho I, Khrapitchev AA, Eichert N, Bauman SE, Compo NR, Martinez MI, Snyder-Mackler N, Brent LJN, Montague MJ, Platt ML, Noonan MAP, Mars RB, Sallet J.

5.1. Abstract

Macaques have been used as models to study brain development in order to better understand human neurodevelopmental and neurodegenerative disorders. However, only few studies have considered investigating connectivity patterns across the whole lifespan. Here, we acquired diffusion imaging data from 24 rhesus macaques (*Macaca mulatta*) ranging from 2.5 months to 25 years old. We were able to create age category templates and surfaces as well as general templates to investigate brain anatomy changes over the macaque lifespan. We assessed brain size and sulcal anatomy as well as white and grey matter ratios as a function of age. We also reconstructed white matter tracts to investigate their anatomy and structural integrity. They allowed us to compare the overall brain connectivity entropy between age categories. The results show that although brain size continues to increase after birth, macaques demonstrate a certain level of maturity from birth with their sulcal anatomy and most of their white matter tracts already present in their adult form. Developmental changes mostly occur in the first 3 years of life with an increase of white matter ratio accompanied by changes in the structural properties of most tracts and localized connectivity of some fronto-parietal projections, confirmed by whole brain connectivity analyses. Overall, this study confirms and completes previous knowledge of macaque brain development and provides more precision to the white matter connectivity changes observed throughout their lifespan.

5.2. Introduction

The brain is mostly modified at two critical periods, during early development and late ageing. Investigating how the brain organization is modified throughout the

complete lifespan and not only these timepoints allows us to better understand their normal proceedings. In turn, these insights can give a better understanding of the impairment happening in neurodevelopmental disorders (e.g., autism, schizophrenia) and neurodegenerative pathologies (e.g., Alzheimer's disease, Parkinson's disease). In humans, the size of the brain continues to increase until early adolescence, with the volume of cerebral grey matter increasing slightly in early years while the volume of white matter increases at higher rates throughout childhood up to adulthood (Courchesne et al., 2000; Matsuzawa et al., 2001). Studies on white matter development have uncovered several important processes responsible for the proper development of brain connectivity. Spanning the pre and post birth period, the pruning process corresponds to the selective removal of some projections to refine the brain connectivity (O'Leary, 1992; Innocenti and Price, 2005). The myelination process leading to better electrical isolation stabilizes these connections (Baumann and Pham-Dinh, 2001). Longitudinal diffusion-weighted imaging studies have been performed in humans to study more precisely white matter changes with age (Lebel et al., 2012; Dubois et al., 2014). They allow us to reconstruct white matter tracts and assess micro-structural characteristics of white matter such as fractional anisotropy (FA) and mean diffusivity (MD).

However, scanning human babies poses several challenges, therefore other primates, such as macaques, have been used as models to study neurodevelopmental processes. By combining developmental and comparative frameworks, these studies can make assumptions on both the developmental and evolutionary trajectory shaping a phenotypic trait and therefore participate in understanding the roots of human cognition (Rosati et al., 2014). While overall developmental processes appear similar between macaques and humans (Shi et al., 2013), the macaque brain is more precocial (reaching

maturity early) compared to humans. Macaque brains are more myelinated upon birth and brain size is closer to adult size (Clancy et al., 2007). Focusing on the early period of life, several studies have shown that the first months after birth are critical for most of the developmental changes in macaques (Malkova et al., 2006; Knickmeyer et al., 2010; Kim et al., 2020). These studies observed an increase of both brain volume and white matter during that period, accompanied by an increase in FA. Therefore, most studies focus on this early period only and whole lifespan studies are scarce (Scott et al., 2016). On the other side of the spectrum, ageing in macaques have been associated with decrease in FA (Makris et al., 2007; Chen et al., 2013). Overall, while imaging protocols and techniques are improving, there is still a limited amount of studies on the connectivity development and ageing in macaques.

Here, we used diffusion-weighted MRI to investigate how whole brain anatomy as well as the structural properties and precise connectivity of white matter projections vary over the rhesus macaque lifespan. We took advantage of the high-resolution diffusion-weighted MRI available in *post mortem* samples and newly developed tools to establish age-specific templates, reconstruct cortical surfaces and white matter tracts for 6 age categories (from infants to seniors). In turn, the definition of 19 white matter tracts allowed us to investigate whole brain connectivity changes across the age range.

5.3. Materials and methods

5.3.1. Data

For this study we used 24 left hemispheres from *post mortem* brains of rhesus macaques (Macaca Mulatta) (see Table 5.1). We classified the individuals in six age categories based on major life events (Liu et al., 2015a): infant (0 to 1 year old), juvenile (3 to 4.9 years old), subadult (5 to 6.9 years old), young adult (7 to 11 years

old), adult (11.1 to 14.9 years old) and senior (15 years old and above). In macaques nutritional weaning occurs between 12 and 18 months. Five years old is considered as the puberty age and seven is the full maturity. The adult group was divided in two (young adult and adult) to represent a similar age span as the other groups. Above 15 years old, macaques are usually considered old. Four individuals, two females and two males, were used in each age category. No brain from subjects between five months old and three years old were available due to population management concerns not related to this study. The brains come from two locations: the University of Oxford's Biomedical Sciences (laboratory macaques) and the field station in Cayo Santiago (free-ranging macaques).

The Oxford brains were obtained from animals involved in independent studies conducted under licenses from the United Kingdom (UK) Home Office in accordance with the UK Animals (Scientific Procedures) Act 1986. Immediately following veterinary euthanasia, brains were transcardially perfused with physiological saline, before being perfused with a 10% neutral buffered formalin solution. Once extracted, brains were stored in 10% neutral buffered formalin solution.

The average annual growth rate of the Cayo Santiago rhesus macaque population is far greater than that of wild populations. Therefore, a necessary population control through capture and removal of animals is conducted by the Caribbean Primate Research Center (CPRC) in accordance with protocols approved by the animal use committee of the University of Puerto Rico (protocol number 338300) (Hernandez-Pacheco et al., 2016). The data in this manuscript comes from the Cayo Biobank Research Unit database, a database created to collect and archive *post mortem* tissues. Immediately following veterinary euthanasia, brains were perfused with physiological saline, removed from the cranium, and sectioned sagittally into left and right

hemispheres. The right hemisphere was cryopreserved for genomics analysis (Chiou et al., 2020) and not used for this study. For a few individuals, the full brain including the right hemisphere was conserved. The left hemispheres or whole brain were conserved in 10% neutral buffered formalin solution. To control for any hemispheric effect, we used six right hemispheres, one for each age category. They are from the same individual as the left hemisphere except for the infant. The only right hemisphere available for this age category came from a sample missing the cerebellum and the brain stem.

Monkey ID	Age category	Age (years)	Sex	Hemisphere used	Provenance
in1	Infant	0 (1 day)	Male	Right	Oxford
in2		0.2	Female	Left	Cayo
in3		0.2	Male	Left	Cayo
in4		0.3	Female	Left	Cayo
in5		0.4	Male	Left	Cayo
ju1	Juvenile	3.2	Female	Left	Cayo
ju2		3.2	Male	Left	Cayo
ju3		3.9	Female	Left and right	Oxford
ju4		4.7	Male	Left	Oxford
su1	Subadult	5	Female	Left and right	Cayo
su2		5.3	Male	Left	Cayo
su3		6.1	Female	Left	Cayo
su4		6.1	Male	Left	Cayo
ya1	Young adult	7.3	Female	Left	Cayo
ya2		9	Female	Left and right	Cayo
ya3		10.2	Male	Left	Cayo
ya4		11	Male	Left	Cayo
ad1	Adult	11.2	Female	Left	Cayo
ad2		11.7	Male	Left and right	Oxford
ad3		12	Male	Left	Cayo
ad4		13.9	Female	Left	Cayo
se1	Senior	15.8	Female	Left and right	Oxford
se2		15.9	Male	Left	Cayo
se3		19.9	Male	Left	Cayo
se4		25.9	Female	Left	Cayo

Table 5.1 Data summary

5.3.2. Imaging protocol

The imaging protocol has been reported previously (Folloni et al., 2019a; Bryant et al., 2020; Eichert et al., 2020) and is the same as chapter 3 and 4. Briefly, all brains were rehydrated in a PBS solution, at least one week prior to scanning and placed in fomblin or fluorinert for the scanning procedure. The diffusion-weighted magnetic resonance imaging (MRI) data were acquired from the whole brain using a 7T preclinical MRI scanner (Varian, Oxford UK). We used a 2D diffusion-weighted spin-echo multi-slice protocol with single line readout (DW-SEMS; TR = 10 s; TE = 26 ms; Matrix size = 128 x 128 with a sufficient number of slices to cover each brain; resolution: 0.6 x 0.6 x 0.6 mm^3). 16 non-diffusion-weighted (b = 0 s/mm^2) and 128 diffusion-weighted (b = 4000 s/mm^2) volumes were acquired with diffusion encoding directions evenly distributed over the whole sphere (single shell protocol).

To assess data quality and the comparability between different brain provenances and ages, we computed the signal to noise ratio (SNR) for each individual scan, the mean diffusivity (MD) and mean fractional anisotropy (FA) in the white matter of each individual as well as in the genu of the corpus callosum. The SNR was defined as the ratio between the mean signal in the brain and the mean signal outside the brain. Values for all measures are comparable between individuals, ages and brain provenance, no systematic bias was observed (Figure 5.1).

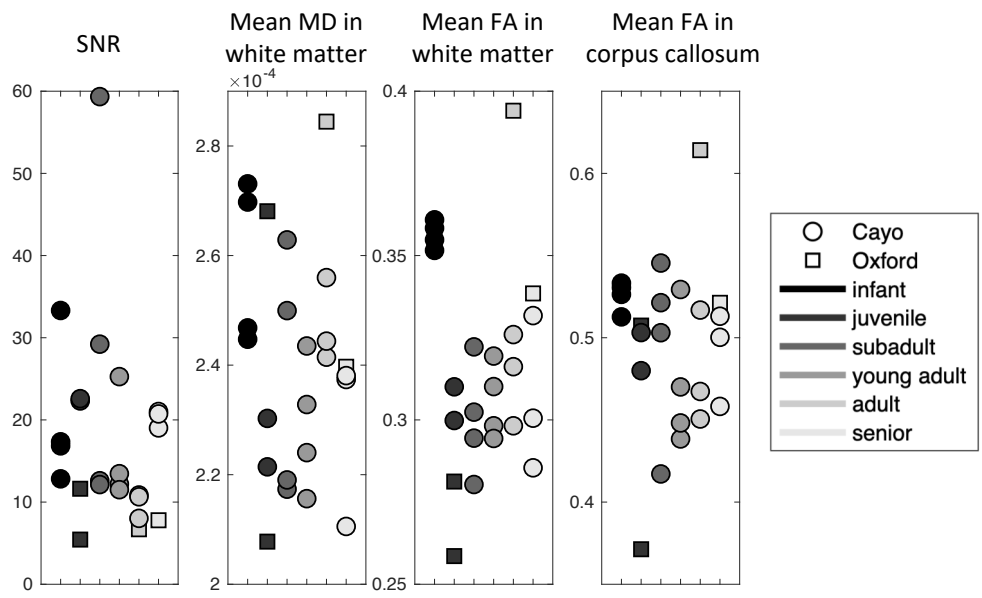

Figure 5.1 Data quality assessment for the left hemispheres.

For each individual, the values of SNR, mean MD and mean FA in white matter as well as mean FA in the corpus callosum are reported. The marker shape code identifies the provenance of the brain while the colour code identifies age category as indicated in the legend. FA: fractional anisotropy; MD: mean diffusivity; SNR: signal to noise ratio.

5.3.3. Diffusion MRI data preprocessing

Data were preprocessed as previously described in chapter 3 and 4 as well (Folloni et al., 2019a; Bryant et al., 2020; Eichert et al., 2020) using the protocol implemented in the module *phoenix* of the MR Comparative Anatomy Toolbox (Mr Cat; www.neuroecologylab.org). After converting the dataset to NIFTI format, we built an image based on the non-diffusion-weighted volumes called *nodif* as well as binary brain mask of this image. Then using tools from FSL (www.fmrib.ox.ac.uk/fsl), we fitted a diffusion tensor model using FSL's *dtifit* and reoriented the data in approximate ACPC (anterior commissure/posterior commissure) conventional orientation which sets the origin at the middle of the anterior commissure. Following the preprocessing, *bedpostX* (Behrens et al., 2007) was used to fit a crossing fibre-model to the data, allowing for three fibre orientations.

A summary of the preprocessing, processing and analysis steps can be found in Figure 5.2.

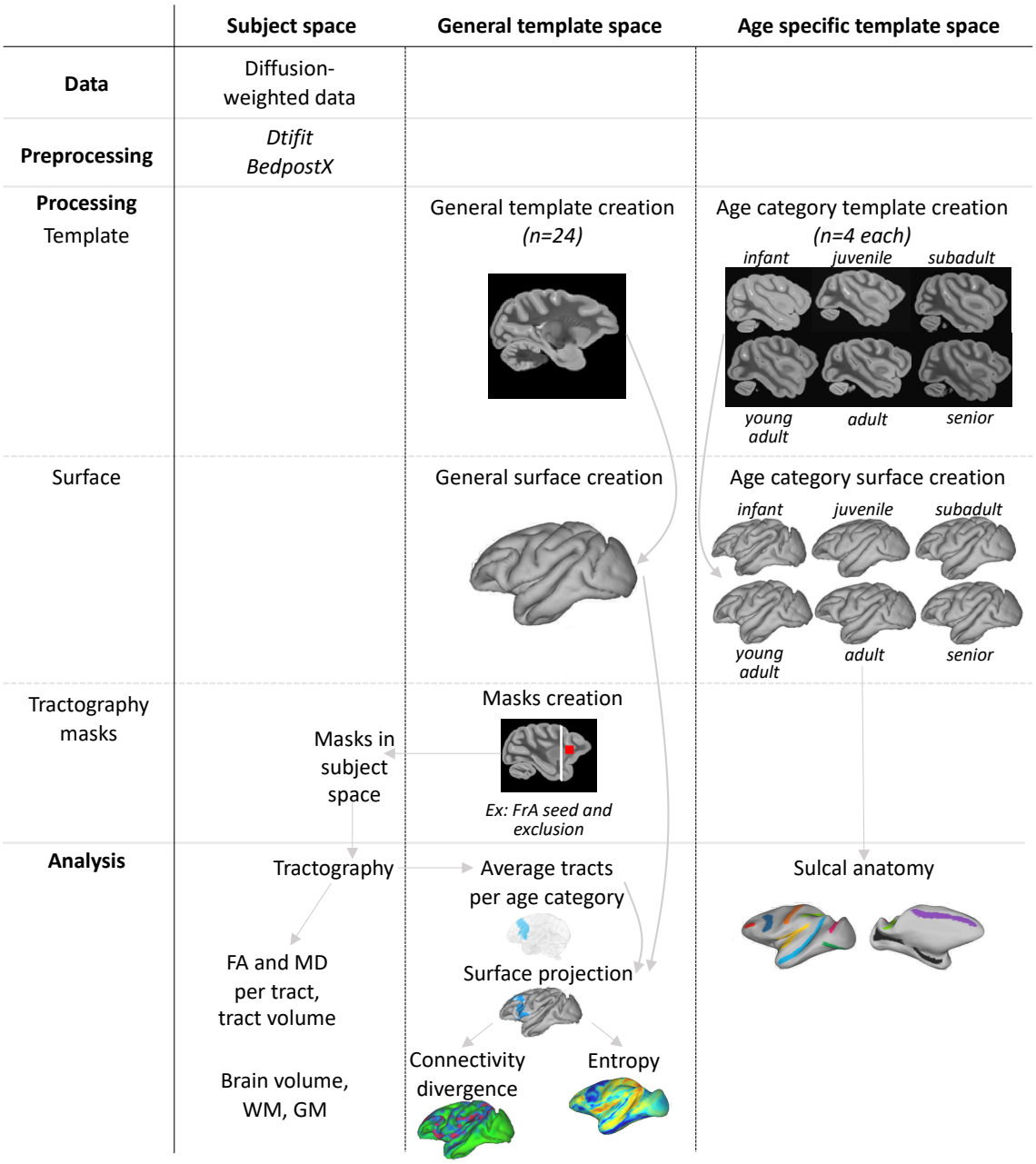

Figure 5.2 Overview of the preprocessing, processing and analysis steps.

Each column represents a different space: subject, general template and age specific template; and contains the steps performed in a given space. From the preprocessed data, we created a general template and age category templates. We created surfaces for each template. The age category specific templates were subsequently used for sulcal anatomy analysis. The general template was used for the tractography, for which we created masks in the general template space that we transformed to each subject space, to perform the tractography in subject space. *(figure legend continues on the following page)*

The tractograms obtained in subject space were used for analysis on the FA and MD for each tract and to assess tract volumes. They were also transformed back to general template space and averaged per age category. Using the previous surface in general template space we obtained a surface representation of these averaged tracts. Using a matrix of all the tracts surface projection, we were able to calculate the connectivity divergence between each age category and the connectivity entropy for each category. Brain volume, as well as WM and GM volumes were assessed in subject space. FA: fractional anisotropy; FrA: frontal aslant; GM: grey matter; MD: mean diffusivity; WM: white matter.

5.3.4. Template creation

We created templates for each of the age category for the left hemisphere as well as a general template for each hemisphere. Because only one individual was available per age category for the right hemisphere, we did not create right hemisphere age category specific template. We applied the method previously used in chapter 4 (Lange et al., 2020b). Conceptually, this method employs a registration based, multi-resolution, iterative template creation strategy including spatial unbiasing of both affine and nonlinear shape changes. Registration is performed using the MultiMOdal Registration Framework (MMORF) (Lange et al., 2020a). MMORF is a multimodal registration tool for simultaneous alignment of datasets with both scalar and tensor MRI images. Here, we utilized the no-diffusion images with T2 contrast (*nodif*) and the tensor images from FSL's *dtifit* (*dti_tensor*). More details on the procedure can be found in chapter 4 (4.3.4).

For the left general template, 24 subjects (four per age category) were used. To assess morphological variability across subjects, we computed the mean positional distance (MPD) by calculating at each voxel for each subject the magnitude of displacement caused by the warp to match the general template (Kovačević et al., 2005; Frey et al., 2011). We then averaged the resulting subject displacement maps (Figure 5.3). Note that voxels with of lower amount of displacement, associated with lower interindividual variability are located mainly in the subcortical regions while regions of

high displacements are mainly located at the extremities of the brain, a pattern observed by others (Frey et al., 2011). The globus pallidus is also displaying high displacement due to its known change of intensity with age (Pozeg et al., 2019).

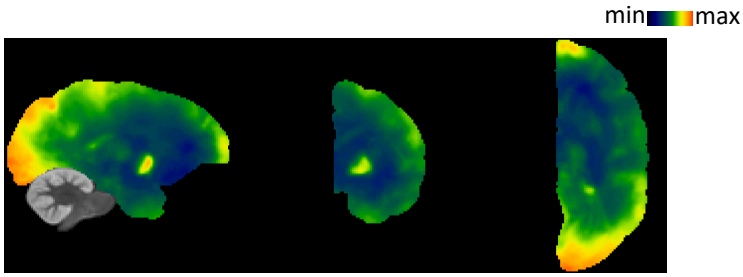

Figure 5.3 Mean displacement map.

Mean positional distance averaged for 24 individuals representing how much a voxel needs to move to match the general left template.

We also created a general template for the right hemisphere with six subjects (one per age category). Because one of the right hemispheres missed the cerebellum and brain stem, we masked out this area of the template when registering this individual. Therefore, the right cerebellum and brain stem template is only based on five individuals. General templates allowed us to define a common space to compare all the individuals.

Because of the wide age range included in the general template, we wanted to ensure proper registration for all individuals. We defined a brain mask and two subcortical masks (hippocampus, caudate and putamen) in the template space that we transformed back to each individual space using the warps obtained with the template creation pipeline. We used subcortical structures as their borders are more clearly defined than cortical areas. In each individual, we could precisely recover the brain mask and subcortical structure masks after transformation to the individual space

(Figure 5.4). The same procedure was performed on the right hemisphere also demonstrating the correctness of the registration (Appendix 5).

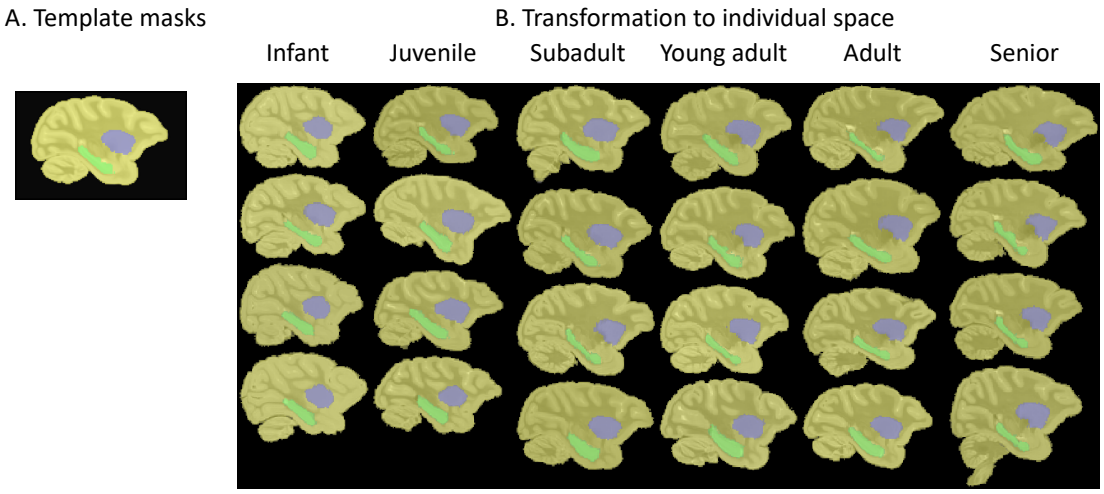

Figure 5.4 Registration quality assessment to the left hemisphere general template.

A. Original masks from the general left hemisphere template on a sagittal slice. **B.** Masks transformed to each individual space. The yellow structures represent the brain mask, the blue structures represent the putamen and caudate nucleus, and the green structures represent the hippocampus.

5.3.5. Surface creation

We created cortical surface for the two general templates (left and right hemispheres) and for each of the age category specific templates (left hemisphere). Surfaces were generated with the preclinical surface pipeline precon_all (https://github.com/neurabenn/precon_all) which is an adaptation of Freesurfer's (Fischl, 2012) recon-all pipeline and has been described in detail previously in chapter 4 (4.3.5). Because this pipeline requires a T1-like contrast image, we converted the T2 contrast of our templates to obtain T1-like contrast images, using FSL tools. Here, we used a hand-edited white matter mask for the segmentation filled with hand-drawn subcortical and non-cortical masks. The filling process uses these masks to remove the cerebellum and brainstem and fill the subcortex between the lateral ventricles beneath the corpus callosum resulting in the prerequisite volumetric image used to produce the

white, pial and mid-thickness surfaces. They were then downsampled in connectome workbench to a sphere with 10,242 vertices. To find the main sulci, we used the sulcal maps from each age category surfaces and clustered them using the workbench command *metric-find-clusters.* We obtained 10 clusters corresponding to the 10 major sulci. As mentioned before due to the small number of right hemispheres available per age category, we did not create age category specific templates for the right hemisphere, therefore we also did not create age category specific surfaces for this hemisphere.

5.3.6. Volume analysis

The volume of the brain for each individual was assessed as the number of voxels in the cerebrum of each individual. This was obtained by transforming a cerebrum mask from the general template spaces to each individual space (left and right hemispheres done separately). We excluded the cerebellum and brainstem because some differences across individuals could be observed, although not based on anatomy. Indeed, the extraction procedure can sometimes alter the integrity of the brain stem and cerebellum. Specifically, the brain stem can be cut differently at its inferior end and the cerebellum was completely missing for one individual.

5.3.7. White matter and grey matter analysis

White matter (WM) and grey matter (GM) masks from the general templates were transformed to each individual space, as well as a cerebrum mask. The ratio WM/cerebrum and GM/cerebrum for each individual was computed. For the left hemisphere, we fitted a linear, a polynomial second degree, and an exponential model to explain the relationship between these ratios and the individual ages. We assessed the goodness of fit with the sum-squared errors and the adjusted R-squared measures. With

a change point analysis, we also investigated at which age the overall mean of the data changes abruptly using the Matlab function *findchangepts.* To investigate if the WM or GM only could drive the effect, we also computed the ratio of WM and GM volume in terms of number of voxels and the absolute volume of WM and GM for each age category.

To further investigate the distribution of GM and WM in each individual brain, we used the globally intensity-normalized *nodif* image (image based on the non-diffusion-weighted volumes with a T2-like contrast) from the template creation. The distribution of intensities in this image gives information on the ratio or grey and white matter voxels. Peaks of voxels belonging to similar range of intensities will associate with either the grey or white matter, as they represent most of the voxels in the brain image. We represented the distribution of intensities as the probability density function (PDF). We obtained local maxima represented by the two peaks of the distribution with the Matlab function *islocalmax* and then assessed the difference between the two peaks.

5.3.8. Tractography

The tracts were reconstructed using probabilistic tractography as implemented in the *Xtract* tool for which we defined seed, target, exclusion and stop masks (Warrington et al., 2020). The masks were defined in the general template space and transformed to each individual diffusion space. The tractography algorithm starts from the seed, the streamlines follow local orientation sampled from the posterior distribution given by *bedpostX.* Only the streamlines that reached or passed through the target and not through the exclusion mask were conserved, the others were excluded. Among the conserved streamlines, the ones reaching the stop mask were terminated there but were not excluded. In each seed voxel 10,000 samples were seeded. We used the default

Xtract options except for the step length which was adjusted to 0.2 mm because of the small voxel size and brain size of our data. For all protocols, a second tractography was run inverting the role of the seed and target as it has been shown to yield more robust results in macaques. For each tract, these resulted in two tractograms transformed back into the general template space and representing the fibre probability distribution at each voxel. They were then added and normalized by the total number of generated streamlines. The normalized tractograms were averaged across subjects (for the left hemisphere) of the same category and log-transformed.

We reconstructed all unilateral tracts, not crossing to the other hemisphere as we had single hemispheres. Tractography protocols used for each tract were defined as in *Xtract* (Warrington et al., 2020) except for modifications concerning the protocols for the inferior longitudinal fascicle (ILF), superior longitudinal fascicle 1 (SLF1) and the arcuate fascicle (AF). The ILF protocol was modified in the definition of seed and target which followed previous definition (Bryant et al., 2020; Roumazeilles et al., 2020), with a seed in the anterior inferior temporal gyrus and a target in the posterior inferior temporal gyrus. For the SLF1 protocol, we added additional coronal exclusion of subcortical areas at the level of the seed and target masks to avoid invading external and internal capsule fibres. For the AF protocol, we used the protocol from chapter 3 (Eichert et al., 2018; Roumazeilles et al., 2020) with a dorsal coronal seed just posterior to the level of the central sulcus. The target was located posteriorly in the caudal end of the Sylvian fissure and anteriorly at the level of the arcuate sulcus. The exclusion mask comprises two subcortical white matter masks to avoid leaking into extreme/external capsule and ventral longitudinal tracts, one mask through the superior parietal cortex and an axial exclusion mask to avoid invading the dorso-frontal territory of the SLF.

We used an in-house Matlab routine to produce three-dimensional visualization of the averaged log-transformed tractograms for each age category, to facilitate the study and the representation of the whole tract anatomy.

To assess each individual tract volume, we log-transformed the normalized tracts for each individual (instead of the age category average as above) and thresholded it at 80%. We assessed the volume of each tract as the number of voxels remaining after threshold and obtained the ratio with the total number of voxels in each individual cerebrum, so that our measure is normalized by the brain size. We investigated linear relationship between the ratio of voxel occupied by each tract and age. Because we have 19 tracts, we corrected the p-value for multiple comparison using the Bonferroni procedure, so the significance level is set at p-value $< 0.05/19$ (0.0026).

5.3.9. Fractional anisotropy and mean diffusivity

The fractional anisotropy (FA) and mean diffusivity (MD) were assessed for each individual tract. For this analysis, we used the individual log-transformed and normalized tracts thresholded at 80% as per their volume analysis. These thresholded tractograms were then used to mask the FA and MD images. The values contained in the resulting FA and MD image were then averaged and reported for each individual. We also used here the change point analysis, identifying the age at which the overall mean of the data changes abruptly, using the Matlab function *findchangepts.* We noticed that for FA and MD one individual was repeatedly an outlier. Because outliers can influence the change point analysis, we plotted a dotted line when the changepoint analysis landed on an outlier. Outliers are defined as values that are more than three scaled median absolute deviations away from the median as per the Matlab function

isoutlier. We also ran the changepoint analysis without the outliers to investigate where would the abrupt change be in this case.

5.3.10. Surface projection maps

We obtained cortical surface representations for each left averaged tract of each age category to investigate the cortical territory reached by these tracts. We used a recently developed approach to reduce the issues caused by gyral bias and superficial white matter (Reveley et al., 2015). This approach multiplies the tractograms obtained with a whole brain connectivity matrix (Mars et al., 2018c) and has been used in several studies before (Bryant et al., 2020; Eichert et al., 2020; Roumazeilles et al., 2020), as well as detailed in chapter 3 and 4. For each individual, we obtained a connectivity matrix representing the connectivity between all the vertices of the downsampled cortical surface and all the voxels in the brain volume. We used the surface derived from the general template and the associated warps to transform the individual images.

As described previously (Bryant et al., 2020; Eichert et al., 2020), to rebalance the weights in the tracts to be more homogenous, connectivity values were weighted by the distance between vertex and voxel. A distance matrix across all vertices of the mid-thickness surface and all brain voxels was computed using Matlab's *pdist2-function* resulting in a matrix of the same size as the connectivity matrix. Each element in the connectivity matrix was then divided by the corresponding value in the vertex-to-voxel distance matrix. We then averaged the matrices across individuals of the same age category. Each of the averaged age-specific tracts from the tractography (not log normalized nor thresholded) were multiplied to this average matrix, to obtain a map representing their connectivity with the cortical surface. The result was smoothed with a

gaussian surface smoothing kernel of 1 mm using the *cifti-smoothing* command from Connectome Workbench (Marcus et al., 2011) and log transformed and thresholded.

5.3.11. Blueprint

The surface projection maps of each left tractogram obtained as previously described can be represented as a column vector and concatenated in a matrix called the connectivity blueprint. This method has been established previously and used to compare different species brain connectivity, as in chapter 3 for instance (Mars et al., 2018c; Roumazeilles et al., 2020). The connectivity blueprint is in effect a matrix that describes how well each vertex of the grey/white matter border, as defined in the surface, is reached by each of the white matter tracts. Because the tracts are defined in a similar way in the different age category, they represent a common space that allows us to compare connectivity fingerprints across two brains, testing whether there are unique connectivity fingerprints in one brain compared with the other.

The connectivity blueprints of different brains can be compared by calculating the Kullback-Leibler (KL) divergence between the connectivity profiles of each vertex in one brain with that of each vertex in the other brain. The KL divergence measures how the probability distribution of likelihoods of one vertex to be reached by each of the tracts is different in one brain from the probability distribution of each vertex in the other brain. For each vertex in one brain, we could then determine another vertex in the other brain that had the minimum KL divergence—in other words, the most similar connectivity profile. If a vertex in one brain has a very similar connectivity profile to that of a vertex in the other brain, meaning that they are reached by a similar combination of tracts, the minimum KL divergence will be low. If, on the other hand, a vertex's fingerprint connectivity profile is unique in one brain, its minimum KL

divergence will be high. With this method, we compared the connectivity blueprint between each consecutive age category (example: from infant to juvenile). We averaged the resulting minimum KL maps across all voxels to investigate the overall divergence from one age category to the next.

5.3.12. Entropy

To further compare the change in connectivity across age category, we calculated a map of the connectivity entropy. The entropy measures whether a region is reached strongly by only a few tracts or equally by multiple tracts (Mars et al., 2018c). We calculated the Shannon's entropy as follow:

$$H(X) = -\sum_{i=1}^{n} log_2(P(x_i))$$

Where H is the entropy at the vertex X, $P(x_1)$ to $P(x_n)$ represent the probability that this vertex is reached by each tract. To investigate how the entropy changes with age, we also calculated the mean of the absolute difference of entropy between each consecutive age category.

5.3.13. Hemispheric variability

We verified that our results could generalized to the right hemisphere by carrying out most of our analysis also on the right hemisphere samples. However, due to the limited number of individuals (six), we were not able to fit any models, find abrupt changes or do the surface analyses. We were able to check that the right hemisphere results follow the same trend as the left hemisphere results (Appendix 5).

5.4. Results

5.4.1. Brain volume increases with age but overall anatomy is already present in infant

The brain volume in number of voxels linearly increases with age in the left hemisphere ($r = 0.53$, $p < 0.01$, Figure 5.5A). Despite this increase in brain size, we can notice from the age-specific left surface anatomy that the overall sulcal and gyral anatomy is conserved from infant to senior with the presence of all major sulci throughout the age range (Figure 5.5B). We were able to identify the arcuate sulcus (AS), the calcarine sulcus (CalS+, defined broadly and extending into the medial temporal lobe), the central sulcus (CeS), the cingulate sulcus (Cing), the inferior occipital sulcus (IOS), the inferior parietal sulcus (IPS), the lateral sulcus (LaS, also called the Sylvian fissure), the lunate sulcus (LuS), the principal sulcus (PS) and the superior temporal sulcus (STS). Previous developmental studies have shown that most sulci appeared at different stages of the embryonic development (Fukunishi et al., 2006; Kashima et al., 2008); our results confirm that if any post-natal changes in sulcal morphology occur, they are limited to the deepness of the sulci.

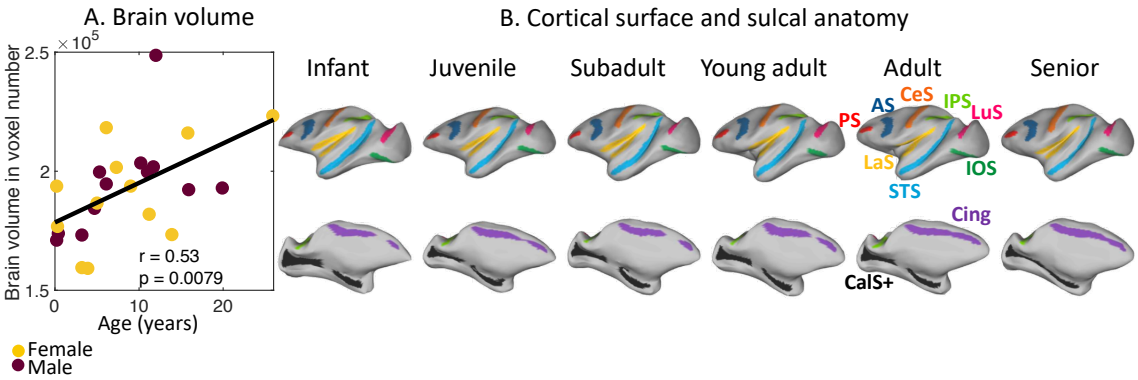

Figure 5.5 Brain volume and cortical anatomy.

A. Brain volume for the left hemisphere of each individual. Linear regression fitted as the black line ($r = 0.53$, $p<0.01$). *(Figure legend continues on the following page)*

B. Left cortical surface for each age category and sulci position. AS: arcuate sulcus; CalS+: calcarine sulcus; CeS: central sulcus; Cing: cingulate sulcus; IOS: inferior occipital sulcus; IPS: inferior parietal sulcus; LaS: lateral sulcus; LuS: lunate sulcus; PS: principal sulcus; STS: superior temporal sulcus.

5.4.2. White matter volume increases with age

When computed in terms of the ratio with the volume of the cerebrum, white matter (WM) and grey matter (GM) relationships with age are better fitted by an exponential model than linear or polynomial models (Figure 5.6A). The WM ratio increases steeply in early years to stabilize later on (linear: sum-squared error = 0.028, adjusted R^2 = 0.30; polynomial: sum-squared error = 0.013, adjusted R^2 = 0.65; exponential: sum-squared error = 0.007, adjusted R^2 = 0.81). The GM ratio follows the inverse relationship decreasing steeply at first to stabilize in later years (linear: sum-squared error = 0.020, adjusted R^2 = 0.42; polynomial: sum-squared error = 0.008, adjusted R^2 = 0.74; exponential: sum-squared error = 0.003, adjusted R^2 = 0.91). An abrupt change in mean of the data is observed between the infant and juvenile for both white matter and grey matter ratios (Figure 5.6A). However, when considering the ratio of white matter and grey matter volumes (Figure 5.6B), it does increase with age suggesting an overall increase of WM volume more than that of GM. This is confirmed by plotting the absolute volume of white and grey matter for each individual (Figure 5.6C). It appears that as brain volume increases, WM volume increases exponentially causing the ratio of GM with cerebrum to decrease but not the absolute volume of GM (r = 0.24, ns, Figure 5.6C).

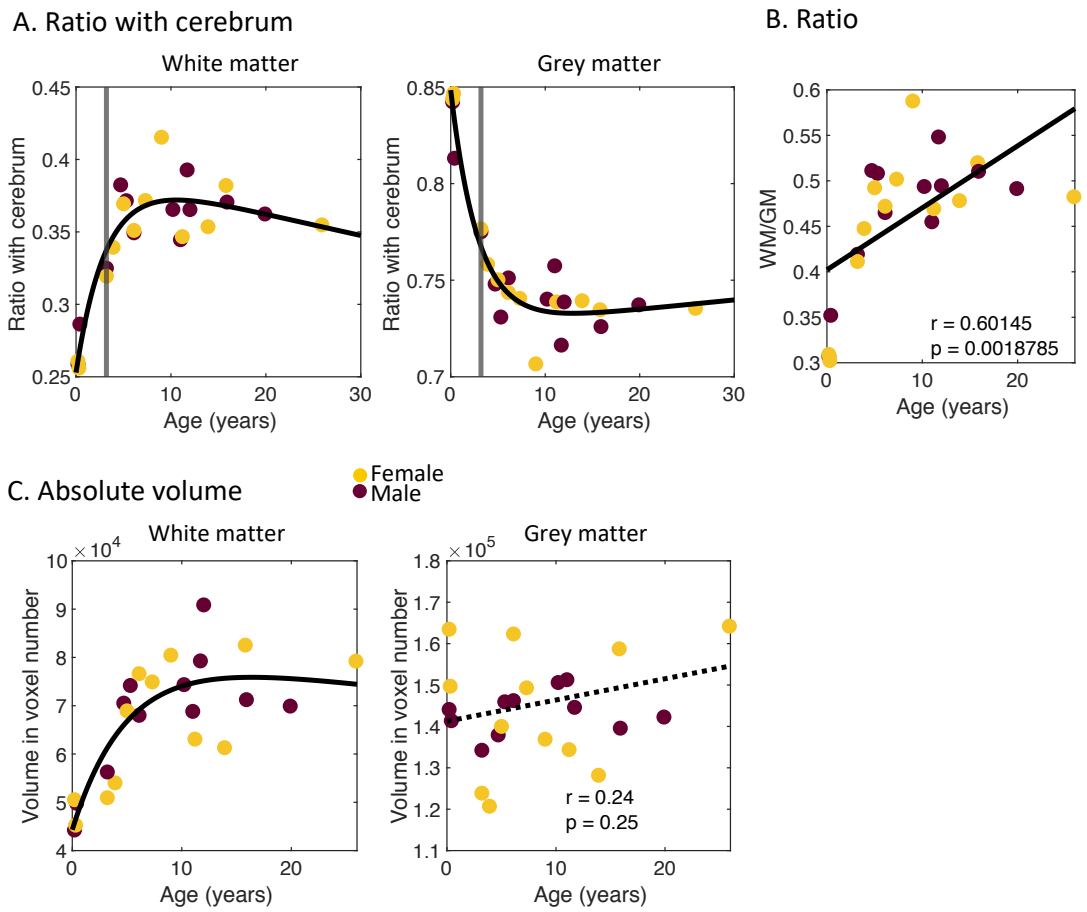

Figure 5.6 White matter and grey matter volume.

A. Ratio of left white matter and grey matter volume with the volume of the left cerebrum with the exponential curve fitted (black line). The grey vertical lines indicate an abrupt change in the mean of the data. **B.** Ratio of white matter volume in terms of number of voxels and grey matter volume for each hemisphere fitted with a linear model. **C.** Absolute volume of white matter and grey matter in terms of voxel number. For the white matter an exponential curve was fitted (black line). For the grey matter, no correlation was found with a linear model (dotted line, r = 0.24, ns). GM: grey matter; WM: white matter.

The distributions of intensities in the intensity-normalized nodif image also confirm that changes are happening in GM and WM across age (Figure 5.7AB). Two peaks can be observed in the distribution, the first one corresponding to darker intensities can be associated with WM and the second one of lighter intensities can be associated with GM. The height of each peak represents the relative likelihood that a given voxel will have this intensity and is therefore another measure of the ratio of GM

and WM. The difference between the probability of the two peaks is considerably higher for the infant that for the other age categories showing a progressive shift toward similar values for each peak (Figure 5.7C).

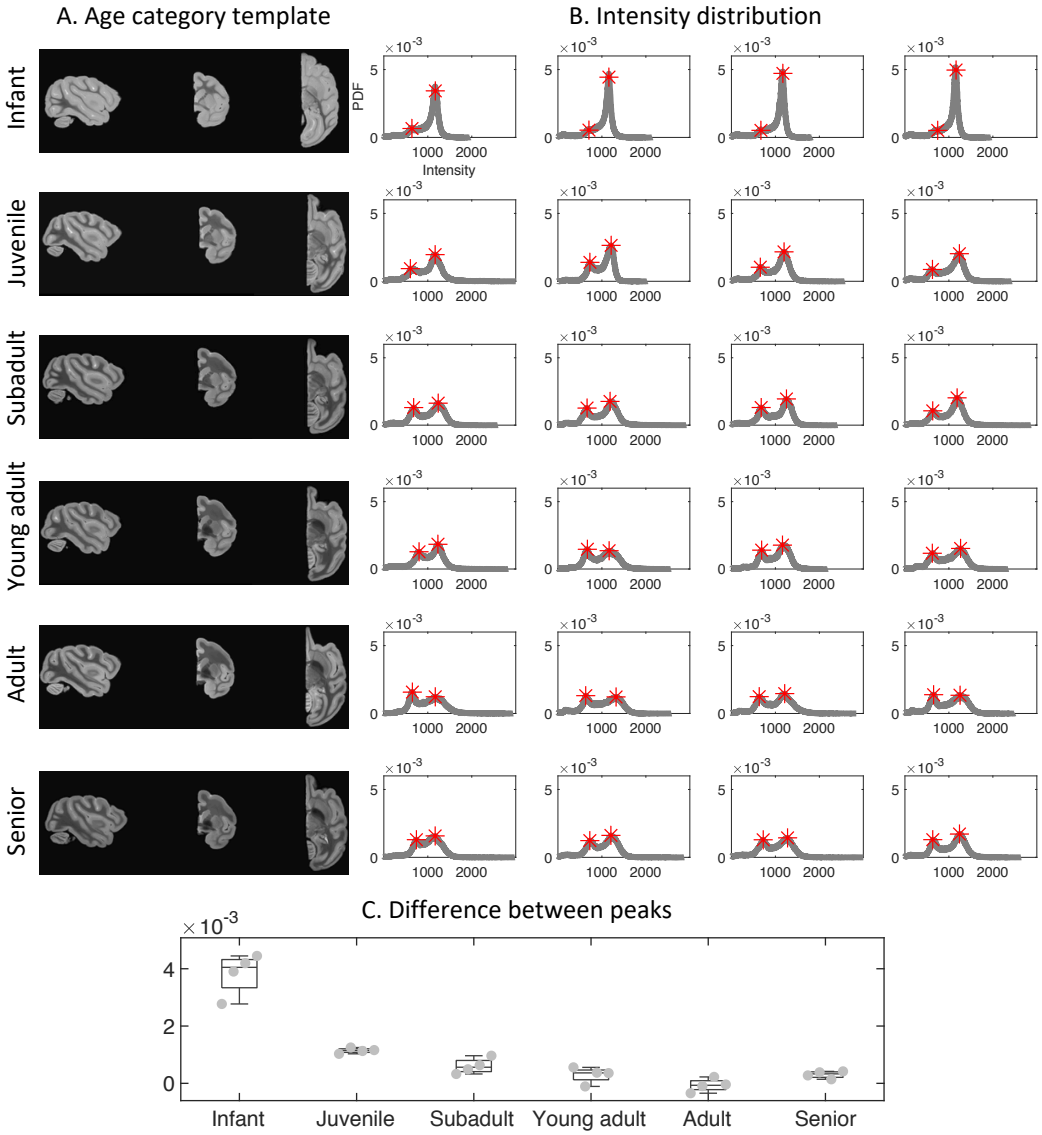

Figure 5.7 Distribution of intensities of the no-diffusion image.

A. Sagittal, coronal, and horizontal slices showing the age category specific templates based on the no-diffusion weighted image (*nodif*) of each individual (left hemisphere). **B.** Distribution of intensities of the normalized *nodif* image for each individual, each row corresponding to one age category. The red stars highlight the local maxima. **C.** Box plot representing the difference between the two peaks for each individual (grey dots). Each box corresponds to one age category, the central mark indicates the median, and the bottom and top edges of the box indicate the 25th and 75th percentiles, respectively. The whiskers extend to the most extreme data points not considered outliers. PDF: probability function distribution.

Similar results concerning white and grey matter volume and intensity distribution can be observed on the right hemisphere (Appendix 5).

5.4.3. Localized modification of tract anatomy with age

To further characterize age-related changes in connectivity, we reconstructed 19 WM tracts across the six age categories. Results show that main tracts and their overall anatomy are already present in infant (Figure 5.8).

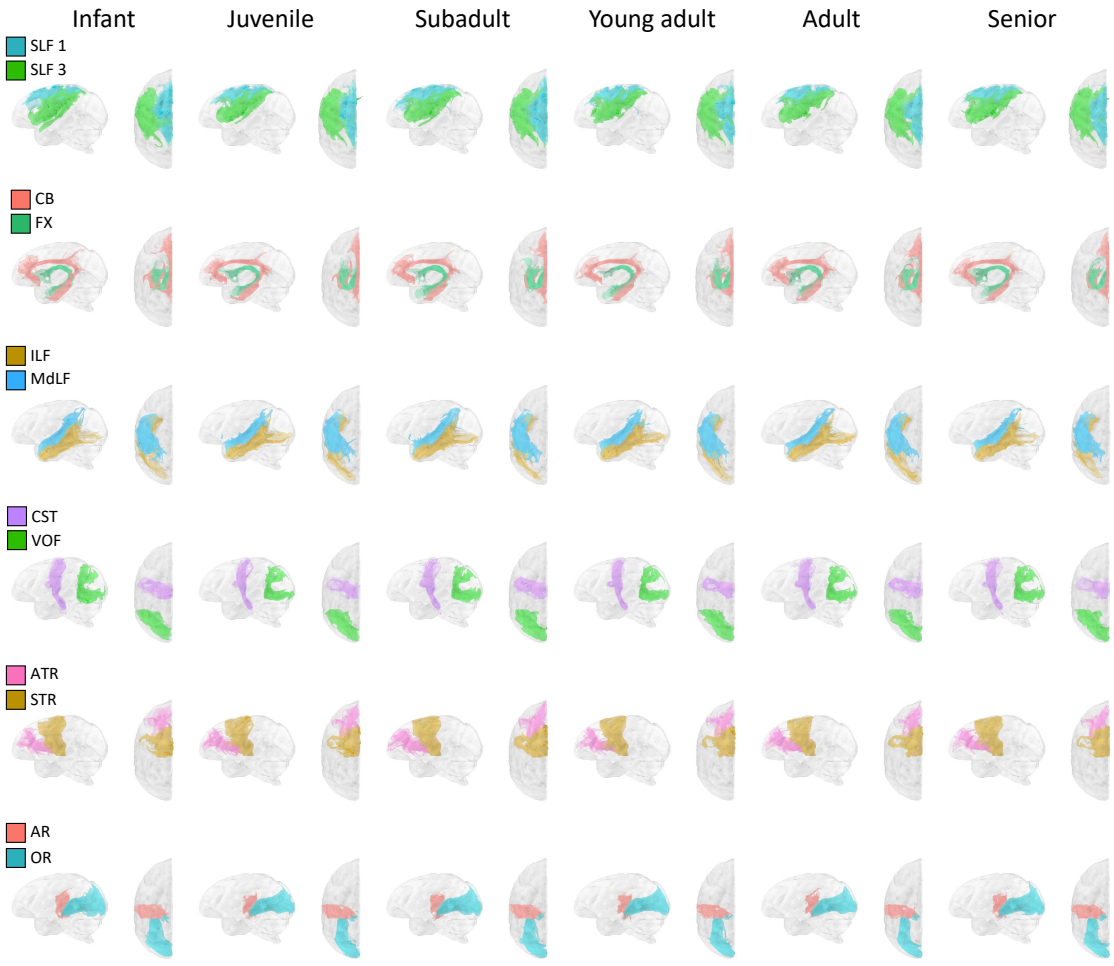

Figure 5.8 Tracts with similar anatomy across age category.

Averaged log transformed, thresholded tractogram represented in a 3D reconstruction showing left and dorsal views.

(Figure legend continues on the following page)

AR: acoustic radiation; ATR: anterior thalamic radiation; CB: cingulum bundle; CST: cortico-spinal tract; FX: fornix; ILF: inferior longitudinal fascicle; MdLF: middle longitudinal fascicle; OR: optic radiation; SLF 1 and 3: superior longitudinal fascicle 1 and 3; STR: superior thalamic radiation; VOF: vertical occipital fascicle.

However, localized differences could be observed across the life span. Three frontal tracts including two fronto-parietal tracts reduce their overall connectivity with age. Indeed, we can observe that the expanse of the arcuate fascicle (AF), the superior longitudinal fascicle 2 (SLF2) and the frontal aslant (FrA) reduces with age (Figure 5.9A), while the relative volume of the last two also significantly decreases with age (SLF2: $r = -0.58$, $p<0.0026$; FrA: $r = -0.50$, $p<0.0026$, corrected for multiple comparison, Figure 5.9B).

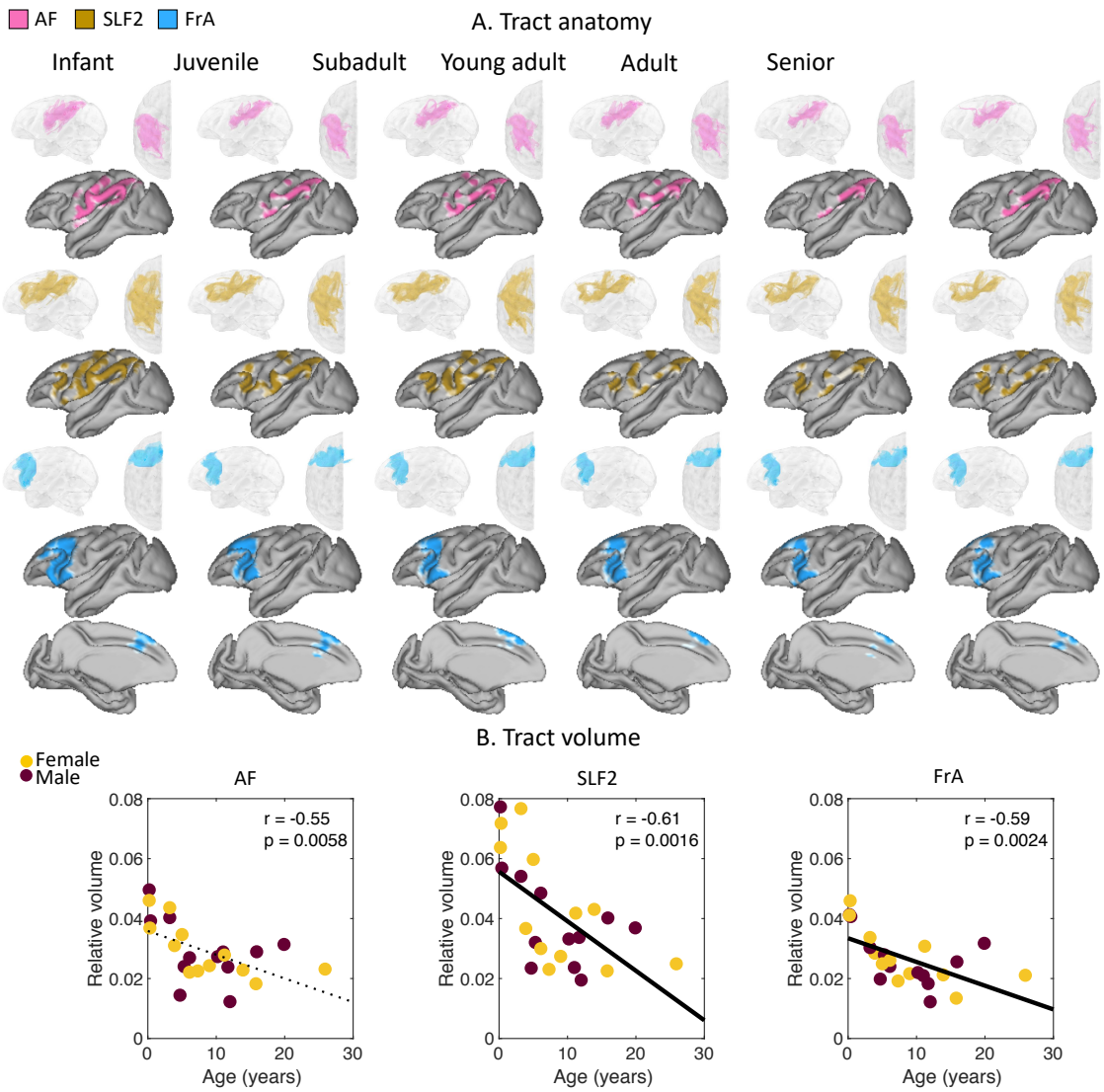

Figure 5.9 Decrease connectivity with age.

A. Left tracts anatomy. At the top, the averaged log transformed, thresholded tractogram is represented in a 3D reconstruction showing left and dorsal views. The bottom lines show projections to the mid-thickness left cortical surface (general template) from the lateral view for all and the medial view as well for the FrA. Lighter colour indicates lower threshold. **B.** Left tract volume relative to brain volume, each individual is represented as a separate dot. The correlation with age is significant for the SLF2 and FrA (Bonferroni corrected). AF: arcuate fascicle; FrA: frontal aslant; SLF2: superior longitudinal fascicle 2.

Two other frontal tracts show more localized differential connectivity although their volumes do not significantly vary with age (Figure 5.10AB). The inferior fronto-occipital fascicle (IFOF) shows a more pronounced connectivity in the medial prefrontal cortex and specifically in the area on the cingulate from juvenile age onward, an

extension not present in infant. Similarly, the uncinate fascicle (UNC) shows an increased frontal connectivity in juveniles onward compared to infants. Although, less evident as only one individual per age category is available, similar observation could be made on the right hemisphere (Appendix 5).

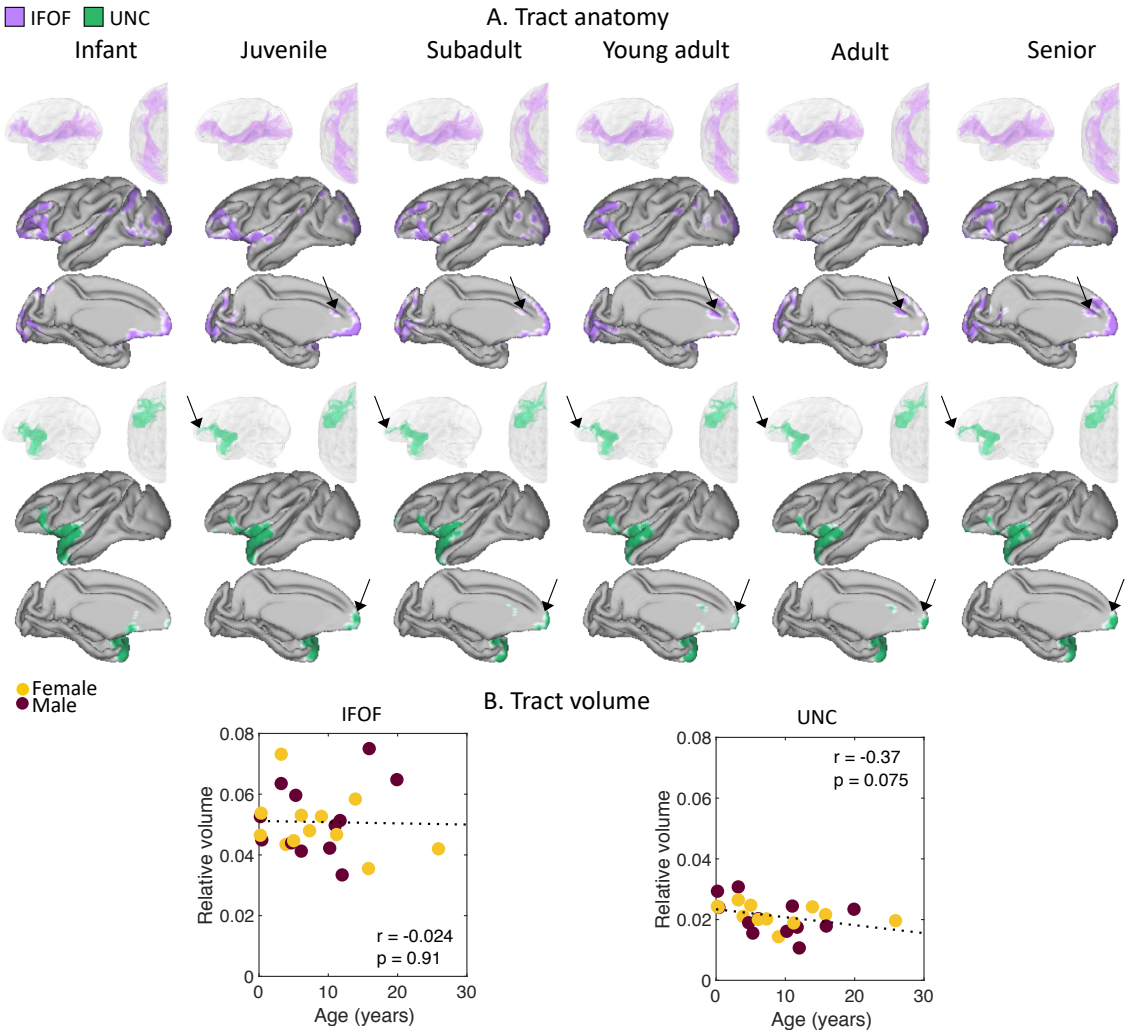

Figure 5.10 Localized frontal connectivity changes with age.

A. Left tracts anatomy. At the top, the averaged log transformed, thresholded tractogram is represented in a 3D reconstruction showing left and dorsal views. The bottom lines show projections to the mid-thickness left cortical surface (general template) from the lateral and medial views. Lighter colour indicates lower threshold. The arrows point out the differences observed between the infants and the other age categories. **B.** Left tract volume relative to brain volume, each individual is represented as a separate dot. IFOF: inferior fronto-occipital fascicle; UNC: uncinate fascicle.

The blueprint analysis, investigating overall brain connectivity change between age category, confirms these results. Indeed, main areas of high minimum divergence between age category are located in fronto-parietal territory (Figure 5.11A). The infant to juvenile minimum KL map, representing divergence in connectivity profiles between the two categories, has a higher mean value than the other minimum KL maps (Figure 5.11B). This difference shows that the connectivity from infant to juvenile undergoes more changes than the connectivity between other consecutive age categories.

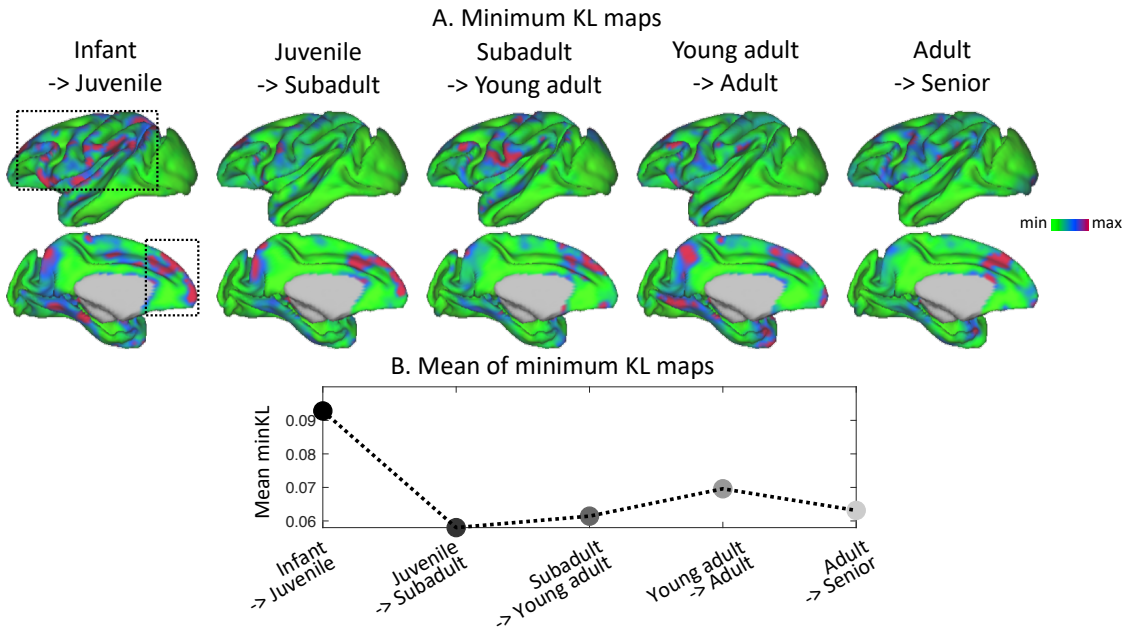

Figure 5.11 Results of the blueprint analysis.

A. Resulting KL divergence maps for younger age predicting older age connectivity represented on the left general template mid-thickness surface. The dotted squares highlight the fronto-parietal and frontal areas where tract differences have previously been observed between age categories. **B.** Averages of each age category minimum KL maps are represented with grey dots. KL: Kullback-Leibler.

5.4.4. FA and MD are mainly affected in early life

Fractional anisotropy (FA) and mean diffusivity (MD) provide structural information about tract integrity. There was no significant correlation between mean FA and mean MD across age in the 19 tracts studied (Figure 5.12AB). However, a change

point analysis revealed that for most of the tracts, the mean changes abruptly from infant to juvenile (16 out of 19 tracts for FA and 14 of 19 tracts for MD after correction for outliers, Figure 5.12C).

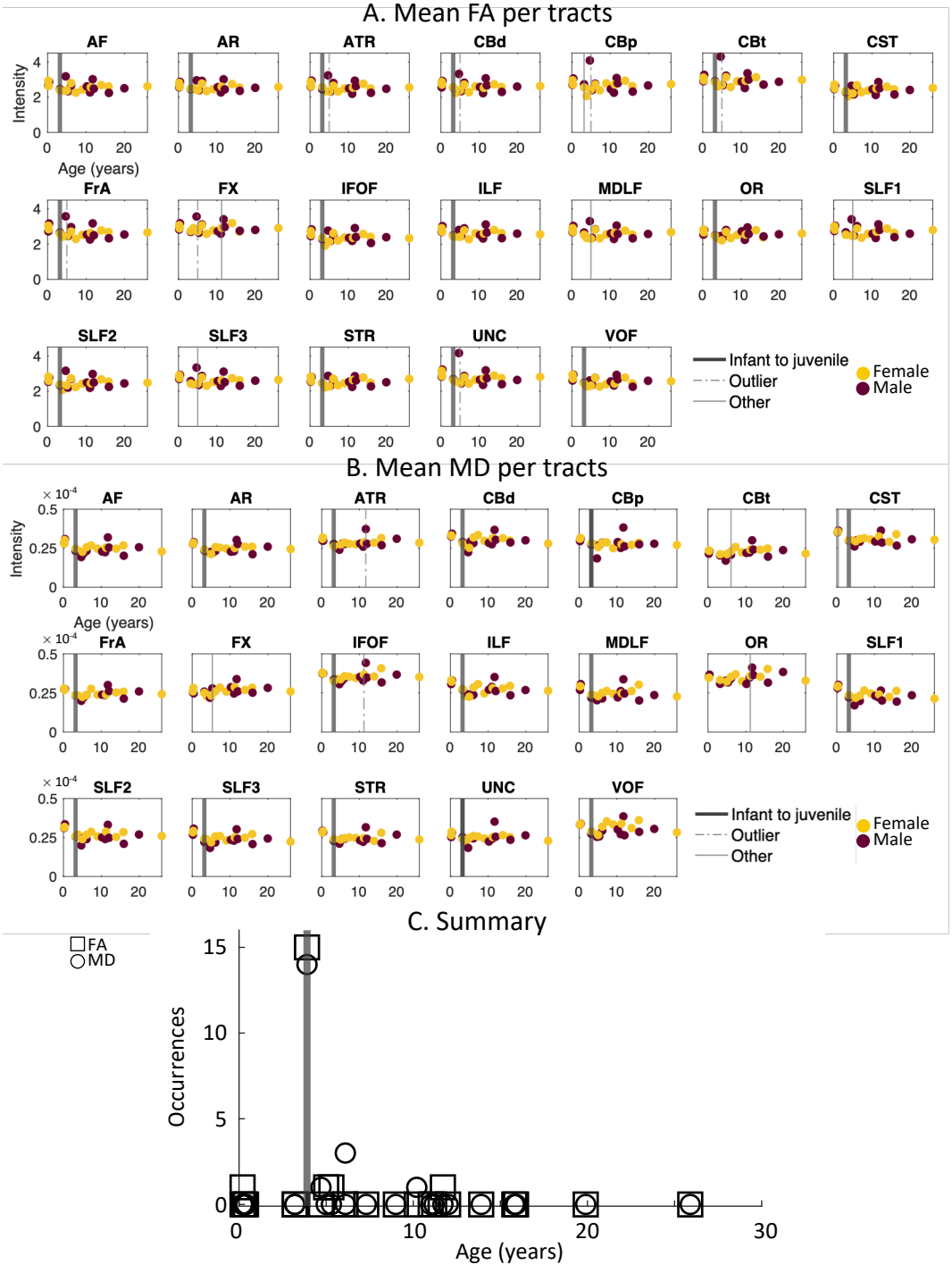

(Figure continues on the following page)

Figure 5.12 FA and MD per tracts.

A. Mean FA and **B.** mean MD per tracts for each individual according to age for the left hemisphere. The grey lines represent the results of the change point analysis. The thick line corresponds to the transition from infants to juveniles, the dotted line corresponds to outliers and the thin line to any other change point identified. **C.** Summary of the change point analysis representing the number of occurrences that a certain point was defined as an abrupt change. The grey line represents the transition from infants to juveniles. FA: Fractional anisotropy, MD: Mean diffusivity. Tract abbreviations can be found in Figure 5.8-9-10.

5.4.5. More entropy changes in early part of life

The entropy in connectivity measures how much a brain voxel is reached by the different tracts. High entropy denotes a brain region connected similarly to several tracts while low entropy corresponds to a brain region highly connected to one tract. Interestingly, we note that similar areas have high and low entropy across age categories (Figure 5.13A). As expected, multimodal areas such as the STS, the prefrontal and parietal areas have high entropy, while primary areas such as the visual cortex or the motor cortex have a lower entropy. The absolute difference of entropy between age category shows that entropy changes more from infant to juvenile and less changes in entropy occur between older age categories (Figure 5.13B). Importantly, the absolute difference is shown here because both increase and decrease (corresponding to pruning) of entropy occur.

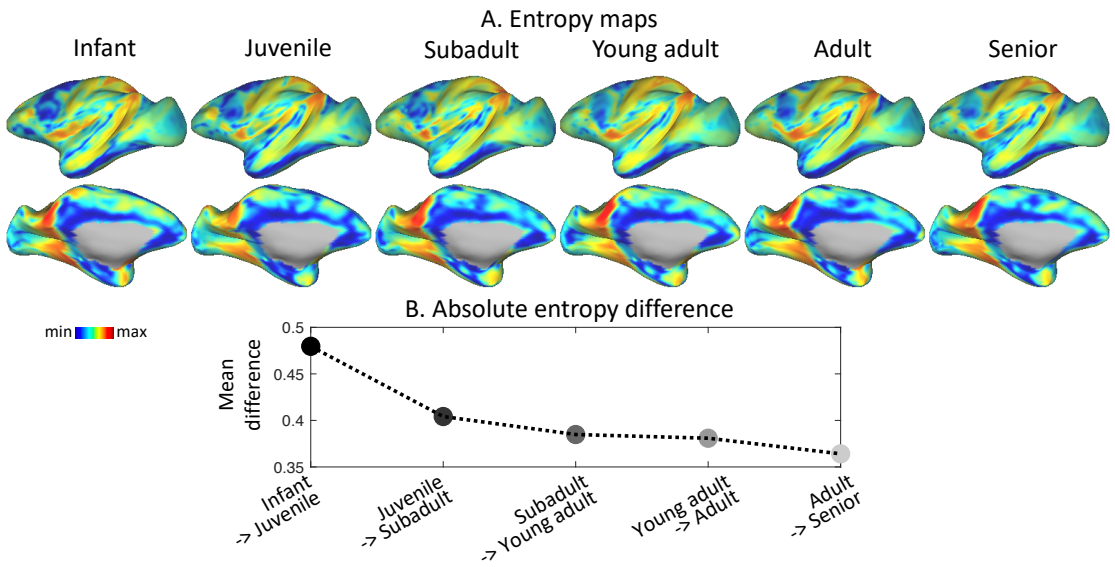

Figure 5.13 Results of the entropy analysis.

A. Entropy maps obtained for each age category represented on the left inflated general template surface. **B.** Averages of the absolute difference between two consecutive age categories are represented with grey dots.

5.5. Discussion

In this study, we investigated the development and aging of the macaque brain using diffusion-weighted MRI in a large sample of rhesus macaques (from 0.2 to 25.9 years old). We were able to assess the effect of age on the brain volume and white matter ratio, the sulcal anatomy, and to investigate white matter tract specific features (Figure 5.14). Indeed, we were able to reconstruct all the major unilateral tracts in the macaque brain to study their anatomy, structural properties and further examine more general connectivity properties. Overall, we observed that although the macaque brain volume slightly increases with age, infant macaque brains already show some adult characteristics, such as the cortical surface sulcal pattern, most of the tract anatomy and similar patterns of high and low entropy across cortical areas. These characteristics are relatively constant throughout the age-span studied here. Some age-related differences could also be observed, mainly from infant to juvenile. They include an increase of

white matter (WM) volume, subtle changes in WM tract anatomy linked with a higher connectivity divergence between infant and juvenile compared to other age categories and more entropy changes in early life.

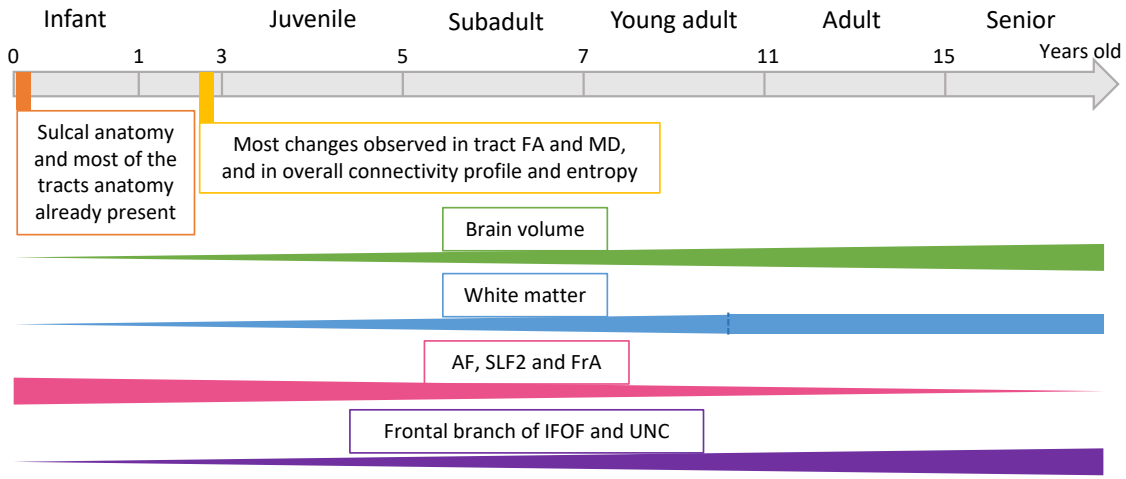

Figure 5.14 Summary figure.

AF: arcuate fascicle, FA: fractional anisotropy; FrA: frontal aslant, IFOF: inferior fronto-occipital fascicle; MD: mean diffusivity; SLF2: superior longitudinal fascicle 2; UNC: uncinate fascicle.

We pointed out important modification of WM characteristics from infants to juveniles, characteristics that stabilize from this juvenile period to old age. Therefore, we identified a similar early critical period for brain development, which was in accordance with previous reports (Malkova et al., 2006; Liu et al., 2015a). Importantly, sulcal anatomy appears already very similar to adult form in macaque infants which is very different from the case of human new-borns. Although already folded at birth the human brain undergoes further regionally specific cortical expansion to reach its adult form, possibly allowing these regions to be more sensitive to post-natal experience (Hill et al., 2010). The shorter period to reach maturity in macaques compared to humans observed neuronally could be a crucial element to explain cognitive differences observed in adulthood between species (Kaplan et al., 2000; Wobber et al., 2014).

Concerning the structural properties of white matter (FA and MD), our data did not show any trend along the macaque lifespan. It corresponds to previous macaque studies identifying most of the fluctuations in the first weeks after birth (Shi et al., 2013; Kim et al., 2020) but is very different from observation in humans showing transient modification of FA and MD throughout the lifespan (Lebel et al., 2012). It is also surprising that we did not observe any ageing effect on FA and MD as was observed in previous human and macaque studies (Chen et al., 2013).

We also observed tract modification along the macaque life span and confirmed this result using the blueprint approach. Although WM tracts cannot be ascribed to specific function as could be done for grey matter (GM) areas, we can try to discuss the possible implications of these results in the light of the current literature. The AF, SLF2 and FrA seem to undergo important pruning with their volume and connectivity extent reducing with age. This could also be associated with an ageing effect as the SLF2, associated with spatial attention and awareness function (Schmahmann et al., 2007), has been previously shown to be altered in its integrity with normal ageing in macaques (Makris et al., 2007). Interestingly, both the AF and FrA have been associated with language functions in humans (Dick et al., 2019), although the development of human AF is mostly following an increase of connectivity with age rather than a decrease as observed here in macaques (Friederici, 2012; Tak et al., 2016). The IFOF and UNC also present some age specific modifications, with localized frontal extension visible in juveniles but not in infants. Overall connectivity analysis, blueprint, and entropy also point towards the main changes happening between infant and juvenile age categories while some aspects remain constant throughout the age range studied. For instance, the blueprint analysis shows that most of the temporal lobe connectivity is already established in early age and does not differ massively throughout the lifespan, while

some GM developmental changes have been identified in the first year around the macaque superior temporal sulcus (Livingstone et al., 2017). Concerning the entropy, its distribution seems very much conserved across the age categories.

Limitations and future directions

One inherent limitation of our study concerns the fact that it is a cross-sectional study and not a longitudinal study, different individuals are represented in the different age category. We tried to counterbalance this effect by acquiring a large amount of data, and more similar data will be acquired in the near future and could be used to confirm our results. We have also shown in the methods section that although we have data of individuals from different age and provenance, the data quality is similar in all cases. Cross-sectional studies could bring concerns about inter-individual variability explaining the results more than the age difference. However, the strong and stable effect we obtained here with different approaches, showing differences mainly between the infants and the rest, is unlikely due to inter-individual differences. Concerning the blueprint analysis, this more sensitive analysis due to the lower threshold used could lead to more noisy results and illustrate some interindividual variability. This could potentially explain the high minimum KL divergence observed in localized areas between some age categories but not others and that are not explained by the tract anatomy. This issue could be resolved with a higher number of subjects per age category.

We have to note that there is a gap in the age range covered between infants and juveniles as no data could be obtained between 5 months old to 3 years old due to colony management issues unrelated to this study (Hernandez-Pacheco et al., 2016). Investigating this missing age range could help to refine our observations. However,

this is not an issue here, as this age range has been covered by other studies (Malkova et al., 2006; Shi et al., 2013; Liu et al., 2015a; Scott et al., 2016) and we were particularly interested in gathering knowledge about the whole lifespan in this study. Another challenge from MRI developmental studies comes from the fact that scanning nonhuman primate new-borns has been proven difficult because of the limited contrast obtained in their brain, as relaxation time is similar between grey and white matter (Liu et al., 2008). Further improvements in the MRI techniques could enable to access WM characteristics from foetal and new-born non-human primates to enrich our understanding of their early development.

Conclusion

In summary, our study provides evidence regarding the developmental schedule of macaque brains. Using a large dataset and newly developed methods, we were able to set an analytic framework with templates and surfaces for all age categories studied. The reconstruction of white matter tracts throughout the brain, in turn, allowed us to go further than previous studies and assess the overall brain connectivity changes between age categories. We reinforce previous findings that most changes happen in the first few years after birth, although some adult brain characteristics are already present in infant macaques. We specifically point out some connectivity modification throughout the life span.

Chapter 6 - Discussion

In this thesis, we aimed to shed light onto the evolutionary roots of the human social brain. Using different magnetic resonance imaging (MRI) techniques in a comparative framework, we were able to further our understanding of the social brain organisation, function, and connectivity in a wide range of primate species and incorporate developmental insights.

6.1. Novelty of the approach

As mentioned in the introduction, comparative neuroscience is a field constantly improving in order to tackle issues that mainly concern the study of more species. Along this thesis, we combined existing approaches and implemented new methods that enabled us to study an unprecedented wide range of primate species.

We benefited from the acquisition of primate brains from several sources such as zoos, laboratory, and free-ranging colonies. We were able not only to acquire anatomical data in the same way in all species and age studied using MRI but also to adapt existing methods in order to analyse them and use the common space framework. We also adapted the methods in the functional domain using appropriate behavioural test in macaques. Combining the functional and structural approaches gave us a more complete picture of the evolutionary processes shaping the primate brain leading to insights never available before.

6.2. Summary of the studies and their findings

6.2.1. Identification of a precursor for theory of mind ability in the last common ancestor of humans and Old World monkeys

First, we relied on a computational framework to design a non-linguistic task in fMRI to investigate theory of mind (TOM) neuronal signature in macaques. We identified a middle superior temporal sulcus (midSTS) area specifically responding to violation of social situation prediction. We reproduced this result in a replication study. We further investigated the properties of this midSTS area by studying its resting-state connectivity and its relationship with the face-responsive network. Overall, we observed that the macaque midSTS area shared computational properties with human area TPJ that are associated with theory of mind, a similar connectivity profile to the rest of the brain, but that it was less dissociated from the face network than human TPJ. In line with recent literature, we concluded that the macaque midSTS could represent a precursor for theory of mind ability in the last common ancestor of humans and Old World monkeys.

6.2.2. A series of changes explain differences between humans and macaques in temporal lobe connectivity

Second, we investigated how the temporal lobe white matter architecture in different primates underlies the expansion and reorganisation of this region observed in the primate phylogeny. Using diffusion-weighted MRI to perform tractography, we reconstructed longitudinal temporal lobe tracts in macaques, gorillas, chimpanzees, and humans. We observed several modifications of white matter anatomy between the different species which allowed us to suggest an evolutionary trajectory for the

longitudinal temporal lobe tracts. The main observations concerned the Inferior longitudinal fascicle (ILF) separation into subcomponents and the more lateral localisation of the inferior fronto-occipital fascicle (IFOF) in great apes but not in macaques. The arcuate fascicle (AF) invaded the temporal lobe more in humans compared to the other species studied. Using the tracts defined, we were able to compare the connectivity profile of the temporal lobe between macaques and humans in a common space framework. We revealed that the medial subcomponent of the human ILF was the most similar to the macaque ILF and it was the AF that contributed most to the distinctive organisation of white matter connectivity in humans compared to macaques. Overall, we argued that differences classically observed between macaques' and humans' temporal lobe cortical organisation are not due to a single change, but the study of additional species brings a finer description of the series of changes responsible.

6.2.3. The simian parietal and frontal elaboration observed in sulcal and white matter anatomy

Third, we extended the study of brain connectivity to early primate species. Using diffusion-weighted MRI and newly developed tools, we were able to create templates and surfaces and reconstruct white matter tracts for the lemurs, squirrel monkeys and macaques. We observed an expanded granular prefrontal cortex associated with the expansion of the ILF and superior longitudinal fascicle complex (SLFc) connectivity in squirrel monkeys and macaques compared to the lemurs. We associated this finding with a parietal and frontal elaboration in simians. We also reported a very developed visual cortex in saimiri which is confirmed by the posterior expansion of the

optic radiation (OR). Overall, this study allowed for a better characterisation of brain anatomy in understudied primate species and illustrate the simian brain elaboration.

6.2.4. The macaque brain undergoes connectivity modification mainly in the first year after birth

Finally, we investigated how the macaque brain connectivity develops throughout the lifespan, in order to better characterise the ontogeny of brain networks in this species. Using a large dataset of diffusion-weighted MRI, we were able to assess brain structural characteristics and connectivity architecture in 6 age categories. We found that most of the parameters studied showed the highest change at the transition between infants (0-1 year old) and juveniles (3-5 years old). Precisely, the expansion of the white matter followed a steeper trend in the first year, such as microstructural connectivity changes seen in fractional anisotropy (FA) and mean diffusivity (MD) across the tracts. Concerning the tracts, we observed a decrease in connectivity with age in three tracts: the AF, the superior longitudinal fascicle 2 (SLF2) and the frontal aslant (FrA) while the IFOF and uncinate fascicle (UNC) demonstrated an increase localized frontal connectivity with age. Overall, the connectivity modifications in terms of connectivity profile and entropy were also more important between infants and juveniles. We concluded that although some brain anatomy is conserved from infant to senior in macaques, most modifications happen in the first year and some localized fronto-parietal connectivity continue to change throughout the lifespan.

6.2.5. A coherent story for the primate social brain evolutionary trajectory

All these studies and conclusions can be linked together to suggest an evolutionary trajectory for the primate social brain (Figure 6.1).

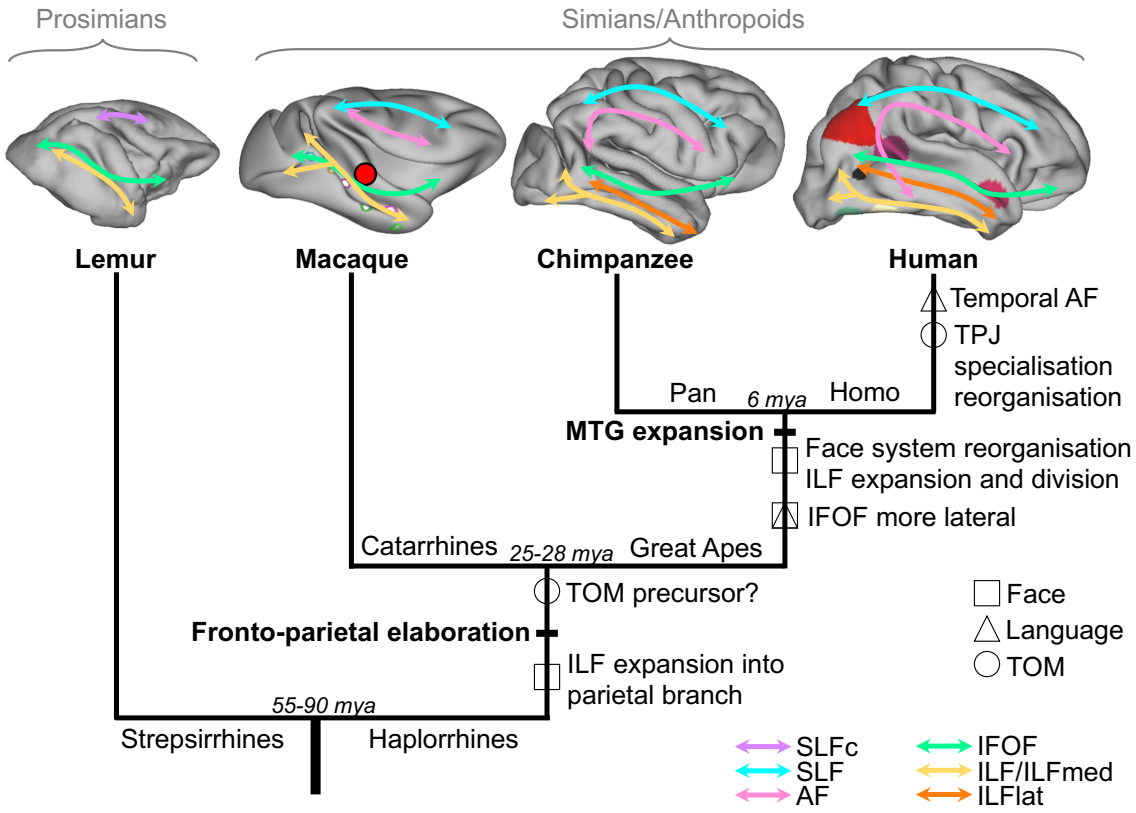

Figure 6.1 Suggested evolutionary trajectory for the primate social brain.

On the simplified primate phylogenetic tree is represented a summary of the results obtained in this thesis. Brain areas and white matter tracts are represented in a simplified version. We classified our findings in terms of their association to three different social abilities (face-associated, language and TOM). TPJ and its possible macaque precursor are represented in red; refer to Figure 1.3 for full colour code of brain areas. AF: arcuate fascicle; IFOF: inferior fronto-occipital fascicle; ILF: inferior longitudinal fascicle; lat: lateral; med: medial; MTG: middle temporal gyrus; SLF: superior longitudinal fascicle, SLFc: superior longitudinal fascicle complex; TOM: theory of mind; TPJ: temporo-parietal junction.

Temporal lobe considerations

The three first studies (chapters 2 to 4) converge in identifying evolutionary trajectory for the temporal lobe and associated social functions. The macaque midSTS was shown as a precursor of the human TPJ supporting mentalizing properties in humans. Differences between the two regions were observed in the further dissociation of the human TPJ from the face-responsive network also present in the temporal lobe. The ILF has previously been identified as a potential tract supporting face-associated abilities (Herbet et al., 2018). Our connectivity studies (chapters 3 and 4) demonstrated an incremental extension of the ILF throughout the primate phylogeny. Its parietal branch, not present in lemurs, was shown as a simian elaboration, while a division in subcomponents was shown as a great apes specialisation. In line with the functional study (chapter 2), the human ILF subcomponent most similar to the macaque ILF was identified as running in the vicinity of the human face areas. These areas are in a completely different location in the two species, but we were able to identify how the underlying connectivity reorganises. We could think that the division of the ILF into subcomponents, with the least similar to the macaque running nearer to the TPJ, could accompany the further specialisation observed in humans compared to macaques. Overall, our studies suggest a cortical and connectivity reorganisation of the temporal lobe associated with the expansion of this region along the primate evolution and provide an interpretation in terms of social functions.

Parietal and frontal considerations

The last three studies (chapters 3 to 5) converge in identifying evolutionary trajectory for the parietal and frontal lobes and the possible implications for language functions. We described a fronto-parietal elaboration in simians compared to

prosimians, observed partly in the expansion of the frontal granular areas and SLFc connectivity (chapter 4). The SLFc, as defined in this study, also includes fibres associated with the AF. The AF has particularly been associated with language functions and we also identified the AF as the main tract contributing to the human different connectivity profile in the temporal lobe (chapter 3). Interestingly, we also identified the AF and the SLF2 as refining their connectivity throughout the macaque lifespan (chapter 5). The IFOF, connecting the frontal and occipital lobe through the temporal lobe, has been identified in all species studied although showing different anatomy in great apes, with a lateral expansion in the middle temporal gyrus. This lateral expansion of the IFOF has been suggested to be implicated in language functions, because carrying information between language-related areas in the human brain (Makris et al., 2009; Almairac et al., 2015) and possibly to allow 'visualisation' of scenes described by speech thanks to its connectivity to the visual cortex (Panesar et al., 2017). Frontal connectivity of the IFOF, as well as the UNC frontal connectivity appeared to expand after the first year of life in macaques. Overall, our studies expand our knowledge of fronto-parietal connectivity evolution and maturation in primates.

6.3. Further considerations and perspectives

6.3.1. Insights into the theory of mind debate

Implicit theory of mind in macaques

As noted in the introduction (1.1.2), theory of mind evolutionary origins are currently highly debated. In the chapter 2 of this thesis, we used the framework of predictive coding associated with theory of mind to investigate a potential neuronal precursor in macaques. This framework proposes that brain areas associated with theory of mind, such as the human TPJ, make inferences about others' thoughts and behaviours

leading to higher activation when the prediction is violated (Behrens et al., 2008; Koster-Hale and Saxe, 2013). We have uncovered a midSTS area in the macaque brain that shares this computational property associated with theory of mind and the TPJ in humans. While our novel method allowed us to conclude that the midSTS constitutes a potential precursor for TPJ in macaques and that macaque brains are able to signal a social prediction error, we cannot conclude firmly on the existence of theory of mind in macaques. Therefore, we are not claiming that macaques possess a full theory of mind as humans, but they share at least some basic mentalizing computations that had not been shown in macaques before. Together with the recent evidence of false belief in macaques (Hayashi et al., 2020), our study reinforces the idea that, at least implicit theory of mind, a fast and automatic process, could have appeared in primate evolution as early as the Old World monkeys common ancestor.

The macaque midSTS as a precursor of human TPJ

Our study argues for the macaque midSTS as a precursor of the human TPJ based on basic mentalizing computation found in both areas. Because of the association to social cognition and mentalizing, we could associate this macaque midSTS specifically to the posterior part of the TPJ (Mars et al., 2012b). Our study also fits in recent literature, arguing for a third visual pathway in primates that would be specialized in dynamic aspects of social perception (Pitcher and Ungerleider, 2021). A midSTS area close to our social prediction area has been identified as the core region of this third pathway in macaques (Yang and Freiwald, 2021). It has been suggested that this macaque third pathway in the dorsal bank and fundus could corresponds to the human third pathway running through the STS (Pitcher and Ungerleider, 2021). This is supported by the expansion of the ILF in humans reported in chapter 3 suggesting more

integration between this third pathway and the face ventral pathway in macaques than in humans. Therefore, differences with human theory of mind in the relationship with other social networks and overall anatomy could explain the unique behavioural features of theory of mind in humans.

It is important to note that an alternative hypothesis has been proposed to the origin of the human TPJ. This second hypothesis is proposing that the inferior parietal lobule (IPL, also called region 7a) corresponds to the human TPJ in macaques (Sliwa and Freiwald, 2017). However, this alternative hypothesis relies solely on a selective response to social interactions in macaques and lacks the connectivity and computational similarities with the TPJ that the midSTS hypothesis has. When considering the expansion of the temporo-parietal area from macaques to humans (Hill et al., 2010) and the fact that the human TPJ is involved in several social functions and not only theory of mind (Patel et al., 2019; Schurz et al., 2021), it is conceivable that several areas in macaques could have reorganised to give the TPJ-pSTS complex in humans. We could suggest that both our social prediction area in the midSTS and the IPL contributed as precursors for the human TPJ. However, only the midSTS constitutes a precursor for mentalizing computation, while the IPL could be involved in other social functions. Interestingly, also in marmosets, both the midSTS and a homologous area to the macaque 7a, the area PG, have been associated with the social brain network (Schaeffer et al., 2020; Cléry et al., 2021). However, to our knowledge mentalizing computations have not been tested yet in New World monkeys, so we cannot infer if they were already present in this primate family or if this characteristic is specific to Old World monkeys.

6.3.2. Implications of white matter reorganisation in the evolutionary framework

Combining cortical and white matter insights

Brain anatomical descriptions and comparisons have classically focused on the grey matter and associated functions. Lately, advances in imaging techniques have favoured a more extended investigation of the whiter matter organisation underlying the grey matter one. We have been able in this thesis to expand our knowledge of white matter organisation in different primate species previously understudied and its developmental trajectory in macaques. Together with observations of cortical reorganisation, defining white matter organisation allows us to fully comprehend differences between primate species. For instance, the gorilla has a slightly less clearly defined fusiform gyrus than their close relatives, chimpanzees. This slight difference was also observable in the connectivity of longitudinal tracts such as the ILF, IFOF and AF. Similarly, we have shown that the very different occipito-parietal anatomy observed between prosimians and simians could be associated with differences in ILF connectivity.

Brain evolution principles and hypotheses

Combining cortical and white matter reorganisation observations, we have also been able to illustrate different principles of brain evolution as introduced previously (1.4.2). The principle of allometry, suggesting that the size of surrounding elements would cause an increase in the size of the encased one, could be observed in the expansion of the temporal lobe in great apes associated with the expansion of the ILF and its subdivision (chapter 3). Similarly, the frontal cortex expansion in simians is associated with an expansion of the SLFc compared to prosimians. We have also

introduced the notion of mosaic evolution, an expansion selective to certain brain structures and lineages. The specific expansion of the visual cortex associated with expansion of the optic radiation in squirrel monkeys constitute a good example of mosaic evolution, as this is not observable in macaques nor in prosimians (chapter 4). We suggested it could be due to the more arboreal-dependent lifestyle of squirrel monkeys which implies more neuronal information processing necessary in visual systems, based on similar observation in rodents (Campi and Krubitzer, 2010). However, in the current state of knowledge, we do not know how much this relative increase in visual cortex size in squirrel monkeys impacts on other brain areas and functions.

In this thesis, we have identified brain modifications in grey matter areas and white matter tracts classically associated with social abilities but also with foraging ones. Indeed, we have previously detailed the implications of our findings for the social brain (6.1.5), but we have also identified a simian fronto-parietal elaboration most commonly associated with decision-making processes underlying foraging (chapter 4). We would therefore suggest that this thesis argues in favour of reconciling the social and ecological hypotheses of brain evolution in that they could have differential explanatory power across different cognitive domains (Rosati, 2017). Even though sociality could have first driven brain evolution, the foraging skills that had to develop to support a large social group and a large brain could have shaped the brain further. Our data and results cannot lead us to conclude on the sequential or simultaneous aspect of the social and foraging pressures on the evolution of the brain, both being so intricately linked in their behavioural phenotypes and brain systems. In this integrative framework, future studies might be able to better account for the different forces at play in primate evolution and in which dimensions humans are unique.

Limitations in the interpretation

We should be cautious in interpreting our results as it is currently limited to link white matter tracts with function and environmental pressure that could have favoured a specific evolutionary trajectory. Relationship between white matter and function has been suggested after brain lesions leading to disconnection that could be matched with task-related fMRI activation patterns (Thiebaut de Schotten et al., 2020). These studies are facilitated by the emergence of large datasets covering the brain connectome and fMRI data and participate in uncovering networks responsible for neurologic and psychiatric symptoms (Fox, 2018). However, lesions due to stroke tend to not be distributed randomly limiting our knowledge access to these regions particularly affected and therefore to a certain set of functions. Direct electrical stimulation has also been suggested as a method to study structural and functional organisation of brain networks including both cortical areas and white matter pathways (Sarubbo et al., 2020). In this thesis, we combine both functional and structural approaches which allows us to make informed network hypotheses based on proximity between functionally identified cortical areas and white matter structure and on previous literature as well. However, our current method cannot allow us to conclude with certainty on the function of a given white matter tract.

The comparative framework used in this thesis has enabled us to make hypotheses on evolutionary trajectory. However, we should observe caution as well in term of evolutionary interpretation, as we are studying distant species that all have continued to evolve since their common ancestor. Our effort to facilitate the integration of more species should contribute to improve these interpretations in the future.

Overall, although there are limitations in interpreting white matter links with function and evolution, our multimodal approach mitigates these limitations and importantly allows to further our understanding underlying brain expansion and reorganisation in primates.

6.3.3. Perspectives

This thesis applies novel frameworks for behavioural and anatomical studies that opens the way to further investigation and allows for applications in more species.

Further applications for the behavioural framework

Our behavioural task from chapter 2 investigating the neuronal correlates of social prediction error could be further adapted to humans. It would allow to match closely the human TPJ and macaque midSTS mentalizing computations. As mentioned previously, to better characterize the evolutionary roots of mentalizing, it could also be adapted to New World monkeys such as the marmosets or the squirrel monkeys for which interests are currently increasing and methods such as functional MRI being refined (Schaeffer et al., 2019; Royo et al., 2021). We have established the relationship between the social prediction error area in macaques and the face patch system, but other social brain networks could be investigated in order to fully comprehend the role of this area in the social brain. For instance, how it integrates with the exclusively social interaction networks observed in macaques and marmosets (Sliwa and Freiwald, 2017; Cléry et al., 2021).

Further applications for the anatomical framework

In chapter 4 and 5, we have applied newly developed methods to create templates and surfaces for different primates' species. These studies constitute a proof of concept and suggest how these methods, available in open access, can be applied and generalized to more species. In turn, the use of similar methods in different species to establish templates and surfaces allows to apply the common space framework and compare very different brain reliably on several levels. In this thesis, we have mainly used the brain connectivity through the white matter tracts reconstruction as a common space between different species or age categories (chapter 3 and 5). Other shared features, mapped on the templates, can be further added and combined to elaborate the evolutionary and developmental hypotheses (Mars et al., 2021).

Regarding the developmental domains, these methods will also allow for better reproducibility between studies and go further than the usual focus on size or regional aspects to instead investigate several features of the whole brain developmental trajectory. They could also lead the way to investigate the brain development of more primate species as this is still quite limited. Using similar methods for developmental and evolutionary research will facilitate the establishment of links between the two. Although, the evo-devo field brings interesting inputs into understanding the roots of primates' cognition, we should remain careful not to overinterpret the findings and also recognise their specific processes.

6.4. Conclusions

In sum, in this thesis we have investigated the social brain structure and function in primates in a comparative and developmental framework, using multi-modal MRI methods in a large range of species. By applying a computational framework to

macaque functional MRI, chapter 2 identified the macaque midSTS as a potential precursor for the human TPJ and mentalizing computations. Chapter 3 focused on the temporal lobe white matter tracts in macaques, gorillas, chimpanzees, and humans to suggest an evolutionary trajectory for the reorganisation of connectivity in this brain lobe associated with social functions. This is further completed in Chapter 4, investigating the cortical anatomy and connectivity of the brain in lemurs, squirrel monkeys and macaques. Chapter 5, using similar methods, provided a different point of view by focusing on developmental brain trajectory in macaques. Overall, this thesis brings evolutionary insights and a novel methodological framework to the field of social comparative neuroscience.

List of references

Acedo-Carmona C, Gomila A (2016) A critical review of Dunbar's social brain hypothesis. Rev Int Sociol 74:e037.

Ainsworth M, Sallet J, Joly O, Kyriazis D, Kriegeskorte N, Duncan J, Schüffelgen U, Rushworth MF, Bell AH (2021) Viewing ambiguous social interactions increases functional connectivity between frontal and temporal nodes of the social brain. J Neurosci:JN-RM-0870-20.

Alcalá-López D, Vogeley K, Binkofski F, Bzdok D (2018) Building blocks of social cognition: Mirror, mentalize, share? Cortex 8:4–18.

Almairac F, Herbet G, Moritz-Gasser S, de Champfleur NM, Duffau H (2015) The left inferior fronto-occipital fasciculus subserves language semantics: a multilevel lesion study. Brain Struct Funct 220:1983–1995.

Alves PN, Foulon C, Karolis V, Bzdok D, Margulies DS, Volle E, Thiebaut de Schotten M (2019) An improved neuroanatomical model of the default-mode network reconciles previous neuroimaging and neuropathological findings. Commun Biol 2:370.

Amiez C, Neveu R, Warrot D, Petrides M, Knoblauch K, Procyk E (2013) The Location of Feedback-Related Activity in the Midcingulate Cortex Is Predicted by Local Morphology. J Neurosci 33:2217–2228.

Amiez C, Sallet J, Hopkins WD, Meguerditchian A, Hadj-Bouziane F, Ben Hamed S, Wilson CRE, Procyk E, Petrides M (2019) Sulcal organization in the medial frontal cortex provides insights into primate brain evolution. Nat Commun 10.

Amiez C, Sallet J, Novek J, Hadj-Bouziane F, Giacometti C, Andersson J, Hopkins WD, Petrides M (2021) Chimpanzee histology and functional brain imaging show that the paracingulate sulcus is not human-specific. Commun Biol 4:54.

Andersson JLR, Skare S, Ashburner J (2003) How to correct susceptibility distortions in spin-echo echo-planar images: Application to diffusion tensor imaging. Neuroimage 20:870–888.

Andersson JLR, Sotiropoulos SN (2016) An integrated approach to correction for off-resonance effects and subject movement in diffusion MR imaging. Neuroimage 125:1063–1078.

Andrew RJ (1963) Evolution of Facial Expression. Am Assoc Adv Sci 142:1034–1041.

Andrews-Hanna JR (2012) The Brain's Default Network and Its Adaptive Role in Internal Mentation. Neurosci 18:251–270.

Andrews-Hanna JR, Smallwood J, Spreng RN (2014) The default network and self-generated thought: component processes, dynamic control, and clinical relevance. Ann N Y Acad Sci 1316:29–52.

Apperly IA, Butterfill SA (2009) Do humans have two systems to track beliefs and belief-like states? Psychol Rev 116:953–970.

Arcaro MJ, Mautz T, Berezovskii VK, Livingstone MS (2020) Anatomical correlates of

face patches in macaque inferotemporal cortex. Proc Natl Acad Sci 117:32667–32678.

Ardesch DJ, Scholtens LH, Li L, Preuss TM, Rilling JK, van den Heuvel MP (2019) Evolutionary expansion of connectivity between multimodal association areas in the human brain compared with chimpanzees. Proc Natl Acad Sci U S A 116:7101–7106.

Arre AM, Santos LR (2021) Mentalizing in Nonhuman Primates. In: The Neural Basis of Mentalizing (Gilead M, Ochsner K., eds), pp 131–147. Cham: Springer International Publishing.

Assaf Y, Bouznach A, Zomet O, Marom A, Yovel Y (2020) Conservation of brain connectivity and wiring across the mammalian class. Nat Neurosci 23:805–808.

Atzil S, Gao W, Fradkin I, Barrett LF (2018) Growing a social brain. Nat Hum Behav 2:624–636.

Avants BB, Tustison N, Johnson H (2009) Advanced Normalization Tools (ANTS). Insight J 2:1–35.

Báez-Mendoza R, Williams ZM (2020) Monkeys Show Theory of Mind. Cell Rep 30:4319–4320.

Balsters JH, Zerbi V, Sallet J, Wenderoth N, Mars RB (2020) Primate homologs of mouse cortico-striatal circuits. Elife 9:1–24.

Bangerter NK, Hargreaves BA, Vasanawala SS, Pauly JM, Gold GE, Nishimura DG (2004) Analysis of Multiple-Acquisition SSFP. Magn Reson Med 51:1038–1047.

Barbas H (2015) General Cortical and Special Prefrontal Connections: Principles from Structure to Function. Annu Rev Neurosci 38:269–289.

Baron-Cohen S (1991) The theory of mind deficit in autism: How specific is it? Br J Dev Psychol 9:301–314.

Barrett RLC, Dawson M, Dyrby TB, Krug K, Ptito M, D'Arceuil H, Croxson PL, Johnson PJ, Howells H, Forkel SJ, Dell'Acqua F, Catani M (2020) Differences in Frontal Network Anatomy Across Primate Species. J Neurosci 40:2094–2107.

Barron HC, Mars RB, Dupret D, Lerch JP, Sampaio-Baptista C (2021) Cross-species neuroscience: closing the explanatory gap. Philos Trans R Soc B Biol Sci 376:20190633.

Barton RA (2006) Primate brain evolution: Integrating comparative, neurophysiological, and ethological data. Evol Anthropol Issues, News, Rev 15:224–236.

Barton RA, Harvey PH (2000) Mosaic evolution of brain structure in mammals. Nature 405:1055–1058.

Barton RA, Venditti C (2013) Human frontal lobes are not relatively large. Proc Natl Acad Sci 110:9001–9006.

Baumann N, Pham-Dinh D (2001) Biology of Oligodendrocyte and Myelin in the Mammalian Central Nervous System. Physiol Rev 81:871–927.

Behrens TEJ, Berg HJ, Jbabdi S, Rushworth MFS, Woolrich MW (2007) Probabilistic diffusion tractography with multiple fibre orientations: What can we gain? Neuroimage 34:144–155.

Behrens TEJ, Hunt LT, Rushworth MFS (2009) The Computation of Social Behavior. Science (80-) 324:1160–1164.

Behrens TEJ, Hunt LT, Woolrich MW, Rushworth MFS (2008) Associative learning of social value. Nature 456:245–249.

Behrens TEJ, Johansen-Berg H, Woolrich MW, Smith SM, Wheeler-Kingshott CAM, Boulby PA, Barker GJ, Sillery EL, Sheehan K, Ciccarelli O, Thompson AJ, Brady JM, Matthews PM (2003) Non-invasive mapping of connections between human thalamus and cortex using diffusion imaging. Nat Neurosci 6:750–757.

Bell AH, Summerfield C, Morin EL, Malecek NJ, Ungerleider LG (2016) Encoding of Stimulus Probability in Macaque Inferior Temporal Cortex. Curr Biol 26:2280–2290.

Bendlin BB, Fitzgerald ME, Ries ML, Xu G, Kastman EK, Thiel BW, Rowley HA, Lazar M, Alexander AL, Johnson SC (2010) White Matter in Aging and Cognition: A Cross-Sectional Study of Microstructure in Adults Aged Eighteen to Eighty-Three. Dev Neuropsychol 35:257–277.

Benito-Kwiecinski S, Giandomenico SL, Sutcliffe M, Riis ES, Freire-Pritchett P, Kelava I, Wunderlich S, Martin U, Wray GA, McDole K, Lancaster MA (2021) An early cell shape transition drives evolutionary expansion of the human forebrain. Cell 184:2084-2102.e19.

Benn RA, Mars RB, Xu T, Rodríguez-Esparragoza L, Montesinos P, Manzano-Patron JP, Lopez-Martin G, Fuster V, Gonzalez-Sanchez J, Duff EP, Ibañez B (2020) A white matter atlas and common connectivity space facilitate the pig as a translational model in neuroscience. bioRxiv.

Bertelsen MF (2019) Issues surrounding surplus animals in zoos. In: Fowler's Zoo and Wild Animal Medicine Current Therapy, Volume 9 (Miller RE, Lamberski N, Calle P, eds), pp 134–136. St. Louis: Elsevier.

Bickart KC, Wright CI, Dautoff RJ, Dickerson BC, Barrett LF (2011) Amygdala volume and social network size in humans. Nat Neurosci 14:163–164.

Blair J, Sellars C, Strickland I, Clark F, Williams A, Smith M, Jones L (1996) Theory of Mind in the psychopath. J Forensic Psychiatry 7:15–25.

Blakemore S-J (2010) The Developing Social Brain: Implications for Education. Neuron 65:744–747.

Blakemore S-J, Mills KL (2014) Is Adolescence a Sensitive Period for Sociocultural Processing? Annu Rev Psychol 65:187–207.

Blazquez Freches G, Haak K V., Bryant KL, Schurz M, Beckmann CF, Mars RB (2020) Principles of temporal association cortex organisation as revealed by connectivity gradients. Brain Struct Funct 225:1245–1260.

Bodin C, Takerkart S, Belin P, Coulon O (2018) Anatomo-functional correspondence in the superior temporal sulcus. Brain Struct Funct 223:221–232.

Borra E, Luppino G (2017) Functional anatomy of the macaque temporo-parieto-frontal connectivity. Cortex 97:306–326.

Brambilla P (2003) Brain anatomy and development in autism: review of structural MRI studies. Brain Res Bull 61:557–569.

Brent LJN, Ruiz-Lambides A, Platt ML (2017) Family network size and survival across the lifespan of female macaques. Proc R Soc B Biol Sci 284:20170515.

Brodmann K (1909) Vergleichende Lokalisationslehre der Großhirnrinde: in ihren Prinzipien dargestellt auf Grund des Zellenbaues. (Barth JA, ed). Leipzig.

Brune M (2005) "Theory of Mind" in Schizophrenia: A Review of the Literature. Schizophr Bull 31:21–42.

Brüne M, Brüne-Cohrs U (2006) Theory of mind—evolution, ontogeny, brain mechanisms and psychopathology. Neurosci Biobehav Rev 30:437–455.

Bryant KL, Ardesch DJ, Roumazeilles L, Scholtens LH, Khrapitchev AA, Tendler BC, Wu W, Miller KL, Sallet J, van den Heuvel MP, Mars RB (2021) Diffusion MRI data, sulcal anatomy, and tractography for eight species from the Primate Brain Bank. Brain Struct Funct.

Bryant KL, Glasser MF, Li L, Jae-Cheol Bae J, Jacquez NJ, Alarcón L, Fields A, Preuss TM (2019) Organization of extrastriate and temporal cortex in chimpanzees compared to humans and macaques. Cortex 118:223–243.

Bryant KL, Li L, Eichert N, Mars RB (2020) A comprehensive atlas of white matter tracts in the chimpanzee. PLOS Biol 18:e3000971.

Bryant KL, Preuss TM (2018) A Comparative Perspective on the Human Temporal Lobe. Digit Endocasts:239–258.

Bubb EJ, Metzler-Baddeley C, Aggleton JP (2018) The cingulum bundle: Anatomy, function, and dysfunction. Neurosci Biobehav Rev 92:104–127.

Buckner RL, Margulies DS (2019) Macroscale cortical organization and a default-like apex transmodal network in the marmoset monkey. Nat Commun 10:1976.

Budday S, Steinmann P, Kuhl E (2015) Physical biology of human brain development. Front Cell Neurosci 9:1–17.

Bullmore E, Sporns O (2012) The economy of brain network organization. Nat Rev Neurosci 13:336–349.

Butterfill SA, Apperly IA (2013) How to Construct a Minimal Theory of Mind. Mind Lang 28:606–637.

Buxton RB (1993) The diffusion sensitivity of fast steady-state free precession imaging. Magn Reson Med 29:235–243.

Byom LJ, Mutlu B (2013) Theory of mind: mechanisms, methods, and new directions. Front Hum Neurosci 7:1–12.

Byrne R (1996) Machiavellian Inteligence. Evol Anthropol 5:172–180.

Calinski T, Harabasz J (1974) A dendrite method for cluster analysis. Commun Stat - Theory Methods 3:1–27.

Call J, Tomasello M (2008) Does the chimpanzee have a theory of mind? 30 years later. Trends Cogn Sci 12:187–192.

Caminiti R, Innocenti GM, Battaglia-Mayer A (2015) Organization and evolution of parieto-frontal processing streams in macaque monkeys and humans. Neurosci Biobehav Rev 56:73–96.

Campi KL, Krubitzer L (2010) Comparative studies of diurnal and nocturnal rodents:

Differences in lifestyle result in alterations in cortical field size and number. J Comp Neurol 518:4491–4512.

Carpendale JIM, Lewis C (2004) Constructing an understanding of mind: The development of children's social understanding within social interaction. Behav Brain Sci 27:79–151.

Carpenter M, Tomasello M (1995) Joint Attention and Imitative Learning in Children, Chimpanzees, and Enculturated Chimpanzees*. Soc Dev 4:217–237.

Caspers S, Eickhoff SB, Rick T, von Kapri A, Kuhlen T, Huang R, Shah NJ, Zilles K (2011) Probabilistic fibre tract analysis of cytoarchitectonically defined human inferior parietal lobule areas reveals similarities to macaques. Neuroimage 58:362–380.

Castelli F, Happé F, Frith U, Frith C (2013) Movement and mind: A functional imaging study of perception and interpretation of complex intentional movement patterns. Soc Neurosci Key Readings 325:155–170.

Catani M, Bambini V (2014) A model for Social Communication And Language Evolution and Development (SCALED). Curr Opin Neurobiol 28:165–171.

Catani M, Jones DK, Donato R, Ffytche DH (2003) Occipito-temporal connections in the human brain. Brain 126:2093–2107.

Catani M, Robertsson N, Beyh A, Huynh V, de Santiago Requejo F, Howells H, Barrett RLC, Aiello M, Cavaliere C, Dyrby TB, Krug K, Ptito M, D'Arceuil H, Forkel SJ, Dell'Acqua F (2017) Short parietal lobe connections of the human and monkey brain. Cortex 97:339–357.

Catani M, Thiebaut De Schotten M (2008) A diffusion tensor imaging tractography atlas for virtual in vivo dissections. Cortex 44:1105–1132.

Chang SWC, Brent LJN, Adams GK, Klein JT, Pearson JM, Watson KK, Platt ML (2013a) Neuroethology of primate social behavior. Proc Natl Acad Sci 110:10387–10394.

Chang SWC, Gariépy J-F, Platt ML (2013b) Neuronal reference frames for social decisions in primate frontal cortex. Nat Neurosci 16:243–250.

Chaplin TA, Yu HH, Soares JGM, Gattass R, Rosa MGP (2013) A conserved pattern of differential expansion of cortical areas in simian primates. J Neurosci 33:15120–15125.

Charvet CJ, Finlay BL (2012) Embracing covariation in brain evolution : Large brains, extended development, and flexible primate social systems. Prog Brain Res 195:71–87.

Charvet CJ, Ofori K, Baucum C, Sun J, Modrell MS, Hekmatyar K, Edlow BL, Van Der Kouwe AJ (2021) Tracing cortical circuits in humans and non-human primates from high resolution connectomic, transcriptomic, and temporal dimensions. bioRxiv:2021.04.30.442016.

Chau BKH, Sallet J, Papageorgiou GK, Noonan MP, Bell AH, Walton ME, Rushworth MFS (2015) Contrasting Roles for Orbitofrontal Cortex and Amygdala in Credit Assignment and Learning in Macaques. Neuron 87:1106–1118.

Chen X, Errangi B, Li L, Glasser MF, Westlye LT, Fjell AM, Walhovd KB, Hu X, Herndon JG, Preuss TM, Rilling JK (2013) Brain aging in humans, chimpanzees

(pan troglodytes), and rhesus macaques (macaca mulatta): Magnetic resonance imaging studies of macro- and microstructural changes. Neurobiol Aging 34:2248–2260.

Chiou KL, DeCasien AR, Montague MJ, Bauman SE, Compo NR, González O, Pliner HA, Spurrell CH, Starita LM, Brent LJ, Higham JP, Martinez MI, Shendure J, Platt ML, Noah S-M (2020) The rhesus macaque brain cell census reveals heterogeneity in aging across cell types. In: American Journal of Physical Anthropology, pp 50–51. Wiley.

Cisek P (2019) Resynthesizing behavior through phylogenetic refinement. Attention, Perception, Psychophys 81:2265–2287.

Clancy B, Finlay BL, Darlington RB, Anand KJS (2007) Extrapolating brain development from experimental species to humans. Neurotoxicology 28:931–937.

Cléry JC, Hori Y, Schaeffer DJ, Menon RS, Everling S (2021) Neural network of social interaction observation in marmosets. Elife 10:1–17.

Clos M, Amunts K, Laird AR, Fox PT, Eickhoff SB (2013) Tackling the multifunctional nature of Broca's region meta-analytically: Co-activation-based parcellation of area 44. Neuroimage 83:174–188.

Connolly CJ (1936) The fissural pattern of the Primate brain. Am J Phys Anthropol 21:301–422.

Constans C, Deffieux T, Pouget P, Tanter M, Aubry JF (2017) A 200-1380-kHz Quadrifrequency Focused Ultrasound Transducer for Neurostimulation in Rodents and Primates: Transcranial in Vitro Calibration and Numerical Study of the Influence of Skull Cavity. IEEE Trans Ultrason Ferroelectr Freq Control 64:717–724.

Courchesne E, Chisum HJ, Townsend J, Cowles A, Covington J, Egaas B, Harwood M, Hinds S, Press GA (2000) Normal Brain Development and Aging: Quantitative Analysis at in Vivo MR Imaging in Healthy Volunteers. Radiology 216:672–682.

Croxson PL, Forkel SJ, Cerliani L, Thiebaut De Schotten M (2018) Structural Variability Across the Primate Brain: A Cross-Species Comparison. Cereb Cortex 28:3829–3841.

Darwin C (1859) On the Origin of Species by Means of Natural Selection, or the Preservation of Favoured Races in the Struggle of Life. London: John Murray.

Davies DL, Bouldin DW (1979) A Cluster Separation Measure. IEEE Trans Pattern Anal Mach Intell PAMI-1:224–227.

de Bruin L, Michael J (2021) Prediction Error Minimization as a Framework for Social Cognition Research. Erkenntnis 86:1–20.

de Ruiter J, Weston G, Lyon SM (2011) Dunbar's Number: Group Size and Brain Physiology in Humans Reexamined. Am Anthropol 113:557–568.

de Waal FBM, Leimgruber K, Greenberg AR (2008) Giving is self-rewarding for monkeys. Proc Natl Acad Sci 105:13685–13689.

de Waal FBM, Suchak M (2010) Prosocial primates: Selfish and unselfish motivations. Philos Trans R Soc B Biol Sci 365:2711–2722.

DeCasien AR, Williams SA, Higham JP (2017) Primate brain size is predicted by diet

but not sociality. Nat Ecol Evol 1:0112.

Decramer T, Swinnen S, van Loon J, Janssen P, Theys T (2018) White matter tract anatomy in the rhesus monkey: a fiber dissection study. Brain Struct Funct 223:3681–3688.

Deffieux T, Younan Y, Wattiez N, Tanter M, Pouget P, Aubry JF (2013) Low-intensity focused ultrasound modulates monkey visuomotor behavior. Curr Biol 23:2430–2433.

Devaine M, Hollard G, Daunizeau J (2014) Theory of mind: Did evolution fool us? PLoS One 9.

Devaine M, San-Galli A, Trapanese C, Bardino G, Hano C, Saint Jalme M, Bouret S, Masi S, Daunizeau J (2017) Reading wild minds: A computational assay of Theory of Mind sophistication across seven primate species. PLoS Comput Biol 13:1–24.

Dhollander T, Raffelt D, Connelly A (2016) Unsupervised 3-tissue response function estimation from single-shell or multi-shell diffusion MR data without a co-registered T1 image. ISMRM Work Break Barriers Diffus MRI:5.

Dhollander T, Raffelt D, Connelly A (2018) Accuracy of response function estimation algorithms for 3-tissue spherical deconvolution of diverse quality diffusion MRI data. 26th Int Soc Magn Reson Med:3–6.

Dick AS, Garic D, Graziano P, Tremblay P (2019) The frontal aslant tract (FAT) and its role in speech, language and executive function. Cortex 111:148–163.

Dobson SD (2009) Socioecological correlates of facial mobility in nonhuman anthropoids. Am J Phys Anthropol 139:413–420.

Donahue CJ, Sotiropoulos SN, Jbabdi S, Hernandez-Fernandez M, Behrens TEJ, Dyrby TB, Coalson T, Kennedy H, Knoblauch K, Van Essen DC, Glasser MF (2016) Using Diffusion Tractography to Predict Cortical Connection Strength and Distance: A Quantitative Comparison with Tracers in the Monkey. J Neurosci 36:6758–6770.

Drayton LA, Santos LR (2016) A decade of theory of mind research on cayo santiago: Insights into rhesus macaque social cognition. Am J Primatol 78:106–116.

Dubois J, Dehaene-Lambertz G, Kulikova S, Poupon C, Hüppi PS, Hertz-Pannier L (2014) The early development of brain white matter: A review of imaging studies in fetuses, newborns and infants. Neuroscience 276:48–71.

Duffau H (2018) The error of Broca: From the traditional localizationist concept to a connectomal anatomy of human brain. J Chem Neuroanat 89:73–81.

Dunbar RIM (1998) The social brain hypothesis. Evol Anthropol 6:178–190.

Dunbar RIM (2009) The social brain hypothesis and its implications for social evolution. Ann Hum Biol 36:562–572.

Dunbar RIM, Shultz S (2007a) Understanding primate brain evolution. Philos Trans R Soc B Biol Sci 362:649–658.

Dunbar RIM, Shultz S (2007b) Evolution in the social brain. Science (80-) 317:1344–1347.

Dunbar RIM, Shultz S (2017) Why are there so many explanations for primate brain evolution? Philos Trans R Soc B Biol Sci 372.

Ecker C (2012) Brain Anatomy and Its Relationship to Behavior in Adults With Autism Spectrum Disorder. Arch Gen Psychiatry 69:195.

Eichert N, Robinson EC, Bryant KL, Jbabdi S, Jenkinson M, Li L, Krug K, Watkins KE, Mars RB (2020) Cross-species cortical alignment identifies different types of anatomical reorganization in the primate temporal lobe. Elife 9.

Eichert N, Verhagen L, Folloni D, Jbabdi S, Khrapitchev AA, Sibson NR, Mantini D, Sallet J, Mars RB (2018) What is special about the human arcuate fasciculus? Lateralization, projections, and expansion. Cortex:1–9.

Eickhoff SB, Thirion B, Varoquaux G, Bzdok D (2015) Connectivity-based parcellation: Critique and implications. Hum Brain Mapp 36:4771–4792.

Eklund A, Nichols TE, Knutsson H (2016) Cluster failure: Why fMRI inferences for spatial extent have inflated false-positive rates. Proc Natl Acad Sci 113:7900–7905.

Emery NJ (2000) The eyes have it: The neuroethology, function and evolution of social gaze. Neurosci Biobehav Rev 24:581–604.

Ercsey-Ravasz M, Markov NT, Lamy C, Van Essen DC, Knoblauch K, Toroczkai Z, Kennedy H (2013) A Predictive Network Model of Cerebral Cortical Connectivity Based on a Distance Rule. Neuron 80:184–197.

Esiri M (2007) Ageing and the brain. J Pathol 211:181–187.

Fasemore TM, Patzke N, Kaswera-Kyamakya C, Gilissen E, Manger PR, Ihunwo AO (2018) The Distribution of Ki-67 and Doublecortin-Immunopositive Cells in the Brains of Three Strepsirrhine Primates: Galago demidoff , Perodicticus potto , and Lemur catta. Neuroscience 372:46–57.

Ferretti F (2016) The Social Brain Is Not Enough: On the Importance of the Ecological Brain for the Origin of Language. Front Psychol 7:1–12.

Filley CM (2021) White matter and human behavior. Science (80-) 372:1265–1266.

Finlay B, Darlington R (1995) Linked regularities in the development and evolution of mammalian brains. Science (80-) 268:1578–1584.

Finlay BL, Darlington RB, Nicastro N (2001) Developmental structure in brain evolution. Behav Brain Sci 24:263–278.

Fischl B (2012) FreeSurfer. Neuroimage 62:774–781.

Fisher C, Freiwald WA (2015) Contrasting specializations for facial motion within the macaque face-processing system. Curr Biol 25:261–266.

Fogassi L, Ferrari PF, Gesierich B, Rozzi S, Chersi F, Rizzolatti G (2005) Parietal Lobe: From Action Organization to Intention Understanding. Science (80-) 308:662–667.

Folloni D, Sallet J, Khrapitchev AA, Sibson N, Verhagen L, Mars RB (2019a) Dichotomous organization of amygdala/temporal-prefrontal bundles in both humans and monkeys. Elife 8:1–23.

Folloni D, Verhagen L, Mars RB, Fouragnan E, Constans C, Aubry JF, Rushworth MFS, Sallet J (2019b) Manipulation of Subcortical and Deep Cortical Activity in the Primate Brain Using Transcranial Focused Ultrasound Stimulation. Neuron 101:1109-1116.e5.

Fonagy P, Gergely G, Jurist EL, Target M (2018) Attachment and Reflective Function: Their Role in Self-Organization. In: Affect Regulation, Mentalization, and the Development of the Self, pp 23–64. Routledge.

Forkel SJ, Thiebaut de Schotten M, Kawadler JM, Dell'Acqua F, Danek A, Catani M (2014) The anatomy of fronto-occipital connections from early blunt dissections to contemporary tractography. Cortex 56:73–84.

Fouragnan EF, Chau BKH, Folloni D, Kolling N, Verhagen L, Klein-Flügge M, Tankelevitch L, Papageorgiou GK, Aubry JF, Sallet J, Rushworth MFS (2019) The macaque anterior cingulate cortex translates counterfactual choice value into actual behavioral change. Nat Neurosci 22:797–808.

Fox MD (2018) Mapping Symptoms to Brain Networks with the Human Connectome. N Engl J Med 379:2237–2245.

Foxley S, Jbabdi S, Clare S, Lam W, Ansorge O, Douaud G, Miller K (2014) Improving diffusion-weighted imaging of post-mortem human brains: SSFP at 7T. Neuroimage 102:579–589.

Frey S, Pandya DN, Chakravarty MM, Bailey L, Petrides M, Collins DL (2011) An MRI based average macaque monkey stereotaxic atlas and space (MNI monkey space). Neuroimage 55:1435–1442.

Friederici AD (2012) Language development and the ontogeny of the dorsal pathway. Front Evol Neurosci 4:1–7.

Friedman H, Haigwood N, Ator N, Newsome W, Allan JS, Golos TG, Kordower JH, Shade RE, Goldberg ME, Bailey MR, Bianchi P (2017) The Critical Role of Nonhuman Primates in Medical Research - White Paper. Pathog Immun 2:352.

Friedrich P et al. (2021) Imaging evolution of the primate brain: the next frontier? Neuroimage 228:117685.

Fukunishi K, Sawada K, Kashima M, Sakata-Haga H, Fukuzaki K, Fukui Y (2006) Development of cerebral sulci and gyri in fetuses of cynomolgus monkeys (Macaca fascicularis). Anat Embryol (Berl) 211:757–764.

Geiger A, Bente G, Lammers S, Tepest R, Roth D, Bzdok D, Vogeley K (2019) Distinct functional roles of the mirror neuron system and the mentalizing system. Neuroimage 202:116102.

Genovesio A, Wise SP, Passingham RE (2014) Prefrontal-parietal function: From foraging to foresight. Trends Cogn Sci 18:72–81.

Ghazanfar AA (2013) Multisensory vocal communication in primates and the evolution of rhythmic speech. Behav Ecol Sociobiol 67:1441–1448.

Glasser MF, Goyal MS, Preuss TM, Raichle ME, Van Essen DC (2014) Trends and properties of human cerebral cortex: Correlations with cortical myelin content. Neuroimage 93:165–175.

Glasser MF, Sotiropoulos SN, Wilson JA, Coalson TS, Fischl B, Andersson JL, Xu J, Jbabdi S, Webster M, Polimeni JR, Van Essen DC, Jenkinson M (2013) The minimal preprocessing pipelines for the Human Connectome Project. Neuroimage 80:105–124.

Glasser MF, Van Essen DC (2011) Mapping Human Cortical Areas In Vivo Based on Myelin Content as Revealed by T1- and T2-Weighted MRI. J Neurosci 31:11597–

11616.

Gómez-Robles A, Hopkins WD, Sherwood CC (2013) Increased morphological asymmetry, evolvability and plasticity in human brain evolution. Proc R Soc B Biol Sci 280:20130575.

Gómez-Robles A, Sherwood CC (2016) Human brain evolution: How the increase of brain plasticity made us a cultural species. Mètode Rev difusió la Investig 2017:35–43.

Goulas A, Zilles K, Hilgetag CC (2018) Cortical Gradients and Laminar Projections in Mammals. Trends Neurosci 41:775–788.

Gould SJ (1966) Allometry and size in ontogeny and phylogeny. Biol Rev 41:587–638.

Gregory C, Lough S, Stone V, Erzinclioglu S, Martin L, Baron-Cohen S, Hodges JR (2002) Theory of mind in patients with frontal variant frontotemporal dementia and Alzheimer's disease: Theoretical and practical implications. Brain 125:752–764.

Gruber T, Clay Z (2016) A Comparison Between Bonobos and Chimpanzees: A Review and Update. Evol Anthropol Issues, News, Rev 25:239–252.

Habbershon HM, Ahmed SZ, Cohen YE (2013) Rhesus Macaques Recognize Unique Multimodal Face-Voice Relations of Familiar Individuals and Not of Unfamiliar Ones. Brain Behav Evol 81:219–225.

Hadj-Bouziane F, Bell AH, Knusten TA, Ungerleider LG, Tootell RBH (2008) Perception of emotional expressions is independent of face selectivity in monkey inferior temporal cortex. Proc Natl Acad Sci 105:5591–5596.

Hampton WH, Unger A, Von Der Heide RJ, Olson IR (2016) Neural connections foster social connections: A diffusion-weighted imaging study of social networks. Soc Cogn Affect Neurosci 11.

Hare B (2001) Can competitive paradigms increase the validity of experiments on primate social cognition? Anim Cogn 4:269–280.

Hare B (2011) From Hominoid to Hominid Mind: What Changed and Why? Annu Rev Anthropol 40:293–309.

Hare B, Call J, Agnetta B, Tomasello M (2000) Chimpanzees know what conspecifics do and do not see. Anim Behav 59:771–785.

Haroush K, Williams ZM (2015) Neuronal Prediction of Opponent's Behavior during Cooperative Social Interchange in Primates. Cell 160:1233–1245.

Hauser MD (2002) The Faculty of Language: What Is It, Who Has It, and How Did It Evolve? Larson RK, Deprez V, Yamakido H, eds. Science (80-) 298:1569–1579.

Haxby J V, Hoffman EA, Gobbini MI (2000) The distributed human neural system for face perception. Trends Cogn Sci 4:223–233.

Hayashi T, Akikawa R, Kawasaki K, Egawa J, Minamimoto T, Kobayashi K, Kato S, Hori Y, Nagai Y, Iijima A, Someya T, Hasegawa I (2020) Macaques Exhibit Implicit Gaze Bias Anticipating Others' False-Belief-Driven Actions via Medial Prefrontal Cortex. Cell Rep 30:4433-4444.e5.

Hecht EE, Gutman DA, Preuss TM, Sanchez MM, Parr LA, Rilling JK (2013) Process Versus Product in Social Learning: Comparative Diffusion Tensor Imaging of Neural Systems for Action Execution–Observation Matching in Macaques,

Chimpanzees, and Humans. Cereb Cortex 23:1014–1024.

Heilbronner SR, Haber SN (2014) Frontal Cortical and Subcortical Projections Provide a Basis for Segmenting the Cingulum Bundle: Implications for Neuroimaging and Psychiatric Disorders. J Neurosci 34:10041–10054.

Herbet G, Lafargue G, Bonnetblanc F, Moritz-Gasser S, Menjot de Champfleur N, Duffau H (2014) Inferring a dual-stream model of mentalizing from associative white matter fibres disconnection. Brain 137:944–959.

Herbet G, Zemmoura I, Duffau H (2018) Functional Anatomy of the Inferior Longitudinal Fasciculus: From Historical Reports to Current Hypotheses. Front Neuroanat 12:1–15.

Herculano-Houzel S, Mota B, Wong P, Kaas JH (2010) Connectivity-driven white matter scaling and folding in primate cerebral cortex. Proc Natl Acad Sci 107:19008–19013.

Hernandez-Fernandez M, Reguly I, Jbabdi S, Giles M, Smith S, Sotiropoulos SN (2019) Using GPUs to accelerate computational diffusion MRI: From microstructure estimation to tractography and connectomes. Neuroimage 188:598–615.

Hernandez-Pacheco R, Delgado DL, Rawlins RG, Kessler MJ, Ruiz-Lambides A V., Maldonado E, Sabat AM (2016) Managing the Cayo Santiago rhesus macaque population: The role of density. Am J Primatol 78:167–181.

Heuer K, Gulban OF, Bazin P-L, Osoianu A, Valabregue R, Santin M, Herbin M, Toro R (2019) Evolution of neocortical folding: A phylogenetic comparative analysis of MRI from 34 primate species. Cortex 118:275–291.

Heyes C (2014) Submentalizing: I Am Not Really Reading Your Mind. Perspect Psychol Sci 9:131–143.

Heyes C (2015) Animal mindreading: what's the problem? Psychon Bull Rev 22:313–327.

Heyes CM (1998) Theory of mind in nonhuman primates. Behav Brain Sci 21:101–114.

Heyes CM, Frith CD (2014) The cultural evolution of mind reading. Science (80-) 344:1243091–1243091.

Hezel DM, McNally RJ (2014) Theory of Mind Impairments in Social Anxiety Disorder. Behav Ther 45:530–540.

Hill J, Inder T, Neil J, Dierker D, Harwell J, Van Essen D (2010) Similar patterns of cortical expansion during human development and evolution. Proc Natl Acad Sci 107:13135–13140.

Horschler DJ, MacLean EL, Santos LR (2020) Do Non-Human Primates Really Represent Others' Beliefs? Trends Cogn Sci 24:594–605.

Horvát S, Gămănuț R, Ercsey-Ravasz M, Magrou L, Gămănuț B, Van Essen DC, Burkhalter A, Knoblauch K, Toroczkai Z, Kennedy H (2016) Spatial Embedding and Wiring Cost Constrain the Functional Layout of the Cortical Network of Rodents and Primates Konopka G, ed. PLOS Biol 14:e1002512.

Hou L, Xiang L, Crow TJ, Leroy F, Rivière D, Mangin JF, Roberts N (2019) Measurement of Sylvian Fissure asymmetry and occipital bending in humans and Pan troglodytes. Neuroimage 184:855–870.

Howell BR, Ahn M, Shi Y, Godfrey JR, Hu X, Zhu H, Styner M, Sanchez MM (2019) Disentangling the effects of early caregiving experience and heritable factors on brain white matter development in rhesus monkeys. Neuroimage 197:625–642.

Hutchison RM, Gallivan JP, Culham JC, Gati JS, Menon RS, Everling S (2012) Functional connectivity of the frontal eye fields in humans and macaque monkeys investigated with resting-state fMRI. J Neurophysiol 107:2463–2474.

Igelström KM, Webb TW, Graziano MSA (2015) Neural Processes in the Human Temporoparietal Cortex Separated by Localized Independent Component Analysis. J Neurosci 35:9432–9445.

Innocenti GM, Price DJ (2005) Exuberance in the development of cortical networks. Nat Rev Neurosci 6:955–965.

Isoda M, Noritake A, Ninomiya T (2018) Development of social systems neuroscience using macaques. Proc Japan Acad Ser B 94:305–323.

Janmaat KRL, Ban SD, Boesch C (2013) Taï chimpanzees use botanical skills to discover fruit: What we can learn from their mistakes. Anim Cogn 16:851–860.

Janmaat KRL, Chapman CA, Meijer R, Zuberbühler K (2012) The use of fruiting synchrony by foraging mangabey monkeys: A “simple tool” to find fruit. Anim Cogn 15:83–96.

Jarvis ED (2019) Evolution of vocal learning and spoken language. Science (80-) 366:50–54.

Jbabdi S, Johansen-Berg H (2011) Tractography: Where Do We Go from Here? Brain Connect 1:169–183.

Jenkinson M, Bannister P, Brady M, Smith S (2002) Improved Optimization for the Robust and Accurate Linear Registration and Motion Correction of Brain Images. Neuroimage 17:825–841.

Jenkinson M, Beckmann CF, Behrens TEJ, Woolrich MW, Smith SM (2012) Fsl. Neuroimage 62:782–790.

Jenkinson M, Smith S (2001) A global optimisation method for robust affine registration of brain images. Med Image Anal 5:143–156.

Jeurissen B, Tournier J-D, Dhollander T, Connelly A, Sijbers J (2014) Multi-tissue constrained spherical deconvolution for improved analysis of multi-shell diffusion MRI data. Neuroimage 103:411–426.

Joiner J, Piva M, Turrin C, Chang SWC (2017) Social learning through prediction error in the brain. npj Sci Learn 2:8.

Kaas JH (2017) The Evolution of Mammalian Brains from Early Mammals to Present-Day Primates. In: Evolution of the Brain, Cognition, and Emotion in Vertebrates (Watanabe S, Hofman MA, Shimizu T, eds), pp 59–80. Tokyo: Springer Japan.

Kaas JH, van Eden CG (2011) Brain Banks Provide a Valuable Resource for Comparative Studies. Brain Behav Evol 77:65–66.

Kaburu SSK, Paukner A, Simpson EA, Suomi SJ, Ferrari PF (2016) Neonatal imitation predicts infant rhesus macaque (Macaca mulatta) social and anxiety-related behaviours at one year. Sci Rep 6:4–11.

Kahnt T, Chang LJ, Park SQ, Heinzle J, Haynes J-D (2012) Connectivity-Based

Parcellation of the Human Orbitofrontal Cortex. J Neurosci 32:6240–6250.

Kanai R, Bahrami B, Roylance R, Rees G (2012) Online social network size is reflected in human brain structure. Proc R Soc B Biol Sci 279:1327–1334.

Kano F, Krupenye C, Hirata S, Tomonaga M, Call J (2019) Great apes use self-experience to anticipate an agent's action in a false-belief test. Proc Natl Acad Sci:201910095.

Kanwisher N, McDermott J, Chun MM (1997) The Fusiform Face Area: A Module in Human Extrastriate Cortex Specialized for Face Perception. J Neurosci 17:4302–4311.

Kaplan H, Hill K, Lancaster J, Hurtado AM (2000) A theory of human life history evolution: Diet, intelligence, and longevity. Evol Anthropol Issues, News, Rev 9:156–185.

Karlsgodt KH, Sun D, Cannon TD (2010) Structural and Functional Brain Abnormalities in Schizophrenia. Curr Dir Psychol Sci 19:226–231.

Kashima M, Sawada K, Fukunishi K, Sakata-Haga H, Tokado H, Fukui Y (2008) Development of cerebral sulci and gyri in fetuses of cynomolgus monkeys (Macaca fascicularis). II. Gross observation of the medial surface. Brain Struct Funct 212:513–520.

Kasper C, Voelkl B (2009) A social network analysis of primate groups. Primates 50:343–356.

Kellner E, Dhital B, Kiselev VG, Reisert M (2016) Gibbs-ringing artifact removal based on local subvoxel-shifts. Magn Reson Med 76:1574–1581.

Kelly C, Uddin LQ, Shehzad Z, Margulies DS, Castellanos FX, Milham MP, Petrides M (2010) Broca's region: linking human brain functional connectivity data and non-human primate tracing anatomy studies. Eur J Neurosci 32:383–398.

Kemp J, Després O, Sellal F, Dufour A (2012) Theory of Mind in normal ageing and neurodegenerative pathologies. Ageing Res Rev 11:199–219.

Kennedy DP, Adolphs R (2012) The social brain in psychiatric and neurological disorders. Trends Cogn Sci 16:559–572.

Keysers C, Fadiga L (2008) The mirror neuron system: New frontiers. Soc Neurosci 3:193–198.

Khalighinejad N, Bongioanni A, Verhagen L, Folloni D, Attali D, Aubry J-F, Sallet J, Rushworth MFS (2020) A Basal Forebrain-Cingulate Circuit in Macaques Decides It Is Time to Act. Neuron 105:370-384.e8.

Kilintari M, Raos V, Savaki HE (2014) Involvement of the Superior Temporal Cortex in Action Execution and Action Observation. J Neurosci 34:8999–9011.

Kim J, Jung Y, Barcus R, Bachevalier JH, Sanchez MM, Nader MA, Whitlow CT (2020) Rhesus Macaque Brain Developmental Trajectory: A Longitudinal Analysis Using Tensor-Based Structural Morphometry and Diffusion Tensor Imaging. Cereb Cortex 30:4325–4335.

Knickmeyer RC, Styner M, Short SJ, Lubach GR, Kang C, Hamer R, Coe CL, Gilmore JH (2010) Maturational Trajectories of Cortical Brain Development through the Pubertal Transition: Unique Species and Sex Differences in the Monkey Revealed

through Structural Magnetic Resonance Imaging. Cereb Cortex 20:1053–1063.

Koster-Hale J, Saxe R (2013) Theory of Mind: A Neural Prediction Problem. Neuron 79:836–848.

Kovačević N, Henderson JT, Chan E, Lifshitz N, Bishop J, Evans AC, Henkelman RM, Chen XJ (2005) A Three-dimensional MRI Atlas of the Mouse Brain with Estimates of the Average and Variability. Cereb Cortex 15:639–645.

Kret ME, Tomonaga M (2016) Getting to the Bottom of Face Processing. Species-Specific Inversion Effects for Faces and Behinds in Humans and Chimpanzees (Pan Troglodytes) Hadjikhani N, ed. PLoS One 11:e0165357.

Krubitzer L (2009) In search of a unifying theory of complex brain evolution. Ann N Y Acad Sci 1156:44–67.

Krubitzer L, Kaas J (2005) The evolution of the neocortex in mammals: How is phenotypic diversity generated? Curr Opin Neurobiol 15:444–453.

Krupenye C (2021) The Evolution of Mentalizing in Humans and Other Primates. In: The Neural Basis of Mentalizing (Gilead M, Ochsner KN, eds), pp 107–129. Cham: Springer International Publishing.

Krupenye C, Kano F, Hirata S, Call J, Tomasello M (2016) Great apes anticipate that other individuals will act according to false beliefs. Science (80-) 354:110–114.

Ku SP, Tolias AS, Logothetis NK, Goense J (2011) FMRI of the Face-Processing Network in the Ventral Temporal Lobe of Awake and Anesthetized Macaques. Neuron 70:352–362.

Kulahci IG, Drea CM, Rubenstein DI, Ghazanfar AA (2014) Individual recognition through olfactory–auditory matching in lemurs. Proc R Soc B Biol Sci 281:20140071.

Kulke L, Johannsen J, Rakoczy H (2019) Why can some implicit Theory of Mind tasks be replicated and others cannot? A test of mentalizing versus submentalizing accounts Król ME, ed. PLoS One 14:e0213772.

Kyriakopoulos M, Vyas NS, Barker GJ, Chitnis XA, Frangou S (2008) A Diffusion Tensor Imaging Study of White Matter in Early-Onset Schizophrenia. Biol Psychiatry 63:519–523.

Lambon Ralph MA, Sage K, Jones RW, Mayberry EJ (2010) Coherent concepts are computed in the anterior temporal lobes. Proc Natl Acad Sci 107:2717–2722.

Lameira AR (2017) Bidding evidence for primate vocal learning and the cultural substrates for speech evolution. Neurosci Biobehav Rev 83:429–439.

Lancaster JL, McKay DR, Cykowski MD, Martinez MJ, Tan X, Valaparla S, Zhang Y, Fox PT (2011) Automated analysis of fundamental features of brain structures. Neuroinformatics 9:371–380.

Lange FJ, Ashburner J, Smith SM, Andersson JLR (2020a) A Symmetric Prior for the Regularisation of Elastic Deformations: Improved anatomical plausibility in nonlinear image registration. Neuroimage 219:116962.

Lange FJ, Smith SM, Bertelsen MF, Khrapitchev AA, Manger PR, Mars RB, Andersson JLR (2020b) Multimodal MRI Template Creation in the Ring-Tailed Lemur and Rhesus Macaque. In: Lecture Notes in Computer Science (including subseries

Lecture Notes in Artificial Intelligence and Lecture Notes in Bioinformatics), pp 141–150. Springer International Publishing.

Large I, Bridge H, Ahmed B, Clare S, Kolasinski J, Lam WW, Miller KL, Dyrby TB, Parker AJ, Smith JET, Daubney G, Sallet J, Bell AH, Krug K (2016) Individual Differences in the Alignment of Structural and Functional Markers of the V5/MT Complex in Primates. Cereb Cortex 26:3928–3944.

Latini F, Mårtensson J, Larsson E, Fredrikson M, Åhs F (2017) Segmentation of the inferior longitudinal fasciculus in the human brain : A white matter dissection and diffusion tensor tractography study. Brain Res 1675:102–115.

Lebel C, Gee M, Camicioli R, Wieler M, Martin W, Beaulieu C (2012) Diffusion tensor imaging of white matter tract evolution over the lifespan. Neuroimage 60:340–352.

Lefebvre L, Reader SM, Sol D (2004) Brains, Innovations and Evolution in Birds and Primates. Brain Behav Evol 63:233–246.

Lerch JP, van der Kouwe AJW, Raznahan A, Paus T, Johansen-Berg H, Miller KL, Smith SM, Fischl B, Sotiropoulos SN (2017) Studying neuroanatomy using MRI. Nat Neurosci 20:314–326.

Leroy F et al. (2015) New human-specific brain landmark: The depth asymmetry of superior temporal sulcus. Proc Natl Acad Sci 112:1208–1213.

Leslie AM (1987) Pretense and representation: The origins of "theory of mind." Psychol Rev 94:412–426.

Liu C, Tian X, Liu H, Mo Y, Bai F, Zhao X, Ma Y, Wang J (2015a) Rhesus monkey brain development during late infancy and the effect of phencyclidine: A longitudinal MRI and DTI study. Neuroimage 107:65–75.

Liu C, Yen CC-C, Szczupak D, Ye FQ, Leopold DA, Silva AC (2019) Anatomical and functional investigation of the marmoset default mode network. Nat Commun 10:1975.

Liu F, Garland M, Duan Y, Stark RI, Xu D, Dong Z, Bansal R, Peterson BS, Kangarlu A (2008) Study of the development of fetal baboon brain using magnetic resonance imaging at 3 Tesla. Neuroimage 40:148–159.

Liu F, Guo W, Fouche J-P, Wang Y, Wang W, Ding J, Zeng L, Qiu C, Gong Q, Zhang W, Chen H (2015b) Multivariate classification of social anxiety disorder using whole brain functional connectivity. Brain Struct Funct 220:101–115.

Liu N, Hadj-Bouziane F, Moran R, Ungerleider LG, Ishai A (2016) Facial Expressions Evoke Differential Neural Coupling in Macaques. Cereb Cortex 27:bhv345.

Livingstone MS, Vincent JL, Arcaro MJ, Srihasam K, Schade PF, Savage T (2017) Development of the macaque face-patch system. Nat Commun 8:1–12.

Lockwood PL, Apps MAJ, Chang SWC (2020) Is There a 'Social' Brain? Implementations and Algorithms. Trends Cogn Sci 24:802–813.

Lockwood PL, Apps MAJ, Valton V, Viding E, Roiser JP (2016) Neurocomputational mechanisms of prosocial learning and links to empathy. Proc Natl Acad Sci 113:9763–9768.

López-Muñoz F, Boya J, Alamo C (2006) Neuron theory, the cornerstone of neuroscience, on the centenary of the Nobel Prize award to Santiago Ramón y

Cajal. Brain Res Bull 70:391–405.

Lopez-Persem A, Verhagen L, Amiez C, Petrides M, Sallet J (2019) The Human Ventromedial Prefrontal Cortex: Sulcal Morphology and Its Influence on Functional Organization. J Neurosci 39:3627–3639.

Lourenço O (2012) Piaget and Vygotsky: Many resemblances, and a crucial difference. New Ideas Psychol 30:281–295.

Low J, Perner J (2012) Implicit and explicit theory of mind: State of the art. Br J Dev Psychol 30:1–13.

Maciej P, Patzelt A, Ndao I, Hammerschmidt K, Fischer J (2013) Social monitoring in a multilevel society: a playback study with male Guinea baboons. Behav Ecol Sociobiol 67:61–68.

Mackey S, Petrides M (2010) Quantitative demonstration of comparable architectonic areas within the ventromedial and lateral orbital frontal cortex in the human and the macaque monkey brains. Eur J Neurosci 32:1940–1950.

Maestripieri D, Roney J (2006) Evolutionary developmental psychology: Contributions from comparative research with nonhuman primates☆. Dev Rev 26:120–137.

Maier-Hein KH et al. (2017) The challenge of mapping the human connectome based on diffusion tractography. Nat Commun 8:1349.

Makris N, Pandya DN (2009) The extreme capsule in humans and rethinking of the language circuitry. Brain Struct Funct 213:343–358.

Makris N, Papadimitriou GM, Kaiser JR, Sorg S, Kennedy DN, Pandya DN (2009) Delineation of the middle longitudinal fascicle in humans: A quantitative, in vivo, DT-MRI study. Cereb Cortex 19:777–785.

Makris N, Papadimitriou GM, van der Kouwe A, Kennedy DN, Hodge SM, Dale AM, Benner T, Wald LL, Wu O, Tuch DS, Caviness VS, Moore TL, Killiany RJ, Moss MB, Rosene DL (2007) Frontal connections and cognitive changes in normal aging rhesus monkeys: A DTI study. Neurobiol Aging 28:1556–1567.

Makris N, Preti MG, Asami T, Pelavin P, Campbell B, Papadimitriou GM, Kaiser J, Baselli G, Westin CF, Shenton ME, Kubicki M (2013) Human middle longitudinal fascicle: Variations in patterns of anatomical connections. Brain Struct Funct 218:951–968.

Malkova L, Heuer E, Saunders RC (2006) Longitudinal magnetic resonance imaging study of rhesus monkey brain development. Eur J Neurosci 24:3204–3212.

Manger PR (2005) Establishing order at the systems level in mammalian brain evolution. Brain Res Bull 66:282–289.

Manger PR, Cort J, Ebrahim N, Goodman A, Henning J, Karolia M, Rodrigus S-L, Šrtkalj G (2008) Is 21st Century Neuroscience too Focussed on the Rat/Mouse Model of Brain Function and Dysfunction? Front Neuroanat 2:1–7.

Mantini D, Gerits A, Nelissen K, Durand J-B, Joly O, Simone L, Sawamura H, Wardak C, Orban GA, Buckner RL, Vanduffel W (2011) Default Mode of Brain Function in Monkeys. J Neurosci 31:12954–12962.

Marciniak K, Atabaki A, Dicke PW, Thier P (2014) Disparate substrates for head gaze following and face perception in the monkey superior temporal sulcus. Elife 3:1–

18.

Marcus DS, Harwell J, Olsen T, Hodge M, Glasser MF, Prior F, Jenkinson M, Laumann T, Curtiss SW, Van Essen DC (2011) Informatics and Data Mining Tools and Strategies for the Human Connectome Project. Front Neuroinform 5:1–12.

Margulies DS, Ghosh SS, Goulas A, Falkiewicz M, Huntenburg JM, Langs G, Bezgin G, Eickhoff SB, Castellanos FX, Petrides M, Jefferies E, Smallwood J (2016) Situating the default-mode network along a principal gradient of macroscale cortical organization. Proc Natl Acad Sci 113:12574–12579.

Margulies DS, Vincent JL, Kelly C, Lohmann G, Uddin LQ, Biswal BB, Villringer A, Castellanos FX, Milham MP, Petrides M (2009) Precuneus shares intrinsic functional architecture in humans and monkeys. Proc Natl Acad Sci 106:20069–20074.

Mars RB, Eichert N, Jbabdi S, Verhagen L, Rushworth MFS (2018a) Connectivity and the search for specializations in the language-capable brain. Curr Opin Behav Sci 21:19–26.

Mars RB, Foxley S, Verhagen L, Jbabdi S, Sallet J, Noonan MP, Neubert FX, Andersson JL, Croxson PL, Dunbar RIM, Khrapitchev AA, Sibson NR, Miller KL, Rushworth MFS (2016a) The extreme capsule fiber complex in humans and macaque monkeys: a comparative diffusion MRI tractography study. Brain Struct Funct 221:4059–4071.

Mars RB, Jbabdi S, Rushworth MFS (2021) A Common Space Approach to Comparative Neuroscience. Annu Rev Neurosci 44:annurev-neuro-100220-025942.

Mars RB, Jbabdi S, Sallet J, O'Reilly JX, Croxson PL, Olivier E, Noonan MP, Bergmann C, Mitchell AS, Baxter MG, Behrens TEJ, Johansen-Berg H, Tomassini V, Miller KL, Rushworth MFS (2011) Diffusion-Weighted Imaging Tractography-Based Parcellation of the Human Parietal Cortex and Comparison with Human and Macaque Resting-State Functional Connectivity. J Neurosci 31:4087–4100.

Mars RB, Neubert F-X, Noonan MP, Sallet J, Toni I, Rushworth MFS (2012a) On the relationship between the "default mode network" and the "social brain." Front Hum Neurosci 6:1–9.

Mars RB, Neubert F-X, Verhagen L, Sallet J, Miller KL, Dunbar RIM, Barton RA (2014) Primate comparative neuroscience using magnetic resonance imaging: promises and challenges. Front Neurosci 8.

Mars RB, O'Muircheartaigh J, Folloni D, Li L, Glasser MF, Jbabdi S, Bryant KL (2019) Concurrent analysis of white matter bundles and grey matter networks in the chimpanzee. Brain Struct Funct 224:1021–1033.

Mars RB, Passingham RE, Jbabdi S (2018b) Connectivity Fingerprints: From Areal Descriptions to Abstract Spaces. Trends Cogn Sci 22:1026–1037.

Mars RB, Sallet J, Neubert F-X, Rushworth MFS (2013) Connectivity profiles reveal the relationship between brain areas for social cognition in human and monkey temporoparietal cortex. Proc Natl Acad Sci 110:10806–10811.

Mars RB, Sallet J, Schuffelgen U, Jbabdi S, Toni I, Rushworth MFS (2012b) Connectivity-based subdivisions of the human right "temporoparietal junction

area": Evidence for different areas participating in different cortical networks. Cereb Cortex 22:1894–1903.

Mars RB, Sotiropoulos SN, Passingham RE, Sallet J, Verhagen L, Khrapitchev AA, Sibson N, Jbabdi S (2018c) Whole brain comparative anatomy using connectivity blueprints. Elife 7:245209.

Mars RB, Verhagen L, Gladwin TE, Neubert F-X, Sallet J, Rushworth MFS (2016b) Comparing brains by matching connectivity profiles. Neurosci Biobehav Rev 60:90–97.

Marticorena DCW, Ruiz AM, Mukerji C, Goddu A, Santos LR (2014) Monkeys represent others' knowledge but not their beliefs. Dev Sci 14:1406–1416.

Martin A, Santos LR (2016) What Cognitive Representations Support Primate Theory of Mind? Trends Cogn Sci 20:375–382.

Masson HL, Isik L (2021) Functional selectivity for naturalistic social interaction perception in the human superior temporal sulcus. bioRxiv:1–25.

Matsuzawa J (2001) Age-related Volumetric Changes of Brain Gray and White Matter in Healthy Infants and Children. Cereb Cortex 11:335–342.

McCloskey MS, Phan KL, Coccaro EF (2005) Neuroimaging and personality disorders. Curr Psychiatry Rep 7:65–72.

McComb K, Semple S (2005) Coevolution of vocal communication and sociality in primates. Biol Lett 1:381–385.

McNab JA, Miller KL (2010) Steady-state diffusion-weighted imaging: Theory, acquisition and analysis. NMR Biomed 23:781–793.

Meltzoff AN, Moore MK (1983) Newborn Infants Imitate Adult Facial Gestures. Child Dev 54:702–709.

Menjot De Champfleur N, Lima Maldonado I, Moritz-Gasser S, MacHi P, Le Bars E, Bonafé A, Duffau H (2013) Middle longitudinal fasciculus delineation within language pathways: A diffusion tensor imaging study in human. Eur J Radiol 82:151–157.

Meunier H (2017) Do monkeys have a theory of mind? How to answer the question? Neurosci Biobehav Rev 82:110–123.

Milham M et al. (2020) Accelerating the Evolution of Nonhuman Primate Neuroimaging. Neuron 105:600–603.

Milham MP et al. (2018) An Open Resource for Non-human Primate Imaging. Neuron 100:61-74.e2.

Miller EK, Nieder A, Freedman DJ, Wallis JD (2003) Neural correlates of categories and concepts. Curr Opin Neurobiol 13:198–203.

Miller KL, McNab JA, Jbabdi S, Douaud G (2012) Diffusion tractography of post-mortem human brains: Optimization and comparison of spin echo and steady-state free precession techniques. Neuroimage 59:2284–2297.

Milton K (1988) Foraging behaviour and the evolution of primate intelligence. In: Machiavellian intelligence: Social expertise and the evolution of intellect in monkeys, apes, and humans., pp 285–305. New York, NY, US: Clarendon Press/Oxford University Press.

Mitchell AS, Thiele A, Petkov CI, Roberts A, Robbins TW, Schultz W, Lemon R (2018) Continued need for non-human primate neuroscience research. Curr Biol 28:R1186–R1187.

Mitchell JP (2005) The false dichotomy between simulation and theory-theory: the argument's error. Trends Cogn Sci 9:363–364.

Montgomery SH, Mundy NI, Barton RA (2016) Brain evolution and development: adaptation, allometry and constraint. Proc R Soc B Biol Sci 283:20160433.

Moran JM (2013) Lifespan development: The effects of typical aging on theory of mind. Behav Brain Res 237:32–40.

Morishima Y, Schunk D, Bruhin A, Ruff CC, Fehr E (2012) Linking Brain Structure and Activation in Temporoparietal Junction to Explain the Neurobiology of Human Altruism. Neuron 75:73–79.

Mott FW, Kelley AM (1908) Complete survey of the cell lamination of the cerebral cortex of the lemur. Proc R Soc London Ser B, Contain Pap a Biol Character 80:488–506.

Murray EA, Wise SP, Graham KS (2016) The Evolution of Memory Systems. Oxford University Press.

Neary D, Snowden J, Mann D (2005) Frontotemporal dementia. Lancet Neurol 4:771–780.

Nelissen K, Vanduffel W, Orban GA (2006) Charting the lower superior temporal region, a new motion-sensitive region in monkey superior temporal sulcus. J Neurosci 26:5929–5947.

Nelson EE, Guyer AE (2011) The development of the ventral prefrontal cortex and social flexibility. Dev Cogn Neurosci 1:233–245.

Neubert F-X, Mars RB, Sallet J, Rushworth MFS (2015) Connectivity reveals relationship of brain areas for reward-guided learning and decision making in human and monkey frontal cortex. Proc Natl Acad Sci 112:E2695–E2704.

Neubert FX, Mars RB, Thomas AG, Sallet J, Rushworth MFS (2014) Comparison of Human Ventral Frontal Cortex Areas for Cognitive Control and Language with Areas in Monkey Frontal Cortex. Neuron 81:700–713.

Nichols T, Brett M, Andersson J, Wager T, Poline JB (2005) Valid conjunction inference with the minimum statistic. Neuroimage 25:653–660.

Nielsen M, Haun D (2016) Why developmental psychology is incomplete without comparative and cross-cultural perspectives. Philos Trans R Soc B Biol Sci 371:20150071.

Noonan MP, Mars RB, Sallet J, Dunbar RIM, Fellows LK (2018) The structural and functional brain networks that support human social networks. Behav Brain Res 355:12–23.

Noonan MP, Sallet J, Mars RB, Neubert F-X, O'Reilly JX, Andersson JL, Mitchell AS, Bell AH, Miller KL, Rushworth MFS (2014) A Neural Circuit Covarying with Social Hierarchy in Macaques. PLoS Biol 12.

Ochiai T, Grimault S, Scavarda D, Roch G, Hori T, Rivière D, Mangin JF, Régis J (2004) Sulcal pattern and morphology of the superior temporal sulcus. Neuroimage

22:706–719.

O'Leary DDM (1992) Development of connectional diversity and specificity in the mammalian brain by the pruning of collateral projections. Curr Opin Neurobiol 2:70–77.

O'Muircheartaigh J, Jbabdi S (2018) Concurrent white matter bundles and grey matter networks using independent component analysis. Neuroimage 170:296–306.

O'Toole AJ, Jonathon Phillips P, Weimer S, Roark DA, Ayyad J, Barwick R, Dunlop J (2011) Recognizing people from dynamic and static faces and bodies: Dissecting identity with a fusion approach. Vision Res 51:74–83.

Olson IR, McCoy D, Klobusicky E, Ross LA (2013) Social cognition and the anterior temporal lobes: A review and theoretical framework. Soc Cogn Affect Neurosci 8:123–133.

Ong WS, Madlon-Kay S, Platt ML (2020) Neuronal correlates of strategic cooperation in monkeys. Nat Neurosci.

Orban GA, Van Essen DC, Vanduffel W (2004) Comparative mapping of higher visual areas in monkeys and humans. Trends Cogn Sci 8:315–324.

Panesar SS, Yeh F-C, Jacquesson T, Hula W, Fernandez-Miranda JC (2018) A Quantitative Tractography Study Into the Connectivity, Segmentation and Laterality of the Human Inferior Longitudinal Fasciculus. Front Neuroanat 12:1–13.

Panesar SS, Yeh FC, Deibert CP, Fernandes-Cabral D, Rowthu V, Celtikci P, Celtikci E, Hula WD, Pathak S, Fernández-Miranda JC (2017) A diffusion spectrum imaging-based tractographic study into the anatomical subdivision and cortical connectivity of the ventral external capsule: uncinate and inferior fronto-occipital fascicles. Neuroradiology 59:971–987.

Paquola C, Vos De Wael R, Wagstyl K, Bethlehem RAI, Hong S-J, Seidlitz J, Bullmore ET, Evans AC, Misic B, Margulies DS, Smallwood J, Bernhardt BC (2019) Microstructural and functional gradients are increasingly dissociated in transmodal cortices Kennedy H, ed. PLOS Biol 17:e3000284.

Parisot S, Arslan S, Passerat-Palmbach J, Wells WM, Rueckert D (2015) Tractography-Driven Groupwise Multi-scale Parcellation of the Cortex. In, pp 600–612.

Parr LA (2011) The evolution of face processing in primates. Philos Trans R Soc B Biol Sci 366:1764–1777.

Parr LA, Hecht E, Barks SK, Preuss TM, Votaw JR (2009) Face Processing in the Chimpanzee Brain. Curr Biol 19:50–53.

Passingham RE, Smaers JB (2014) Is the prefrontal cortex especially enlarged in the human brain? Allometric relations and remapping factors. Brain Behav Evol 84:156–166.

Passingham RE, Smaers JB, Sherwood CC (2017) Evolutionary Specializations of the Human Prefrontal Cortex. In: Evolution of Nervous Systems, 2nd ed. (Kass J., Preuss TM, eds), pp 207–226. Elsevier.

Passingham RE, Stephan KE, Kötter R (2002) The anatomical basis of functional localization in the cortex. Nat Rev Neurosci 3:606–616.

Passingham RE, Wise SP (2012) The Neurobiology of the Prefrontal Cortex. Oxford University Press.

Patel GH, Sestieri C, Corbetta M (2019) The evolution of the temporoparietal junction and posterior superior temporal sulcus. Cortex.

Paxinos G, Huang X., Toga A. (2000) The Rhesus Monkey Brain in Stereotaxic Coordinates. Acad Press San Diego.

Pearlman-Avnion S, Ron N, Ezekiel S (2018) Ageing and theory of mind abilities: The benefits of social interaction. Educ Gerontol 44:368–377.

Perelman P, Johnson WE, Roos C, Seuánez HN, Horvath JE, Moreira MAM, Kessing B, Pontius J, Roelke M, Rumpler Y, Schneider MPC, Silva A, O'Brien SJ, Pecon-Slattery J (2011) A Molecular Phylogeny of Living Primates Brosius J, ed. PLoS Genet 7:e1001342.

Perretta G (2009) Non-human primate models in neuroscience research. Scand J Lab Anim Sci 36:77–85.

Perrodin C, Kayser C, Abel TJ, Logothetis NK, Petkov CI (2015) Who is That? Brain Networks and Mechanisms for Identifying Individuals. Trends Cogn Sci 19:783–796.

Peters M, Ploog D (1973) Communication among primates. Annu Rev Physiol 35:221–242.

Petrides M (2005) Lateral prefrontal cortex: architectonic and functional organization. Philos Trans R Soc B Biol Sci 360:781–795.

Petrides M (2011) The human cerebral cortex: an MRI atlas of the sulci and gyri in MNI stereotaxic space. Amsterdam: Academic Press.

Phillips KA, Bales KL, Capitanio JP, Conley A, Czoty PW, 't Hart BA, Hopkins WD, Hu S-L, Miller LA, Nader MA, Nathanielsz PW, Rogers J, Shively CA, Voytko M Lou (2014) Why primate models matter. Am J Primatol 76:801–827.

Pinsk MA, Arcaro M, Weiner KS, Kalkus JF, Inati SJ, Gross CG, Kastner S (2009) Neural representations of faces and body parts in macaque and human cortex: A comparative fMRI study. J Neurophysiol 101:2581–2600.

Pitcher D, Ungerleider LG (2021) Evidence for a Third Visual Pathway Specialized for Social Perception. Trends Cogn Sci 25:100–110.

Popivanov ID, Jastorff J, Vanduffel W, Vogels R (2014) Heterogeneous single-unit selectivity in an fMRI-defined body-selective patch. J Neurosci 34:95–111.

Pouget P, Frey S, Ahnine H, Attali D, Claron J, Constans C, Aubry JF, Arcizet F (2020) Neuronavigated Repetitive Transcranial Ultrasound Stimulation Induces Long-Lasting and Reversible Effects on Oculomotor Performance in Non-human Primates. Front Physiol 11:1–13.

Povinelli D, Vonk J (2012) We don't need a microscope to explore the chimpanzee's mind. Ration Anim 19:1–28.

Pozeg P, Forget J, Meuli RA, Maeder P (2019) Age, But Not Repeated Exposure to Gadoterate Meglumine, Is Associated With T1- and T2-Weighted Signal Intensity Changes in the Deep Brain Nuclei of Pediatric Patients. Invest Radiol 54:537–548.

Premack D, Woodruff G (1978) Does the chimpanzee have a theory of mind? Behav

Brain Sci 1:515–526.

Preuss TM (2011) The human brain: rewired and running hot. Ann N Y Acad Sci 1225:E182–E191.

Preuss TM, Goldman-Rakic PS (1991) Myelo- and cytoarchitecture of the granular frontal cortex and surrounding regions in the strepsirhine primate Galago and the anthropoid primate Macaca. J Comp Neurol 310:429–474.

Price CJ (2000) The anatomy of language: contributions from functional neuroimaging. J Anat 197:332–359.

Pyles JA, Verstynen TD, Schneider W, Tarr MJ (2013) Explicating the Face Perception Network with White Matter Connectivity Ptito M, ed. PLoS One 8:e61611.

Quesque F, Rossetti Y (2020) What Do Theory-of-Mind Tasks Actually Measure? Theory and Practice. Perspect Psychol Sci 15:384–396.

Radinsky L (1975) Primate Brain Evolution: Comparative studies of brains of living mammal species reveal major trends in the evolutionary development of primate brains, and analysis of endocasts from fossil primate braincases suggests when these specializations occurred. Am Sci 63:656–663.

Raff RA (2000) Evo-devo: the evolution of a new discipline. Nat Rev Genet 1:74–79.

Raichle ME, MacLeod AM, Snyder AZ, Powers WJ, Gusnard DA, Shulman GL (2001) A default mode of brain function. Proc Natl Acad Sci 98:676–682.

Rakoczy H, Harder-Kasten A, Sturm L (2012) The decline of theory of mind in old age is (partly) mediated by developmental changes in domain-general abilities. Br J Psychol 103:58–72.

Reader SM, Laland KN (2002) Social intelligence, innovation, and enhanced brain size in primates. Proc Natl Acad Sci 99:4436–4441.

Reveley C, Gruslys A, Ye FQ, Glen D, Samaha J, Russ BE, Saad Z, Seth AK, Leopold DA, Saleem KS (2017) Three-dimensional digital template atlas of the macaque brain. Cereb Cortex 27:4463–4477.

Reveley C, Seth AK, Pierpaoli C, Silva AC, Yu D, Saunders RC, Leopold DA, Ye FQ (2015) Superficial white matter fiber systems impede detection of long-range cortical connections in diffusion MR tractography. Proc Natl Acad Sci 112:E2820–E2828.

Rilling JK (2006) Human and NonHuman primate brains: Are they allometrically scaled versions of the same design? Evol Anthropol 15:65–77.

Rilling JK (2014) Comparative primate neuroimaging: Insights into human brain evolution. Trends Cogn Sci 18:46–55.

Rilling JK, Glasser M, Jbabdi S, Andersson J, Preuss T (2012) Continuity,divergence,and the evolution of brain language pathways. Front Evol Neurosci 3:1–6.

Rilling JK, Glasser MF, Preuss TM, Ma X, Zhao T, Hu X, Behrens TEJ (2008) The evolution of the arcuate fasciculus revealed with comparative DTI. Nat Neurosci 11:426–428.

Rizzolatti G (2005) The mirror neuron system and its function in humans. Anat Embryol (Berl) 210:419–421.

Rizzolatti G, Craighero L (2004) The mirror-neuron system. Annu Rev Neurosci 27:169–192.

Rizzolatti G, Fadiga L, Gallese V, Fogassi L (1996) Premotor cortex and the recognition of motor actions. Cogn Brain Res 3:131–141.

Rizzolatti G, Fogassi L (2014) The mirror mechanism: recent findings and perspectives. Philos Trans R Soc B Biol Sci 369:20130420–20130420.

Rocchi F, Oya H, Balezeau F, Billig AJ, Kocsis Z, Jenison RL, Nourski K V., Kovach CK, Steinschneider M, Kikuchi Y, Rhone AE, Dlouhy BJ, Kawasaki H, Adolphs R, Greenlee JDW, Griffiths TD, Howard MA, Petkov CI (2021) Common fronto-temporal effective connectivity in humans and monkeys. Neuron 109:852-868.e8.

Rosabal F (1967) Cytoarchitecture of the frontal lobe of the squirrel monkey. J Comp Neurol 130:87–108.

Rosati AG (2017) Foraging Cognition: Reviving the Ecological Intelligence Hypothesis. Trends Cogn Sci 21:691–702.

Rosati AG, Hare B (2009) Looking past the model species: diversity in gaze-following skills across primates. Curr Opin Neurobiol 19:45–51.

Rosati AG, Wobber V, Hughes K, Santos LR (2014) Comparative Developmental Psychology: How is Human Cognitive Development Unique? Evol Psychol 12:147470491401200.

Roumazeilles L, Eichert N, Bryant KL, Folloni D, Sallet J, Vijayakumar S, Foxley S, Tendler BC, Jbabdi S, Reveley C, Verhagen L, Dershowitz LB, Guthrie M, Flach E, Miller KL, Mars RB (2020) Longitudinal connections and the organization of the temporal cortex in macaques, great apes, and humans. PLOS Biol 18:e3000810.

Rousseeuw PJ (1987) Silhouettes: A graphical aid to the interpretation and validation of cluster analysis. J Comput Appl Math 20:53–65.

Royo J, Forkel SJ, Pouget P, Thiebaut de Schotten M (2021) The squirrel monkey model in clinical neuroscience. Neurosci Biobehav Rev 128:152–164.

Ruff CC, Fehr E (2014) The neurobiology of rewards and values in social decision making. Nat Rev Neurosci 15:549–562.

Rushworth MFS, Mars RB, Sallet J (2013) Are there specialized circuits for social cognition and are they unique to humans? Curr Opin Neurobiol 23:436–442.

Sakai T, Mikami A, Tomonaga M, Matsui M, Suzuki J, Hamada Y, Tanaka M, Miyabe-Nishiwaki T, Makishima H, Nakatsukasa M, Matsuzawa T (2011) Differential prefrontal white matter development in chimpanzees and humans. Curr Biol 21:1397–1402.

Sallet J, Mars RB, Noonan MP, Andersson JL, O'Reilly JX, Jbabdi S, Croxson PL, Jenkinson M, Miller KL, Rushworth MFS (2011) Social Network Size Affects Neural Circuits in Macaques. Science (80-) 334:697–700.

Sallet J, Mars RB, Noonan MP, Neubert F-X, Jbabdi S, O'Reilly JX, Filippini N, Thomas AG, Rushworth MF (2013) The Organization of Dorsal Frontal Cortex in Humans and Macaques. J Neurosci 33:12255–12274.

Sandel AA, Miller JA, Mitani JC, Nunn CL, Patterson SK, Garamszegi LZ (2016)

Assessing sources of error in comparative analyses of primate behavior: Intraspecific variation in group size and the social brain hypothesis. J Hum Evol 94:126–133.

Sansalone G, Allen K, Ledogar JA, Ledogar S, Mitchell DR, Profico A, Castiglione S, Melchionna M, Serio C, Mondanaro A, Raia P, Wroe S (2020) Variation in the strength of allometry drives rates of evolution in primate brain shape. Proc R Soc B Biol Sci 287:20200807.

Sarubbo S, Petit L, De Benedictis A, Chioffi F, Ptito M, Dyrby TB (2019) Uncovering the inferior fronto-occipital fascicle and its topological organization in non-human primates: the missing connection for language evolution. Brain Struct Funct 0:0.

Sarubbo S, Tate M, De Benedictis A, Merler S, Moritz-Gasser S, Herbet G, Duffau H (2020) Mapping critical cortical hubs and white matter pathways by direct electrical stimulation: an original functional atlas of the human brain. Neuroimage 205:116237.

Saxe R (2005) Against simulation: the argument from error. Trends Cogn Sci 9:174–179.

Schaeffer DJ, Adam R, Gilbert KM, Gati JS, Li AX, Menon RS, Everling S (2017) Diffusion weighted tractography in the common marmoset monkey at 9.4 T. J Neurophysiol:jn.00259.2017.

Schaeffer DJ, Gilbert KM, Hori Y, Gati JS, Menon RS, Everling S (2019) Integrated radiofrequency array and animal holder design for minimizing head motion during awake marmoset functional magnetic resonance imaging. Neuroimage 193:126–138.

Schaeffer DJ, Selvanayagam J, Johnston KD, Menon RS, Freiwald WA, Everling S (2020) Face selective patches in marmoset frontal cortex. Nat Commun 11:4856.

Schafroth JL, Basile BM, Martin A, Murray EA (2021) No evidence that monkeys attribute mental states to animated shapes in the Heider–Simmel videos. Sci Rep 11:3050.

Schilling KG, Gao Y, Stepniewska I, Wu T-L, Wang F, Landman BA, Gore JC, Chen LM, Anderson AW (2017) The VALiDATe29 MRI Based Multi-Channel Atlas of the Squirrel Monkey Brain. Neuroinformatics 15:321–331.

Schmahmann JD, Pandya DN (2006a) Composite Summary of Cerebral White Matter Fiber Pathways in the Rhesus Monkey. In: Fiber Pathways of the Brain, pp 533–554. Oxford University Press.

Schmahmann JD, Pandya DN (2006b) Fiber pathways of the brain. Oxford: Oxford University Press.

Schmahmann JD, Pandya DN (2006c) Inferior Longitudinal Fasciculus. In: Fiber Pathways of the Brain, pp 441–454. Oxford University Press.

Schmahmann JD, Pandya DN, Wang R, Dai G, D'Arceuil HE, De Crespigny AJ, Wedeen VJ (2007) Association fibre pathways of the brain: Parallel observations from diffusion spectrum imaging and autoradiography. Brain 130:630–653.

Schmelz M, Call J (2016) The psychology of primate cooperation and competition: a call for realigning research agendas. Philos Trans R Soc B Biol Sci 371:20150067.

Schurz M, Maliske L, Kanske P (2020) Cross-network interactions in social cognition:

A review of findings on task related brain activation and connectivity. Cortex 130:142–157.

Schurz M, Perner J (2015) An evaluation of neurocognitive models of theory of mind. Front Psychol 6:1–9.

Schurz M, Tholen MG, Perner J, Mars RB, Sallet J (2017) Specifying the brain anatomy underlying temporo-parietal junction activations for theory of mind: A review using probabilistic atlases from different imaging modalities. Hum Brain Mapp 38:4788–4805.

Schurz M, Radua J, Aichhorn M, Richlan F, Perner J (2014) Fractionating theory of mind: A meta-analysis of functional brain imaging studies. Neurosci Biobehav Rev 42:9–34.

Schurz M, Radua J, Tholen MG, Maliske L, Margulies DS, Mars RB, Sallet J, Kanske P (2021) Toward a hierarchical model of social cognition: A neuroimaging meta-analysis and integrative review of empathy and theory of mind. Psychol Bull 147:293–327.

Schwiedrzik CM, Zarco W, Everling S, Freiwald WA (2015) Face Patch Resting State Networks Link Face Processing to Social Cognition. PLoS Biol 13:1–27.

Scott JA, Grayson D, Fletcher E, Lee A, Bauman MD, Schumann CM, Buonocore MH, Amaral DG (2016) Longitudinal analysis of the developing rhesus monkey brain using magnetic resonance imaging: birth to adulthood. Brain Struct Funct 221:2847–2871.

Semendeferi K, Lu A, Schenker N, Damasio H (2002) Humans and great apes share a large frontal cortex. Nat Neurosci 5:272–276.

Shaw RC, Greggor AL, Plotnik JM (2021) The Challenges of Replicating Research on Endangered Species. Anim Behav Cogn 8:240–246.

Shepherd (2010) Following gaze: gaze-following behavior as a window into social cognition. Front Integr Neurosci 4:1–13.

Shi Y, Short SJ, Knickmeyer RC, Wang J, Coe CL, Niethammer M, Gilmore JH, Zhu H, Styner MA (2013) Diffusion tensor imaging-based characterization of brain neurodevelopment in primates. Cereb Cortex 23:36–48.

Silk JB (2003) Social Bonds of Female Baboons Enhance Infant Survival. Science (80-) 302:1231–1234.

Slater DA, Melie-Garcia L, Preisig M, Kherif F, Lutti A, Draganski B (2019) Evolution of white matter tract microstructure across the life span. Hum Brain Mapp 40:2252–2268.

Sliwa J, Duhamel J-R, Pascalis O, Wirth S (2011) Spontaneous voice-face identity matching by rhesus monkeys for familiar conspecifics and humans. Proc Natl Acad Sci 108:1735–1740.

Sliwa J, Freiwald WA (2017) A dedicated network for social interaction processing in the primate brain. 749:745–749.

Smaers JB, Gómez-Robles A, Parks AN, Sherwood CC (2017) Exceptional Evolutionary Expansion of Prefrontal Cortex in Great Apes and Humans. Curr Biol 27:714–720.

Smaers JB, Soligo C (2013) Brain reorganization, not relative brain size, primarily characterizes anthropoid brain evolution. Proc R Soc B Biol Sci 280.

Smaers JB, Vanier DR (2019) Brain size expansion in primates and humans is explained by a selective modular expansion of the cortico-cerebellar system. Cortex 118:292–305.

Sotiropoulos SN, Jbabdi S, Xu J, Andersson JL, Moeller S, Auerbach EJ, Glasser MF, Hernandez M, Sapiro G, Jenkinson M, Feinberg DA, Yacoub E, Lenglet C, Van Essen DC, Ugurbil K, Behrens TEJ (2013) Advances in diffusion MRI acquisition and processing in the Human Connectome Project. Neuroimage 80:125–143.

Spadacenta S, Dicke PW, Thier P (2019) Reflexive gaze following in common marmoset monkeys. Sci Rep 9:15292.

Stevens HE, Leckman JF, Coplan JD, Suomi SJ (2009) Risk and Resilience: Early Manipulation of Macaque Social Experience and Persistent Behavioral and Neurophysiological Outcomes. J Am Acad Child Adolesc Psychiatry 48:114–127.

Stiles J, Jernigan TL (2010) The Basics of Brain Development. Neuropsychol Rev 20:327–348.

Striedter GF et al. (2014) NSF Workshop Report: Discovering General Principles of Nervous System Organization by Comparing Brain Maps across Species. Brain Behav Evol 83:1–8.

Sueur C, Jacobs A, Amblard F, Petit O, King AJ (2011) How can social network analysis improve the study of primate behavior? Am J Primatol 73:703–719.

Sugranyes G, Kyriakopoulos M, Corrigall R, Taylor E, Frangou S (2011) Autism Spectrum Disorders and Schizophrenia : Meta- Analysis of the Neural Correlates of Social Cognition. 6.

Sussman RW, Garber PA, Cheverud JM (2005) News and views: Importance of cooperation and affiliation in the evolution of primate sociality. Am J Phys Anthropol 128:84–97.

Sutton RS, Barto A. (1998) Reinforcement learning: An introduction. MIT Press.

Tak HJ, Kim JH, Son SM (2016) Developmental process of the arcuate fasciculus from infancy to adolescence: A diffusion tensor imaging study. Neural Regen Res 11:937–943.

Takemura H, Pestilli F, Weiner KS, Keliris GA, Landi SM, Sliwa J, Ye FQ, Barnett MA, Leopold DA, Freiwald WA, Logothetis NK, Wandell BA (2017) Occipital White Matter Tracts in Human and Macaque. Cereb Cortex 27:3346–3359.

Taubert J, Wardle SG, Flessert M, Leopold DA, Ungerleider LG (2017) Face Pareidolia in the Rhesus Monkey. Curr Biol 27:2505-2509.e2.

Thiebaut de Schotten M, Dell'Acqua F, Forkel S, Simmons A, Vergani F, Murphy DGM, Catani M (2011a) A Lateralized Brain Network for Visuo-Spatial Attention. Nat Preced 14:1245–1246.

Thiebaut de Schotten M, Ffytche DH, Bizzi A, Dell'Acqua F, Allin M, Walshe M, Murray R, Williams SC, Murphy DGM, Catani M (2011b) Atlasing location, asymmetry and inter-subject variability of white matter tracts in the human brain with MR diffusion tractography. Neuroimage 54:49–59.

Thiebaut De Schotten M, Dell'Acqua F, Valabregue R, Catani M (2012) Monkey to human comparative anatomy of the frontal lobe association tracts. Cortex 48:82–96.

Thiebaut de Schotten M, Foulon C, Nachev P (2020) Brain disconnections link structural connectivity with function and behaviour. Nat Commun 11:5094.

Tibshirani R, Walther G, Hastie T (2001) Estimating the number of clusters in a data set via the gap statistic. J R Stat Soc Ser B (Statistical Methodol 63:411–423.

Tomasello M (2019) Becoming Human. Harvard University Press.

Tomasello M, Carpenter M, Call J, Behne T, Moll H (2005) Understanding and sharing intentions: The origins of cultural cognition. Behav Brain Sci 28:675–691.

Tomasello M, Hare B, Lehmann H, Call J (2007) Reliance on head versus eyes in the gaze following of great apes and human infants: the cooperative eye hypothesis. J Hum Evol 52:314–320.

Tomasello M, Kruger AC, Ratner HH (1993) Cultural learning. Behav Brain Sci 16:495–511.

Tournier J-D, Calamante F, Connelly A (2007) Robust determination of the fibre orientation distribution in diffusion MRI: Non-negativity constrained super-resolved spherical deconvolution. Neuroimage 35:1459–1472.

Tournier J-D, Calamante F, Connelly A (2013) Determination of the appropriate b value and number of gradient directions for high-angular-resolution diffusion-weighted imaging. NMR Biomed 26:1775–1786.

Tremblay S, Sharika KM, Platt ML (2017) Social Decision-Making and the Brain: A Comparative Perspective. Trends Cogn Sci 21:265–276.

Tsao DY, Freiwald WA, Knutsen TA, Mandeville JB, Tootell RBH (2003) Faces and objects in macaque cerebral cortex. Nat Neurosci 6:989–995.

Tsao DY, Moeller S, Freiwald WA (2008) Comparing face patch systems in macaques and humans. Proc Natl Acad Sci 105:19514–19519.

Ugurbil K et al. (2013) Pushing spatial and temporal resolution for functional and diffusion MRI in the Human Connectome Project. Neuroimage 80:80–104.

van den Heuvel MP, Bullmore ET, Sporns O (2016) Comparative Connectomics. Trends Cogn Sci 20:345–361.

van der Bijl W, Kolm N (2016) Why direct effects of predation complicate the social brain hypothesis. BioEssays 38:568–577.

Van Essen DC, Dierker DL (2007) Surface-based and probabilistic atlases of primate cerebral cortex. Neuron 56:209–225.

Van Essen DC, Drury HA, Dickson J, Harwell J, Hanlon D, Anderson CH (2001) An integrated software suite for surface-based analyses of cerebral cortex. J Am Med Informatics Assoc 8:443–459.

Van Essen DC, Smith J, Glasser MF, Elam J, Donahue CJ, Dierker DL, Reid EK, Coalson T, Harwell J (2017) The Brain Analysis Library of Spatial maps and Atlases (BALSA) database. Neuroimage 144:270–274.

Van Essen DC, Smith SM, Barch DM, Behrens TEJ, Yacoub E, Ugurbil K (2013) The WU-Minn Human Connectome Project: An overview. Neuroimage 80:62–79.

Van Overwalle F, Baetens K (2009) Understanding others' actions and goals by mirror and mentalizing systems: A meta-analysis. Neuroimage 48:564–584.

Ventura-Antunes L, Mota B, Herculano-Houzel S (2013) Different scaling of white matter volume, cortical connectivity, and gyrification across rodent and primate brains. Front Neuroanat 7:1–12.

Verhagen L, Gallea C, Folloni D, Constans C, Jensen DEA, Ahnine H, Roumazeilles L, Santin M, Ahmed B, Lehericy S, Klein-Flügge MC, Krug K, Mars RB, Rushworth MFS, Pouget P, Aubry JF, Sallet J (2019) Offline impact of transcranial focused ultrasound on cortical activation in primates. Elife 8:1–28.

Vijayakumar S, Sallet J, Verhagen L, Folloni D, Medendorp WP, Mars RB (2019) Mapping multiple principles of parietal–frontal cortical organization using functional connectivity. Brain Struct Funct 224:681–697.

Vincent JL, Patel GH, Fox MD, Snyder AZ, Baker JT, Van Essen DC, Zempel JM, Snyder LH, Corbetta M, Raichle ME (2007) Intrinsic functional architecture in the anaesthetized monkey brain. Nature 447:83–86.

von Bonin G, Bailey P (1947) The Neocortex of Macaca Mulatta, University. Urbana, IL.

Vos de Wael R, Royer J, Tavakol S, Wang Y, Paquola C, Benkarim O, Eichert N, Larivière S, Xu T, Misic B, Smallwood J, Valk SL, Bernhardt BC (2021) Structural Connectivity Gradients of the Temporal Lobe Serve as Multiscale Axes of Brain Organization and Cortical Evolution. Cereb Cortex:1–14.

Wang Y, Metoki A, Alm KH, Olson IR (2018) White matter pathways and social cognition. Neurosci Biobehav Rev 90:350–370.

Wang Y, Olson IR (2018) The Original Social Network: White Matter and Social Cognition. Trends Cogn Sci 22:504–516.

Warrington S, Bryant KL, Khrapitchev AA, Sallet J, Charquero-Ballester M, Douaud G, Jbabdi S, Mars RB, Sotiropoulos SN (2020) XTRACT - Standardised protocols for automated tractography in the human and macaque brain. Neuroimage 217:116923.

Wattiez N, Constans C, Deffieux T, Daye PM, Tanter M, Aubry J-F, Pouget P (2017) Transcranial ultrasonic stimulation modulates single-neuron discharge in macaques performing an antisaccade task. Brain Stimul 10:1024–1031.

Whiten A, van de Waal E (2017) Social learning, culture and the 'socio-cultural brain' of human and non-human primates. Neurosci Biobehav Rev 82:58–75.

Whiten A, van Schaik CP (2007) The evolution of animal 'cultures' and social intelligence. Philos Trans R Soc B Biol Sci 362:603–620.

Wilson B, Kikuchi Y, Sun L, Hunter D, Dick F, Smith K, Thiele A, Griffiths TD, Marslen-Wilson WD, Petkov CI (2015) Auditory sequence processing reveals evolutionarily conserved regions of frontal cortex in macaques and humans. Nat Commun 6:8901.

Wimmer H, Perner J (1983) Beliefs about beliefs: Representation and constraining function of wrong beliefs in young children's understanding of deception.

Cognition 13:103–128.

Winkler AM, Ridgway GR, Webster MA, Smith SM, Nichols TE (2014) Permutation inference for the general linear model. Neuroimage 92:381–397.

Wittmann MK, Kolling N, Faber NS, Scholl J, Nelissen N, Rushworth MFS (2016) Self-Other Mergence in the Frontal Cortex during Cooperation and Competition. Neuron 91:482–493.

Wittmann MK, Lockwood PL, Rushworth MFS (2018) Neural Mechanisms of Social Cognition in Primates. Annu Rev Neurosci 41:99–118.

Wobber V, Herrmann E, Hare B, Wrangham R, Tomasello M (2014) Differences in the early cognitive development of children and great apes. Dev Psychobiol 56:547–573.

Woolrich MW, Behrens TEJ, Beckmann CF, Jenkinson M, Smith SM (2004) Multilevel linear modelling for FMRI group analysis using Bayesian inference. Neuroimage 21:1732–1747.

Woolrich MW, Ripley BD, Brady M, Smith SM (2001) Temporal autocorrelation in univariate linear modeling of FMRI data. Neuroimage 14:1370–1386.

Wu Y, Sun D, Wang Y, Wang Y (2016) Subcomponents and Connectivity of the Inferior Fronto-Occipital Fasciculus Revealed by Diffusion Spectrum Imaging Fiber Tracking. Front Neuroanat 10:1–13.

Xiang H, Van Leeuwen TM, Dediu D, Roberts L, Norris DG, Hagoort P (2015) L2-Proficiency-Dependent Laterality Shift in Structural Connectivity of Brain Language Pathways. Brain Connect 5:349–361.

Xu T, Nenning K-H, Schwartz E, Hong S-J, Vogelstein JT, Goulas A, Fair DA, Schroeder CE, Margulies DS, Smallwood J, Milham MP, Langs G (2020) Cross-species functional alignment reveals evolutionary hierarchy within the connectome. Neuroimage 223:117346.

Yang Z, Freiwald WA (2021) Joint encoding of facial identity, orientation, gaze, and expression in the middle dorsal face area. Proc Natl Acad Sci 118:e2108283118.

Yarnykh VL (2007) Actual flip-angle imaging in the pulsed steady state: A method for rapid three-dimensional mapping of the transmitted radiofrequency field. Magn Reson Med 57:192–200.

Yeo BTT, Krienen FM, Sepulcre J, Sabuncu MR, Lashkari D, Hollinshead M, Roffman JL, Smoller JW, Zollei L, Polimeni JR, Fischl B, Liu H, Buckner RL (2011) The organization of the human cerebral cortex estimated by intrinsic functional connectivity. J Neurophysiol 106:1125–1165.

Yeshurun Y, Nguyen M, Hasson U (2021) The default mode network: where the idiosyncratic self meets the shared social world. Nat Rev Neurosci 22:181–192.

Yin Z, Zhou X, Bakal C, Li F, Sun Y, Perrimon N, Wong STC (2008) Using iterative cluster merging with improved gap statistics to perform online phenotype discovery in the context of high-throughput RNAi screens. BMC Bioinformatics 9:264.

Yoshida K, Saito N, Iriki A, Isoda M (2012) Social error monitoring in macaque frontal cortex. Nat Neurosci 15:1307–1312.

Yovel G, Freiwald WA (2013) Face recognition systems in monkey and human: are they the same thing? F1000Prime Rep 5:1–8.

Yushkevich PA, Piven J, Hazlett HC, Smith RG, Ho S, Gee JC, Gerig G (2006) User-guided 3D active contour segmentation of anatomical structures: Significantly improved efficiency and reliability. Neuroimage 31:1116–1128.

Zhang Y, Brady M, Smith S (2001) Segmentation of brain MR images through a hidden Markov random field model and the expectation-maximization algorithm. IEEE Trans Med Imaging 20:45–57.

Zuberbühler K, Janmaat K (2010) Foraging Cognition in Nonhuman Primates. In: Primate Neuroethology, pp 64–83. Oxford University Press.

Appendices

Appendix 1: Cluster number verification

As stated in the main text (chapter 3), in our initial analyses we performed a connectivity-based parcellation of coronal sections through the temporal cortex white matter (Figure 3.1A) to establish the bodies of main white matter tracts that we then reconstructed (Figure 3.1B). We hypothesized three main clusters for the macaque, corresponding to the MdLF, IFOF, and ILF, and four clusters for the human, corresponding to MdLF, IFOF, and two ILF subdivisions based on the work by Latini and colleagues (Latini et al., 2017).

To determine the number of clusters in data, different algorithms have been used (see Eickhoff et al., 2015 for a review). However, in the connectivity-based parcellation field it is well-known that different algorithms tend to converge on different solutions. Therefore, previous studies have used multiple algorithms and chosen a solution that was appropriate to the point they wanted to convey (Kelly et al., 2010; Kahnt et al., 2012; Clos et al., 2013; Neubert et al., 2014). However, the situation might be alleviated in the comparative context, where we are merely interested in whether all solutions point in the same direction between different brains, rather than in 'the' correct number of clusters. In this respect, our hypothesis is that great ape and human brains show a greater number of clusters in the temporal cortex white matter, which we interpret as a greater complexity of the white matter. We want to precise that we do not claim that the exact number of clusters should be three in macaques and four in apes. Rather, we want to show that by using the same approach in the different brains and finding a larger

number of clusters in some brains than in others, we can make a comparative statement about the complexity of the brains.

Below, we describe various ways of assessing cluster number. We originally tested the number of clusters by means of consistency across subjects, which has been the preferred method in our lab in the past (Mars et al., 2011; Sallet et al., 2013; Neubert et al., 2014). We then also employed the hierarchy index, a popular measure that relies on the hierarchical nature of biological data as a confirmatory measure. Finally, to further test the hypothesis of greater complexity in great apes, we employed a variety of other methods from the literature and, acknowledging that they are likely to give slightly different absolute numbers of clusters, investigated whether each method indicates a greater number of clusters in the great apes and humans compared to the macaque 'baseline' number of clusters.

We used the consistency across subjects as the main goal of the clustering was to define the masks for the subsequent tract reconstruction. These masks are defined based on probability maps from the clustering of the different subjects. Therefore, if there is no consistency across subjects in the clustering result, the maps will contain only low probability and it will not be possible to define non-overlapping masks for the tract reconstruction. When we ran the clustering analysis with one more cluster in macaques (four for the posterior and middle ROIs and five for the anterior ROI), we noticed that the clustering would then lead to divide either the MdLF, IFOF or ILF associated cluster without consistency across subjects and ROIs (Appendix figure 1.1A). In contrast in humans and chimpanzees, when we ran the clustering analysis with one less cluster (three for the posterior and middle ROIs and four for the anterior ROI), we could notice that the clustering would cluster together the two ILF subcomponents (Appendix figure 1.1A). This consistency analysis confirmed that a higher number of

clusters in the macaque did not yield a reliable parcellation of white matter. This result is also in line with the results from the hierarchy analysis.

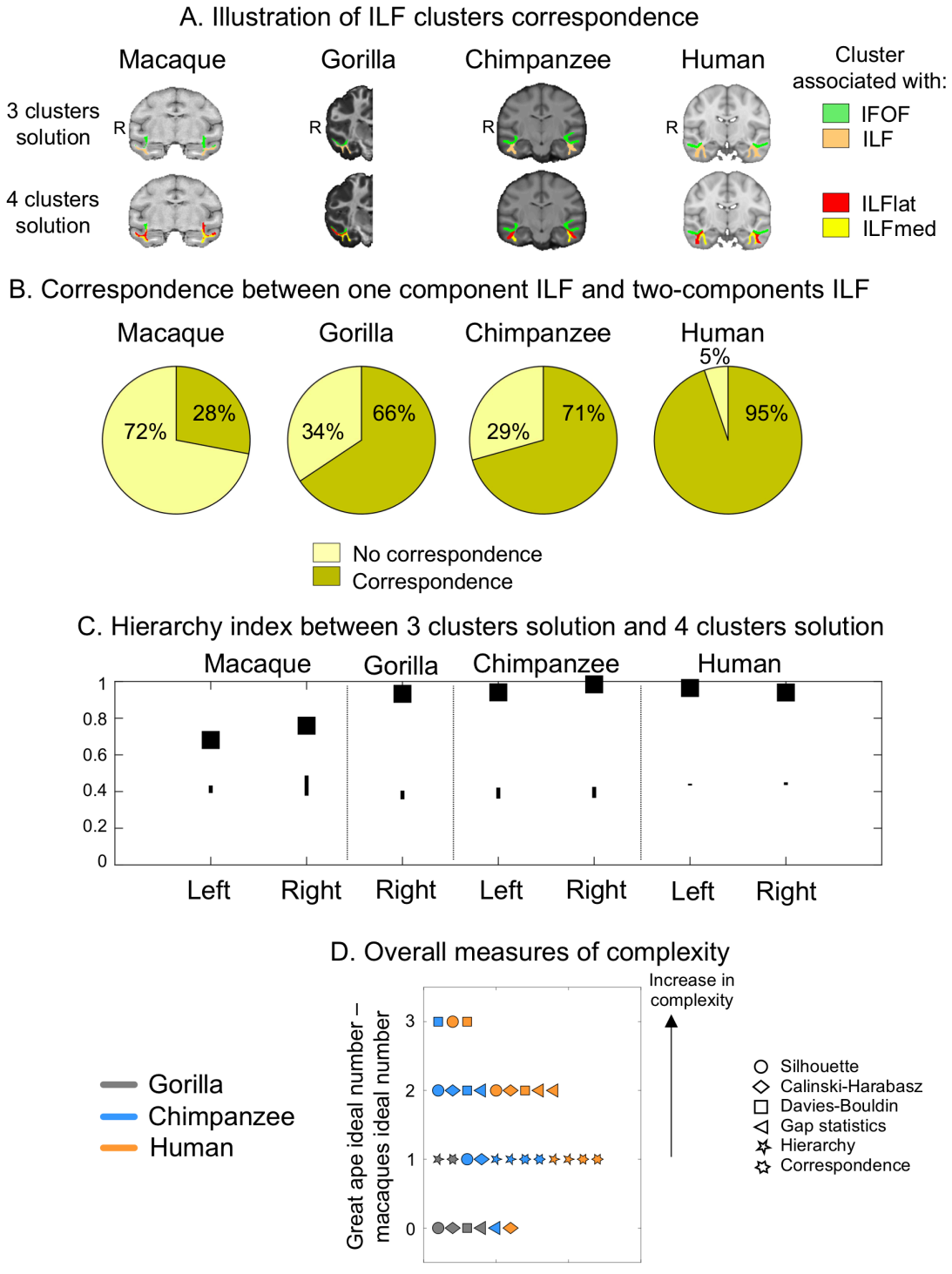

Appendix figure 1.1 Verification of cluster number reliability.

(Figure legend continues on the following page)

A. Illustration of the correspondence between ILF clusters in the middle (seed) ROI when defined as one ILF (three-cluster solution, top row) or the sum of the two subcomponents (four-cluster solution, bottom row), shown from the clustering results obtained across species (thresholded at two individuals' overlap for macaques, two for chimpanzee, and four for humans). (The IFOF is not visible on the macaque left hemisphere four-cluster solution because the hypothetical ILF subcomponents are invading that space.) R denotes right hemisphere. **B.** Correspondence between ILF as defined as a single cluster in the three-cluster solution and as defined by the sum of two clusters in the four-cluster solution, shown as their percentage overlap. If the ILF is reliably split into subclusters, the "correspondence" should be high. **C.** Hierarchy index between the three-cluster and four-cluster solutions is represented in black squares for all species. The black lines represent the range of hierarchy index values obtained with 1,000 random permutations of cluster labelling. **D.** Results from all measures investigating cluster number solutions. The y-axis represents the results of the subtraction of macaques' ideal cluster number from the great apes' cluster number. Each symbol corresponds to a different measure. IFOF: inferior fronto-occipital fascicle; ILF: inferior longitudinal fascicle; ILFlat: inferior longitudinal fascicle lateral; ILFmed: inferior longitudinal fascicle medial.

We further verified the choice of clusters by assessing the hierarchical nature of the cluster assignment in the low versus the high-cluster solution. Many studies on cortical organization have shown a hierarchical organization, where one can define organization from networks, to clusters of areas, to areas, to patches, etc. This hierarchical organization means that when one divides a larger part (e.g., a brain network) into more constituency parts (e.g., brain areas) no aspect (e.g., voxel) will jump from one high-level unit to another. In other words, all voxels classified as belonging to the same brain areas previously belonged to the same brain network. If this is not the case, the finer level parcellation is likely to be incorrect. We tested whether our choice of ILF subdivisions in humans and great apes, but not macaques, was consistent with this notion in two ways. First, as part of the consistency analysis, we added the two clusters from the two-components solution (i.e., high number of clusters solution) for all individuals and calculated its overlap with the cluster from the one ILF solution for all individuals (i.e., low number of cluster solution). This showed a larger overlap in humans compared to macaques (Appendix figure 1.1B). Thus, in humans a

three-cluster solution would lead to a cluster associated with ILF that we could reliably split into two subcomponents in a four-cluster solution, but this was not the case in the macaque. In both gorilla and chimpanzee, the difference between a three- and four-cluster solution led to a separation of ILF into two subcomponents although less reliable than in the human (Appendix figure 1.1AB).

We performed a more formal test by calculating the Hierarchy Index (Kahnt et al., 2012) between the three-cluster and four-cluster solutions in the middle ROI. This index represents the probability that a given cluster in the four-cluster solution comes from only one cluster in the three-cluster solution. A perfectly hierarchical subdivision would have a hierarchy index equal to one. We found that for all samples apart from the macaque the hierarchy index was close to one (0.93 for gorilla and 0.96 and 0.95 for chimpanzees and humans respectively when averaged over the two hemispheres, Appendix figure 1.1C). In contrast, the macaque's hierarchy index, again averaged over the two hemispheres, was only 0.72, much closer to the value observed for hierarchy based on 1000 random permutations of cluster labels (0.40, average over all species and hemispheres, Appendix figure 1.1C). As the macaque was the only one demonstrating such a low hierarchy index, departing from the perfect value of one, compared to other species, this reinforces the argument in favour of a three-cluster solution in macaques and four-cluster solution in others. The difference between the human and macaque can also be represented graphically. Appendix figure 1.2 demonstrates which cluster in the low-cluster solution each voxel of ILFlat and ILFmed in a high-cluster solution was assigned to. As can be seen, human ILFmed and ILFlat voxels were previously almost exclusively assigned to ILF, whereas macaque ILFmed voxels in the left hemisphere and ILFlat voxels in both hemispheres were assigned almost equally from ILF and IFOF in low-cluster solution.

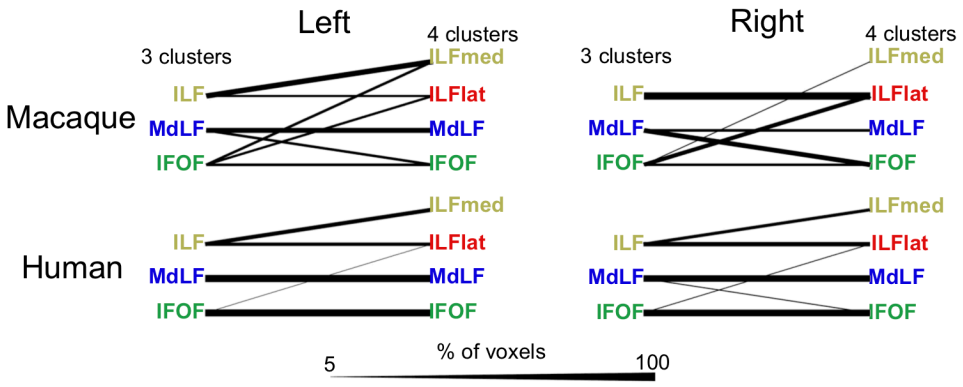

Appendix figure 1.2 Voxel distributions in the three- to four-cluster solutions in the middle ROI.

The lines link the clusters between the two clustering solutions according to whether they have voxels in common; the thickness of the line represents the percentage of the three-cluster voxels that have been allocated to the four clusters. In humans, the clear division of the ILF in the three-cluster solution into ILFmed and ILFlat in the four-cluster solution can be observed. This division is not apparent in macaques. IFOF: inferior fronto-occipital fascicle; ILF: inferior longitudinal fascicle; ILFlat: inferior longitudinal fascicle lateral; ILFmed: inferior longitudinal fascicle medial; MdLF: middle longitudinal fascicle.

Finally, to further confirm the higher complexity found in great apes than in macaques, we performed the clustering of the middle ROI in all species imposing one to five clusters and calculated four additional measures that should indicate the best number of clusters among the ones tried (Calinski-Harabasz (Calinski and Harabasz, 1974), Davies-Bouldin (Davies and Bouldin, 1979), silhouette (Rousseeuw, 1987) and gap statistics (Tibshirani et al., 2001)). We performed the Calinski-Harabasz, Davies-Bouldin and silhouette measure as part of the in-built Matlab function *evalcluster*s. The gap statistic was performed using the Matlab file exchange function written by Alessandro Crimi (https://www.mathworks.com/matlabcentral/fileexchange/37905-gap-statistics) and modified to use a normal distribution as the reference distribution (as suggested in Yin et al., 2008). Although, as shown in previous literature, the different

measures differed in their final solution (Eickhoff et al., 2015), we report here that they still point toward a higher complexity for the humans and chimpanzees than for the macaques, with a more ambiguous result for the gorilla. To represent this result efficiently, the ideal number of clusters given for macaques were subtracted from the ideal number given for the apes by each of the four measures. The motivation behind this manipulation is to show that if this subtraction leads to positive number in general, it means that the complexity is higher for the apes. In other words, that the measures point toward a higher number of clusters for apes than macaques (Appendix figure 1.1D). We also included the results from the hierarchy and correspondence analysis in this representation, which point toward a four-cluster solution as a better solution for apes and a three-cluster solution as a better solution for macaques.

Appendix 2: Clustering and tract reconstruction using other tractography techniques

Tractography algorithms can be error prone (Jbabdi and Johansen-Berg, 2011). This is particularly true when tractography is performed in a manner that is unconstrained by the use of anatomical priors (Maier-Hein et al., 2017). However, these errors can be different when using different algorithms. Therefore, to mitigate the possibility that some of the results may be affected by false positive/negative tracts, we repeated our analyses using different tractography techniques. In addition to the probabilistic tractography using FSL from the main text, we performed deterministic tracking using FSL and an entirely separate implementation from a separate software suite, namely MRTrix3 (www.mrtrix.org).

First, we investigated whether we could replicate the first part of the analysis pipeline, the connectivity-based clustering. We performed the same unconstrained

tractography as previously described from all the voxels in temporal lobe white matter ROIs to all the voxels in the brain but using deterministic tractography instead of probabilistic. In order to do so, we transformed the outputs of the *bedpostX* model (macaque, chimpanzee *in vivo,* humans) and SSFP-based ball-and-two-sticks model (gorilla) to use only the peak orientations of the uncertainty distribution for subsequent deterministic tractography with FSL *probtrackx2*. We also turned off probabilistic interpolation (Behrens et al., 2003) and instead used nearest neighbour interpolation, i.e., similar to traditional deterministic tracking. However, unlike traditional deterministic algorithms, we did not save individual streamlines, but we instead saved voxel-wise visitation counts which were directly comparable with the probabilistic tractography results. Streamline seeding was randomly jittered within each voxel. We increased this jitter for the deterministic version to allow for a sufficient amount of streamlines to be generated (0.25 for macaques, 0.3 for gorilla, 0.5 for chimpanzees and humans). All other parameters were kept the same and we were then able to follow the exact same procedure as defined for the probabilistic version. Briefly, we computed the similarity matrix representing how each voxel in the temporal lobe white matter ROIs is connected to the rest of the brain. This similarity matrix underwent k-means clustering to reveal which voxels of the ROI share similar connectivity. With the same logic as before, based on the current knowledge of tract anatomy (Schmahmann et al., 2007; Catani and Thiebaut De Schotten, 2008; Latini et al., 2017), we could determine which cluster belonged to each tract for each subject. Adding the clusters belonging to the same tracts for all subjects, we obtained probability maps of cluster position in each ROI.

We tested the similarity of these cluster positions with the ones we found using the probabilistic algorithm. For both clustering results, we obtained a winner-takes-all

map from the probability maps, which assigns each voxel of the ROI to the tract cluster with the highest probability. We compared the probabilistic and deterministic winner-takes-all maps by calculating the Dice coefficient between these two maps for each ROI of each species. This coefficient assesses how two clustering results are similar to each other (Parisot et al., 2015; O'Muircheartaigh and Jbabdi, 2018). We obtained Dice coefficients ranging between 0.59 and 0.98 (mean across all ROIs and all species of 0.80). Importantly, all of these coefficients were significantly different to coefficients calculated using 1000 randomly permuted clustering results (difference tested at $p < 0.01$ using permutation test, mean of Dice coefficient between permuted results of 0.27, Appendix figure 2.1). The randomly permuted clustering results were obtained by assigning randomly one of the possible cluster identification to each voxel. In other words, by randomizing the order of the values in the vectors representing the cluster identification of each voxel in the ROIs obtained with the two techniques and calculating the Dice coefficient between these two randomized vectors. This result reinforces our confidence on the position of the clusters described previously. A visual inspection also shows that the clusters obtained with both techniques are very similar (Appendix figure 2.1).

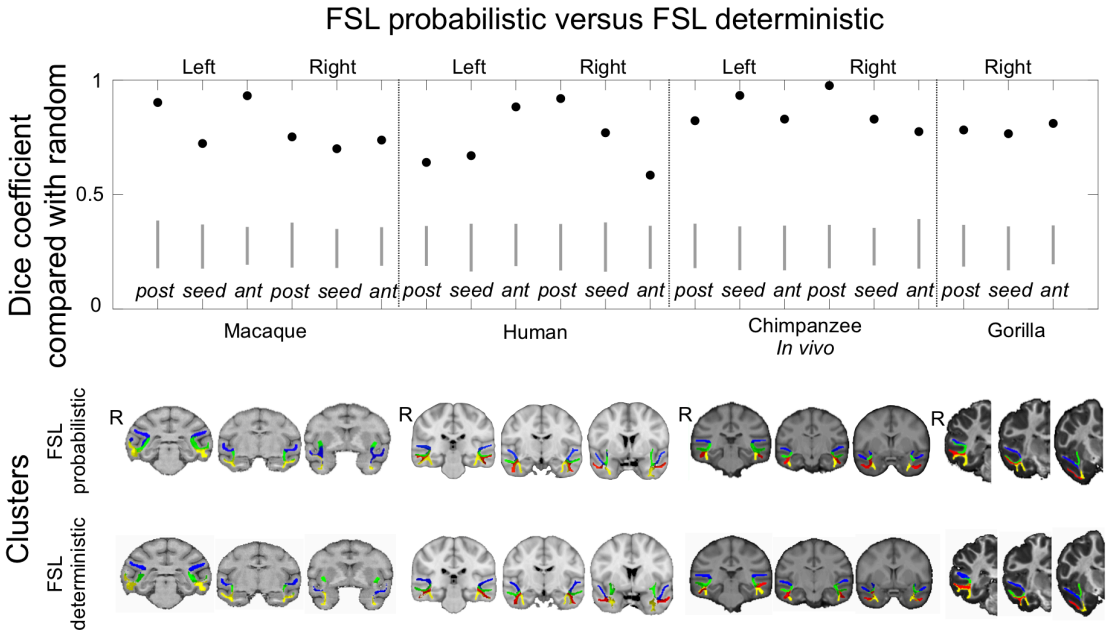

Appendix figure 2.1 FSL probabilistic and deterministic clustering results.

The top panel shows the Dice coefficients in black dots between the clustering results obtained with probabilistic and deterministic tractography for each ROI. The light-grey lines represent the range of Dice coefficients obtained between 1,000 random permutations of cluster solutions. The bottom panels show the clustering results obtained with probabilistic (top) and deterministic (bottom) tractography for each ROI. As in Figure 3.2 and Figure 3.3, the clustering results are thresholded to show the overlap between at least two subjects out of four in macaques and four out of 10 in humans; no thresholding is applied in chimpanzees and gorilla. R denotes right hemisphere. ant: anterior; FSL: FMRIB software library; post: posterior; ROI: region of interest.

Second, we investigated whether we can replicate the tract reconstruction step of our analysis pipeline. We performed the same tractography as previously described, starting from the seed masks, and constrained by two waypoints which were anterior and posterior to the seed. All masks for the MdLF, IFOF and ILF had been defined in the clustering step. For AF, we used the masks as described earlier. We also used the same exclusion and termination masks described previously. However, for the tractography itself, we used two different tractography techniques.

One was the deterministic tractography from FSL, which we used as described for deterministic clustering. We also changed here the jitter of the streamline random

sampling from the seed (from 1mm with the probabilistic algorithm to 3mm for all species with the deterministic algorithm). We were then able to follow the exact same procedure as defined for the probabilistic version. We normalized each tract by the number of streamlines generated, averaged the tracts across species and down-sampled the results before log-transforming them.

The other technique used for this tractography step was performed using the MRtrix3 package (www.mrtrix.org). We followed guidelines from the developers of this package as to which fitting model to use with the different preprocessed data in our hands. As the gorilla and chimpanzee *post mortem* brains were scanned using diffusion-weighted steady-state free precession (DW-SSFP) protocols, we were not able to use MRtrix to analyse these data. This is because DW-SSFP has a different signal formation mechanism, which requires different modelling (Miller et al., 2012), compared to spin-echo data which MRtrix was designed for. The *in vivo* chimpanzee data, while being spin-echo, have a resolution that is considered too low for the type of algorithm used by MRtrix. Therefore, we could only perform this step on the *post mortem* macaque and *in vivo* human data. To estimate the fibre orientation distribution, MRtrix first requires to estimate a response function modelling the signal expected at a given high-anisotropy voxel and uses it as a kernel to perform constrained spherical deconvolution. In humans, we used the Dhollander algorithm to estimate the response function (Dhollander et al., 2016, 2018), because it is described as the default and best suited for multi-shell data. Then we applied a multi-shell multi-tissue constrained spherical deconvolution (Jeurissen et al., 2014) which estimates the fibre orientation distributions for each tissue type (white matter, grey matter, and cerebrospinal fluid). We performed intensity normalization to correct for global intensity differences to make the fibre orientation distributions comparable between subjects. In macaques, we estimated the response

function using the Tournier algorithm (Tournier et al., 2013) because it is described as being robust with a wide range of single shell data. Then, we applied the constrained spherical deconvolution to estimate the fibre orientation distributions of the white matter (Tournier et al., 2007). To finally perform the streamlines tractography, we used the tckgen tool from MRtrix with the default probabilistic algorithm iFOD2, which stands for second order integration over fibre orientation distributions. Where possible similar settings to the FSL-based probabilistic tractography technique were applied. We used the same masks (only converted to MRtrix format), the step sizes were species-dependent (0.5 for humans and 0.25 for macaques), and we seeded 10,000 streamlines per voxel of the seed image to match the number of samples used in FSL. Finally, MRtrix implementation of waypoint inclusion imposes that streamlines must traverse all waypoint masks to be accepted while FSL allows to traverse only one. Therefore, we conducted the MRtrix tractography once with the waypoint anterior and once with the posterior one and added the two results. As for the other tractography techniques, we transformed the results of each individual back to standard space and normalized the tracts by dividing them by the number of streamlines generated, then averaged the tracts across species and down-sampled the results before log-transforming them (Appendix figure 2.2).

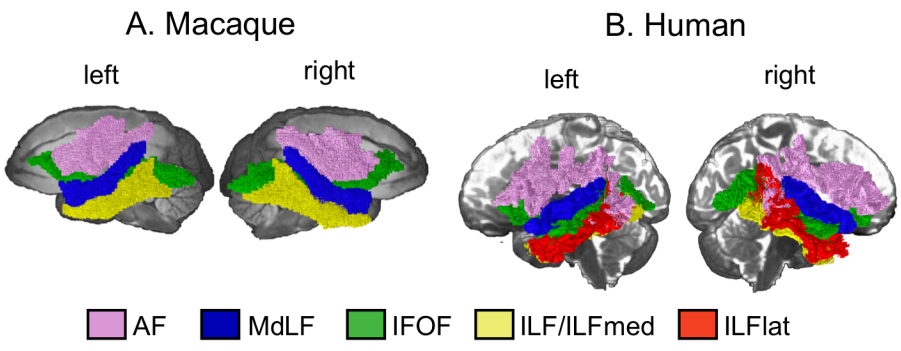

(Figure continues on the following page)

Appendix figure 2.2 MRtrix results showing tractography streamlines for temporal lobe tracts in macaques (A) and humans (B).

Tractograms were log transformed and normalized for display. Blue, MdLF; green, IFOF; yellow, ILF (macaque) or ILFmed (human); red, ILFlat; pink, AF. Thresholds for the tracts are as follows: 0.82 for MDLF; 0.82 for IFOF; 0.8 for ILF, ILFmed, and ILFlat; and 0.8 for AF. AF: arcuate fascicle; IFOF: inferior fronto-occipital fascicle; ILF: inferior longitudinal fascicle; ILFlat: inferior longitudinal fascicle lateral; ILFmed: inferior longitudinal fascicle medial; MdLF: middle longitudinal fascicle.

Anatomically, the tracts obtained with the different techniques followed a very similar path and confirmed their characteristics described earlier (Appendix figure 2.3-6, panels A). The tracts obtained by computing the overlap between the different techniques also demonstrates the overall conserved pattern (Appendix figure 2.3-6, panels A Overlap). In all analyses, the main course of the tracts is preserved, with MdLF running dorsally to ILF and IFOF generally running more medially. The IFOF was the only one of these three to reach the frontal cortex in any species. Although this frontal extension was less pronounced in the deterministic tracking, the overall course of the tract was similar. The AF was also successfully reconstructed in all species using all techniques and the temporal extension in the human was apparent.

We also computed the overlap of each tract obtained with the different techniques with the tracts obtained with FSL probabilistic tractography. More precisely this overlap was calculated as the number of voxels overlapping between a tract of interest and each of the tracts obtained with FSL probabilistic divided by the total number of voxels of the tract of interest. The pattern of overlap of the tracts obtained with other techniques is similar to the one obtained with FSL probabilistic and the tracts most overlapping is always the one we were trying to reconstruct (Appendix figure 2.3-6, panels B). Therefore, not only the tracts have a similar pathway, but they also have a similar organization with respect to each other across the different techniques.

Overall, the different results (clustering and tract reconstruction) obtained using the FSL probabilistic tractography could be reproduced with other techniques, arguing for the robustness of our results and against them emanating from false positives.

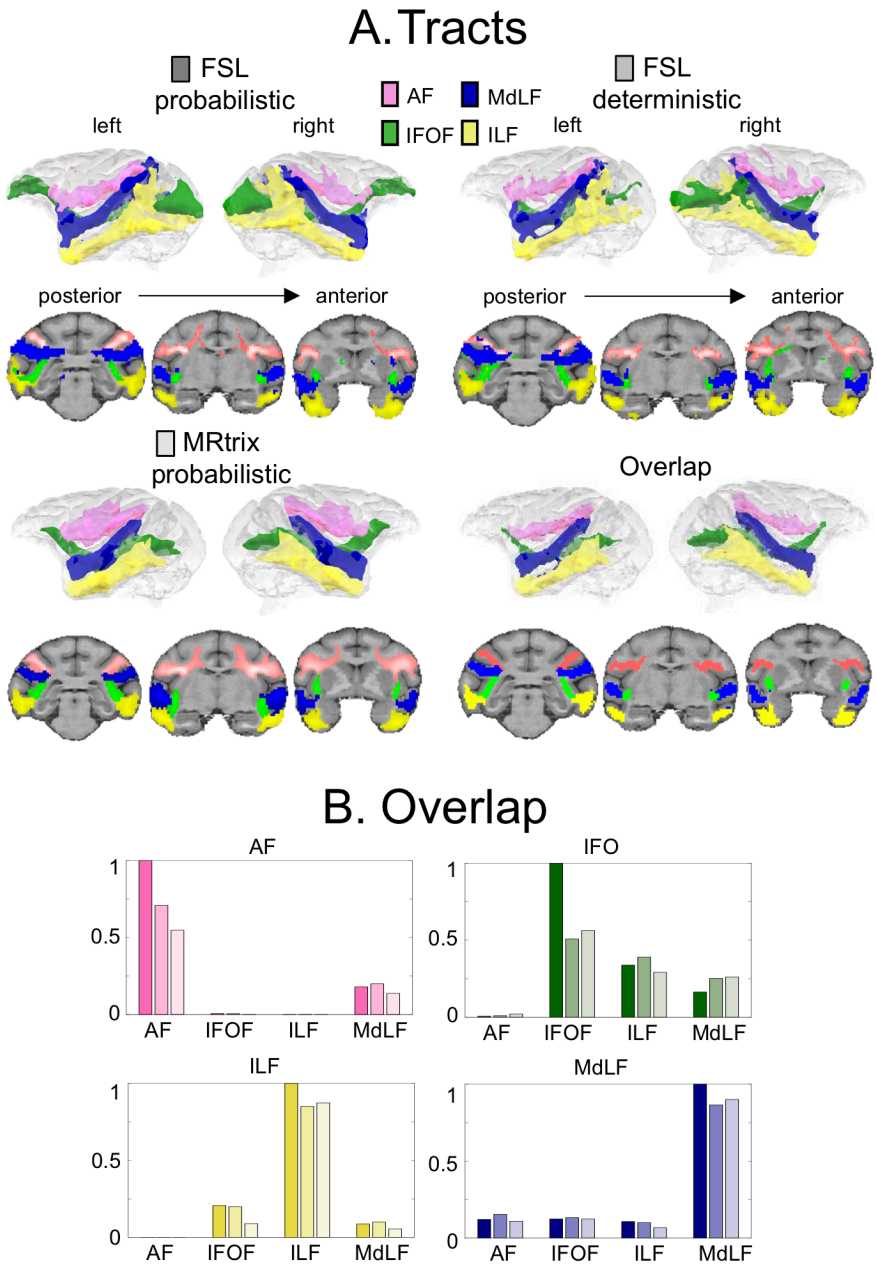

Appendix figure 2.3 Comparison of tract reconstruction using different tractography techniques in macaques.

(Figure legend continues on the following page)

A. Comparison of tract anatomy obtained using FSL probabilistic, FSL deterministic, and MRtrix probabilistic techniques, as well as overlapping tracts between the three. The top panels show the 3D representation of the tracts, and the bottom ones show their organization on coronal sections. Thresholds for the tracts with FSL probabilistic and deterministic techniques are as follows: 0.7 for MDLF; 0.75 for IFOF; 0.7 for ILF; and 0.75 for AF. Thresholds for the tracts with MRtrix are as follows: 0.82 for MDLF; 0.82 for IFOF; 0.8 for ILF; and 0.8 for AF. The overlap is binarized. **B.** Comparison of tract overlap when reconstructed with different techniques. We calculated the number of voxels overlapping between a tract of interest and each of the tracts obtained with FSL probabilistic divided by the total number of voxels of the tract of interest. The darker colour represents the overlap of the tract of interest obtained with FSL probabilistic, and the lighter colour represents the overlap of the tract of interest obtained with MRtrix and the colour in between the tract of interest obtained with FSL deterministic. AF: arcuate fascicle; FSL: FMRIB Software Library; IFOF: inferior fronto-occipital fascicle; ILF: inferior longitudinal fascicle; ILFmed: inferior longitudinal fascicle medial; MdLF: middle longitudinal fascicle.

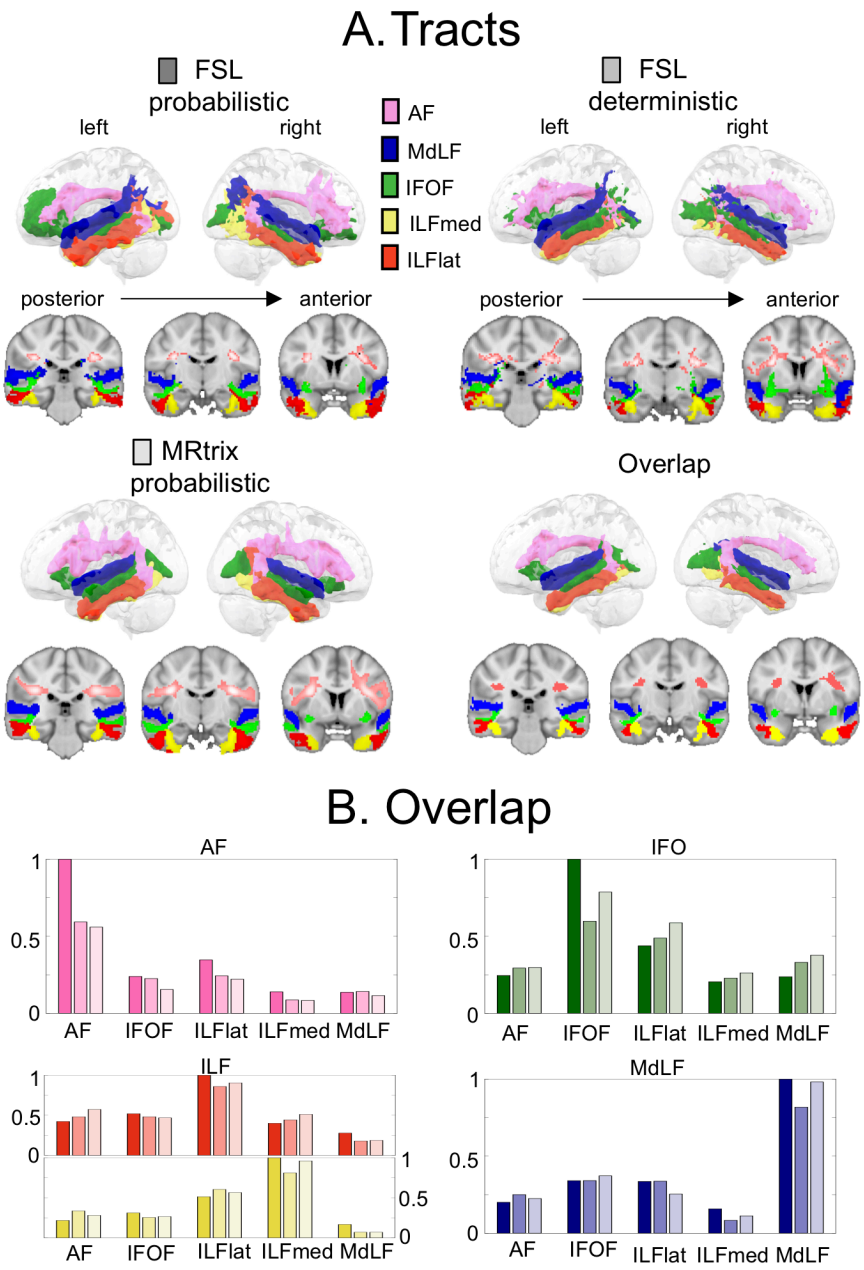

Appendix figure 2.4 Comparison of tract reconstruction using different tractography techniques in humans.

A. Comparison of tract anatomy obtained using FSL probabilistic, FSL deterministic, and MRtrix probabilistic techniques, as well as overlapping tracts between the three. The top panels show the 3D representation of the tracts, and the bottom ones show their organization on coronal sections. Thresholds for the tracts with FSL probabilistic and deterministic techniques are as follows: 0.7 for MDLF; 0.75 for IFOF; 0.7 for ILFlat and ILFmed; and 0.75 for AF. Thresholds for the tracts with MRtrix are as follows: 0.82 for MDLF; 0.82 for IFOF; 0.8 for ILFlat and ILFmed; and 0.8 for AF. The overlap is binarized.

(Figure legend continues on the following page)

B. Comparison of tract overlap when reconstructed with different techniques. We calculated the number of voxels overlapping between a tract of interest and each of the tracts obtained with FSL probabilistic divided by the total number of voxels of the tract of interest. The darker colour represents the overlap of the tract of interest obtained with FSL probabilistic, and the lighter colour represents the overlap of the tract of interest obtained with MRtrix and the colour in between the tract of interest obtained with FSL deterministic. AF: arcuate fascicle; FSL: FMRIB Software Library; IFOF: inferior fronto-occipital fascicle; ILFlat: inferior longitudinal fascicle lateral; ILFmed: inferior longitudinal fascicle medial; MdLF: middle longitudinal fascicle.

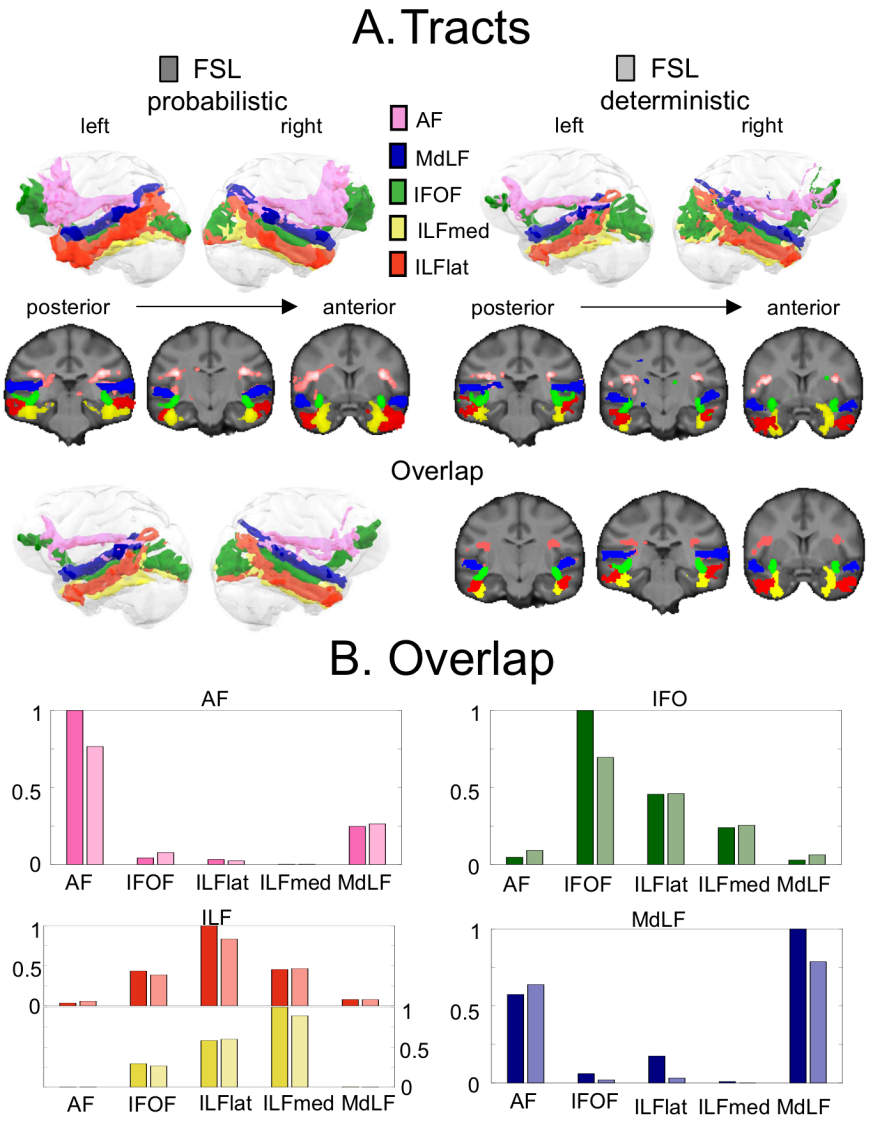

Appendix figure 2.5 Comparison of tract reconstruction using different tractography techniques in chimpanzees *in vivo*.

A. Comparison of tract anatomy obtained using FSL probabilistic and FSL deterministic techniques, as well as overlapping tracts between the two. The top panels show the 3D representation of the tracts, and the bottom ones show their organization on coronal sections.

(Figure legend continues on the following page)

Thresholds for the tracts with FSL probabilistic and deterministic techniques are as follows: 0.7 for MDLF; 0.75 for IFOF; 0.7 for ILFlat and ILFmed; and 0.75 for AF. The overlap is binarized. **B.** Comparison of tract overlap when reconstructed with different techniques. We calculated the number of voxels overlapping between a tract of interest and each of the tracts obtained with FSL probabilistic divided by the total number of voxels of the tract of interest. The darker colour represents the overlap of the tract of interest obtained with FSL probabilistic, and the lighter colour represents the overlap of the tract of interest obtained with FSL deterministic. AF: arcuate fascicle; FSL: FMRIB Software Library; IFOF: inferior fronto-occipital fascicle; ILFlat: inferior longitudinal fascicle lateral; ILFmed: inferior longitudinal fascicle medial; MdLF: middle longitudinal fascicle.

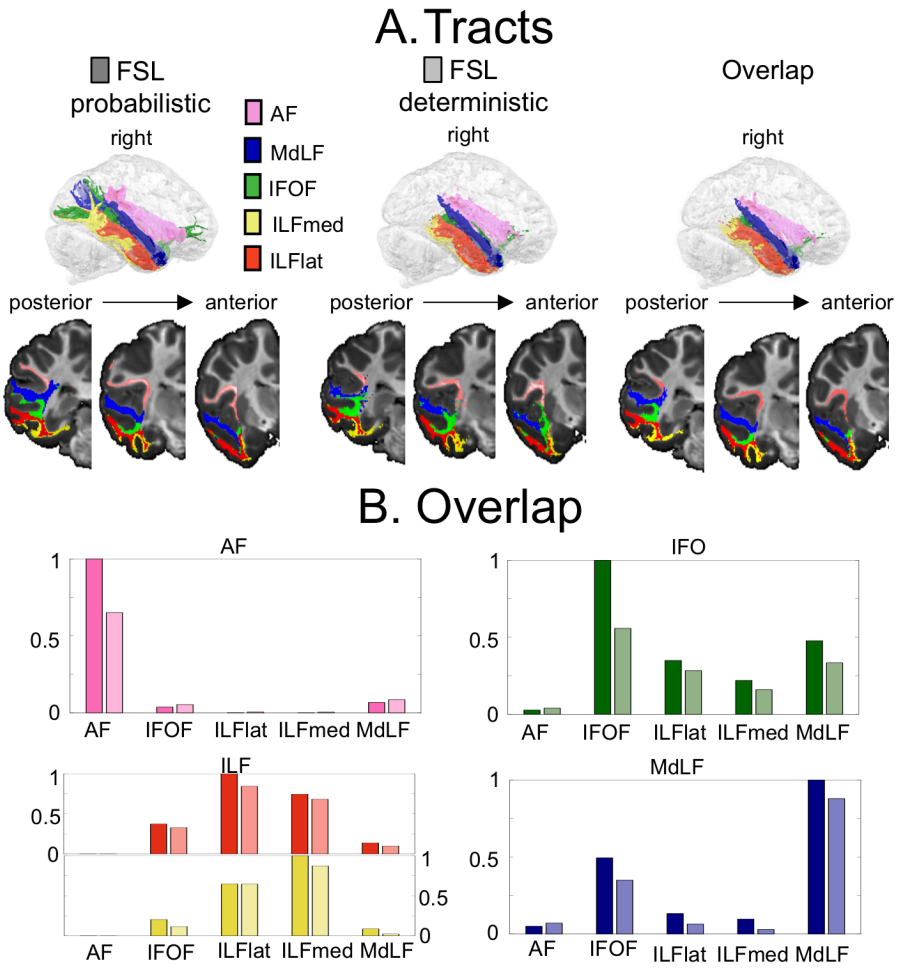

Appendix figure 2.6 Comparison of tract reconstruction using different tractography techniques in gorilla *post mortem*.

A. Comparison of tract anatomy obtained using FSL probabilistic and FSL deterministic techniques, as well as overlapping tracts between the two. The top panels show the 3D representation of the tracts, and the bottom ones show their organization on coronal sections. Thresholds for the tracts with FSL probabilistic and deterministic techniques are as follows: 0.7 for MDLF; 0.75 for IFOF; 0.7 for ILFlat and ILFmed; and 0.75 for AF. The overlap is binarized.

(Figure legend continues on the following page)

B. Comparison of tract overlap when reconstructed with different techniques. We calculated the number of voxels overlapping between a tract of interest and each of the tracts obtained with FSL probabilistic divided by the total number of voxels of the tract of interest. The darker colour represents the overlap of the tract of interest obtained with FSL probabilistic, and the lighter colour represents the overlap of the tract of interest obtained with FSL deterministic. AF: arcuate fascicle; FSL: FMRIB Software Library; IFOF: inferior fronto-occipital fascicle; ILFlat: inferior longitudinal fascicle lateral; ILFmed: inferior longitudinal fascicle medial; MdLF: middle longitudinal fascicle.

Appendix 3: Tractography as the best method to study white matter in a large range of species.

The research of white matter tracts commonly relies on different methods across species. All of these methods have their advantages and inconveniences and capture different aspects of the underlying biology. Therefore, when comparing the white matter organization in different species, we should use the same technique to be able to compare like-with-like.

We argue here that tractography is the method that fits best our study aim (chapter 3). In the macaque monkey, tract tracing approaches have been previously widely used. They are precise techniques to follow the path of an axon but require very invasive experiments. This is also the case for blunt dissection studies. Therefore, their use in a large range of primate species including humans is not ethically supported. Tractography, which relies on diffusion MRI data, is a non-invasive alternative and the only viable option as a method available in all species.

There are technical limitations of tractography and if used incorrectly the method can lead to high false positive and false negative rates and biases due to the definition of seeds and waypoints to guide the algorithm. We have dealt with this issue by defining our seeds and waypoints based on a data-driven method clustering together white matter voxels according to their connectivity to the rest of the brain. The underlying idea is that if voxels, around the same anatomical region, have very similar

connectivity to the rest of the brain then they should be part of the same tract. This approach was restricted to the core of the tract and the result was compared with outcomes from previous tractography studies but also tract tracing and dissection. In a recent paper from our lab (Folloni et al., 2019a), it has been shown that using features from tract tracing studies can help guide reliable tractography results in both humans and macaques; this was illustrated for a tract that is usually particularly difficult to reconstruct with tractography, the amygdalofugal pathway.

To establish a relationship between the probabilistic tractography results and those obtained using other methods, we here also compare our tractography results with tracts obtained with other methods. When using different methods, we cannot expect to obtain exactly the same results. However, we note here that the core of the tracts resulting from our tractography protocol in macaques is very similar to what have been reconstructed using tract tracing results (Schmahmann et al., 2007) (Appendix figure 3.1A), indicating that the number of false positives and negatives is low. Specifically, the ILF and MdLF are very much the same, but we can notice some differences for the AF and IFOF (Appendix figure 3.1A). Regarding the AF, it seems to invade the territory of the Superior longitudinal fascicle (SLF) in some parts. However, this is a known issue when using tractography for the AF, as pointed out in the pioneering study from Rilling and colleagues (Rilling et al., 2008) where AF and SLF III are treated as one bundle in humans, chimpanzees, and macaques.

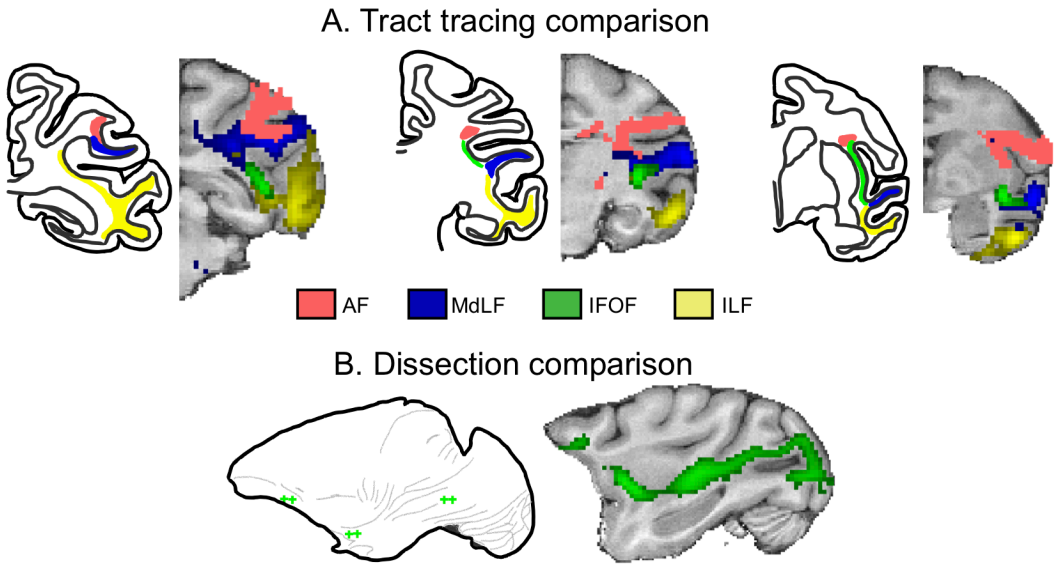

Appendix figure 3.1 Comparison of the macaque tractography results with the tract tracing and dissection literature.

A. Comparison with tract tracing results redrawn from previous report (Schmahmann and Pandya, 2006b). Tracts to be compared are highlighted in similar colours. Blue, MdLF; green, IFOF; yellow, ILF; pink, AF. **B.** Comparison with the dissection results redrawn from previous report (Decramer et al., 2018); the green crosses illustrate the IFOF pathway. AF: arcuate fascicle; IFOF: inferior fronto-occipital fascicle; ILF: inferior longitudinal fascicle; MdLF: middle longitudinal fascicle.

Concerning the IFOF, its extent from the frontal lobe to the occipital lobe has been controversial, as tracer data commonly shows terminations in the middle part of the temporal cortex in macaques (Thiebaut De Schotten et al., 2012). We presume this discrepancy to be due to the nature of the IFOF as a multisynaptic pathway. Tract tracing can only reveal mono-synaptic connections and therefore might fail to reconstruct the full IFOF pathway (Mars et al., 2016a). A recent blunt dissection study showed that an IFOF similar to the one reported by our tractography results can be identified in macaques, running from the frontal lobe to the occipital lobe (Decramer et al., 2018) (Appendix figure 3.1B). We are therefore confident that the fibre bundle identified in this study corresponds to tracts previously shown in the literature and that it has a firm biological basis.

We also verified our approach by comparing the results obtained with two other tractography techniques, one using the same software (FSL) but with a deterministic algorithm and one using a completely different package, MRtrix3 (www.mrtrix.org). The three different methods yield very similar tracts and anatomical organization (Appendix 2). We are therefore confident that the probabilistic tractography results do not only reflect false positives and false negatives.

Appendix 4: Left hemisphere results for chapter 3

Result figures for the left hemisphere as shown in the main text of chapter 3 for the right hemisphere.

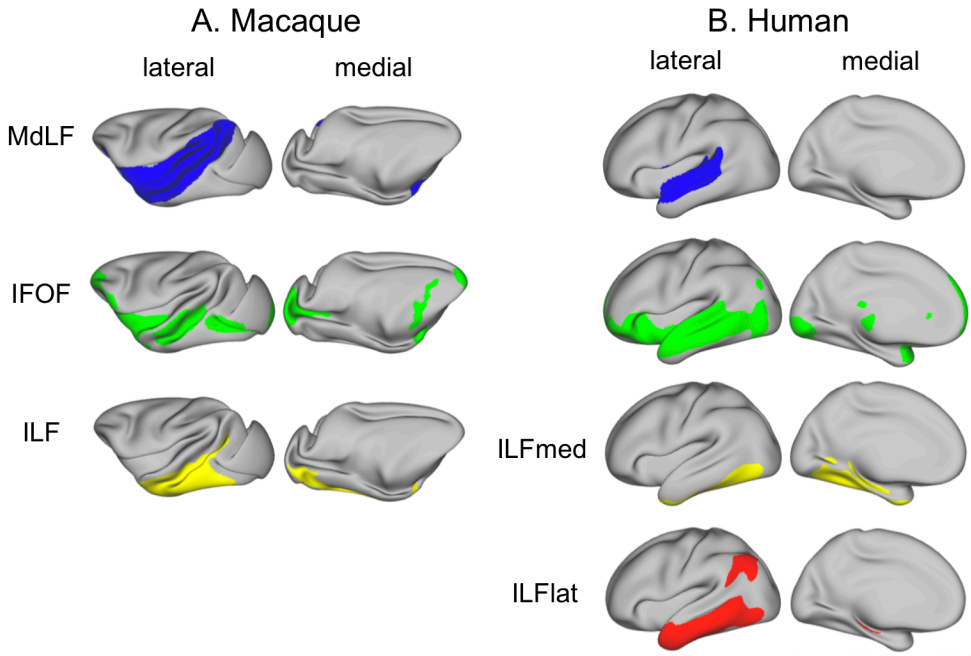

Appendix figure 4.1 Surface projection of longitudinal temporal tracts in macaques (A) and humans (B).

Shown are the group averages of the normalized, log-transformed, and thresholded tracts in the left hemisphere only (for space-saving purpose). Blue, MdLF; green, IFOF; yellow, ILF (macaque) or ILFmed (humans); red, ILFlat. Thresholds for the tracts are as follows: 0.7 for MDLF; 0.75 for IFOF; and 0.7 for ILF, ILFmed, and ILFlat. IFOF: inferior fronto-occipital fascicle; ILF: inferior longitudinal fascicle; ILFlat: inferior longitudinal fascicle lateral; ILFmed: inferior longitudinal fascicle medial; MdLF: middle longitudinal fascicle.

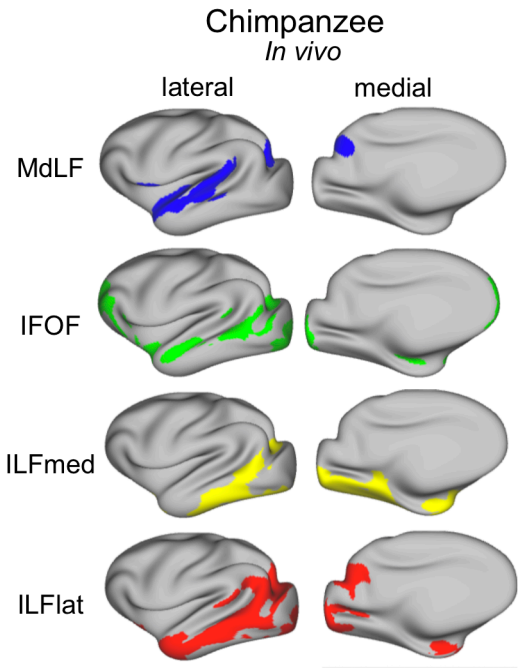

Appendix figure 4.2 Surface representation of longitudinal temporal tracts in chimpanzees.

Shown are the group averages of the normalized, log-transformed, smoothed and thresholded left tracts. Blue, MdLF; green, IFOF; yellow, ILFmed; red, ILFlat. Thresholds for the tracts are as follows: 0.7 for MDLF; 0.75 for IFOF; and 0.7 for ILFmed and ILFlat. IFOF: inferior fronto-occipital fascicle; ILFlat: inferior longitudinal fascicle lateral; ILFmed: inferior longitudinal fascicle medial; MdLF: middle longitudinal fascicle.

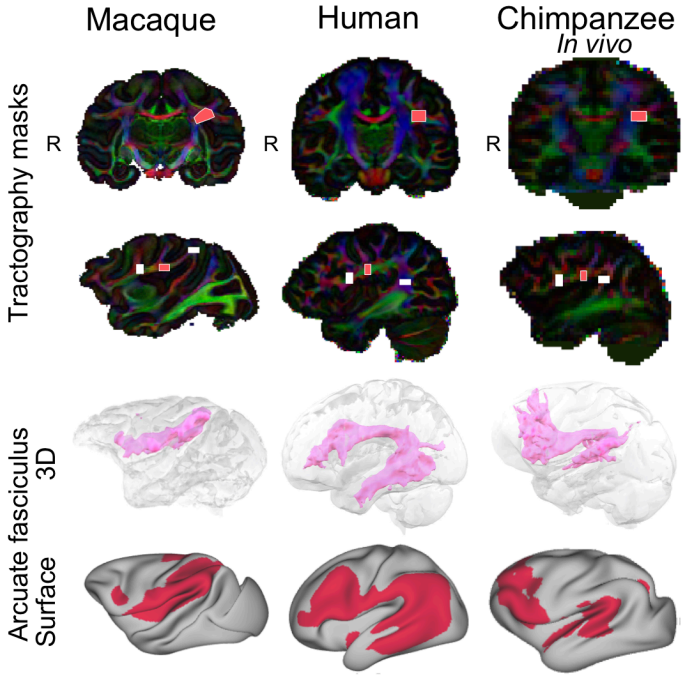

(Figure continues on the following page)

Appendix figure 4.3 AF tractography protocols and results.

Top panel: AF tractography masks example for one individual macaque, human, and chimpanzee, represented on the principal eigenvector (V1) map weighted by the fractional anisotropy map. The light-pink mask represents the seed, and the white masks represent the anterior and posterior waypoints. Bottom panel: 3D and surface representation of the left tractogram obtained for AF. Threshold of 0.75. R denotes right hemisphere. AF: arcuate fascicle.

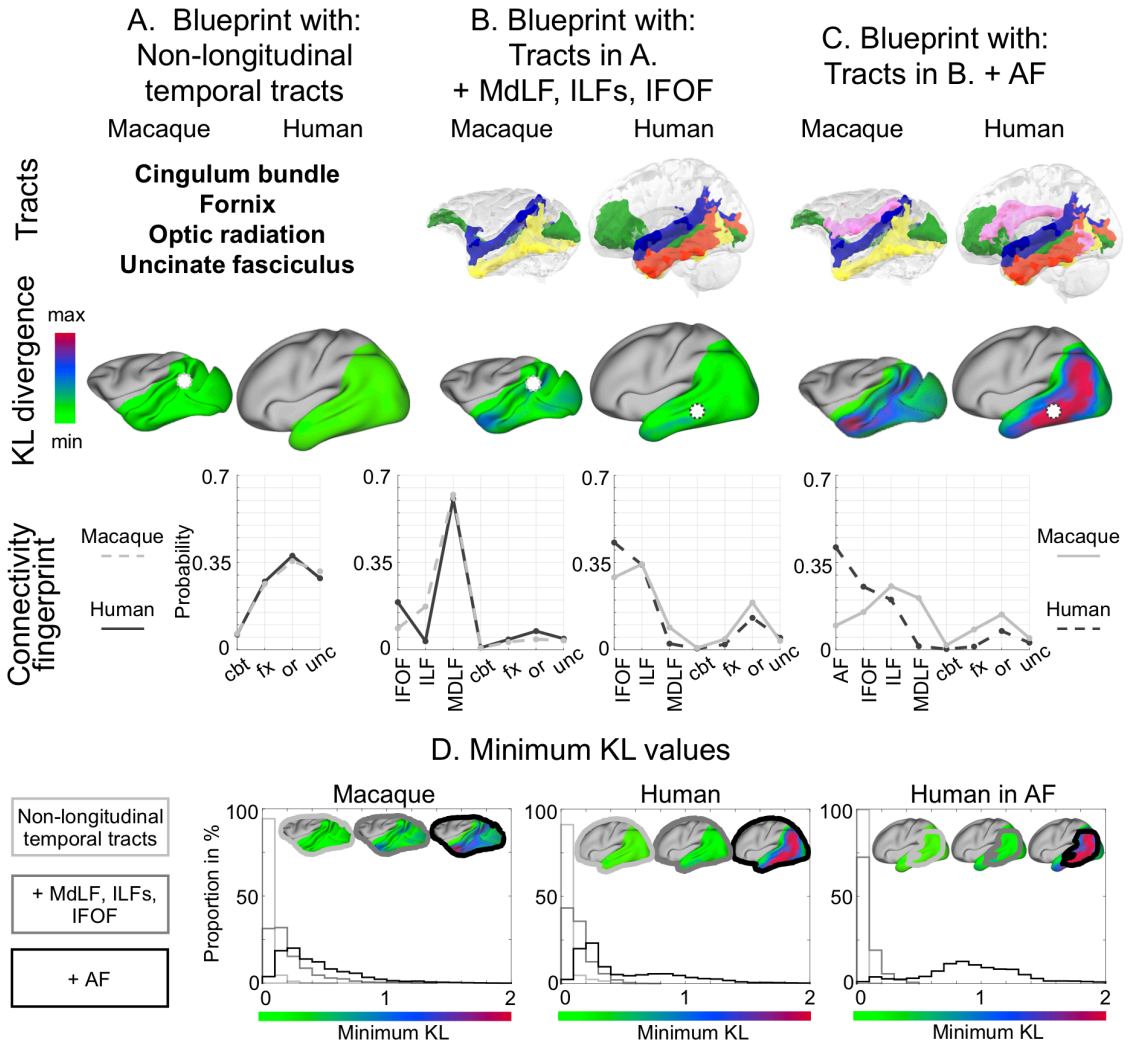

Appendix figure 4.4 Results of the blueprint analysis.

The figure reports results on the left hemisphere. Shown are the tracts used (top row), the resulting KL divergence (middle row) for human predicting macaque (left) and macaque predicting human (right), and the connectivity fingerprints (bottom row). The greener the vertices of the KL divergence map in one brain, the more their connectivity profile is similar to that of vertices in the other brain. The connectivity fingerprints show the probability of the vertex, highlighted by a white sphere in the brain above, to be reached by each tract (dotted line).

(Figure legend continues on the following page)

The solid line represents the probability of being reached by each tract in the other species, calculated as the mean over the 10 vertices with the smallest KL divergence with the initial species' vertex of interest. **A.** Blueprints established using the cbt, the fx, the or, and the unc. **B.** Blueprints established with the tracts in (A) and adding the MdLF, ILF (both subcomponents combined in humans), and IFOF. **C.** Blueprints established with the tracts in (B) and adding the AF. Blue, MdLF; green, IFOF; yellow, ILF (macaque) or ILFmed (human); red, ILFlat; pink, AF. **D.** Distribution of minimum KL values obtained for each blueprint. From left to right for the macaque, the human, and masked with the human AF. Light grey, nonlongitudinal tracts; grey, adding MdLF, ILFs, and IFOF; black, adding AF. AF: arcuate fascicle; cbt: temporal part of the cingulum bundle; fx: fornix; IFOF: inferior fronto-occipital fascicle; ILF: inferior longitudinal fascicle; ILFlat: inferior longitudinal fascicle lateral; ILFmed: inferior longitudinal fascicle medial; KL: Kullback–Leibler; MdLF: middle longitudinal fascicle; or: optic radiation; unc: uncinate fascicle.

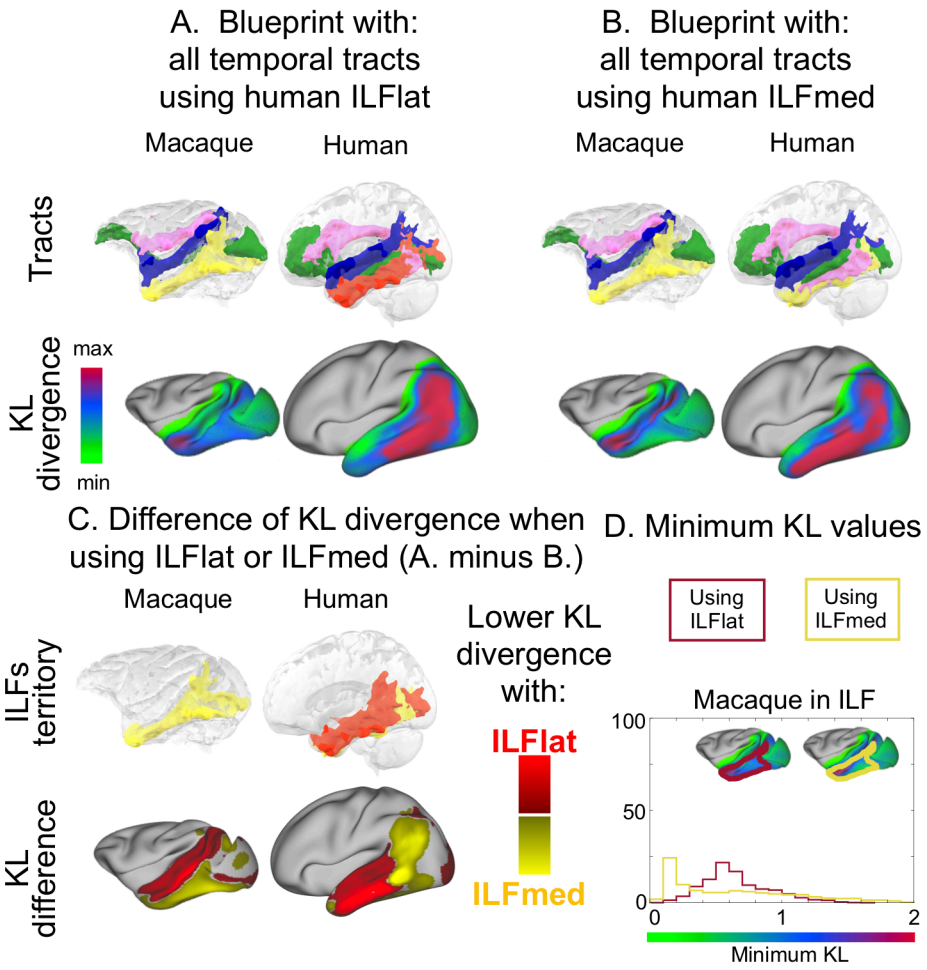

Appendix figure 4.5 Blueprint method to determine differences between the human ILFs.

A. Blueprint established as in Appendix figure 4. 4C but with the ILFlat for humans (no ILF med). **B.** Blueprint established as in (A) but with the ILFmed for humans (no ILFlat).

(Figure legend continues on the following page)

C. The different ILF tractograms are represented on the top row. On the bottom row is shown the KL difference between the two maps established in (A) and (B). More yellow vertices means that using ILFmed in humans as macaques' ILF homologous results in lower KL divergence between the two species at these vertices, whereas more red applies to ILFlat. Blue, MdLF; green, IFOF; yellow, ILF (macaque) or ILFmed (human); red, ILFlat; pink, AF. **D.** Distribution of minimum KL values in the macaque's ILF territory obtained for the blueprints with the different human ILF subcomponents. Red, with human ILFlat; yellow, with human ILFmed. IFOF: inferior fronto-occipital fascicle; ILF: inferior longitudinal fascicle; ILFlat: inferior longitudinal fascicle lateral; ILFmed: inferior longitudinal fascicle medial; KL: Kullback–Leibler; MdLF: middle longitudinal fascicle.

Appendix 5: Right hemisphere results for chapter 5

Result figures including the right hemisphere data to verify hemispheric variability in chapter 5.

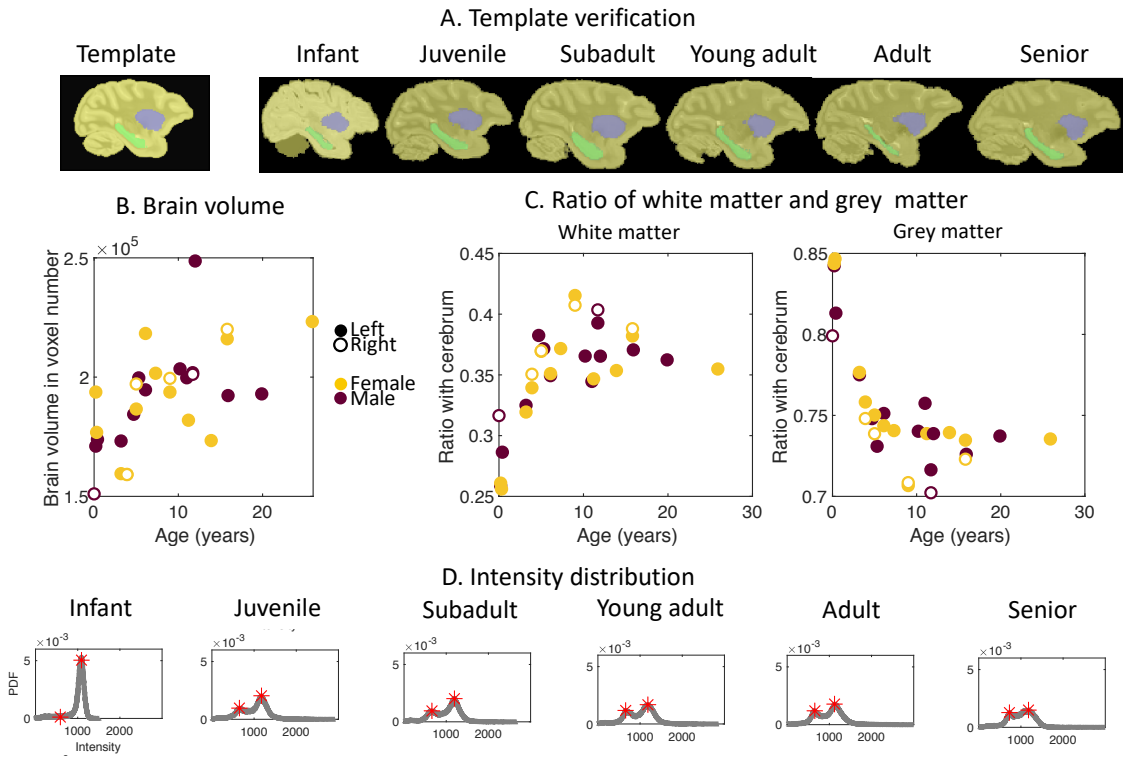

Appendix figure 5.1 Right hemisphere results for template verification and whole brain measure.

(Figure legend continues on the following page)

A. Registration quality assessment to the right hemisphere general template showing the original masks from the general right hemisphere template on a sagittal slice and the transformed masks to each individual space. The yellow structures represent the brain mask, the blue structures represent the putamen and caudate nucleus, and the green structures represent the hippocampus. **B.** Brain volume for all available hemispheres, left (filled dots) and right (outline dots). Note that the right hemisphere values are following the same trend as the left hemisphere values. **C.** Ratio of left (filled dots) and right (outline dots) white matter and grey matter volume with the volume of the cerebrum. Note that the right hemisphere values are following the same trend as the left hemisphere values. **D.** Distribution of intensities of the normalized nodif image for each individual right hemisphere, each row corresponding to one age category. The red stars highlight the local maxima. PDF: probability function distribution.

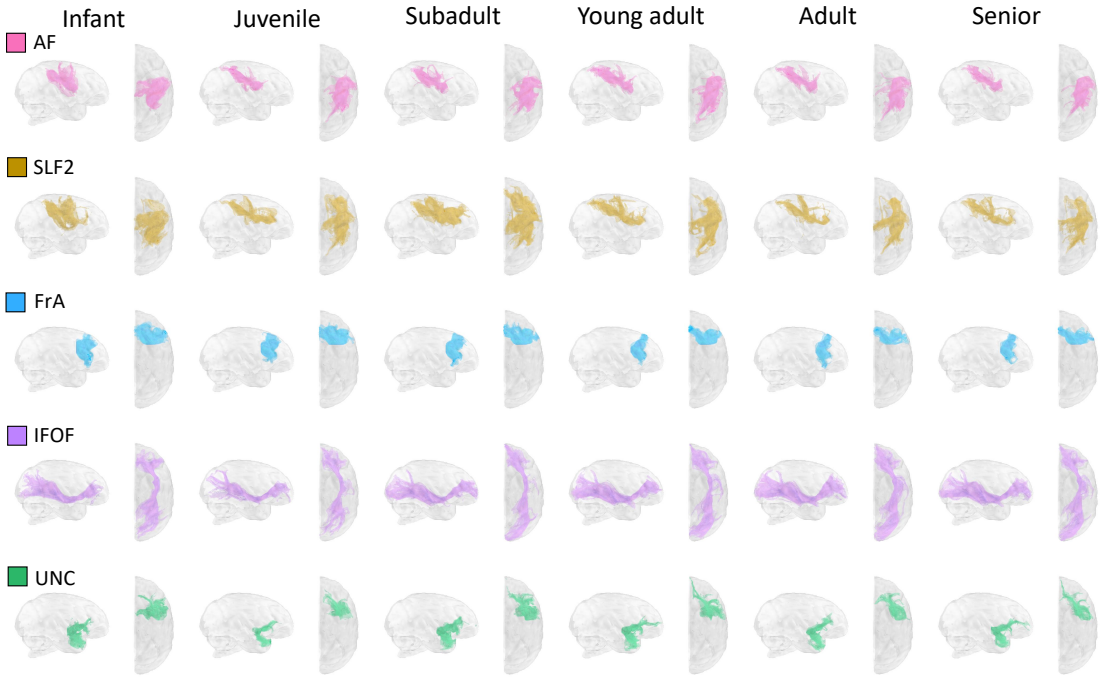

Appendix figure 5.2 Right hemisphere tractography results.

Right hemisphere tract anatomy representing the averaged log transformed, thresholded tractogram in a 3D reconstruction showing right and dorsal views. Although less evident that for the left hemisphere we can note that similar trends are observable in the tracts of interest on the right hemisphere. AF: arcuate Fascicle, IFOF: inferior fronto-occipital fascicle, FrA: frontal aslant, SLF2: superior longitudinal fascicle, UNC: uncinate fascicle.